

MASS TRANSFER PROCESSES OF ODORANTS IN AERIAL BOUNDARY LAYERS

CHAYAN KUMER SAHA

PHD THESIS · SCIENCE AND TECHNOLOGY · 2011



AARHUS UNIVERSITY

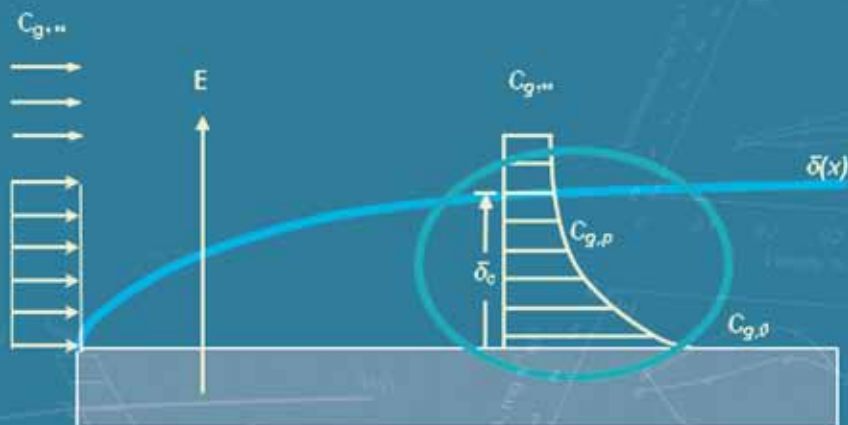


Fig. 2.6 - Comparison of ammonia emission fluxes at various distances from the surface.

MASS TRANSFER PROCESSES OF ODORANTS IN AERIAL BOUNDARY LAYERS

CHAYAN KUMER SAHA

PhD THESIS · SCIENCE AND TECHNOLOGY · 2011



AARHUS UNIVERSITY

Department of Biosystems Engineering
Science and Technology
Research Centre Foulum
Aarhus University
P.O. Box 50
DK-8830 Tjele

Preface

This thesis is submitted as a partial fulfillment of the requirements for the Doctor of Philosophy (PhD) degree at the Aarhus University, Faculty of Science and Technology.

This thesis presents PhD research between May 2008 and March 2011 in the Department of Biosystems Engineering, Aarhus University. The experiments were carried out at Air Physics Lab and the experimental building for fattening pigs, Research Centre Bygholm, Horsens, and also at Research Center Foulum, Department of Biosystems Engineering. The work was part of the ROSES project, “Reduction of Odour Source in and Emission from Swine Buildings” under the program “Animal Husbandry, the Neighbours and the Environments”, funded by the Danish Ministry of Food, Agriculture and Fisheries (Grant number: 3304-VMP-05-032-01). Part of the fund was also provided by the School of Food, Agriculture and Environment (SAFE) and the Department of Biosystems Engineering.

This thesis is based on the work presented in four published research articles and three submitted manuscripts to academic journals. They are entitled:

1. **Saha, C. K.**, Zhang, G and Ni. J.-Q., 2010. Airflow and concentration characterisation and ammonia mass transfer modelling in wind tunnel studies. **Biosystems Engineering**, Vol. 107 (4), P 328-340.
2. **Saha, C.K.**, Wu, W., Zhang, G., and Bjerg, B., 2011. Assessing effect of wind tunnel sizes on air velocity boundary layers and on ammonia emission estimation using computational fluid dynamics (CFD). **Submitted to a peer review journal.**
3. **Saha, C. K.**, Zhang, G., and Kai, P., 2011. Ammonia emission process affected by ventilation airflow, pen partition and location of emission surface and ammonia mass transfer modelling in a model pig house. **Submitted to a peer review journal.**
4. **Saha, C.K.**, Zhang, G, Ni, J.-Q. and Ye, Z., 2011. Similarity criteria for estimating gas emission from scale models. **Biosystems Engineering**, Vol. 108(3), P 227-236.
5. **Saha, C.K.**, Feilberg, A., Zhang, G., and Adamsen, A. P., 2011. Effect of airflow on odorants emissions in a model pig house- A laboratory study using Proton-Transfer-Reaction Mass Spectrometry (PTR-MS). **Submitted to a peer review journal.**
6. Ye, Z., **Saha, C.K.**, Li, B., Tong, G., Wang, C., Zhu, S., and Zhang, G., 2009. Effect of environmental deflector and curtain on air exchange rate in slurry pit in a scaled livestock building. **Biosystems Engineering**, Vol. 104 (4), P 522-533.
7. **Saha, C.K.**, Zhang, G, Kai, P. and Bjerg, B., 2010. Effects of a partial pit ventilation system on indoor air quality and ammonia emission from a fattening pig room. **Biosystems Engineering**, Vol. 105 (3), P 279-287.

During this study, I spent six months in Purdue Agricultural Air Quality Laboratory (PAAQL), Department of Agricultural and Biological Engineering, Purdue University, USA and acquired skills on online measurement techniques, data analysis, and data quality control. I attended two international conferences on subjects directly related to this PhD study and made one oral and one poster presentations. I also presented four posters at internal seminars. Additionally, I was involved in organizing practical exercises for MSc and PhD students, and teaching MSc students at Faculty of Science and Technology, Aarhus University. I was also involved in the measurements and data collection of full scale experimental climate laboratory, Ruballegård, Horsens.

In addition, the following publication was produced during the PhD study:

1. Ye, Z., Zhang, G., Li, B., Seo, I., Kai, P., **Saha, C.K.**, Wang, C, and Li, B., 2009. Airflow characteristics at manure surface affected by ventilation rate, floor slat opening and headspace in slurry pit. **Biosystems Engineering**, Vol. 104 (1), P 97-105.

Acknowledgements

I would like to acknowledge a few people who have been involved in this study in various ways.

First and foremost I would like to sincerely thank my principal supervisor, Dr. Guoqiang Zhang, Senior Scientist, Aarhus University for giving me the opportunity to work on this project and for his expert guidance, continuous support, and stimulating input on this research venture. His broad knowledge, high academic standards and personal integrity motivated me to move forward, academically and personally. I would like to express sincere gratitude to my co-supervisor and host of my research stay at Purdue University, Dr. Jiqin Ni, Research Associate Professor for his valuable time, careful and instructive comments, and suggestions on every publication that we prepared together and on this PhD thesis. I will remain forever grateful for the important skills that you taught me.

I am indebted to Dr. Anders Feilberg, Senior Scientist, Department of Biosystems Engineering, Aarhus University, who gave me much help in my odour measurement research. I benefited from many discussions with him on the volatile organic compounds emission. I would also like to give sincere thanks to Dr. Anders Peter S. Adamsen, Senior scientist and head of the research unit, for his assistance, support and suggestion about extended experiment. My sincere thank goes to Dr. Morten Dam Rasmussen, Head of the Department of Biosystems Engineering for his generosity, believing on me, and giving me flexibility in work.

I am grateful to the following individuals with whom I co-authored the papers included in this thesis: Dr. Peter Kai and Wentao Wu from Aarhus University; Dr. Bjarne Bjerg from KU-Life; Dr. Zhangying Ye and Dr. Songming Zhu from Zhejiang University, China; Dr. Boamin Li and Dr. Chaoyuan Wang from China Agricultural University, China; and Dr. Guohong Tong from Shenyang Agricultural University, China. Thank you all for helping remove nonsense whilst adding sense to the papers.

This work would not have been possible without the tireless assistance from the lab technicians at Aarhus University, in particular Jan Ove Johnsen, Peter Ravn, Preben Jansen Dahl, Steffen Gold Christensen, and Claudia Nagy. I would also like to thank Anja Torup Hansen, department secretary, and Britt-Ea Jansen, information officer for their help with smiling faces whenever I asked for. My special thanks to Ole Juul Jørgensen for his assistance in the moving phase of the department.

Many thanks go to all my colleagues at the Faculty of Science and Technology at Aarhus University, although I am not listing your names here. It was your faces of smile and acts of kindness that made my PhD work much enjoyable.

Above all, I am deeply indebted to my wife Papia Roy, who has always been my great helper, and our daughter Pushpita Saha for their understanding, patience and support, and for sharing all the difficulties and happiness during this PhD study. My parents and brothers were also very supportive and always believed in my ability to excel.

Finally, I thank God for giving me strength and good health during the course of this study.

(Chayan Kumer Saha)

Abstract

Odorants from pig production systems affect human and animal health, and surrounding atmosphere negatively, both directly and indirectly. Identification of different factors that influence release behaviours of ammonia (NH_3), hydrogen sulphide (H_2S), and volatile organic compounds (VOCs) are essential to develop emission abatement technologies. Air is the main transport medium of these gases and VOCs from livestock buildings to the atmosphere. Therefore, the main objective of this thesis was to obtain fundamental knowledge about mass transfer process of odorants from slurry surface boundary layers to the room air space, and about release of odorants from animal slurry by giving emphasis on the effects of air velocity, turbulence intensity, ventilation rate, and different geometrical sizes of the air space.

Both experimental and modelling approaches were used to generate knowledge on mass transfer process. The experiments were conducted in wind tunnels, scale models, a 2D model chamber, and a full scale pig house. Statistical modelling was used to relate different factors with emission and mass transfer processes. Computational fluid dynamics (CFD) modelling technique was used for simulation and for answering questions that were raised from the experimental results.

Air velocity and turbulence intensity both affect ammonia emission and mass transfer processes. Ammonia mass transfer coefficient (AMTC) increased with the increase of air velocity and turbulence intensity. Although it was technically difficult to measure ammonia concentrations in the boundary layer above the emission surface using existing techniques, the CFD simulation of five different sizes of wind tunnels showed that concentration boundary layer decreased with the increase in inlet velocity. Therefore, the AMTC was faster and ammonia emission increased in higher air velocity. The CFD simulation also revealed that the wind tunnel heights significantly affected the thickness of velocity and concentration boundary layer and therefore the ammonia emissions from the tunnels ($P < 0.001$). This factor needs to be considered for accurate emission estimation or modelling.

The scale model study showed that the airflow was not always parallel to the emission surface. In addition, the height and length of the scale models affected the airflow characteristics and ammonia emissions. The AMTC was correlated with jet momentum number, and from that to the inlet opening, inlet air velocity, length of the scale model (width of building in reality), and height of the room. Non-dimensional normalised emission rate and jet momentum ratio (R_m) were proposed for studies that compare scale models of different dimensions or compare scale models and full rooms.

Mass transfer of odorants in different ventilation rates using Proton Transfer Reaction Mass Spectrometry (PTR-MS) showed that volatile fatty acids (VFAs), phenols, ketones, and indoles were affected and could be controlled by ventilation rate or air phase boundary. Therefore, emissions of these gases and odorants can be potentially reduced and indoor air quality can be improved by controlling or guiding the airflow.

The results of this PhD study demonstrated some possible techniques to improve air quality, such as optimising ventilation control strategies, control of airflow by using a deflector on the side wall and curtain in the slurry pit, and adapting partial pit ventilation system. Some of these methods should be tested in pig houses and optimised for practical implementation.

Resume på dansk

Lugtstoffer fra svineproduktion har en negativ indvirkning på både menneskers og dyrs sundhed og på den omgivende atmosfære, både direkte og indirekte. For at kunne udvikle teknologier til reduktion af emissionen er det afgørende at få identificeret de forskellige faktorer, der påvirker frigivelsen af ammoniak (NH_3), svovlbrinte (H_2S) og flygtige organiske forbindelser (VOCs).

Luften er det vigtigste transportmiddel for disse gasser og flygtige organiske forbindelser fra stalde til atmosfæren. Derfor var denne afhandlings hovedformål at opnå en grundlæggende viden, dels om overførslen af lugtstoffer fra grænselaget ved gyllens overflade til staldluften, dels om sammenhængen mellem lufthastighed, turbulens, luftstrøm og luftrumets geometriske udformning.

Både eksperimenter og modellering blev anvendt for at skaffe viden om massetransportfænomenerne. Forsøgene blev udført i vindtunneler, på skalamodeller, i et 2D modelkammer og i en fuldskala svinestald. Statistisk modellering blev benyttet til at sammenholde forskellige faktorer med emission og luftbevægelse. Numerisk modellering ved hjælp af Computational Fluid Dynamics (CFD) blev brugt til simulering med henblik på at besvare spørgsmål, som de eksperimentelle studier rejste.

Såvel lufthastigheden som turbulensintensiteten påvirker massetransporten og dermed emissionen af gasser. Ammoniaks massetransportkoefficient (AMTC) blev forøget med stigende lufthastighed og turbulensintensitet. Selv om det var teknisk vanskeligt at måle ammoniakkoncentrationen i grænselaget over emissionsoverfladen, viste CFD simuleringer i de fem forskellige størrelser vindtunneler, at grænselagskoncentrationen af ammoniak faldt med stigende lufthastighed. Derfor forøgedes AMTC og ammoniakemissionen med stigende lufthastighed. CFD simuleringer viste også, at vindtunnellens højde påvirkede grænselaget for luft og ammoniakkoncentrationen væsentligt, og dermed havde indflydelse på emissionen af ammoniak fra tunnelerne ($P < 0,001$). Denne faktor skal tages i betragtning med henblik på nøjagtig estimering eller modellering af gasemissioner.

Skalamodelundersøgelsen viste, at luftstrømning ikke altid var parallel med emissionsoverfladen. Desuden påvirkede skalamodellernes højde og længde både luftstrømmens egenskaber og ammoniakemission. AMTC blev påvirket af luftstrålens moment, åbningen af luftindtaget hastigheden af luftindtaget, skalamodellens længde (dvs. bygningens bredde), og rummets højde, hvorved nogle skaleringsproblemer kan undgås. Non-dimensional normaliseret emission og jet momentum ratios (R_m) er foreslået benyttet til sammenligning af skalamodeller med forskellige dimensioner og ved sammenligning mellem skalamodeller og fuldskala.

Transport af lugtstoffer i luften i forskellige ventilationsmængde blev undersøgt ved hjælp af Proton Transfer Reaction massespektrometri (PTR-MS). Undersøgelserne viste, at emissionen af flygtige fedtsyrer (VFAs), phenoler, ketoner og indoler blev påvirket af ventilationsmængde, luftfase grænselaget. Derfor kan emissionen af disse gasser og lugtstoffer potentielt reduceres, og kvaliteten af staldluften kan forbedres gennem styring af luftstrømmen.

Resultaterne af studiet peger på mulige teknikker til at forbedre luftkvaliteten i stalde, såsom optimering af ventilationsstyringen, ændring af luftstrøm ved hjælp af deflektor på sidevæggen og gardin i gyllekummen, samt anvendelse af lokal ventilation af gyllekummen. Nogle af disse metoder bør testes og optimeres til praktisk brug i svinestalde.

Table of Contents

Preface.....	i
Acknowledgements.....	iii
Abstract.....	iv
Resume på dansk.....	v
Table of Contents.....	vi
Chapter 1. General introduction.....	1
1.1. Environmental impact of livestock production.....	2
1.2. Housing systems design and need of fundamental study to reduce environmental impact ..	3
1.3. Mass transfer processes of odorants from emission surface to free air stream	5
1.4. Technologies for emission measurement and for fundamental study and their challenges ..	9
1.5. Objectives.....	11
1.6. Outline of this thesis.....	11
References.....	13
Chapter 2. Airflow and concentration characterisation and ammonia mass transfer modelling in wind tunnel studies	17
<i>Abstract</i>	18
2.1. Introduction	19
2.2. Materials and Methods	22
2.2.1. Wind tunnel.....	22
2.2.2. Ammonia aqueous solution.....	23
2.2.3. Measurement.....	24
2.2.4. Statistical modelling and sensitivity analysis.....	26
2.2.5. Ammonia emission and AMTC model comparison	26
2.3. Results and discussion.....	27
2.3.1. Ammonia concentration profile	27
2.3.2. Wind velocity profile	29
2.3.3. Turbulence intensity profile	31
2.3.4. Effect of wind velocity and turbulence intensity on ammonia concentration and emission.....	32
2.3.5. Modelling of ammonia mass transfer coefficient	34

2.3.6.	Comparison of ammonia emissions in three wind tunnel studies.....	36
2.3.7.	Comparison of mass transfer coefficients in three wind tunnel studies.....	37
2.4.	Conclusions	37
	Acknowledgements.....	38
	References.....	38
	Chapter 3. Assessing effect of wind tunnel sizes on air velocity and concentration boundary layers and on ammonia emission estimation using computational fluid dynamics (CFD).....	43
3.1.	Introduction	46
3.2.	Theoretical background.....	47
3.2.1.	Mass transfer from an emitting surface.....	47
3.2.2.	Boundary layer theory.....	48
3.3.	Methods and materials.....	49
3.3.1.	CFD modelling.....	49
3.3.2.	Experiment for model validation	52
3.3.3.	Statistical modelling and sensitivity analysis.....	54
3.4.	Results and discussion.....	54
3.4.1.	Grid independency	54
3.4.2.	CFD model validation.....	55
3.4.3.	Effect of inlet velocity and wind tunnel sizes on velocity and concentration boundary layer thickness	56
3.4.4.	Effect of inlet velocity and wind tunnel sizes on ammonia emission.....	61
3.5.	Conclusions	63
	References.....	64
	Chapter 4. Ammonia emission process affected by ventilation airflow, pen partition and location of emission surface and ammonia mass transfer modelling in a model pig house	69
4.1.	Introduction	71
4.2.	Materials and methods.....	73
4.2.1.	Scale model.....	73
4.2.2.	Ammonia aqueous solution.....	74
4.2.3.	Experimental set-ups.....	74
4.2.4.	Measurement.....	75
4.2.5.	Estimation of ammonia emission and ammonia mass transfer coefficient.....	77
4.2.6.	Modelling and sensitivity analysis.....	78

4.2.7. Ammonia emission and ammonia mass transfer coefficient model Comparison.....	80
4.3. Results and discussion.....	80
4.3.1. Effect of ventilation control strategies on airflow patterns and airflow characteristics inside the scale model.....	81
4.3.2. Effect of ventilation control strategies on ammonia concentration and emissions.....	85
4.3.3. Effect of emission source locations and pen partition on ammonia emissions.....	86
4.3.4. Modelling of ammonia mass transfer coefficient	87
4.3.5. Comparison of different scale model studies.....	91
4.4. Conclusion.....	93
Acknowledgements.....	93
References.....	94
Chapter 5 . Similarity criteria for estimating gas emission from scale models	97
5.1. Introduction	99
5.2. Theory	100
5.3. Materials and Methods	102
5.3.1. Experimental facilities	102
5.3.2. Ammonia aqueous solution.....	103
5.3.3. Experimental design.....	104
5.3.4. Measurement.....	105
5.3.5. Estimation of ammonia emission rate and calculation of non-dimensional parameters	106
5.4. Results and discussion.....	106
5.4.1. Air flow pattern.....	106
5.4.2. Ammonia concentration.....	107
5.4.3. Ammonia emission rate	108
5.4.4. Comparison of similarity parameters Re and Rm	110
5.5. Conclusions	114
Acknowledgements.....	114
References.....	115
Chapter 6. Effect of airflow on odorants emissions in a model pig house- A laboratory study using proton-transfer-reaction mass spectrometry (PTR-MS)	117
<i>Abstract</i>	118
6.1. Introduction	119

6.2. Materials and Methods	121
6.2.1. Experimental room and model pig house	121
6.2.2. Pig slurry	122
6.2.3. Measurements and instruments.....	123
6.2.4. Concentration and emission flux calculations	125
6.3. Results and Discussion.....	127
6.3.1. Manure composition	127
6.3.2. Concentration and temporal variations	129
6.3.3. Effect of ventilation rate on VICs and VOCs emissions	133
6.4. Conclusion.....	136
Acknowledgements.....	137
References.....	137
Chapter 7. Effect of environmental deflector and curtain on air exchange rate in slurry pit in a scaled livestock building.....	143
<i>Abstract</i>	144
7.1. Introduction	145
7.2. Materials and methods.....	146
7.2.1. Experimental facility.....	146
7.2.2. Measurements	148
7.2.3. Statistical and estimation methods.....	150
7.3. Results and discussion.....	151
7.3.1. Effect of environmental deflector	152
7.3.2. Effect of slurry pit curtain.....	158
7.4. Conclusions	163
Acknowledgements.....	163
References.....	164
Chapter 8. Effects of a partial pit ventilation system on indoor air quality and ammonia emission from a fattening pig room	167
<i>Abstract</i>	168
8.1. Introduction	169
8.2. Material and methods	170
8.2.1. Experimental pig house.....	170
8.2.2. Ventilation systems.....	171

8.2.3.	Animals and feeding	172
8.2.4.	Measurements	172
8.2.5.	Observations	173
8.2.6.	Computation of ammonia emission rate and data analysis	174
8.3.	Results and discussion.....	174
8.3.1.	Ammonia concentration.....	176
8.3.2.	Ammonia emission	178
8.3.3.	Lying locations.....	180
8.4.	Conclusion.....	181
Acknowledgements.....		181
References.....		182
Chapter 9. General discussion and conclusions		185
9.1.	Effect of air velocity & turbulence intensity on boundary layer and ammonia emission from aqueous ammonia solution	186
9.2.	Effect of chamber or wind tunnel dimensions on airflow characteristics and mass transfer process.....	187
9.3.	Mass transport behaviour of different gases and odours.....	188
9.4.	Technologies for improving indoor air quality, and reducing odorants emissions.....	190
9.4.1.	Ventilation strategy	190
9.4.2.	Location of emission surface	191
9.4.3.	Deflector and curtain.....	191
9.4.4.	Partial pit ventilation.....	191
9.5.	Future perspectives.....	192
9.6.	General conclusions	193
References.....		194
Appendix - A. Pictorial views of different experimental set-ups		197

Chapter 1
General introduction

1.1. Environmental impact of livestock production

Intensive livestock production is a profitable sector, which contributes substantially to the economics of many European countries in terms of employment and export of products. But intensive livestock farming in general, and pig production in particular, is under more pressure and some structural changes in the pig production sector are expected in the coming years because of environmental problems. Pig production in Europe is concentrated in several regions characterized by large scale intensive farms. Main pig producing areas can be found in the north (Denmark, the Netherlands, Belgium, Brittany in France, Niedersachsen in Germany) and in south (Lombardy in Italy, Cataluña and Galicia in Spain) (EC, 2003). Denmark, with 5.5 Million inhabitants and a population density of almost 130.24 inhabitants per square km, houses 12.6 million pigs and is hence the fifth largest pig-producing country in the EU in terms of number of pigs – only exceeded by Germany, Spain, Poland, and France as per 2005 (DAC, 2007).

Intensive pig production is connected with a number of environmental effects, which include aerial emissions, e.g., odorants (ammonia, hydrogen sulphide, volatile organic compounds (VOCs)), non-CO₂ greenhouse gases (methane and nitrous oxide) and particulate matter, and discharge to soils and surface waters (e.g., nitrogen, phosphorous, and heavy metals). Odour is a complex mixture of various volatile compounds, which contribute to odour nuisance from pig production facilities (Schiffman et al., 2001). Odorous compounds are classified into four main groups: (1) ammonia and volatile amines, (2) sulphurous compounds, (3) volatile fatty acids, and (4) indolic and phenolic compound (Hobbs et al., 1997; Mackie et al., 1998). Among these odorants, Ammonia has negative effects on human and animal health, ecological damage, and malodorous emission (Bull and Sutton, 1998; Portejoie et al., 2002). Hydrogen sulphide is considered the most dangerous gas in animal buildings and manure storage, and has been responsible for animal as well as human deaths in animal facilities (Campagna et al., 2004; Oesterhelweg and Puschel, 2008). In atmospheric chemistry, VOCs also play central roles through their reactions with the hydroxyl radical (OH), by indirect production of ozone and organic aerosol following their photochemical oxidation (Andreae and Crutzen, 1997). Both ozone and organic aerosol have direct health effects for humans, as they are harmful to our respiratory system.

In recent years, odour emissions from animal housing and manure land application are being increasingly considered a nuisance in most European countries with intensive livestock production as the scale of livestock operation expands and an increasing number of rural residential developments are built in traditional farming areas (EC, 2003). Ammonia has been given most attention as the key air pollutant as it is emitted in the highest quantities. Particularly, around 50% of ammonia emissions from pig production stem from pig houses and slurry storage in the Netherlands, Denmark and France (van der Peet-Schwering et al., 1999). In the USA, 90% of the atmospheric NH₃ emission also comes from animal production and emissions from slurries and manures (Davison and Cape, 2003). Nearly all the information on the reduction of emissions from

animal housing reported on the reduction of ammonia emission. It is assumed that techniques to reduce ammonia emissions will reduce emissions of the other gaseous substances as well.

In Denmark, producers with livestock farms larger than 75 livestock unit (LU) (1 LU equals to 100 kg nitrogen in the manure prior to application) must obtain environmental authorisation if the farm wishes to extend and modify their production. The ammonia emission must be reduced by 25% in 2009 and onwards compared with a reference pig facility (partially slatted floor). In practice this corresponds to a reduction of approximately 40% if the farmer wishes to build a pig house with fully slatted floor (Anonymous, 2007). Producers with livestock farms larger than 15 LU must currently comply with the new rules on nuisance distance for odour when extending or modifying their production. The new rules stipulate that a livestock farm must not exceed the maximum odour emission corresponding to 5 OU_E/m^3 in urban areas, 7 OU_E/m^3 in total dwellings, and 15 OU_E/m^3 in individual dwellings in rural areas. This is a significant tightening compared with previous odour regulations (Anonymous, 2007). Though often, national legislation pushes farmers towards the application of certain techniques, the requirements of the large grocery retailers can also affect the choice and operation of production techniques. It should be borne in mind that techniques applied under the scope of "animal welfare" legislation are not always associated with the best environmental performance. One of the major challenges in the modernisation of pig production is the need to balance the reduction or elimination of the polluting effects on the environment with increasing animal welfare demands, while at the same time maintaining a profitable business (EC, 2003).

In order to reduce the environmental impacts of livestock production, the quantification of emission and behaviour of transportation of ammonia, hydrogen sulphide, and VOCs from pig production facilities are important not only for estimation of emission factors from a regulatory standpoint, but also for developing efficient emission abatement technologies and control strategies to reduce emission of gases and odours.

1.2. Housing systems design and need of fundamental study to reduce environmental impact

Housing systems design is one of the approaches in order to reduce emission of gaseous compounds from animal house to atmosphere (EC, 2003). The most commonly used housing type in large swine feeding operations is total confinement where pigs are raised in stalls or pens in environmentally controlled buildings (Arogo et al., 2003) (Fig. 1.1) . Housing has been developed to give shelter and provide comfortable and dry environment for animals, with the purpose of increasing production and to facilitate feeding. Feed and water are provided as inputs for animal growth. Air is supplied through ventilation system to provide optimum living conditions for pigs. A well-managed, functioning, efficient ventilation system effectively draws fresh air into a building and removes stale air containing a proportion of microbes, dust, harmful gases, odours, and water vapour. Inefficient ventilation is detrimental to pig and staff performance (particularly on hot days)

and costs more to run (Sommer et al., 2006). Energy is used for heating/cooling, lighting, and ventilation of room air. At the end of the production system, we get finishing pigs; manure for fertilization of agricultural land for crop production, which can be used again for animal feed.

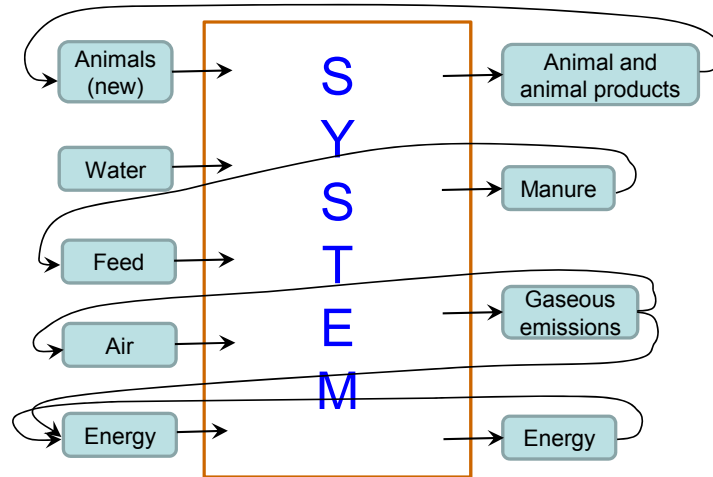


Fig. 1.1- Closed production cycles and systems

The design of a housing system, i.e., the combination of the floor-system, manure collection and the manure removal system, determines to a large extent the level of the emission of gaseous compounds. In close housing system based on slurry, the sources of odours are the soiled area of the solid floor, slats, side of the slurry store, and the surface of the slurry stored below the slatted floor (Fig. 1.2). Sommer et al. (2006) mentioned that the physics and chemistry of these sources of odours may differ; therefore, splitted the housing compartment into odour emission elements typical for each emitting surface. They also pointed out that by characterizing the important elements, these may then be combined as appropriate to calculate odours emissions from different housing types.

It is generally conceded that in buildings with partially slatted floors, the majority of the emission is derived from the slurry channels and floor emissions account between 11 and 40% of the emissions from the pens, the variation being related to variation in the animals soiling the solid floor and size of the slatted area (Aarnink et al., 1996; Hoeksma et al., 1992). The magnitude of soiled area is related to the animal behavior, which can be controlled partly through design of pens, position of feeders and drinkers and indoor climate.

The major transportation medium of gases from the above mentioned sources is ventilation air. To improve the air quality inside animal buildings and to reduce the impact of agricultural air pollution on atmospheric environment, knowledge about how volatiles are transferred from different sources to room air space and outdoor atmosphere is still needed. Knowledge is also needed about the effects of aerodynamic characteristics on the transfer of volatiles by different factors like air velocities and turbulence intensities, etc. Studies have shown that the airflow type

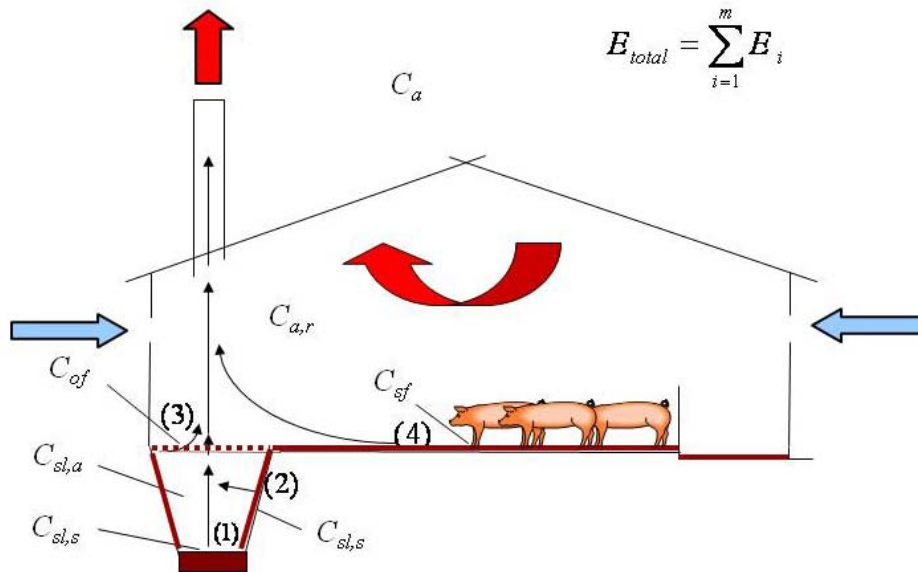


Fig. 1.2- Emission sources from a pig house. The emission of gases from the house is given by the sum of emission from each source in the animal house: (1) slurry surface, (2) soiled walls of slurry channel, (3) slats above the slurry channel or store, and (4) soiled floor (Adapted from Sommer et al., 2006). Where, C and E mean concentration and emission respectively. Subscripts a, r, of, sf, sl, and s mean air, room, slatted floor, soiled floor, slurry pit, and slurry respectively.

(laminar or turbulent) and the thickness of the air boundary layer are of major importance for the release and transport of volatiles from solid and liquid surfaces to air (Rong et al., 2009). The interaction between air movements in the room and in the slurry channel will affect the odorant concentration in the channel and in the room air. Better understanding of the exchange mechanisms between air and the slurry surface in the slurry channel and between air and soiled surfaces and animals in the room is needed.

1.3. Mass transfer processes of odorants from emission surface to free air stream

The processes of odorants release are essentially the transfer of gaseous odorants from manure surface to free air stream. Mass transfer due to convection involves transfer between a moving fluid and a surface or between two relative immiscible moving fluids (Incropera et al., 2007). Two theories are mostly used to describe the volatilization process: the two-film theory and the boundary layer theory (Ni, 1999). In two-film theory, the mass transfer between two films is controlled by the rates of diffusion through film of each side of interface (Fig. 1.3). The instantaneous gas release is the function of the concentration of gas in the air in immediate contact with gas concentration in liquid phase. The liquid phase concentration is a function of the chemical composition of the solution and transformations within the manure that either increase or decrease the concentration in the liquid. The rate of emission is further determined by the concentration gradient and resistance to

gas transport between the air in immediate contact with the emitting surface and the free atmosphere as controlled by atmospheric transport processes and barriers to the transport. The air above the surface can be envisaged as a laminar or turbulent-free layer close to the surface and, above this, a turbulent layer. Gas at the liquid-air interface is transported through a laminar or turbulent layer to the free atmosphere by turbulent diffusion and advection (Sommer et al., 2006).

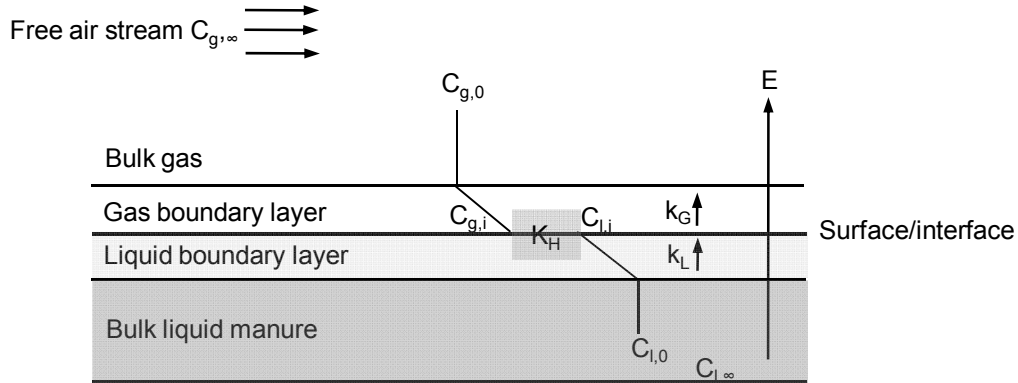


Fig. 1.3- Two-film theory and relationships between dimensionless Henry law constant, transfer coefficients, concentration and phases

The equilibrium of gas phase concentration with the liquid phase gas concentration is controlled by the Henry constant (K_H) (Roberts and Dandliker, 1983; Sommer et al., 2006). The dimensionless K_H describes the volatilisation. This equilibrium situation may be expressed as (Hudson and Ayoko, 2008a):

$$K_H = \frac{C_{g,i}}{C_{l,i}} \quad (1.1)$$

where K_H is the dimensionless Henry law coefficient; $C_{g,i}$ and $C_{l,i}$ represent the gas and liquid phase concentration (mass/volume), respectively. The liquid-film and gas-film transfer resistances of a solute are related to the respective mass transfer coefficients as follows:

$$E = k_G (C_{g,i} - C_{g,0}) = k_L (C_{l,0} - C_{l,i}) \quad (1.2)$$

where E is the volatilisation flux (mass/area-time); k_G is the gas-film transfer coefficient or velocity (length/time); k_L is the liquid-film transfer coefficient or velocity (length/time); $C_{g,i}$ and $C_{l,i}$ represent the gas and liquid phase concentration (mass/volume), respectively; $C_{g,0}$ and $C_{l,0}$ is the bulk air phase and bulk water phase concentration (mass/volume), respectively.

The concentrations $C_{g,i}$ and $C_{l,i}$ cannot be measured directly, therefore k_G and k_L cannot be determined individually either. The overall flux or transfer of chemical from one phase to the other and direction of transfer can therefore be described using dimensionless Henry constant (Eq. 1.1) as

$$E = K_G (K_H \times C_{l,0} - C_{g,0}) = K_L \left(C_{l,0} - \frac{C_{g,0}}{K_H} \right) \quad (1.3)$$

$$\frac{1}{K_G} = \frac{1}{k_G} + \frac{K_H}{k_L} \quad (1.4)$$

$$\frac{1}{K_L} = \frac{1}{k_L} + \frac{1}{K_H \times k_G} \quad (1.5)$$

where K_G is overall mass transfer coefficient in the gas film (length/time); K_L is the overall mass transfer coefficient in the liquid film (length/time).

Hudson and Ayoko (2008a) mentioned the ranges of values of K_H for which the mass transfer process is dominated by one of the two mass transfer coefficients k_G or k_L . Consideration of typical air and water exchange velocities and relative viscosities of air and water (Schwarzenbach et al., 2003) reveals that when values of K_H are significantly smaller than approximately 10^{-3} , air-phase control over mass transfer dominates, whereas when values of K_H are significantly larger than approximately 10^{-3} , water-phase control of over mass transfer dominates. Therefore, many odorous compounds are expected to be affected by ventilation air and airflow characteristics as it is for ammonia.

Ni (1999) reviewed ammonia emission models which used the two-film theory and found that the ammonia transfer in the gas phase was the major focus in these models. In most of the published models, it was assumed that, for highly soluble gases such as ammonia, the transfer through the gas film controls the interface transport system (Arogo et al., 1996; Zhang, 1992). In practice, $C_{g,i}$ was approximated by the gas phase concentration at the emission surface $C_{g,0}$. The thicknesses of the gas and liquid films were not defined. The ammonia flux was calculated based on the concentration difference between the gas phase concentration at the immediate emission surface and the gas concentration in the free air stream (Ni et al., 1999).

$$E = k_G (C_{g,0} - C_{g,\infty}) \quad (1.6)$$

where $C_{g,\infty}$ is the gas concentration in the free air stream (mass/volume). In Eq. (1.6), the application of the two-film theory in the models of odours release from manure is simplified. It actually does not include the mass transfer across the films.

On the other hand, in the boundary layer theory, when a free air stream flows over a surface and the gas phase concentration at the surface $C_{g,0}$ differs from that in the free air stream $C_{g,\infty}$, a concentration boundary will develop (Incropera et al., 2007; Ni, 1999) (Fig. 1.4).

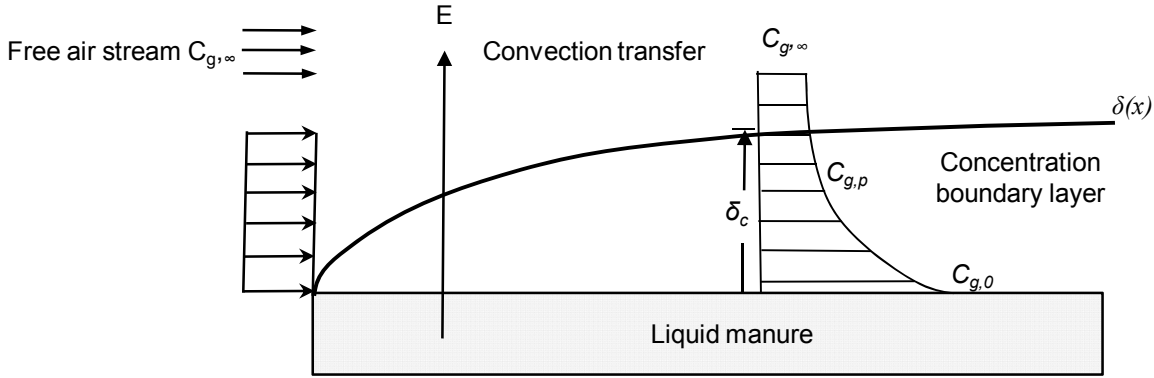


Fig. 1.4- concentration boundary layer theory

The concentration boundary layer (δ_c) is defined in this study as the region of the fluid in which concentration gradient exist, and its thickness, δ_c is typically defined as the value of vertical distance for which the fluid concentration equals 99% of that in the free air stream (Incropera et al., 2007) (Eq. (1.7)).

$$\frac{C_{g,0} - C_{g,p}}{C_{g,0} - C_{g,\infty}} = 0.99 \quad (1.7)$$

where, $C_{g,0}$ is surface concentration (mass/volume); $C_{g,p}$ is concentration at a specific point (mass/volume); $C_{g,\infty}$ is concentration at the free air stream (mass/volume).

Conditions within the concentration boundary layer determine the convective mass transfer. The boundary layer theory has a simpler structure than the two-film theory, and it has been used in the models of ammonia released from applied fertilizer (Vandermolen et al., 1990) and stored pig slurry (Olesen and Sommer, 1993). In those models, the gas phase ammonia concentration difference was taken between the slurry surface and a specified height above the surface, and the flux equation took a form similar to Eq. (1.6).

The gaseous phase boundary layer can be perceived as a resistance that limits the transfer of odorants from liquid manure or soil surface into the free air stream. Boundary layer theory has been used most extensively to estimate the gas phase mass transfer coefficient (k_c) in controlled laboratory environments. The boundary layer thickness is taken as being the thickness of the viscous boundary layer region. Because the main effect of viscosity is to slow the fluid flowing speed near a wall, the edge of the viscous region is at the point where the fluid velocity or concentration is essentially equal to that at the free stream (Fig. 1.4). With increasing distance from

the leading edge, the effects of gas molecules penetrate further into free the air stream and the concentration boundary layer grows (δ increase with x).

The primary factors affecting the resistance are ventilation rate, outlet area, airflow characteristics above the floors, air exchange rate in the slurry channel, and airflow characteristics in the slurry channel (Sommer et al., 2006). The transfer of gas from a slurry surface to the air stream above the slurry surface depends mainly on the dynamic structure of the airflow in the boundary layer (Bird et al., 2007) and the airflow pattern (Morsing et al., 2008).

The effects of air velocity and air temperature on ammonia emission in a scale model of a dairy cow house were found (Elzing and Monteny, 1997; Wang et al., 2006). Morsing *et al.* (2008) found that the ammonia emission was significantly affected by the different airflow patterns related to the floor type and the slurry channel layout. The influence of air velocity, turbulence and ventilation rate on ammonia emission rate was reported by Ye et al. (2008b). The effects of headspace heights on the slurry pit, the slatted floor opening, and the ventilation rate on ammonia emission and airflow characteristics using real slurry were studied (Ye et al., 2008a; Ye et al., 2009). The scale of a pig building of their study was 1:12.5. Topp et al. (2001) indicated that local airflow affected pollutant emission from the indoor building surface. Zhang et al. (2008) investigated the effects of three different ventilation control strategies on ammonia emission and estimated air exchanges between the manure pit headspace and the room space. The scale model that Zhang et al. (2008) and Ye et al. (2008b) used were 1:12.5 pig house models. In these works, the air velocity and the local airflow pattern above the emission surface were not reported. To make a step forward to apply the results in full scale, it is very important to assess the correlations of floor air velocities and AMTC from the emission source and how they are affected by room geometry (room height and room length), inlet height, and mean inlet air velocity. Additionally, none of the above mentioned studies investigated ventilation effects on other odorants except ammonia. But, the investigation of ventilation effects on other volatile inorganic and organic compounds' emission is necessary to find similarities or dissimilarities in behaviour with ammonia. This knowledge may help to decide which odorants can be reduced by applying similar techniques related to airflow guidance/ventilation strategies for reducing ammonia emission.

1.4. Technologies for emission measurement and for fundamental study and their challenges

There are different devices/methods used for estimation of emission of volatiles from area sources, generating fundamental knowledge of volatilisation process from slurry surface affected by different factors (e.g., velocity and temperature etc.), and also for model development purposes. These devices include dynamic flux chambers (DFC), which were also called hood or wind tunnel (Hudson and Ayoko, 2008b), and model house of animal building (Morsing et al., 2008). By working principle, a DFC is a typical wind tunnel with an open bottom covering the emission surface, and is flushed with incoming air at a known velocity or flow rate (Gao and Yates, 1998;

Peu et al., 1999; Reichman and Rolston, 2002). The inlet and outlet of a wind tunnel may vary depending on its specific configurations. Airflow created in the wind tunnel is mainly parallel to the emission surface. On the other hand, model house is a model that scales down from full scale animal building. Ventilation fan is used at the exhaust for supplying fresh air into the room from air inlet due to negative pressure, and removing polluted air from the room. Airflow above the floor or the emission surface may not be always parallel to the surface.

A variety of wind tunnels have been used to collect odour samples from area sources at intensive livestock farming operations and were tabulated in the recent review by Hudson and Ayoko (2008). The emission data obtained from the different wind tunnels are difficult to comprehend by the general community, thereby creating difficulties for various regulatory agencies and producers. There is no standard for the design of emission sampling wind tunnels. Variations in tunnel geometry are reflected in different length/width ratio, emission surface area, and height of the tunnel. The tunnel sizes were found to affect gas and odour emission rate (Frechen et al., 2004; Hudson et al., 2009; Smith and Watts, 1994). Smaller tunnel height could enhance emission rate due to the larger wind speed gradient at the release surface. Shah et al. (2006) concluded that wind tunnels may not be appropriate for determining ammonia fluxes; but they can be used to compare emissions and test models. Ye et al. (2008b) and Rong et al. (2009) used two different sizes of wind tunnels to study air velocity and turbulence intensity effects on ammonia mass transfer process, but obtained two different results. The results from Ye et al. (2008b) demonstrated irregular ammonia emission patterns related to wind velocity and relative turbulence intensity (RTI) and were substantially different from the study of Rong et al. (2009). However, a complex relationship existed between emission estimates derived from different devices (Hudson and Ayoko, 2009; Hudson et al., 2009), which need to be quantified.

Comparing with a wind tunnel, a scale model may generate airflow conditions that are more closely related to full-scale room in terms of airflow patterns (Ye et al., 2008b). The flow and thermal conditions in a small-scale test chamber cannot adequately represent the whole range of conditions in a real building, though the flow pattern may be similar in model with different scales, (Yang, 1999). An important characteristic of airflow in scale model is the turbulence scale. The size of main eddy in a model air space is related to the height of the model and that may affect the mass transfer process. Bjerg et al. (1999) found that the relation between room width and room height influenced the development of three-dimensional airflow. Topp et al. (1997) reported that using small-scale test chambers, a difference in scale may lead to different emission rates. But, Chen (2009) concluded in his recent review that small-scale experimental models are very effective and economical to study ventilation performance in buildings. However, in addition to scaling issues associated with thermo-fluid dimensionless parameters, it can be rather challenging to scale down complex flow geometry. The airflow pattern/magnitude of the floor air velocities and emission of

scale model should correspond to full scale situation. Better method for comparing scale model study with full scale is needed.

1.5. Objectives

As discussed above, the interaction between air movements in the room and in the slurry channel affects the odorant concentration in the channel and in the room air. Geometric sizes may also affect the emission process. Different gases and odours may behave differently. Better understanding of the exchange mechanisms between air and slurry surface in the slurry channel and between air and soiled surfaces and animals in the room is still needed. Therefore, the main objective of the PhD thesis was to obtain fundamental knowledge about mass transfer process of odorants from slurry surface boundary layers to the room air space and about release of odorants from animal slurry by giving emphasis on the effects of air velocity, turbulence intensity, and turbulence scale, ventilation rate, and different geometrical sizes of the air space. The ultimate goal of such studies is to provide fundamental information for designing a healthy indoor environment and reducing pollutant emissions. The specific objectives were to study the effects of:

- air velocities and turbulence intensities on ammonia release and transport mechanism in mechanically ventilated swine buildings;
- wind tunnels geometrical sizes on aerodynamic characteristics of aerial boundary layer and ammonia emissions from slurry surface;
- scale models geometrical sizes (1:12.5 and 1:6) on ammonia concentration and emission or transport phenomena from slurry surface to aerial boundary layer;
- ventilation rates on VICs (NH_3 and H_2S) and VOCs emission from pig slurry; and
- airflow guidance above the slurry surface (i.e., in slurry pit) and soiled surface on the reduction of odorants concentration in room air and emission from the emission surfaces.

1.6. Outline of this thesis

The starting point of the research theme was to generate fundamental knowledge of mass transfer processes of odorants from animal slurry, giving special emphasis on airflow characteristics, which can help to develop model and emission abatement technology to meet the requirement of the current strict environmental regulation on new animal production facilities. Initially, a major odour compound ammonia (NH_3) was selected to study the effect of airflow characteristics and geometric scales on mass transfer process using wind tunnels and scale models (Chapter 2, 3, 4, and 5). Ammonia was relatively easy to measure with available instrument and it was assumed that it had the same behaviour of other odorous compounds. Later investigation was carried to identify other odorous compounds from slurry and their similarities/dissimilarities in mass transfer process with NH_3 (Chapter 6). Finally, two cases are presented (2D chamber study and full scale experimental

facilities with pigs inside) to demonstrate how guidance of airflow using different techniques reduced emission and improved indoor air quality. A short summary of each chapter is given below:

Chapter 2 (“Airflow and concentration characterisation and ammonia mass transfer modelling in wind tunnel studies”) gives an overview of ammonia mass transfer process affected by airflow characteristics (i.e., air velocity and turbulent intensity) above the emission surface of air side boundary layer. The concentration boundary layer was measured, but the technical difficulty to experimentally determine ammonia concentration at the immediate liquid surface was demonstrated. An ammonia mass transfer model was developed and compared with the studies of similar methodologies. The possible effect of geometric sizes on ammonia emission measurement and mass transfer process are discussed.

Chapter 3 (“Assessing effect of wind tunnel sizes on air velocity boundary layers and on ammonia emission estimation using computational fluid dynamics (CFD)”) presents a computational fluid dynamics (CFD) study to investigate the effects of wind tunnel size and inlet air velocity on velocity and concentration boundary layers, and on ammonia mass transfer process, which were difficult to investigate thoroughly only by using physical experiments.

Chapter 4 (“Ammonia emission process affected by ventilation airflow, pen partition and location of emission surface and ammonia mass transfer modelling in a model pig house”) deals with airflow characteristics above the emission surface for different inlet velocities and inlet opening height and their effects on ammonia emission process in a model pig house (scale model). It was assumed that airflow pattern and characteristics may not be the same as wind tunnel, but close to full scale pig house. The effect of pen partition and location of emission surface were also investigated. Ammonia mass transfer modelling was performed taking into account the dimensions of the scale model and the inlet velocity. Chapter 5 (“Similarity criteria for estimating gas emission from scale models”) discusses techniques to compare scale model study with full scale situation or the studies with the models of different sizes.

Chapter 6 (“Effect of airflow on odorants emissions in a model pig house - A laboratory study using Proton-Transfer-Reaction Mass Spectrometry (PTR-MS)”) describes temporal variation and ventilation effects on odorants, which include volatile inorganic compounds (NH_3 and H_2S) and volatile organic compounds (e.g., Phenols, VFAs, Indoles, Ketones etc.).

Chapter 7 and 8 are case studies. Chapter 7 (“Effect of environmental deflector and curtain on air exchange rate in slurry pit in a scaled livestock building”) illustrates the effects of a deflector in the wall and curtain in the slurry pit on slurry pit air exchange rates, and possible improvement of indoor air quality using a 2D scaled livestock building. Chapter 8 (“Effects of a partial pit ventilation system on indoor air quality and ammonia emission from a fattening pig room”) describes and discusses the performance of a partial pit ventilation system on indoor air quality and ammonia emission without effecting pig behaviour. Furthermore, this study simulated possible emission reduction using air purification system.

Finally, Chapter 9 (“General discussion and conclusions”) summarizes and discusses the main findings of this thesis, and makes recommendation for future research.

References

- Aarnink, A. J. A., vandenBerg, A. J., Keen, A., Hoeksma, P., and Versteegen, M. W. A. (1996). Effect of slatted floor area on ammonia emission and on the excretory and lying behaviour of growing pigs. *Journal of Agricultural Engineering Research*, 64(4), 299-310.
- Andreae, M. O., and Crutzen, P. J. (1997). Atmospheric aerosols: Biogeochemical sources and role in atmospheric chemistry. *Science*, 276(5315), 1052-1058.
- Anonymous (2007). Annual report on Danish Pig production-Research and Development. Danish Pig Production. October 2007 (1st edn.). Tafdrup@co, Denmark.
- Arogo, J., Day, D. L., Christianson, L. L., Riskowski, G. L., and Zhang, R. (1996). Evaluation of mass transfer coefficient of ammonia from liquid swine manure . First International Conference on Air Pollution from Agricultural Operation. Kansas City, Missouri, USA, 111-118.
- Arogo, J., Westerman, P. W., and Heber, A. J. (2003). A review of ammonia emissions from confined swine feeding operations. *Transactions of the ASAE*, 46(3), 805-817.
- Bird, B. R., Stewart, W. E., and Ligtfoot, E. E. (2007). *Transport Phenomena* (revised second edition). NewYork, N. Y. :John Wiley and Sons.
- Bjerg, B., Morsing, S., Svidt, K., and Zhang, G. (1999). Three-dimensional airflow in a livestock test room with two-dimensional boundary conditions. *Journal of Agricultural Engineering Research*, 74(3), 267-274.
- Bull, K. R., and Sutton, M. A. (1998). Critical loads and the relevance of ammonia to an effects-based nitrogen Protocol. *Atmospheric Environment*, 32(3), 565-572.
- Campagna, D., Kathman, S. J., Pierson, R., Inserra, S. G., Phifer, B. L., Middleton, D. C., Zarus, G. M., and White, M. C. (2004). Ambient hydrogen sulfide, total reduced sulfur, and hospital visits for respiratory diseases in northeast Nebraska, 1998-2000. *Journal of Exposure Analysis and Environmental Epidemiology*, 14(2), 180-187.
- Chen, Q. Y. (2009). Ventilation performance prediction for buildings: A method overview and recent applications. *Building and Environment*, 44(4), 848-858.
- DAC (2007). Agriculture in Denmark. Facts and Figures 2007. *Danish Agricultural Council*, ISBN 87-90891-48-1.
- Davison, A. W., and Cape, J. N. (2003). Atmospheric nitrogen compounds - issues related to agricultural systems. *Environment International*, 29(2-3), 181-187.
- EC (2003). Integrated Pollution Prevention and Control (IPCC). Reference Document on Best Available Technique for Intensive Rearing of Poultry and Pigs. European Commission, http://ec.europa.eu/environment/ipcc/brefs/ilf_bref_0703.Pdf.

- Elzing, A., and Monteny, G. J. (1997). Ammonia emission in a scale model of a dairy-cow house. *Transactions of the ASAE*, 40(3), 713-720.
- Frechen, F. B., Frey, M., Wett, M., and Loser, C. (2004). Aerodynamic performance of a low-speed wind tunnel. *Water Science and Technology*, 50(4), 57-64.
- Gao, F., and Yates, S. R. (1998). Laboratory study of closed and dynamic flux chambers: Experimental results and implications for field application. *Journal of Geophysical Research-Atmospheres*, 103(D20), 26115-26125.
- Hobbs, P. J., Misselbrook, T. H., and Pain, B. F. (1997). Characterisation of odorous compounds and emissions from slurries produced from weaner pigs fed dry feed and liquid diets. *Journal of the Science of Food and Agriculture*, 73(4), 437-445.
- Hoeksma, P., Verdoes, N., Oosthoek, J., and Voermans, J. A. M. (1992). Reduction of Ammonia Volatilization from Pig Houses Using Aerated Slurry As Recirculation Liquid. *Livestock Production Science*, 31(1-2), 121-132.
- Hudson, N., and Ayoko, G. A. (2008a). Odour sampling 1: Physical chemistry considerations. *Bioresource Technology*, 99(10), 3982-3992.
- Hudson, N., and Ayoko, G. A. (2008b). Odour sampling. 2. Comparison of physical and aerodynamic characteristics of sampling devices: A review. *Bioresource Technology*, 99(10), 3993-4007.
- Hudson, N., and Ayoko, G. A. (2009). Comparison of emission rate values for odour and odorous chemicals derived from two sampling devices. *Atmospheric Environment*, 43(20), 3175-3181.
- Hudson, N., Ayoko, G. A., Dunlop, M., Duperouzel, D., Burrell, D., Bell, K., Gallagher, E., Nicholas, P., and Heinrich, N. (2009). Comparison of odour emission rates measured from various sources using two sampling devices. *Bioresource Technology*, 100(1), 118-124.
- Incropera, F. P., DeWitt, D. P., Bergman, T. L., and Lavine, A. S. (2007). *Fundamentals of Heat and Mass Transfer. Sixth Edition, John Wiley & Sons.*
- Mackie, R. I., Stroot, P. G., and Varel, V. H. (1998). Biochemical identification and biological origin of key odor components in livestock waste. *Journal of Animal Science*, 76(5), 1331-1342.
- Morsing, S., Strom, J. S., Zhang, G., and Kai, P. (2008). Scale model experiments to determine the effects of internal airflow and floor design on gaseous emissions from animal houses. *Biosystems Engineering*, 99(1), 99-104.
- Ni, J. Q. (1999). Mechanistic models of ammonia release from liquid manure: a review. *Journal of Agricultural Engineering Research*, 72(1), 1-17.
- Oesterhelweg, L., and Puschel, K. (2008). "Death may come on like a stroke of lightning ..." - Phenomenological and morphological aspects of fatalities caused by manure gas. *International Journal of Legal Medicine*, 122(2), 101-107.

- Olesen, J. E., and Sommer, S. G. (1993). Modeling Effects of Wind-Speed and Surface Cover on Ammonia Volatilization from Stored Pig Slurry. *Atmospheric Environment Part A-General Topics*, 27(16), 2567-2574.
- Peu, P., Beline, F., and Martinez, J. (1999). A floating chamber for estimating nitrous oxide emissions from farm scale treatment units for livestock wastes. *Journal of Agricultural Engineering Research*, 73(1), 101-104.
- Portejoie, S., Martinez, J., and Landmann, G. (2002). Ammonia of farm origin: impact on human and animal health and on the natural habitat. *Productions Animales*, 15(3), 151-160.
- Reichman, R., and Rolston, D. E. (2002). Design and performance of a dynamic gas flux chamber. *Journal of Environmental Quality*, 31(6), 1774-1781.
- Roberts, P. V., and Dandliker, P. G. (1983). Mass-Transfer of Volatile Organic Contaminants from Aqueous-Solution to the Atmosphere During Surface Aeration. *Environmental Science & Technology*, 17(8), 484-489.
- Rong, L., Nielsen, P. V., and Zhang, G. Q. (2009). Effects of airflow and liquid temperature on ammonia mass transfer above an emission surface: Experimental study on emission rate. *Bioresource Technology*, 100(20), 4654-4661.
- Schiffman, S. S., Bennett, J. L., and Raymer, J. H. (2001). Quantification of odors and odorants from swine operations in North Carolina. *Agricultural and Forest Meteorology*, 108(3), 213-240.
- Schwarzenbach, R., Gschwend, P., and Imboden, D. (2003). *Environmental Organic Chemistry*. 2nd Edition, John Wiley & Sons, New York.
- Shah, S. B., Westerman, P. W., and Arogo, J. (2006). Measuring ammonia concentrations and emissions from agricultural land and liquid surfaces: A review. *Journal of the Air & Waste Management Association*, 56(7), 945-960.
- Smith, R. J., and Watts, P. J. (1994). Determination of Odor Emission Rates from Cattle Feedlots .2. Evaluation of 2 Wind Tunnels of Different Size. *Journal of Agricultural Engineering Research*, 58(4), 231-240.
- Sommer, S. G., Zhang, G. Q., Bannink, A., Chadwick, D., Misselbrook, T., Harrison, R., Hutchings, N. J., Menzi, H., Monteny, G. J., Ni, J. Q., Oenema, O., and Webb, J. (2006). Algorithms determining ammonia emission from buildings housing cattle and pigs and from manure stores. *Advances in Agronomy*, 89, 261-335.
- Topp, C., Nielsen, P. V., and Heiselberg, P. (1997). Evaporation controlled emission in weighted rooms. *Proceedings of Healthy Building/IAQ' 97, Washington D C, USA*, 3, 557-562.
- Topp, C., Nielsen, P. V., and Heiselberg, P. (2001). Influence of local airflow on the pollutant emission from indoor building surfaces. *Indoor Air-International Journal of Indoor Air Quality and Climate*, 11(3), 162-170.

- van der Peet-Schwering, C., Aarnink, A. J. A., Rom, H. B., and Dourmad, J. Y. (1999). Ammonia emissions from pig houses in The Netherlands, Denmark and France. *Livestock Production Science*, 58(3), 265-269.
- Vandermolen, J., Beljaars, A. C. M., Chardon, W. J., Jury, W. A., and Vanfaassen, H. G. (1990). Ammonia Volatilization from Arable Land After Application of Cattle Slurry .2. Derivation of A Transfer Model. *Netherlands Journal of Agricultural Science*, 38(3), 239-254.
- Wang, C. Y., Li, B. M., Zhang, G. Q., Rom, H. B., and Strom, J. S. (2006). Model estimation and measurement of ammonia emission from naturally ventilated dairy cattle buildings with slatted floor designs. *Journal of the Air & Waste Management Association*, 56(9), 1252-1259.
- Yang, X. D. (1999). Study of Building Material Emissions and Indoor Air Quality. PhD Thesis, MIT, USA.
- Ye, Z., Zhang, G., Li, B., Strom, J. S., and Dahl, P. J. (2008a). Ammonia Emissions Affected by Airflow in A Model Pig House: Effects of Ventilation Rate, Floor Slat Opening, and Headspace Height in A Manure Storage Pit. *Transactions of the ASABE*, 51(6), 2113-2122.
- Ye, Z., Zhang, G., Li, B., Strom, J. S., Tong, G., and Dahl, P. J. (2008b). Influence of airflow and liquid properties on the mass transfer coefficient of ammonia in aqueous solutions. *Biosystems Engineering*, 100(3), 422-434.
- Ye, Z., Zhang, G., Seo, I. H., Kai, P., Saha, C. K., Wang, C., and Li, B. (2009). Airflow characteristics at the surface of manure in a storage pit affected by ventilation rate, floor slat opening, and headspace height. *Biosystems Engineering*, 104(1), 97-105.
- Zhang, G., Bjerg, B., Strom, J. S., Morsing, S., Kai, P., Tong, G., and Ravn, P. (2008). Emission effects of three different ventilation control strategies - A scale model study. *Biosystems Engineering*, 100(1), 96-104.
- Zhang, R. H. (1992). Degradation of swine manure and a computer model for predicting the desorption rate of ammonia from an under-floor pit . PhD dissertation. Library, University of Illinois, Urbana IL.

Chapter 2

Airflow and concentration characterisation and ammonia mass transfer modelling in wind tunnel studies

Paper I:

Saha, C. K., Zhang, G and Ni. J.-Q., 2010. Airflow and concentration characterisation and ammonia mass transfer modelling in wind tunnel studies. Biosystems Engineering, Vol 107 (4), P 328-340.

Abstract

The ammonia mass transfer process was modelled by investigating the airflow characteristics above ammonia release surfaces in a wind tunnel and evaluating the effect of wind tunnel dimensions on ammonia emission and the mass transfer process. A laboratory experiment was conducted using a $0.35 \times 0.35 \text{ m}^2$ cross section wind tunnel at 0.1 to 0.4 m s^{-1} mean wind velocities and 11% to 30% reference turbulence intensities. A 0.1-m thick ammonia concentration boundary layer and 0.03 to 0.1 m thick wind velocity boundary layers were observed at the tested velocities and turbulence intensities. Increases in wind velocity did not significantly affect ammonia concentration profiles, but reduced tunnel outlet ammonia concentrations and increased emissions. An inverse-relationship between turbulence intensities and wind velocity was also observed. The highest turbulence intensities were located close to the ammonia release surface where wind velocities were the lowest. An ammonia mass transfer coefficient model was developed as a function of wind velocity and turbulence intensity. Comparisons with two similar studies revealed that characteristics of wind velocity and ammonia emission were significantly affected by wind tunnel geometric dimensions.

Key words: Air velocity, ammonia release, boundary layer, gas emission, turbulence intensity

Nomenclature		u_A	average wind velocity at specific point, m s^{-1}
A	ammonia release surface area, m^2	u'	wind velocity fluctuation, m s^{-1}
a	model constant	VR	wind tunnel ventilation rate, $\text{m}^3 \text{ s}^{-1}$
b	model constant	Δk_G	change in AMTC, m s^{-1}
C	ammonia concentration, mg m^{-3}	ΔI	change in input parameter, m s^{-1} or %
c	model constant	ΔP	pressure difference, pa
E	emission rate, mg s^{-1}	Subscripts	
\bar{I}	average value of input parameter, m s^{-1} or %	a	bulk air
k_G	ammonia mass transfer coefficient, m s^{-1}	D	Dissociation
\bar{k}_G	average ammonia mass transfer coefficient, m s^{-1}	H	Henry
K	constant	in	wind tunnel inlet
Sr	relative sensitivity, %	out	wind tunnel outlet
T	temperature, K	p	point
Ti	turbulence intensity, %	s	ammonia release surface
u	average wind velocity in tunnel, m s^{-1}	∞	free stream outside the boundary layer

2.1. Introduction

Ammonia (NH₃) in and from animal houses at high concentrations and emission rates is one of the most important agricultural environmental problems related to human and animal health since it causes ecological damage, loss of nitrogen from manures as fertiliser, causes changes in biodiversity, and produces malodorous emissions (e.g., Aneja et al., 2008; Bull & Sutton, 1998; Portejoie et al., 2002; Webb et al., 2005). Approximately 50% of the NH₃ emissions in the Netherlands, Denmark, and France were estimated as coming from pig housing and slurry storage (van der Peet-Schwering et al., 1999).

Ammonia release from liquid slurry in animal buildings and open fields is a process of convective mass transfer that allows dissolved ammonia to be transferred from immediate liquid surface into free air stream. Ammonia emission is a process of ammonia emanating from an enclosure, to outside the enclosure or to atmosphere (Ni, 1999). Identification and quantification of different factors that are involved in these processes are important for modelling agricultural ammonia emissions and helping to develop emission abatement technologies.

Significant progress in studying ammonia transfer from liquid animal slurry has been made since the first research was conducted in the early 1970s (Hashimoto and Ludington, 1971). Transfer of gaseous ammonia from the immediate liquid manure surface into the free bulk air stream can usually be described by a core mechanistic model, in which both a physical understanding and a quantitative description of the ammonia release are given (Ni, 1999). Under steady state conditions, and without any sink in the enclosure, e.g., a biofilter to convert ammonia in animal building, ammonia emission equals ammonia release and the core model can be expressed as:

$$E = k_G \cdot A(C_s - C_a) \quad (2.1)$$

where E is emission rate, mg s⁻¹; k_G is ammonia mass transfer coefficient (AMTC), m s⁻¹; A is ammonia release surface area, m²; C_s is gaseous ammonia concentration at the immediate liquid surface, mg m⁻³; C_a is the ammonia concentration in the bulk air, mg m⁻³.

However, limited by the technology required to acquire an in-depth knowledge related to this process, the AMTC has always been determined empirically. Experiments using wind tunnels (e.g., Loubet et al., 1999a; Loubet et al., 1999b; Rong et al., 2009; Ye et al., 2008a) or similar devices, e.g., flow-through emission chamber (Liu et al., 2007), have been conducted by different researchers to study the mass transfer of ammonia from soil surface or from aqueous solutions. Ammonia emission from a wind tunnel can be expressed as:

$$E = VR(C_{out} - C_{in}) \quad (2.2)$$

where E is emission rate, mg s^{-1} ; VR is wind tunnel ventilation rate, $\text{m}^3 \text{s}^{-1}$; C_{out} is ammonia concentration at the wind tunnel outlet, mg m^{-3} ; C_{in} is ammonia concentration at the wind tunnel inlet, mg m^{-3} .

Rearranging Eqs. (2.1) and (2.2), Eq. (2.3) below is obtained (Ye et al., 2008a).

$$k_G = \frac{VR(C_{out} - C_{in})}{A(C_s - C_a)} \quad (2.3)$$

Because C_a is the concentration of bulk air outside the concentration boundary layer, it can be approximately assumed as C_{in} . C_{out} and VR can be experimentally determined, and A is a constant. Therefore, the AMTC k_G in a wind tunnel can be calculated using Eq. (2.3) if C_s is known. However, although the gaseous ammonia concentration in the bulk air stream can be easily measured, it is still difficult to measure it at the immediate liquid surface. Therefore, the C_s is almost always theoretically calculated by using Henry's constant, dissociation constant, association constant, total ammoniac nitrogen (TAN) concentration, and pH value (e.g., Arogo et al., 1999; Bliss et al., 1995; Ni, 1999).

Nevertheless, ammonia concentration in the liquid slurry surface is under dynamic equilibrium and decreases during the process of ammonia release to the free air stream. The loss of ammonia from the liquid slurry surface is compensated by an upward diffusion of ammonia mass inside the slurry. The diffusion is controlled by temperature and concentration gradient in the liquid. Mass transfer in liquid phase is much slower than in gaseous phase. These characteristics make it even more difficult to study the gaseous ammonia at the liquid manure surface in order to verify the theory and improve the knowledge of ammonia release. Ignoring the dynamic nature of the gaseous ammonia concentration at the liquid manure surface risks misinterpretation of the ammonia release mechanism described in Eq. (2.1). To avoid this potential problem, a new methodology has been used by employing aqueous ammonia circulation to provide a stable liquid surface ammonia concentration while investigating the mass transfer coefficients in wind tunnels (Rong et al., 2009; Ye et al., 2008a).

Boundary layer theory is used most extensively to estimate the k_G in controlled laboratory environments. The boundary layer thickness is taken as being the thickness of the viscous boundary layer region. Because the main effect of viscosity is to slow fluid near a wall, the edge of the viscous region is at the point where the fluid velocity or concentration is essentially equal to that at the free stream. The edge of a velocity boundary layer is usually defined as the point at which the air velocity equals 99% of that in the free air stream (Incropera et al., 2007) (Eq. (2.4)).

$$u_p = 0.99u_\infty \quad (2.4)$$

where, u_p is air velocity at a specific point, m s^{-1} ; u_∞ is air velocity in free air stream, m s^{-1} .

Similarly, the edge of a concentration boundary layer is the point at which the fluid concentration equals 99% of that in the free air stream (Incropera et al., 2007) (Eq. (2.5)).

$$\frac{C_s - C_p}{C_s - C_\infty} = 0.99 \quad (2.5)$$

where, C_s is surface concentration, mg m^{-3} ; C_p is concentration at a specific point, mg m^{-3} ; C_∞ is concentration at the free air stream, mg m^{-3} .

Characteristics of wind in tunnels, including wind velocity, turbulence intensity, and air temperature, have been found to greatly affect ammonia concentration and emission rates (Loubet et al., 1999a; Loubet et al., 1999b; Sohn et al., 2005; Rong et al., 2009). In a recent review of mass transfer processes in the context of odour sampling, Hudson and Ayoko (2008) noticed that air turbulence was significant to air-liquid transfer velocities for all solutes. Turbulence levels can be described in terms of turbulence intensity, which is the ratio of the root mean square (RMS) of velocity fluctuations to the mean velocity (Eq. (2.6)).

$$Ti = \frac{\sqrt{u'^2}}{u_A} \times 100 \quad (2.6)$$

Where, Ti is turbulence intensity, %; u_A is average wind velocity at specific point, m s^{-1} ; u' is wind velocity fluctuation at the measuring point. The velocity fluctuation can be determined from the difference between the instantaneous velocity and the average velocity over the integration time. Rong et al. (2009) also found that the boundary layer thickness of air velocity increased sharply when the velocity was reduced from 0.2 to 0.1 m s^{-1} .

In addition to the wind characteristics, the tunnel sizes were also found to affect gas and odour emission rate (Hudson et al., 2009; Smith and Watts, 1994). Smaller tunnel heights can enhance emission rates by increasing the wind speed gradient at the release surface and larger aerodynamic roughness led to a larger air exchange rate. A nonlinear relationship of mass transfer process with air velocity and air turbulence intensity was found in a scale model and a wind tunnel by Ye et al. (2008a). Moreover, a complex relationship exists between emission estimates derived from different devices (Hudson et al., 2009).

There is still limited knowledge available on mass transfer process affected by the characteristics of wind and some contradictory results have been reported. Therefore, more laboratory experimental investigations using improved and comparable methodologies are required. The objective of this work was to contribute to the fundamental knowledge of ammonia mass transfer process in wind tunnel studies. The specific objectives were to: 1. characterise aerial and airflow boundary layers above an ammonia release surface; 2. model ammonia mass transfer as affected by the airflow characteristics; and 3. compare and interpret the results in this study with results in the literature on ammonia mass transfer.

2.2. Materials and Methods

2.2.1. Wind tunnel

The experiment was carried out at the Air Physics Lab, Research Centre Bygholm, Faculty of Agricultural Sciences, Aarhus University, Denmark, using a 3.67-m long wind tunnel (Fig. 2.1). The wind tunnel was constructed of polystyrene sheets and contained a 0.60-m long section for profile measurement. One side of the tunnel wall that covered this section was made of a 0.8-m long transparent glass to enable velocity and turbulence intensity measurement using a Laser Doppler anemometer and for visual inspection when measuring velocity, turbulence intensity, and ammonia concentration above the liquid surface.

Airflow into the tunnel was via a 0.17-m thick smooth-surface contraction section fitted around the edges of the 0.35 (H) × 0.35 (W) m² wind tunnel inlet opening. Three different levels of wind reference turbulence intensities (RTI) were generated to provide relatively constant airflow conditions above the liquid surface in the profile measurement section. The lowest turbulence intensity level was obtained when using a blank screen S-0 (i.e., no perforated screen plate) between the contraction section and the wind tunnel inlet. Screens S-a and S-b that had 24 and 16 equally spaced 0.03-m diameter holes were used to create medium and high level RTIs, respectively. Four mean wind velocities of 0.1, 0.2, 0.3, and 0.4 m s⁻¹ in the tunnel were also created for the study by controlling the speed of the fan that was installed at the tunnel exhaust. The room air temperature and relative humidity were kept at 22.0 ± 0.5°C (mean ± standard deviation) and 29 ± 3 %, respectively. The exhaust air temperature and relative humidity were kept at 20.0 ± 0.4°C and 31 ± 3 %, respectively, depending on the tunnel airflow rates.

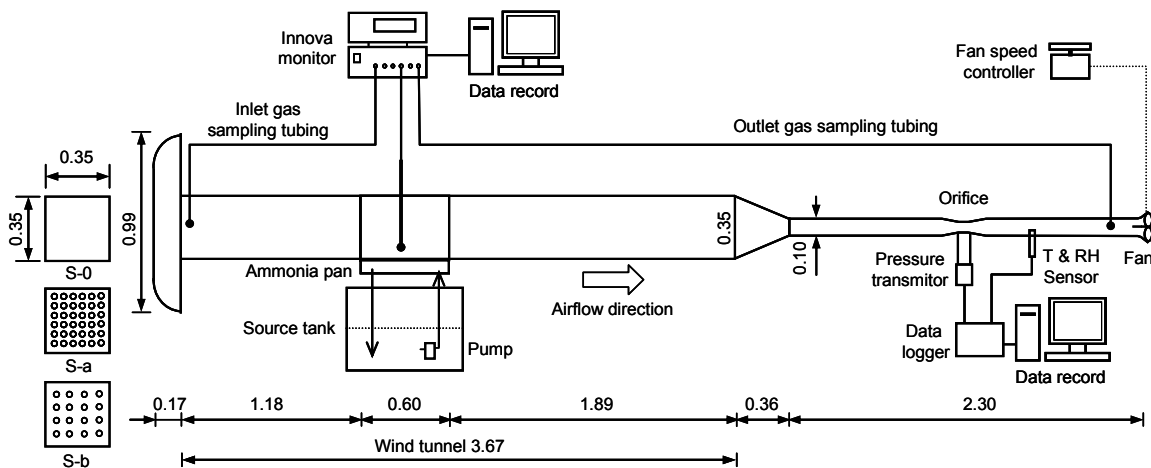


Fig. 2.1 - Schematic of the wind tunnel and the laboratory experiment set-up (all dimensions are in m). The screens “S-0” (blank screen without a perforated screen plate), “S-a”, and “S-b” were used in the inlet for generating different turbulences above the ammonia pan.

The profile measurement section was 1.18 m downwind from the wind tunnel inlet and designed to characterise wind and ammonia inside the tunnel. It measured 0.60 (L) × 0.35 (W) × 0.35 (H) m³ and had a 0.09-m deep ammonia aqueous solution pan below the bottom of the tunnel main body (Fig. 2.2). An ammonia source tank of 0.77 (L) × 0.56 (W) × 0.45 (H) m³ and was installed underneath the ammonia solution pan. A 0.36-m long reducer and a 2.30-m long and 0.10-m diameter round duct were connected to the outlet of the wind tunnel. An orifice and a 200-mm diameter variable-speed axial-flow ventilation fan (Type CK 200 B CBU, Lindab A/S, Denmark) were installed in the round duct. The wind tunnel air flow was driven by the fan and controlled via a Danfoss VLT[®] variable-speed drive (Type 3508, Nordborg, Denmark).

2.2.2. Ammonia aqueous solution

Two aqueous solutions were prepared for the experiment. An ammonium chloride (NH₄Cl) solution was made as an ammonia source. A buffer solution of sodium carbonate (Na₂CO₃) and sodium hydrogen carbonate (NaHCO₃) was used to keep the constant pH of the aqueous solution. The ammonia solution had a 16,500 mg l⁻¹ TAN concentration and a target pH value of 8.8, which were higher than pig manure, to facilitate the study and maintain a robust balance between ammonium and ammonia during the experiment. The solution was kept circulating with a 6-mm diameter hose and a pump (Type PA1000, Heissner, Germany) during the measurements between the solution pan and the underneath ammonia source tank, in which a 0.25-m deep ammonia solution was kept. The stability of the ammonia aqueous solution was tested prior to the experiment to ensure that the ammonia emission rate under specific conditions could allow the experiment to be performed under steady state. The continuous circulation maintained a 0.09-m deep reservoir of ammonia solution in the pan and provided a constant free ammonia concentration at the immediate liquid surface (C_s in Eq. (2.3)) during the ammonia release process.

Liquid samples taken from the return flow were checked for TAN concentration and pH value before and after each experimental trial. The TAN measurement was made according to ISO 7150/1. The pH was measured with a pH detector (Type Sension 1, HACH-LANGE, Bronshoj, Denmark). The TAN and pH of ammonia solution, Eq. (2.7) from Jayweera and Mikkelsen (1990), and Eq. (2.8) from van der Molen et al. (1990) were used to calculate the C_s in Eq. (2.3).

$$K_D = 10^{-\left(0.0897 + \frac{2729}{T}\right)} \quad (2.7)$$

where K_D is dissociation constant, dimensionless; T is temperature, K.

$$K_H = 10^{-\left(1.69 + \frac{1477.7}{T}\right)} \quad (2.8)$$

where K_H is Henry's constant, dimensionless; T is temperature, K.

2.2.3. Measurement

2.2.3.1. Ammonia concentration

Ammonia concentration was measured at eight different heights (0.005, 0.01, 0.015, 0.03, 0.06, 0.1, 0.16, and 0.34 m) and three locations in the X-Y plane (C to E in Fig. 2.2).

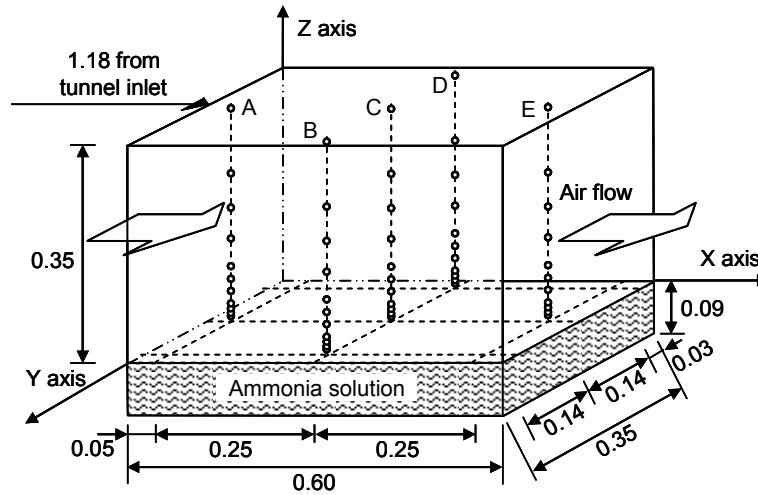


Fig. 2.2 - The profile measurement section in the wind tunnel (all dimensions are in m). Measurement points (indicated by circles) were above the ammonia solution along the Z axis and at five different locations in the X-Y plane, in which “A” to “E” were for wind measurement and “C” to “E” were for ammonia measurement.

The measurements were performed simultaneously with the measurements of wind velocity at locations C, D, and E and sequentially at the inlet and outlet of the tunnel using a Brüel & Kjær Photoacoustic multi-gas monitor (Type 1312, Innova AirTech Instruments, Ballerup, Denmark) and a multiplexer (Type 1309, Innova AirTech Instruments, Ballerup, Denmark). The accuracy of the monitor for ammonia measurement was ± 0.1 ppm depending on the filter setting. The sample integration time configured in the monitor for the experiment was 20 s. The tunnel inlet and outlet measurement provided ammonia concentrations in the incoming and outgoing air. The measurement time at each of the 26 points was 40 min before switching to another point. It was found that at least 10-15 min were required for the ammonia concentration reading to stabilize following measurement of higher ammonia concentration samples. Therefore, the ‘old’ air in the instruments was flushed out to ensure that it was completely replaced by the ‘new’ air; this was especially important when the ammonia concentration of ‘old’ air was very high. The wind tunnel was operated for at least 30 min to let the airflow conditions to stabilize for each experimental trial before measuring the ammonia concentrations.

2.2.3.2. Ventilation rate

A FMU/FMDRU 100-80 flow meter (Lindab A/S, Denmark), which was based on an orifice tapping principle, was used to measure the ventilation airflow rates in the tunnel at 1 m from the wind tunnel exhaust (Fig. 2.1). The error of the flow measuring method was 5-10% depending on the distance to the flow disturbance. The flow meter consisted of two reducers joined together with measurement nozzles. By measuring the pressure difference between the measurement nozzles, the ventilation rate in the duct was calculated using Eq. (2.9), which was provided by the manufacturer of the flow meter based on factory calibrations (Lindab A/S, Denmark).

$$VR = 0.00732\sqrt{\Delta P} \quad (2.9)$$

where VR is ventilation rate, $\text{m}^3 \text{s}^{-1}$; ΔP is pressure difference, Pa .

The pressure differences were measured using a differential pressure sensor (Model 694, Huba Control, Würenlos, Switzerland) with a measurement range of 10-300 Pa, an accuracy of $\pm 0.7\%$, and a resolution of 0.1% of full scale. The pressure sampling period was every 10 s and the averaged data were saved every min in a data logger (Model CR215, Campbell Scientific, Logan, UT, USA).

2.2.3.3. Wind velocity and turbulence intensity

Wind velocity and turbulent intensity profile measurements were taken at 11 different vertical heights (0.003, 0.005, 0.010, 0.015, 0.03, 0.045, 0.06, 0.1, 0.16, 0.23, and 0.34 m) and at five locations in the X-Y plane (A to E in Fig. 2.2). Measurements were not taken at vertical height of 0.23 m for locations B and D due to a sampling error.

A Laser Doppler Anemometer (Type 58N40-FVA enhanced, DANTEC Dynamics, Skovlunde, Denmark) was used to measure the wind velocities and turbulence intensities. It measured the velocity using light beams at a point in a flow seeded by small particles which could follow the turbulent motion of the flow. It sensed true velocity component, and measured that component in a sequence of near instantaneous samples. The signal was time series and this allowed common statistical data analysis of the velocity information. The integration time for velocity measurement for each point was 8 min. The mean wind velocities in the tunnel measured with the anemometer were compared with the tunnel ventilation rates measured with the flow meter for consistencies. Three RTI, 11%, 20% and 30%, corresponding to wind tunnel inlet screens S-0, S-a, and S-b, respectively, were determined. The RTIs were the mean turbulence intensities at the centre of the profile measurement section in the wind tunnel (location: $X=0.3 \text{ m}$, $Y=0.17 \text{ m}$, and $Z=0.16 \text{ m}$, Fig. 2.2) under four different wind velocities (0.1, 0.2, 0.3 and 0.4 m s^{-1}).

2.2.3.4. Temperature and relative humidity

The experimental room air temperature and relative humidity were measured with a temperature/humidity probe (Model Testo 400, Gmbh & Co, Lenzkirch, Germany) that had accuracies of $\pm 0.1^\circ\text{C}$ and $\pm 1\%$, respectively. The wind tunnel exhaust air temperature and relative humidity was measured with a Vaisala Intercap Humidity and Temperature Probe (Model HMP50, Vaisala, Woburn, MA, USA) with accuracies of $\pm 0.1^\circ\text{C}$ and $\pm 3\%$ at 20°C , respectively.

2.2.4. *Statistical modelling and sensitivity analysis*

The wind tunnel experimental data were used to develop a statistical model and were analysed to obtain the AMTC with nonlinear regression using DataFit Program (Version 8.2.79, Oakdale Engineering, Oakdale, PA, USA). The AMTC was modelled as a function of wind velocity and turbulence intensity as expressed in Eq. (2.10).

$$k_G = a \cdot u^b T_i^c \quad (2.10)$$

where k_G is AMTC, m s^{-1} ; a , b , and c are model constants; u is wind velocity, m s^{-1} ; T_i is wind turbulence intensity, %.

A sensitivity analysis was performed to determine the relative change rates in ammonia mass transfer coefficient with changes in the model parameters (wind velocity and turbulence intensity). Relative sensitivity values were calculated for the different input parameter ranges using the method outlined by Zerihun et al. (1996). The relative sensitivity for each input factor was calculated using Eq. (2.11) for specified ranges within the factor while keeping the other factors that were not being tested constant at their mean values (Liang et al., 2002; Ye et al., 2008b).

$$Sr = \frac{\Delta k_G \cdot \bar{I}}{\Delta I \cdot k_G} \quad (2.11)$$

where Sr is relative sensitivity, %; Δk_G is change in mass transfer coefficient, m s^{-1} ; \bar{k}_G is average ammonia mass transfer coefficient, m s^{-1} ; ΔI is change in input parameter over the range being considered, m s^{-1} or %; \bar{I} is average value of the input parameter, m s^{-1} or %.

2.2.5. *Ammonia emission and AMTC model comparison*

Results from this study and those from Ye et al. (2008a) and Rong et al. (2009) were used for comparing ammonia emissions and AMTC models. The three studies employed similar methodologies and experimental conditions, including isothermal condition and constant liquid surface ammonia concentration with ammonia solution circulation, but used three wind tunnels of different sizes (Table 2.1). The cross sections of the wind tunnels were

Table 2.1 - Experimental conditions with three wind tunnels (WT) for ammonia mass transfer studies.

Parameter	This study	Rong et al. (2009)	Ye et al. (2008a)
WT dimension (W×H×L), m ³	0.35×0.35×3.67	0.5×0.5×4.99	0.15×0.15×2.00
WT cross-section (H×L), m ²	0.123	0.250	0.0135 ^a
Ammonia surface (W×L), m ²	0.35×0.6	0.43×0.62	0.15×0.3
Air temperature, °C	22.0 ± 0.5	22.3	22.0
Liquid temperature, °C	20.0 ± 0.4	22.3 ^b	22.0
Ammonia solution pH	8.8	8.98	9.0 ^c
TAN, mg l ⁻¹	16,500	6800	8200
C _s , mg m ⁻³ ^d	1758	984	1226
Ventilation rates, m ³ s ⁻¹	0.014 to 0.048	0.025 to 0.10	0.005 to 0.020
Inlet air velocities, m s ⁻¹	0.1 to 0.4	0.1 to 0.4	0.1 to 0.6 ^d
RTI, %	11 to 30	10 to 35	5 to 21

^aOnly the top part of 0.09 m height was used for airflow. The bottom part of 0.06 m height was used to store ammonia solution. ^bOnly the test at 22.3 °C liquid temperature and 0.1 to 0.4 m s⁻¹ air velocities were compared in this study. ^cThis pH was one of the three pH values tested by Ye et al. (2008a). ^dCalculated with actual pH, TAN, and Eqs. (2.7) and (2.8).

0.15×0.15 m² used by Ye et al. (2008a) and 0.5×0.5 m² by Rong et al. (2009). In the study of Ye et al. (2008a), only the top 0.09 m tunnel height was used for airflow. The bottom 0.06 m height was used to store ammonia solution. Two AMTC models were developed using the published data by Ye et al. (2008a) and Rong et al. (2009) with the same procedure as in this study, including the dissociation constant and Henry's constant as described in Eqs. (2.7) and (2.8), respectively, for calculating the C_s.

2.3. Results and discussion

2.3.1. Ammonia concentration profile

The profiles of net ammonia concentrations in this study (Fig. 2.3), which were the concentrations at the profile measurement section minus tunnel inlet concentrations, were similar to the results reported by other researchers using wind tunnels (Loubet et al., 1999b; Sohn et al., 2005). The concentrations were at the maximum close to the release surface, tapering rapidly with height above the surface (Sohn et al., 2005). Considerable ammonia concentration gradients were observed at the bottom of the tunnel. The maximum ammonia concentration was 563 ppm measured at 0.005 m above the release surface while the calculated C_s at the immediate ammonia solution surface was 2483 ppm (or 1758 mg m⁻³ at 101 kPa, Table 2.1). At the height above 0.1 m, the net concentrations decreased to only about 1 ppm and became almost constant for most of the profile curves shown in Fig. 2.3, indicating a concentration boundary layer thickness of approximately 0.1 m.

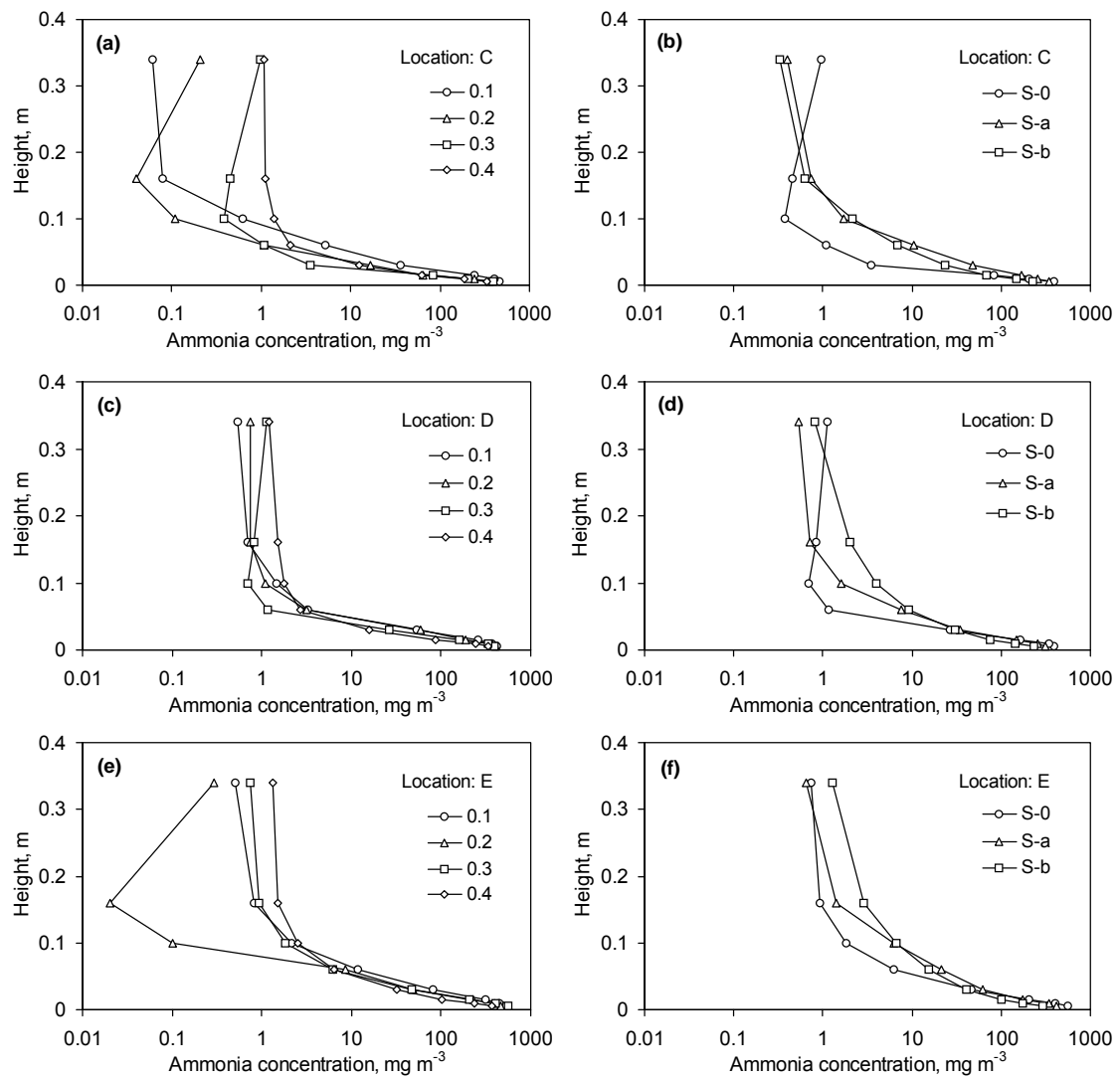


Fig. 2.3 - Ammonia concentration profiles with four mean wind velocities: (a) at C, (c) at D, and (e) at E sampling locations, and with three tunnel inlet screens: (b) at C, (d) at D, and (f) at E sampling locations. The tunnel inlet ammonia concentrations were subtracted.

The large ammonia concentration gradients within the 0.1 m thick boundary layer illustrated the technical difficulty to experimentally determine the C_s , because a small variation in height gave a significant difference in ammonia concentrations. Therefore it is necessary to estimate the C_s by using the Henry constant, the dissociation constant, and the known TAN and pH values. The circulating ammonia aqueous solution during the experiments provided a continuously renewed ammonia emission source in the wind tunnel to ensure a constant C_s .

2.3.2. Wind velocity profile

Horizontal wind velocities at different heights increased with the increase in the mean velocities at all sampling locations along the length (Fig. 2.4a, c, and e) and the width (Fig. 2.4b, d, and f) of the wind tunnel above the profile measurement section (Fig. 2.2). At the lowest mean velocity of 0.1 m s^{-1} using the blank tunnel inlet screen (S-0), the velocity differences among the five sampling locations were not significant (Fig. 2.4a and b). More variations in wind velocities along the tunnel length were demonstrated with the increase in mean wind velocities and in wind turbulence levels using S-a and S-b as shown in Fig. 2.4a, c, and e. The vertical wind velocity profiles were less uniform at different sampling locations when using inlet screens S-a (Fig. 2.4c and d) and S-b (Fig. 2.4e and f) compared with S-0 (Fig. 2.4a and b).

The profiles along the tunnel length (Fig. 2.4a, c, and e) at all four mean velocities showed that the wind velocities close to the tunnel mid-height at 0.16 m were generally the highest at location A, closest to the tunnel inlet, and decreased at locations C and E. The lowest wind velocities were recorded at the bottom of the profiles, which were logarithmic in profile. Although not all the wind velocity profiles in Fig. 2.4 show regular and clear trends, they show a general pattern related to velocity boundary layer. Wind velocities at different measurement points increased rapidly from heights at 0.003 m - 0.005 m and continued to increase, but slower, until at 0.03 m at low mean wind velocity of 0.1 m s^{-1} . At the highest mean velocity of 0.4 m s^{-1} , this rapid velocity increase did not change until at height of approximately 0.06 m. However, more velocity variations were seen above the height of 0.03 m when screens S-a and S-b were used and along the width of the tunnel.

The rapid increase in wind velocities from the ammonia release surface to 0.03 or 0.06 m heights indicated the development of the wind velocity boundary layers. In some profiles curves, this velocity increasing trend extended to 0.1 m height, e.g., at mean velocity of 0.1 m s^{-1} and location B shown in Fig. 2.4b. The relatively stable wind velocities with small variations at different heights from 0.03 or 0.06 to 0.23 m (Fig. 2.4a, c, and e) and from 0.03 or 0.06 to 0.16 m (Fig. 2.4b, d, and f) at all sampling locations indicated a zone of free-stream velocities. The similar wind velocity variations at heights of 0.01 m and 0.34 m, which was 0.01 m from the tunnel ceiling, demonstrated the symmetric nature of the boundary layer.

Although a slight increase in boundary layer thickness with the decrease in mean wind velocities were seen, the wind velocity boundary thickness did not exhibit a clear correlation with the mean wind velocities. This disagreed with the results obtained by Rong et al. (2009), who reported that the boundary layer thickness sharply increased when the wind velocity was reduced from 0.2 to 0.1 m s^{-1} .

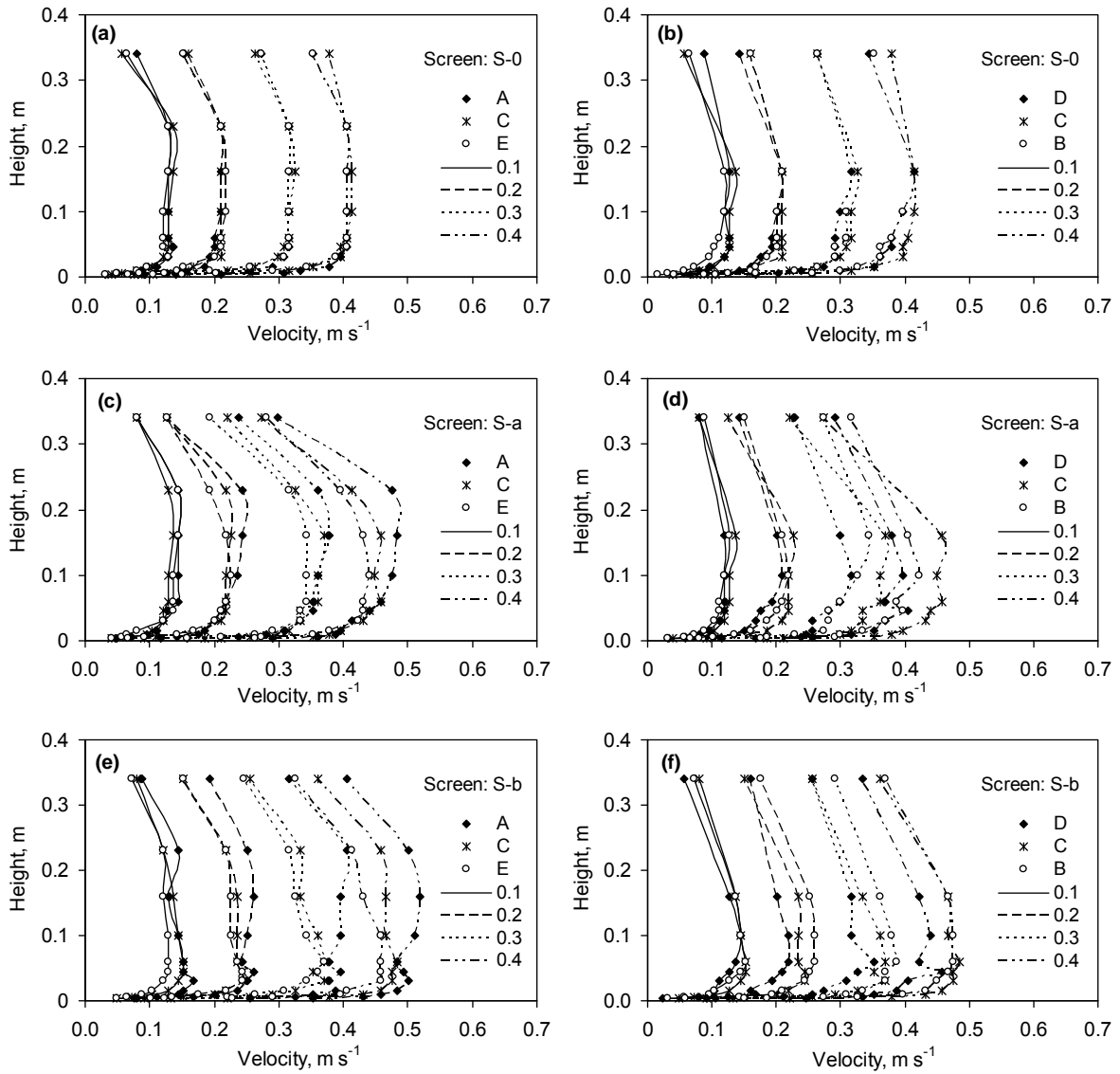


Fig. 2.4 - Wind velocity profiles with 0.1, 0.2, 0.3, and 0.4 m s⁻¹ mean wind velocities at A, C, and E sampling locations: (a) using inlet screen S-0, (c) using S-a, and (e) using S-b, and at D, C, and B sampling locations: (b) using S-0, (d) using S-a, and (f) using S-b.

The vertical wind velocity profiles did not demonstrate consistent variations along the tunnel width at measurement locations B, C, and D. The reason could be that there were only three sampling locations along the tunnel width and the sampling locations B and D were 0.04m and 0.03 m from the wind tunnel sidewalls, respectively (Fig. 2.2). Therefore, the effects of wind tunnel side walls on the velocities at small distances, e.g., 0.003 and 0.01 m, were not obtained. However, because the wind tunnel was built centrally symmetric, wind velocity profiles along the width similar to those along the height of the tunnel were expected.

The reduced wind velocities close to the ammonia release surface and the tunnel ceiling were caused by shear effects, which were the results of wind friction with the release surface and the tunnel ceiling. Similar results showing that wind friction from the wall weakens the jet and ultimately reduces the wind velocity, have been reported in the studies of wall jets and airflow in rooms (Adre and Albright, 1994; Strom et al., 2002; Zhang et al., 2000). At higher mean wind velocities, the shear effects were larger.

2.3.3. Turbulence intensity profile

Compared with the wind velocity profiles, the turbulence intensity profiles were less distinguishable among the four different mean velocities (Fig. 2.5), except for a few vertical profile curves, e.g., when measured at location B with 0.1 m s^{-1} mean air velocity (Fig. 2.5b).

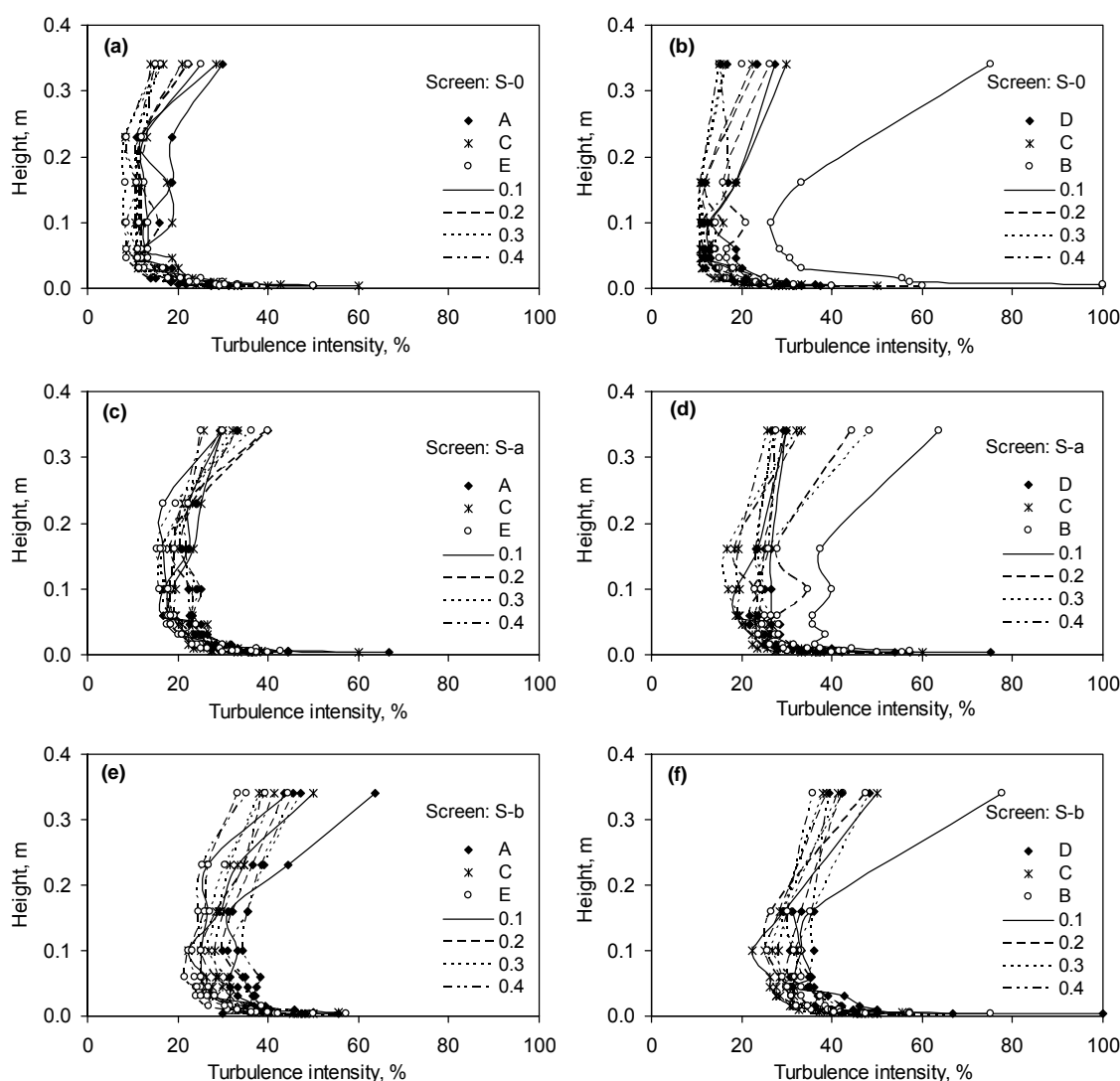


Fig. 2.5 - Turbulence intensity profiles with $0.1, 0.2, 0.3,$ and 0.4 m s^{-1} mean wind velocities at A, C, and E sampling locations: (a) using inlet screen S-0, (c) using S-a, and (e) using S-b, and at D, C, and B sampling locations: (b) using S-0, (d) using S-a, and (f) using S-b.

However, there was a clear inverse-relationship between the profiles of the turbulence intensities and the profiles of wind velocities. The highest turbulence intensities were located where the wind velocities were the lowest, i.e., close to the ammonia release surface and the wind tunnel ceiling. Both liquid and wall surfaces affected the airflow characteristics. Turbulence intensities increased when wind had contact with the liquid surface and the tunnel walls. These characteristics were similar to the results obtained by Loubet et al. (1999b) and Sohn et al. (2005).

The lowest turbulence intensities from the four mean wind velocities were all observed at the mid-height of the wind tunnel where wind speed was the highest along the tunnel length (Fig 2.5a, c, and 2.5e) as well as across the tunnel width (Fig. 2.5b, d, and f). The turbulence intensities were higher when using screens S-a and S-b as compared with a blank screen (S-0) at the wind tunnel inlet. Higher turbulence intensities at lower flow rates indicated higher intermittence (Townsend, 1976).

2.3.4. Effect of wind velocity and turbulence intensity on ammonia concentration and emission

Under isothermal conditions and at different wind velocities and RTI, ammonia concentrations in the wind tunnel inlet and outlet ranged from 1.5 to 3.5 mg m⁻³ and 12.0 to 30.6 mg m⁻³, respectively (Table 2.2). The fact that the inlet ammonia concentrations were above outdoor ambient levels, usually below 0.2 mg m⁻³ (Huber and Kreutzer, 2002), was because the tests were conducted in an enclosed laboratory environment. However, because the ammonia emissions were calculated by multiplying the tunnel ventilation rate with the ammonia concentration difference between the outlet and inlet in this mass transfer study, the effect of the small inlet ammonia concentration variations was considered to be negligible.

Table 2.2 - Effect of wind velocity and reference turbulence intensity (RTI) on wind tunnel ammonia concentrations.

Velocity, m s ⁻¹	RTI (%)	Inlet concentration, mg m ⁻³ (SD) ^[a]	Outlet concentration, mg m ⁻³ (SD) ^[a]
0.1	11	2.9 (0.3)	28.0 (1.3)
0.2	11	2.6 (0.3)	18.8 (0.8)
0.3	11	2.1 (0.2)	14.0 (0.7)
0.4	11	2.0 (0.1)	12.0 (0.4)
0.1	20	3.5 (0.2)	30.6 (1.6)
0.2	20	2.9 (0.4)	21.4 (1.3)
0.3	20	2.4 (0.2)	17.0 (1.4)
0.4	20	1.5 (0.2)	14.3 (0.8)
0.1	30	2.2 (0.2)	28.5 (2.6)
0.2	30	2.6 (0.2)	21.9 (2.0)
0.3	30	2.7 (0.3)	18.2 (2.1)
0.4	30	3.0 (0.3)	15.9 (1.3)

^a SD = standard deviation. The RTIs were the mean turbulence intensities at the centre of the profile measurement section in the wind tunnel (location: X=0.3 m, Y=0.17 m, and Z=0.16 m, Fig. 2.2)

The tunnel outlet ammonia concentrations were inversely correlated to the mean wind velocities (Table 2.2). The profile concentrations above the release surface did not vary considerably at all four mean wind velocities (Fig. 2.3a, c and e). This difference between the inlet/outlet concentrations and the profile concentrations could be related to the thickness of ammonia concentration boundary layer that only occupied 0.1 m height zone in the tunnel of 0.35 m height. The outlet ammonia concentration was the highest at the lowest wind velocity. The majority of the air flowed through the low concentration zone. At higher velocities, more air with low ammonia concentration was carried to the outlet, causing the mean outlet concentration to decrease.

The concentration profile patterns at measurement locations C, D, and E were similar at all four different wind velocities (Fig. 2.3a, c and e). This implied that, at RTI of more than 11%, the wind turbulence was sufficient to mix gaseous ammonia and maintain a stable concentration profile along the length of the release surface. However, ammonia concentration boundary layer was slightly thinner at low turbulence intensity when using S-0, compared with other two screens, at all three measurement locations. At measurement locations D and E, the concentration boundary layer was also a little thinner when using S-a than using S-b (Fig. 2.3b, d and f).

Increasing turbulence intensity was expected to lower the thickness of the gaseous boundary layer (Leyris et al., 2005; Rong et al., 2009). Rong et al. (2009) found that the boundary layer thickness increased slightly over the velocities ranging from 0.2 to 0.4 m s⁻¹ and increased significantly at 0.1 m s⁻¹. Although greater concentration fluctuations in this study were observed at the bottom of the concentration boundary layer, where air velocities were low and turbulence intensities were high (Fig. 2.3), such a phenomenon was not observed by Rong et al. (2009). According to boundary layer theory, air velocity affects the boundary layer thickness over the liquid surface. Increasing air velocity should result in a thinner concentration boundary layer at the liquid-gaseous interface (Haslam et al., 1924). However, the conclusion made by Haslam et al. (1924) was based on a velocity range from 0.015 to 0.4 m s⁻¹. Within a narrower velocity range from 0.1 to 0.4 m s⁻¹, a similar phenomenon was not observed in this study.

Higher wind velocities induced by higher tunnel ventilation rate resulted in more intensive dilution that lowered outlet ammonia concentrations at all three RTI levels. Increasing wind velocity had evident effect on increasing ammonia emissions at all three RTI (Fig. 2.6a). This was in good agreement with the work by other researchers on soluble gases including ammonia (Arogo et al., 1999; Mackay and Yeun, 1983). It also agreed with the study by Vlek and Stumpe (1978), who reported that ammonia evaporation losses increased linearly with the increasing airflow rates.

Increases in RTI from 11% to 30% also resulted in a general trend of increase in ammonia emission fluxes with only one exception at 0.1 m s⁻¹ and 30% (Fig. 2.6a). This inconsistent instance of the effects of wind velocity and RTI on ammonia emission might be related to the Laser Doppler anemometer only being capable of taking one-dimensional measurements. Therefore, only

horizontal wind fluctuations were measured and the vertical fluctuations were not taken into account.

2.3.5. Modelling of ammonia mass transfer coefficient

Using nonlinear model fitting and the experimental data presented in Table 2.2, an AMTC model was obtained with the wind velocity as the only independent variable (Eq. (2.12)).

$$k_{G-1} = 0.00232 \times u^{0.33} \quad (R^2=0.71) \quad (2.12)$$

At 95% confidence interval, the standard errors for the model parameters $a=2.32 \times 10^{-3}$ and $b=0.33$ were 7.05×10^{-4} and 0.213, respectively. The standard error of the estimate was 1.55×10^{-4} .

An improved AMTC model with higher correlation coefficient, $R^2=0.93$ compared with $R^2=0.71$ in Eq. (2.12), was obtained as a function of both wind velocity and RTI above the release surface (Eq. (2.13)).

$$k_{G-2} = 0.00126 \times u^{0.34} Ti^{0.21} \quad (R^2=0.93) \quad (2.13)$$

At 95% confidence interval, the standard errors for the model parameters $a=1.26 \times 10^{-3}$, $b=0.34$, and $c=0.21$ were 3.6×10^{-4} , 0.077, and 0.089, respectively. The standard error of the estimate was 7.87×10^{-5} . Comparison of the differences between the two models (Eqs. (2.12) and (2.13)) showed that the effects of turbulence intensity on the mass transfer modelling cannot be ignored.

The AMTC increased with the increasing turbulence intensity at all four different wind velocities presented in Table 2.2. The AMTC increased 10 % when the turbulence intensity increased 57.4 % at the same wind velocity. This agreed with the results reported by Leyris et al. (2005) and Rong et al. (2009) and could be related with the slight change in boundary layer thickness due to the increasing turbulence intensity.

Model sensitivity analysis using Eq. (2.11) showed that the mass transfer coefficient was more sensitive at lower wind velocities than at high velocities. The relative sensitivity was 75.2% for wind velocity interval between 0.05 to 0.10 m s⁻¹ and 25.1% for wind velocity interval between 0.35 to 0.4 m s⁻¹. The mass transfer coefficient was also more sensitive at lower than at higher turbulence intensities. The relative sensitivity was 47.2% for turbulence intensity interval between 5 to 10% and 6.1% for turbulence intensity interval between 95 to 100%. The results also showed that the model was more sensitive to the wind velocity than to the turbulence intensity. These results were in agreement with the study of Rong et al. (2009).

However, the AMTC modelled in this study to describe the relationship between the wind characteristics and the ammonia emissions was only obtained in laboratory experiments using a particular wind tunnel. The quantitative correlation could be different in the case of ammonia emissions using other wind tunnels, from real slurry, or in commercial animal buildings due to scale

effects, the presence of animals, and dynamic changes in liquid slurry, air temperature, the pH of slurry, building ventilation, and other yet unknown factors.

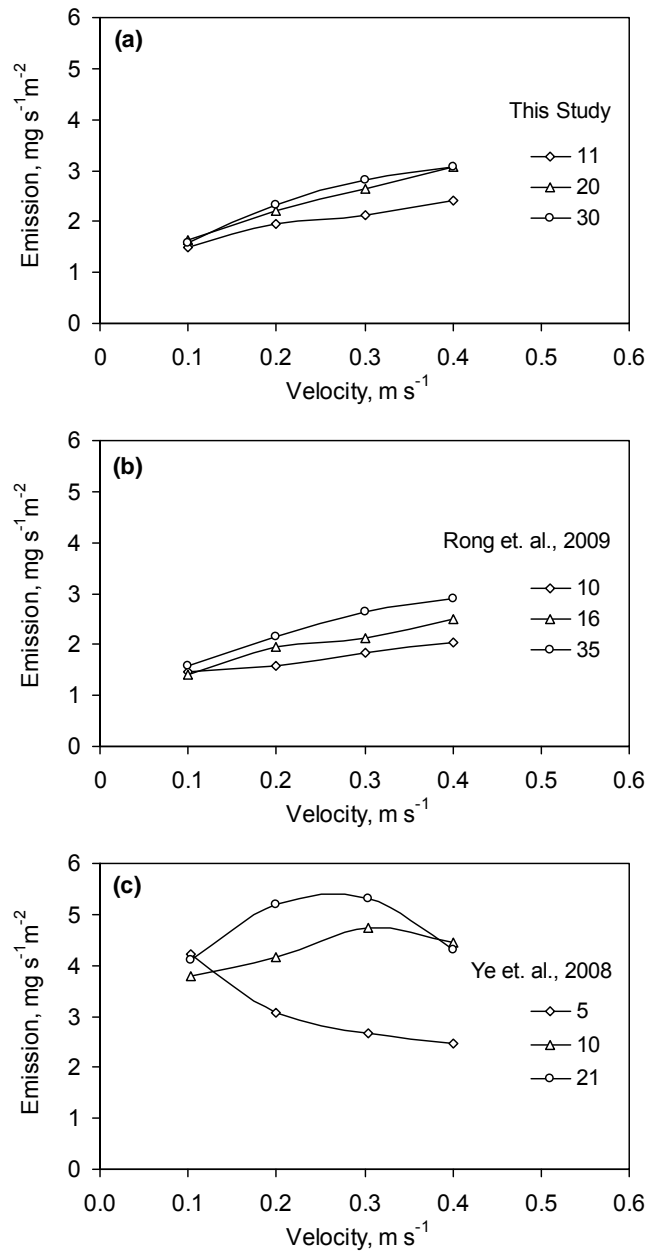


Fig. 2.6 - Comparison of ammonia emission fluxes at three different reference turbulence intensities from three wind tunnel studies: (a) this study, (b) from Rong et al. (2009), and (c) from Ye et al. (2008a).

2.3.6. Comparison of ammonia emissions in three wind tunnel studies

Different ammonia emissions were observed at the same wind velocities but slightly different turbulence intensities at three wind tunnel studies (Fig. 2.6). The ammonia emissions from this study were similar to those obtained by Rong et al. (2009), especially at low wind velocities. At 0.1 m s^{-1} wind velocity and 11% RTI, the ammonia emission in this study was $1.504 \text{ mg s}^{-1} \text{ m}^2$ versus $1.455 \text{ mg s}^{-1} \text{ m}^2$ at the same wind velocity and 10% RTI by Rong et al. (2009). Different RTI had less effect on ammonia emissions at low wind velocities of 0.1 and 0.2 m s^{-1} compared with at higher wind velocities of 0.3 and 0.4 m s^{-1} in both studies. A general trend of increasing ammonia emissions induced by increasing wind velocity was clearly shown in Fig. 2.6a and b.

The results obtained by Ye et al. (2008a) demonstrated irregular ammonia emission patterns related to wind velocity and RTI and were substantially different from the other two studies. Wind velocities from 0.1 to 0.4 m s^{-1} were inversely correlated to ammonia emissions at low RTI of 5%. At higher RTI of 10% and 20%, increase in wind velocities from 0.1 to 0.3 m s^{-1} resulted in an increase in ammonia emissions. However, further increase in wind velocities from 0.3 to 0.4 m s^{-1} caused a decrease in ammonia emissions at 10% and 20% RTI (Fig. 2.6c).

The experiments conducted by Rong et al. (2009) and Ye et al. (2008a) used similar methodologies and laboratory experimental setups as this study. The major differences among the three studies were the wind tunnel size and the TAN concentration in ammonia solution (Table 2.1). Therefore, the three sets of data provided a rare opportunity for comparison. The wind tunnel in this study had a larger cross section area (0.123 m^2) than that of 0.0135 m^2 in the wind tunnel used by Ye et al. (2008a), but smaller than the 0.25 m^2 used by Rong et al. (2009).

The experiment in this study employed TAN that had almost twice the concentration as the TAN used by Rong et al. (2009), but with a lower pH of 8.8 versus 8.98 by Rong et al. (2009). The calculated C_s was 1758 and 984 mg m^{-3} in this study and in Rong et al. (2009), respectively (Table 2.1). However, the expected ammonia emissions that should have been much higher due to the higher C_s in this study than in Rong et al. (2009) were not observed, indicating that the mass transfer coefficients were different in the two studies. In addition, Ye et al. (2008a) used a C_s of 1226 mg m^{-3} , lower than found in this study, but they obtained the highest ammonia emissions among the three tests (Fig. 2.6). At 10% RTI, the ammonia emissions were almost twice as high as those obtained by Rong et al. (2009). These phenomena suggested that the wind tunnel size played an important role in the ammonia emissions and agreed with the work of other researchers. Smith and Watts (1994) found that odour emissions using a large wind tunnel were consistently lower than those in a smaller tunnel. Wind tunnel heights were related to sweep wind speed and gas emissions, as indicated by Frechen et al. (2004). Hudson and Ayoko (2008) concluded that different devices (chamber, hood, or wind tunnels) could be expected to provide equivalent emission rate estimates.

Ammonia concentration profiles in Fig. 2.3 showed that the concentration boundary layer had a thickness of about 0.1 m . The headspace above the ammonia release surface in the wind tunnel by

Ye et al. (2008a) was only 0.09 m height, lower than the boundary layer in this study. Frechen et al. (2004) noticed that reduction of tunnel height increases the sweep wind speed. If the ammonia concentration boundary layer above the emission surface had similar thicknesses in the three tunnel studies, the smallest tunnel was expected to have the largest proportion of ventilation air passing through the high ammonia concentration zone above the release surface and therefore result in the highest ammonia releases, and vice versa. This could explain the ammonia emission differences among the three studies.

2.3.7. Comparison of mass transfer coefficients in three wind tunnel studies

Statistically modelled AMTCs as a function of wind velocity and turbulence intensity among the three wind tunnel studies demonstrated similar differences among the three studies as found in the ammonia emission differences (Fig. 2.6), although all the AMTC values ranged from 1.06×10^{-3} to $4.3 \times 10^{-3} \text{ m s}^{-1}$ and were within the range of 1.17×10^{-2} to $1.3 \times 10^{-6} \text{ m s}^{-1}$ reviewed by Ni (1999). The models obtained for this study (k_{G-2} , Eq. (2.13)) and the study of Rong et al. (2009) (k_{G-3} , Eq. (2.14)) had R^2 of 0.93 and 0.94, respectively. The R^2 for the model of Ye et al. (2008a) was only 0.46 (k_{G-4} , Eq. (2.15)), indicating a higher uncertainty when using wind velocity and turbulence intensity to model ammonia emissions. The k_{G-2} and k_{G-3} were positively correlated to both wind velocity and turbulence intensity; but the k_{G-4} was inversely correlated to wind velocity although positively correlated to turbulence intensity.

$$k_{G-3} = 0.00179 \times u^{0.38} Ti^{0.24} \quad (R^2=0.94) \quad (2.14)$$

$$k_{G-4} = 0.00171 \times u^{-0.0038} Ti^{0.28} \quad (R^2=0.46) \quad (2.15)$$

This disagreement among the three studies was unexpected because the AMTCs were obtained based on the known ammonia emission rates as shown in Fig. 2.6. Therefore, the discrepancy could be contributed to the differences in tunnel sizes.

Predicting mass transfer coefficients based on wind characteristics (velocity and turbulence intensity) has been used in ammonia emission studies, e.g., Teye and Hautala, (2008) and Cortus et al. (2008). However, previous work by other researchers, e.g., Smith and Watts (1994) and Hudson and Ayoko (2008), and the comparison among the three wind tunnels clearly shows that the relationship between the AMTC and the wind characteristics is highly device-dependent. Therefore, while the factors such as wind characteristics, air and liquid temperature, pH and TAN of liquids or slurry, etc. are indispensable in AMTC study, it remains critically important to investigate the effect of geometric scale of the enclosures on boundary layers and ammonia emissions.

2.4. Conclusions

Using a wind tunnel under laboratory conditions provided a controlled environment that allowed comprehensive investigations on wind and ammonia concentration characterisation and ammonia

emissions. An inverse-relationship between wind velocities and turbulence intensities was observed. A quasi-constant thickness of 0.1 m ammonia concentration boundary layer was found at different wind velocities and turbulence intensities. The large ammonia concentration gradients within the 0.1 m thick boundary layer demonstrated technical difficulty to experimentally determine the ammonia concentration at the immediate liquid surface, because a small variation in height meant a significant difference in ammonia concentrations. A statistical model of ammonia mass transfer coefficient was developed as a function of wind velocity and turbulence intensity to calculate ammonia emission from the wind tunnel. While this study confirmed some previous research findings in the literature, disagreements with other research were also found. Comparison with different studies revealed that there might be a significant effect of tunnel size on ammonia mass transfer. More knowledge about ammonia mass transfer needs to be obtained in the future studies in order to apply it under field conditions for emission modelling and abatement.

Acknowledgements

This research was performed as part of ROSES project “Reduction of Odour Source in and Emission from Swine Buildings” under the program “Animal Husbandry, the Neighbours and the Environment” funded by the Danish Ministry of Food, Agriculture and Fisheries (Grant Number: 3304-VMP-05-032-01). The authors also appreciate the technical support of Preben Jensen Dahl and Peter Ravn at Air Physics Lab, Research Centre Bygholm, University of Aarhus, Denmark.

References

- Adre N; Albright L D (1994). Criterion for establishing similar air-flow patterns (isothermal) in slotted-inlet ventilated enclosures. *Transactions of the ASAE*, 37(1), 235-250.
- Aneja V P; Blunden J; James K; Schlesinger W H; Knighton R; Gilliam W; Jennings G; Niyogi D; Cole S (2008). Ammonia assessment from agriculture: US status and needs. *Journal of Environmental Quality*, 37(2), 515-520.
- Arogo J; Zhang R H; Riskowski G L; Christianson L L; Day D L (1999). Mass transfer coefficient of ammonia in liquid swine manure and aqueous solutions. *Journal of Agricultural Engineering Research*, 73(1), 77-86.
- Bliss P J; Jiang K Y; Schulz T J (1995). The development of a sampling system for the determination of odor emission rates from areal surfaces. 2. Mathematical-model. *Journal of the Air & Waste Management Association*, 45(12), 989-994.
- Bull K R; Sutton M A (1998). Critical loads and the relevance of ammonia to an effects-based nitrogen Protocol. *Atmospheric Environment*, 32(3), 565-572.
- Cortus E L; Lemay S P; Barber E M; Hill G A; Godbout S (2008). A dynamic model of ammonia emission from urine puddles. *Biosystems Engineering*, 99(3), 390-402.

- Frechen F B; Frey M; Wett M; Loser C (2004). Aerodynamic performance of a low-speed wind tunnel. *Water Science and Technology*, 50(4), 57-64.
- Hashimoto A G; Ludington D C (1971). Ammonia desorption from concentrated chicken manure slurries, *Livestock Waste Management and Pollution Abatement*, Proceedings of the International Symposium on Livestock Wastes. St. Joseph, MI: ASAE, pp. 117-121.
- Haslam R T; Hershey R L; Keen R H (1924). Effect of gas velocity and temperature on rate of absorption. *Industrial and Engineering Chemistry*, 16(12), 1224-1230.
- Huber C; Kreutzer K (2002). Three years of continuous measurements of atmospheric ammonia concentrations over a forest stand at the Hoglwald site in southern Bavaria. *Plant and Soil*, 240(1), 13-22.
- Hudson N; Ayoko G A (2008). Odour sampling 2. Comparison of physical and aerodynamic characteristics of sampling devices: A review. *Bioresource Technology*, 99(10), 3993-4007.
- Hudson N; Ayoko G A; Dunlop M; Duperouzel D; Burrell D; Bell K; Gallagher E; Nicholas P; Heinrich N (2009). Comparison of odour emission rates measured from various sources using two sampling devices. *Bioresource Technology*, 100 (1), 118-124.
- Incropera F P; DeWitt D P; Bergman T L; Lavine A S (2007). *Fundamentals of Heat and Mass Transfer* (6th ed.), New Jersey, USA: John Wiley & Sons.
- Jayaweera G R; Mikkelsen D S (1990). Ammonia volatilization from flooded soil systems: A computer model. I. Theoretical aspects. *Soil Science Society of America Journal*, 54(5), 1447-1455.
- Leyris C; Guillot J M; Fanlo J L; Pourtier L (2005). Comparison and development of dynamic flux chambers to determine odorous compound emission. rates from area sources. *Chemosphere*, 59(3), 415-421.
- Liang Z S; Westerman P W; Arogo J (2002). Modeling ammonia emission from swine anaerobic lagoons. *Transactions of the ASAE*, 45(3), 787-798.
- Liu Z F; Wang L J; Beasley D; Oviedo E (2007). Effect of moisture content on ammonia emissions from broiler litter: A laboratory study. *Journal of Atmospheric Chemistry*, 58(1), 41-53.
- Loubet B; Cellier P; Flura D; Genermont S (1999a). An evaluation of the wind-tunnel technique for estimating ammonia volatilization from land: Part 1. Analysis and improvement of accuracy. *Journal of Agricultural Engineering Research*, 72(1), 71-81.
- Loubet B; Cellier P; Genermont S; Flura D (1999b). An evaluation of the wind-tunnel technique for estimating ammonia volatilization from land: Part 2. Influence of the tunnel on transfer processes. *Journal of Agricultural Engineering Research*, 72(1), 83-92.
- Mackay D; Yeun A T K (1983). Mass transfer coefficient correlations for volatilization of organic solutes from water. *Environmental Science & Technology*, 17(4), 211-217.
- Ni J Q (1999). Mechanistic models of ammonia release from liquid manure, a review. *Journal of Agricultural Engineering Research*, 72(1), 1-17.

- Portejoie S; Martinez J; Landmann G (2002). Ammonia of farm origin: impact on human and animal health and on the natural habitat, *Productions Animales*, 15(3), 151-160.
- Rong L; Nielsen P V; Zhang G Q (2009). Effects of airflow and liquid temperature on ammonia mass transfer above an emission surface: Experimental study on emission rate. *Bioresource Technology*, 100(20), 4654-4661.
- Smith R J; Watts P J (1994). Determination of odor emission rates from cattle feedlots. 2. Evaluation of 2 wind tunnels of different size. *Journal of Agricultural Engineering Research*, 58(4), 231-240.
- Sohn J H; Smith R J; Hudson N A; Choi H L (2005). Gas sampling efficiencies and aerodynamic characteristics of a laboratory wind tunnel for odour measurement. *Biosystems Engineering*, 92(1), 37-46.
- Strom J S; Zhang G; Morsing S (2002). Predicting near-floor air velocities for a slot-inlet ventilated building by jet velocity decay principles. *Transactions of the ASAE*, 45(2), 407-413.
- Teye F K; Hautala M (2008). Adaptation of an ammonia volatilization model for a naturally ventilated dairy building. *Atmospheric Environment*, 42(18), 4345-4354.
- Townsend A A (1976). *The Structure of Turbulent Shear Flow* (2nd ed.). Cambridge: Cambridge University Press.
- van der Molen J; Beljaars A C M; Chardon W J; Jury W A; Vanfaassen H G (1990). Ammonia volatilization from arable land after application of cattle slurry. 2. derivation of a transfer model. *Netherlands Journal of Agricultural Science*, 38(3), 239-254.
- van der Peet-Schwering C M C; Aarnink A J A; Rom H B; Dourmad J Y (1999). Ammonia emissions from pig houses in The Netherlands, Denmark and France. *Livestock Production Science*, 58(3), 265-269.
- Vlek P L G; Stumpe J M (1978). Effects of solution chemistry and environmental conditions on ammonia volatilization losses from aqueous systems. *Soil Science Society of America Journal*, 42(3), 416-421.
- Webb J ; Menzi H; Pain B F; Misselbrook T H; Dammgen U; Hendriks H; Dohler H (2005). Managing ammonia emissions from livestock production in Europe. *Environmental Pollution*, 135(3), 399-406.
- Ye Z; Zhang G; Li B; Strom J S; Tong G; Dahl P J (2008a). Influence of airflow and liquid properties on the mass transfer coefficient of ammonia in aqueous solutions. *Biosystems Engineering*, 100(3), 422-434.
- Ye Z; Zhang G; Li B; Strom J S; Dahl P J (2008b). Ammonia emissions affected by airflow in a model pig house: effects of ventilation rate, floor slat opening, and headspace height in a manure storage pit. *Transactions of the ASABE*, 51(6), 2113-2122.
- Zerihun D; Feyen J; Reddy J M (1996). Sensitivity analysis of furrow-irrigation performance parameters. *Journal of Irrigation and Drainage Engineering-ASCE*, 122(1), 49-57.

Zhang G; Morsing S; Bjerg B; Svidt K; Strom J S (2000). Test room for validation of airflow patterns estimated by computational fluid dynamics. *Journal of Agricultural Engineering Research*, 76(2), 141-148.

Chapter 3

Assessing effect of wind tunnel sizes on air velocity and concentration boundary layers and on ammonia emission estimation using computational fluid dynamics (CFD)

Paper II:

Saha, C.K., Wu, W., Zhang, G., and Bjerg, B 2011. Assessing effect of wind tunnel sizes on air velocity and concentration boundary layers and on ammonia emission estimation using computational fluid dynamics (CFD). Submitted to a peer review journal.

Abstract

The objective of this study was to investigate the effect of different geometric sizes of wind tunnels on aerial boundary layers above the emission surface and therefore their effect on ammonia emission using CFD tool. Five wind tunnels of different sizes were used for the CFD simulation. Detail experimental measurements on air velocity and concentration profiles above the emission surface were realized using average inlet velocities of 0.1, 0.2, 0.3 and 0.4 m s⁻¹ in two wind tunnels under isothermal condition. The TAN (Total Ammoniacal Nitrogen) and pH of ammonia aqueous solution were kept constant during the experiments. The boundary conditions necessary for the CFD study were obtained from the measured experimental data. The CFD model used for simulations was first validated using the data from the two wind tunnel experiments. For assessing the effects of wind tunnel size, the air velocity range of 0.1 to 0.6 m s⁻¹ was used in CFD investigations. It was found that the velocity and concentration boundary layer thickness decreased with the increase of inlet air velocity where the concentration boundary was thinner than the corresponding velocity boundary layer. Wind tunnel sizes affected both velocity and concentration boundary layer thicknesses ($P < 0.001$). The velocity and concentration boundary layer was thicker in a wind tunnel with larger heights than in small height. The over estimation of ammonia emission of smaller wind tunnels were observed comparing to the largest wind tunnel or open field situation ($P < 0.001$). Non-linear regression equations were developed for velocity boundary layer thickness (δ_u), concentration boundary layer thickness (δ_c), and ammonia mass transfer coefficient (k_G) as a function of wind tunnel height (H) and average inlet velocity (u_m), which given clear quantitative indication of effects of H , and u_m on δ_u , δ_c , and k_G respectively.

Key words: boundary layer thickness, wind tunnel size, CFD simulation, mass transfer, ammonia emission

3.1. Introduction

Dynamic Flux Chamber (DFC) methods have, for several decades, been used for estimating emission of odour, ammonia and greenhouse gases from area sources including open manure storages, and manure field applications (Hudson and Ayoko, 2008). By working principle, a DFC is a typical wind tunnel with a part of open bottom facing the emission surface, and flushed with incoming air at a known velocity or flow rate (Gao and Yates, 1998; Peu et al., 1999; Reichman and Rolston, 2002). The inlet and outlet of the wind tunnel may be varied following differences of the specific configuration of a DFC.

A range of wind tunnels have been used to collect odour samples from area sources at intensive livestock farming operations which are tabulated in the recent review of Hudson and Ayoko (2008). The emission data obtained from the different wind tunnels are difficult to comprehend by the general community, thereby creating difficulties for the various regulatory agencies and producers. In addition, there is no standard for the design of emission sampling wind tunnels. Variations in tunnel geometry include differences in the length/width ratio, the emission surface area and the height of the tunnel. The tunnel sizes were found to affect both gas and odour emission rates (Frechen et al., 2004; Hudson et al., 2009; Smith and Watts, 1994). Smaller tunnel height could enhance emission rate due to the larger wind speed gradient at the release surface. However, a complex relationship exists between emission estimates derived from different devices (Hudson et al., 2009; Hudson and Ayoko, 2009). In our recent study (Saha et al., 2010); we found that there might be an effect of wind tunnel size on ammonia mass transfer processes. However, a systematic study is needed to quantify and estimate the effects of geometry design and dimension on the air-flow characteristics in the chambers and their effect on emissions.

The experimental method is very expensive and time consuming to investigate the effects of wind tunnel dimensions on emission, due to a large number of experimental setups when both information for airflow characteristics and mass transfer process in the space are needed. Besides, the number of points that can be measured is limited. It is also very difficult to obtain comprehensive knowledge of air velocity and concentration pattern in boundary layers by using direct measurement methods (Saha et al., 2010). Direct measurement requires a measurement agent that unavoidably interferes with airflow and concentration pattern, and consequently affects the measurement output.

In line with the rapid development in computer technology, computational fluid dynamics (CFD) has matured to a stage where it provides substantial insight into phenomena that occur in dynamic air-flow system (Chen, 2009; Norton et al., 2010). As a simulation technique, it can be used to solve real or hypothetical fluid problems, and so, it has potential to be used as a design technique. However, it is still important to validate part of CFD simulation experimentally and the

yardstick of success is the level of agreement that can be attained between numerical predictions and experiments (Xia and Sun, 2002).

Computational fluid dynamics techniques have been used to study ventilation performance (Bjerg et al., 2002; Chen, 2009; Norton et al., 2007; Norton et al., 2009; Zhang et al., 1999) and contaminant dispersion and transfer in buildings (Baklanov, 2000; Quinn et al., 2001; Sun et al., 2002; Topp et al., 2001; Vallee et al., 2008; Zhang et al., 1999). The influence of pen partitions and heated simulated pigs on air-flow in a slot ventilated test room and CFD has been evaluated as a tool to predict airflow in a livestock room (Bjerg et al., 2000). Bjerg et al. (1999) found through CFD simulation that the relationship between room width and room height had a crucial three-dimensional effects on the airflow. Recently, Rong et al. (2010) used CFD to study surface concentration distributions on the emission surface and evaluated the ability of turbulence models to predict the NH₃ mass transfer process in the boundary conditions measured in experiments. They found that the concentration, velocity, and temperature profiles simulated in CFD reasonably agree with the measurements, and recommended shear stress transport (SST) $k-\omega$ model for predicting the transfer process in the boundary layer. They also found that NH₃ concentration of the emission surfaces increases with decreases of air velocity, and that local mass transfer coefficient decreased with increased concentration boundary layer thickness. But the effects of wind tunnel sizes on airflow boundary layer and concentration boundary layer were not evaluated in their CFD simulation or in other previous investigations.

The overall aim of this study was to conduct an assessment of the effect of different geometric sizes of wind tunnels on air velocity and concentration boundary layer, and their effect on ammonia emission using CFD method. The CFD model was first validated using two wind tunnel experiments data before being applied to different simulation scenarios.

3.2. Theoretical background

3.2.1. Mass transfer from an emitting surface

Ammonia (NH₃) transfer from the immediate liquid manure surface or from manure fertilizer applied open field into the free bulk air stream by diffusion or convection. The transfer process of this gaseous NH₃ can usually be described by a core mechanistic model, in which both a physical understanding and a quantitative description of the ammonia release are given (Ni, 1999). Ammonia emission flux equals ammonia release under steady state conditions without any sink in the enclosure. Ammonia convective mass transfer from animal manure is expressed by the core model, which can be written as Eq. (3.1).

$$E = k_G(C_s - C_a) \quad (3.1)$$

where E is emission flux ($\text{mg s}^{-1}\text{m}^{-2}$); k_G is ammonia mass transfer coefficient (AMTC) (m s^{-1}); C_s is gaseous ammonia concentration at the immediate liquid surface (mg m^{-3}); C_a is the ammonia concentration in the bulk air (mg m^{-3}).

However, due to limitation of available technology to acquire in-depth knowledge related to this process, the AMTC has always been determined empirically. Ammonia emission flux from a wind tunnel can be expressed as:

$$E = \frac{VR}{A_s}(C_o - C_i) \quad (3.2)$$

where E is emission flux ($\text{mg s}^{-1}\text{m}^{-2}$); VR is wind tunnel ventilation rate ($\text{m}^3 \text{s}^{-1}$); A_s is ammonia release surface area (m^2); C_o is ammonia concentration at the wind tunnel outlet (mg m^{-3}); C_i is ammonia concentration at the wind tunnel inlet (mg m^{-3}).

Equation (3.2) can be written as:

$$E = u_m \frac{A_c}{A_s}(C_o - C_i) \quad (3.3)$$

where, u_m is average velocity in wind tunnel (m s^{-1}); A_c is cross sectional area of corresponding wind tunnel (m^2); A_s is ammonia release surface area (m^2); C_o is ammonia concentration at the wind tunnel outlet (mg m^{-3}); C_i is ammonia concentration at the wind tunnel inlet (mg m^{-3}).

Re-arranging Eqs. (3.2) and (3.3), Eq. (3.4) below is obtained (Ye et al., 2008a).

$$k_G = \frac{u_m \cdot A_c}{A_s} \cdot \frac{(C_o - C_i)}{(C_s - C_a)} \quad (3.4)$$

In this study, C_i and C_a were considered zero for CFD simulation. A_c and A_s were fixed for the specific wind tunnel. Average inlet velocity, u_m was boundary value for simulation. C_s was assumed constant value at the surface for the simulation. Therefore, the AMTC k_G in a wind tunnel can be calculated using Eq. (3.4) for further analysis.

3.2.2. Boundary layer theory

The concept of boundary layers gives the understanding of convection heat and mass transfer between a surface and a fluid flow past. For isothermal case, mass transfer is the main issue in boundary layer. The gaseous phase boundary layer can be perceived as a resistance that limits the transfer of ammonia from liquid manure or soil surface into the free air stream. Boundary layer theory is used most extensively to estimate the gas phase mass transfer coefficient (k_G) in controlled laboratory environments. The boundary layer thickness is taken as being the thickness of the viscous boundary layer region. Because the main effect of viscosity is to slow fluid near a wall, the edge of the viscous region is at the point where the fluid velocity or concentration is essentially equal to that at the free stream (Fig. 3.1). With the increasing distance of leading edge, the effects of viscosity or species transfer penetrate further into free air stream and boundary layers grow (δ increase with x).

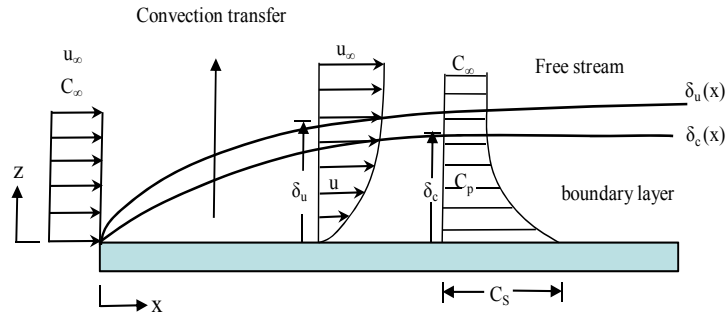


Fig. 3.1- Typical velocity and concentration boundary layer over a flat surface

Note: δ_u – thickness of velocity boundary layer; u_∞ - velocity of free air stream; u - velocity at specific point; δ_c – thickness of concentration boundary layer; C_∞ - concentration of gaseous NH_3 in free air stream; C_p – concentration of gaseous NH_3 at specific point above the emission surface; C_s –concentration of gaseous NH_3 at immediate liquid surface; x – horizontal distance; z - vertical distance. Adapted from: Incropera et al. (2007)

The edge of a velocity boundary layer (δ_u) is usually defined as the vertical distance of the point at which the air velocity equals 99% of that in the free air stream (Incropera et al., 2007) (Eq. (3.5)).

$$u_p = 0.99u_\infty \quad (3.5)$$

where, u_p is air velocity at a specific point (m s^{-1}); u_∞ is air velocity in free air stream (m s^{-1}).

Similarly, The concentration boundary layer (δ_c) is defined in this study as the region of the fluid in which concentration gradient exist, and its thickness, δ_c , is typically defined as the value of vertical distance (height inside the wind tunnel in this case) for which the fluid concentration equals 99% of that in the free air stream (Incropera et al., 2007)(Eq. (3.6)).

$$\frac{C_s - C_p}{C_s - C_\infty} = 0.99 \quad (3.6)$$

where, C_s is surface concentration (mg m^{-3}); C_p is concentration at a specific point (mg m^{-3}); C_∞ is concentration at the free air stream (mg m^{-3}), which was zero for this study.

3.3. Methods and materials

3.3.1. CFD modelling

3.3.1.1. Numerical method

The CFD model was based on the description of the experimental wind tunnel. The airflow pattern and NH_3 mass transfer in the tunnel are governed by the conservation laws of mass, momentum and

energy. The result of CFD calculation is the solution of conservative transport equations for mass, momentum and energy. Commercial code Fluent 12.0 (Fluent, 2009), used in this work, is based on the finite volume approach. SIMPLE algorithm (Versteeg and Malalasekera, 2007) is used for velocity-pressure correction and the second-order upwind scheme (Versteeg and Malalasekera, 2007) for convective terms is used to reduce the numerical diffusion. The convergence is not assumed to be reached until the velocity magnitude at a specific point above the emission surface has stabilized.

3.3.1.2. Wind tunnel design and model set up in CFD

The wind tunnels used for CFD simulation are listed in details in Table 3.1. According to the review by Hudson and Ayoko (2008), the length, width, and height of wind tunnels or DFCs varied from 0.1 m to 15.6 m, 0.03 m to 7.3 m, 0.002 m to 4.5 m respectively. Five different sizes were chosen

Table 3.1: Wind tunnels (WT) and their design dimensions. S, Y and R were denoted for Saha et al. (2010), Ye et al.(2008b), and Rong et al. (2009) studies.

Parameter	S-WT1/10th	Y-WT	S-WT	R-WT	S-WT10t
WT length (L) (m)	0.367	2.00	3.67	4.99	36.7
WT width (W) (m)	0.035	0.15	0.35	0.5	3.5
WT height (H) (m)	0.035	0.15	0.35	0.5	3.5
WT airflow cross-section area (m ²)	0.0123	0.0135 ^[a]	0.123	0.25	12.3
Ammonia release surface area (m ²)	0.06×0.035	0.3×0.15	0.6×0.35	0.62×0.43	6.0×3.5
Emission source distance from the inlet (m)	0.1175	0.65	1.175	2.05	11.75
Air velocity and concentration profile measuring location (m)	X=0.138, Y=0.0175	X=0.8, Y=0.075	X=1.38, Y=0.175	X=2.36, Y=0.25	X=13.8, Y=1.75
Air temperature (°C)	22	22.0	22.0	22.3	22
Inlet air velocity range (m s ⁻¹) ^[b]	0.1-0.6	0.1-0.6	0.1-0.6	0.1-0.6	0.1-0.6

^[a] Only the top part of 0.09m height was used for airflow. The bottom part of 0.06m height was used to ammonia solution. ^[b]In both S-WT and R-WT studies, the inlet velocity ranges of 0.1 to 0.4 m s⁻¹ were used in their experiment.

for assessing their effects on airflow and concentration characteristics above the emission surface inside wind tunnel and therefore on ammonia emission. The dimensions of three wind tunnels, Y-WT, S-WT, and R-WT, were adapted from the experimental studies by Ye et al. (2008b), Saha et al. (2010), and Rong et al (2009) respectively. The dimensions of the other two, S-WT1/10th and S-WT10t, were scaled to 1:10 and 10:1 referring to S-WT, the one by Saha et al. (2010). The width

and height of S-WT1/10th tunnel were higher than Ravikrishna et al. (1998) dynamic flux chamber, but $1/10^{\text{th}}$ of wind tunnel used by Saha et al. (2010). On the other hand, dimensions of the S-WT10t tunnel, especially width and height were lower than the big tunnel used by Hansen et al. (2006), but 10 times bigger than wind tunnel used by Saha et al. (2010). The S-WT10t can be considered as an open field situation. Inlet average velocity used in CFD simulation was from 0.1 to 0.6 m s^{-1} . The computational domain used is a simple rectangular main working section of a wind tunnel. This can be shown as an example of section A-A in Fig. 3.2 for S-WT.

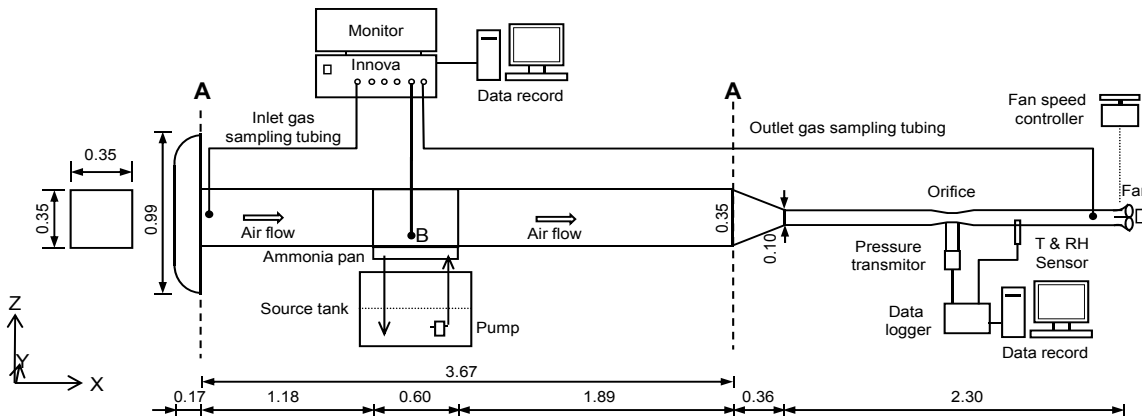


Fig. 3.2 - Schematic of the wind tunnel and the laboratory experiment set-up (all dimensions are in m). A-A section was only considered for CFD simulation.

3.3.1.3. The turbulent airflow model

The shear stress transport (SST) $k-\omega$ model (Menter, 1994) was used for this study. The SST $k-\omega$ model carries out calculations by means of a $k-\omega$ model near wall and a transformed $k-\epsilon$ model in regions far from walls (Menter, 1994). The switch between two models is controlled by blending functions (Zhai et al., 2007). Rong et al. (2010) successfully applied this model in their wind tunnel studies and found SST $k-\omega$ suitable to study mass transfer process in aerial boundary layer compared to the standard $k-\epsilon$ model. An advantage that the $k-\omega$ model has over the $k-\epsilon$ model is that its performance is improved for boundary layers under adverse pressure gradients as the model can be applied to the wall boundary, without using empirical log-law wall functions. This SST $k-\omega$ model provides enhanced resolution of boundary layer on viscous flows (Menter, 1994).

3.3.1.4. Boundary condition

Accurate use of CFD techniques involves defining boundary conditions that match the case being modelled closely enough. Three different types of boundary conditions were adopted in the present computations: velocity inlet, pressure outlet, and wall.

The flow quantities can be extrapolated from interior fluid field. All the wind tunnel surfaces are specified as wall boundary with no-slip condition. For CFD model validation, the inlet air velocity and turbulence intensity were provided according to the data obtained by experimental measurements. For the extended simulations, the inlet air velocity was varied from 0.1 m s⁻¹ to 0.6 m s⁻¹ and constant turbulence intensity of 10% was used in all cases.

The constant NH₃ mass fraction of 7.175×10^{-4} was assumed on the emission surface in all cases for comparison of different wind tunnels' results. It was assumed that the absolute value of ammonia mass fraction on emission surface has no effect on the distribution of the normalized ammonia concentration, which was defined as,

$$m_f = \frac{C_p - C_i}{C_o - C_i} \quad (3.7)$$

where, C_p is the ammonia concentration at the specific point above the emission surface of wind tunnel (mg m⁻³); C_i is ammonia concentration at the inlet of the wind tunnel (mg m⁻³); C_o is ammonia concentration at the outlet of wind tunnel (mg m⁻³).

3.3.1.5. Grid independency

According to the requirement of SST $k-\omega$ model, the flow must be solved to wall directly, in the viscous sub-layer. Thus the y^+ value should be smaller than 1. A grid independency analysis was conducted to ensure that the resolution of the mesh was not influencing the results. The optimum grid distribution was achieved by completing a grid-independence control, during which a number of different simulations were run with different mesh, until the velocity and gas distribution were constant.

3.3.2. *Experiment for model validation*

Model validation is important to ensure adequate results and is necessary before analyzing the airflow pattern, concentration profile, and ammonia emission obtained from the CFD simulations of different size of wind tunnels.

The data used for CFD model validation was generated from an experiment carried out at the Air Physics Lab, Research Centre Bygholm, Faculty of Agricultural Sciences, Aarhus University, Denmark. The wind tunnel (S-WT) used was 3.67-m long, constructed of Polystyrene sheet and contained a 0.60-m long working section for velocity and concentration profile measurement (Fig. 3.2). One side of the tunnel wall that covered this section was made of a 0.8-m long transparent glass for measuring velocity and turbulence intensity using a Laser Doppler Anemometer (Type 58N40-FVA enhanced, DANTEC Dynamics, Skovlunde, Denmark) and for visual inspection when measuring velocity, turbulence intensity, and ammonia concentration above the liquid surface.

An aqueous solution mixed of ammonium chloride (NH_4Cl) solution and a buffer solution of sodium carbonate (Na_2CO_3) and sodium hydrogen carbonate (NaHCO_3) was used in experiment as an ammonia source. The buffer solution was used to keep the constant pH of the aqueous solution. The ammonia solution had a $16,500 \text{ mg l}^{-1}$ TAN concentration and a target pH value of 8.8, which were higher than pig manure, to facilitate the study and maintain a robust balance between ammonium and ammonia during the experiment. The solution was kept circulating with a 6-mm diameter hose and a pump (Type PA1000, Heissner, Germany) during the measurements between the solution pan and the underneath ammonia source tank, in which a 0.25 m deep ammonia solution was kept. The stability of the ammonia aqueous solution was tested prior to the experiment to ensure that the ammonia emission rate under specific conditions could allow the experiment to be performed under steady state.

Four mean wind velocities of 0.1, 0.2, 0.3, and 0.4 m s^{-1} in the tunnel were created for the study by controlling the speed of the fan that was installed at the tunnel exhaust. The measuring location B above the emission surface is shown in Fig. 3.2, and exact location of measurement is described in Table 3.1.

The experimental room air temperature and relative humidity were measured with a temperature/humidity probe (Model Testo 400, Gmbh & Co, Lenzkirch, Germany) that had accuracies of $\pm 0.1^\circ\text{C}$ and $\pm 1\%$, respectively. The wind tunnel exhaust air temperature and relative humidity was measured with a Vaisala Intercap Temperature and Humidity Probe (Model HMP50, Vaisala, Woburn, MA, USA) that had accuracies of $\pm 0.1^\circ\text{C}$ and $\pm 3\%$ at 20°C , respectively. The room air temperature and relative humidity were kept at $22.0 \pm 0.5^\circ\text{C}$ and $29 \pm 3\%$, respectively.

Ammonia concentration was measured sequentially at eight different heights of location B, (see Fig. 3.2) and at the inlet and outlet of the tunnel using a Brüel & Kjær Photoacoustic Multi-gas Monitor (Type 1312, Innova AirTech Instruments, Ballerup, Denmark) and a multiplexer (Type 1309, Innova AirTech Instruments, Ballerup, Denmark). The minimum detection limit of the Multi-gas monitor for ammonia measurement was 0.2 ppm depending on the filter setting. The measurement time at each of the points was 40 min before switching to another point to avoid the delay effects due to channel switching (Rom and Zhang, 2010). The system was operated for at least 30 min to let the airflow conditions to stabilize for each experimental trial before concentration profile measurement. More details description of the measurement and results can be found in the report of Saha et al. (2010).

In addition to the experiment mentioned above, the measured air velocity and concentration profiles in R-WT by Rong et al. (2009) was used for CFD model validation. We assumed that if the SST model can give satisfactory prediction as the experiment results of two wind tunnels (S-WT and R-WT), then this model can also be used for simulating the characteristics of airflow and concentration in other wind tunnels (S-WT1/10th, Y-WT, and S-WT10t) if other criteria of model fulfilled (e.g., grind independency, boundary condition etc.).

3.3.3. Statistical modelling and sensitivity analysis

The wind tunnels' simulation data were used to develop a statistical model and were analysed to obtain the velocity boundary layer thickness (δ_u), concentration boundary layer thickness (δ_c), and the AMTC (k_G) with nonlinear regression using DataFit Program (Version 8.2.79, Oakdale Engineering, Oakdale, PA, USA). The δ_u , δ_c , and AMTC were modelled as a function of wind tunnel height, and average inlet velocity as expressed in Eq. (3.8).

$$D = a \times H^b u_m^c \quad (3.8)$$

where D is δ_u or δ_c or AMTC (k_G) (m or m s^{-1}); a , b , and c are model constants; H is height of the wind tunnel (m); u_m is average wind tunnel velocity (m s^{-1}).

A sensitivity analysis was performed to determine the relative change rates in ammonia mass transfer coefficient with changes in the model parameters (wind tunnel height and average wind tunnel air velocity). Relative sensitivity values were calculated for the different input parameter ranges using the method outlined by Zerihun et al. (1996). The relative sensitivity for each input factor was calculated using Eq. (3.9) for specified ranges within the factor while keeping the other factors that were not being tested constant at their mean values (Liang et al., 2002; Ye et al., 2008a)

$$Sr = \frac{\Delta P \cdot \bar{I}}{\Delta I \cdot \bar{P}} \quad (3.9)$$

where Sr is relative sensitivity (%); ΔP is change in dependent variables (i.e., change in k_G , or δ_u or δ_c) (m or m s^{-1}); \bar{P} is average of dependent variables (i.e., k_G , or δ_u or δ_c) (m or m s^{-1}); ΔI is change in input parameter over the range being considered (m or m s^{-1}); \bar{I} is average value of the input parameter (m or m s^{-1}).

3.4. Results and discussion

3.4.1. Grid independency

The result of the grid independence for wind tunnel S-WT1/10th, Y-WT, S-WT, and S-WT10t are displayed in Fig. 3.3. No large differences between the solutions on the last two meshes can be observed. The 667550 grids were considered for the investigations in S-WT1/10th, S-WT, and S-WT10t wind tunnels. For wind tunnel R-WT, the grid independence has been conducted by Rong et al. (2010), the final grids' number was 561680. The optimum grid was 909696 for wind tunnel Y-WT, which were determined by grid independence study as shown in Fig. 3.3b.

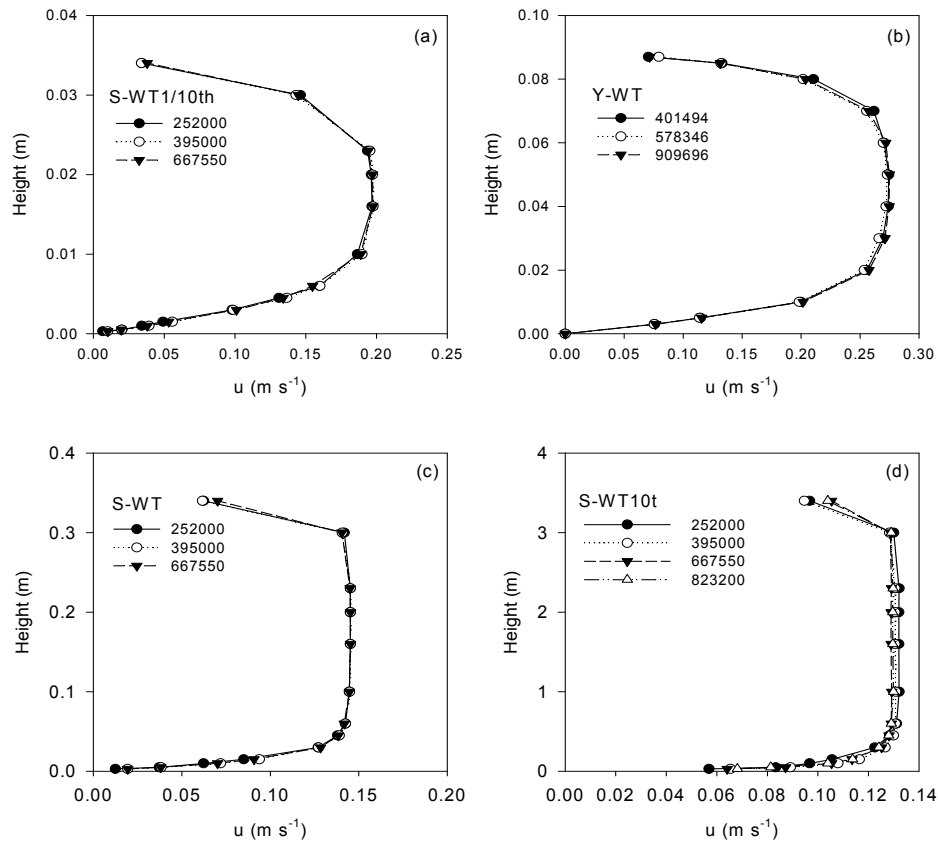


Fig. 3.3 - Grid independence studies of four wind tunnels at the inlet velocity of 0.1 m s^{-1} for the wind tunnels (a) S-WT1/10th, (c) S-WT, and (d) S-WT10t and at the inlet velocity of 0.2 m s^{-1} for (b) Y-WT. Number in the legends are grid numbers.

3.4.2. CFD model validation

The comparisons between the experimental and the numerical data of velocity and concentration profiles confirm the validity of the numerical model used in the CFD simulation (Fig. 3.4 and Fig. 3.5). The characteristics of measured velocity, and concentration profiles were reasonably revealed by the numerical simulation with the SST model. The coefficient of determination (R^2) values of measurement and simulated velocities for S-WT, and R-WT were 0.98 (Fig. 3.4a2), and 0.93 (Fig. 3.4b2) respectively. The coefficient of determination (R^2) values of measurement and simulated concentrations for S-WT, and R-WT were 0.99 (Fig. 3.5a2), and 0.97 (Fig. 3.5b2) respectively.

However, there are discrepancies at the near-wall area between simulated and measured velocity. One explanation could be possible uncertainty might exist for laser-doppler anemometer precisely located at the specific measurement positions, although the much attention was paid to it. The discrepancies in measured concentration and simulated concentration could be because of difficulty in measuring concentrations near the emission surface, where a very small difference in measurement height might give large differences in concentration (Saha et al., 2010). In spite of the

uncertainties in the experiment and simulation, the preliminary results illustrate that numerical model is feasible for modelling characteristics of airflow and concentration above the emission surface in a emission measurement facility like a wind tunnel or a dynamic flux chamber, and consequently the emission process. The SST model is thereby applied further in the following simulation cases.

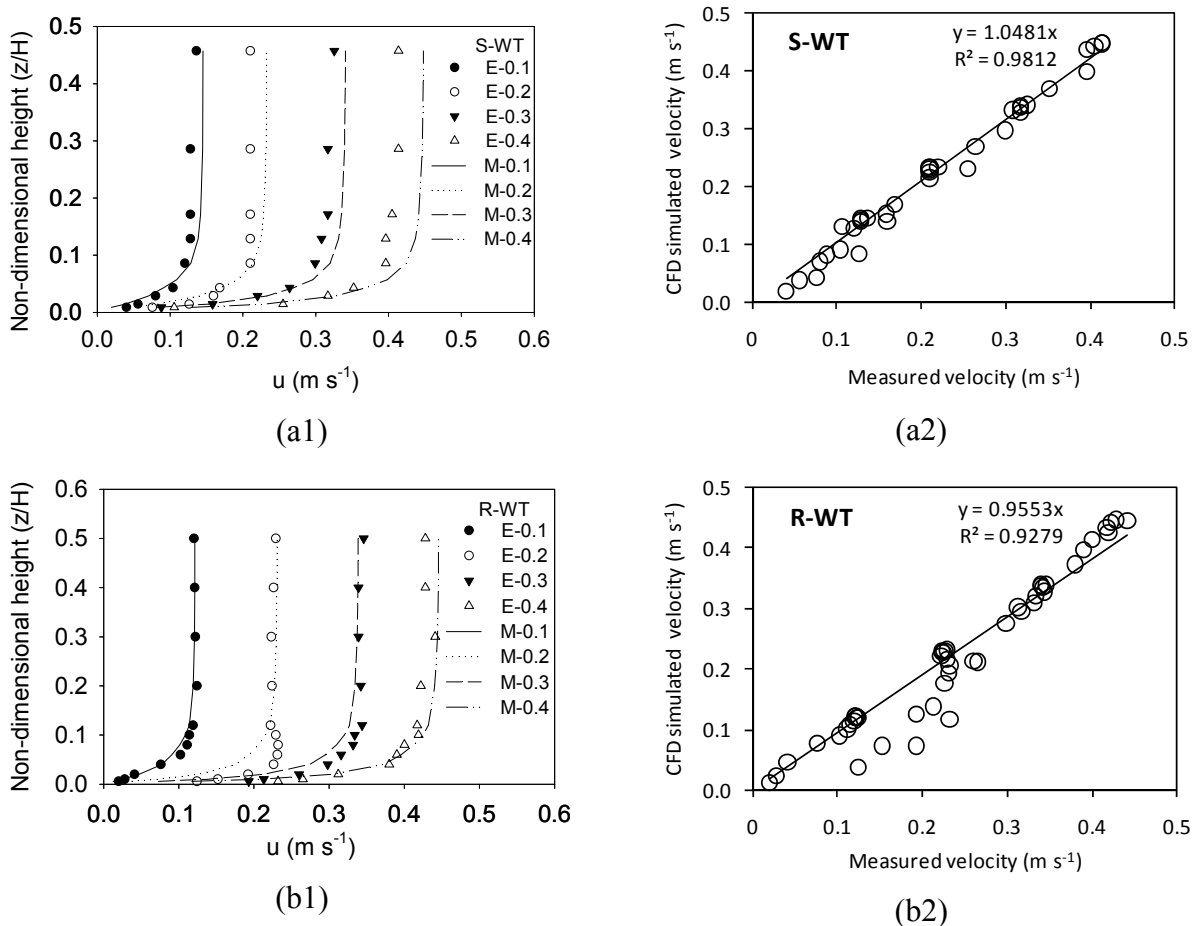


Fig. 3.4 - Comparison of velocity profiles between simulations and measurements of two wind tunnels (a) S-WT and (b) R-WT. where E represent experiment and M represent model.

3.4.3. Effect of inlet velocity and wind tunnel sizes on velocity and concentration boundary layer thickness

The simulated and measured non-dimensional velocity profiles and concentration profiles above the emission surface in S-WT and R-WT are showed in Fig. 3.4 and Fig. 3.5. They are in accordance with the universal logarithm velocity profiles description. Air velocity at different heights increased with increase of mean air velocity Fig. 3.6. The lowest air velocities were found at the bottom of the profiles, which became lower again when it reached close to the ceiling. The reduced wind velocities close to the ammonia release surface and the tunnel ceiling were caused by shear effects,

which were the results of wind friction on the release surface and the tunnel ceiling. Similar results of such friction may also be found in a wall jet development in a room space, where wall weakened the jet and ultimately reduced the wind velocity near to the wall (Adre and Albright, 1994; Strom et al., 2002; Zhang et al., 2000).

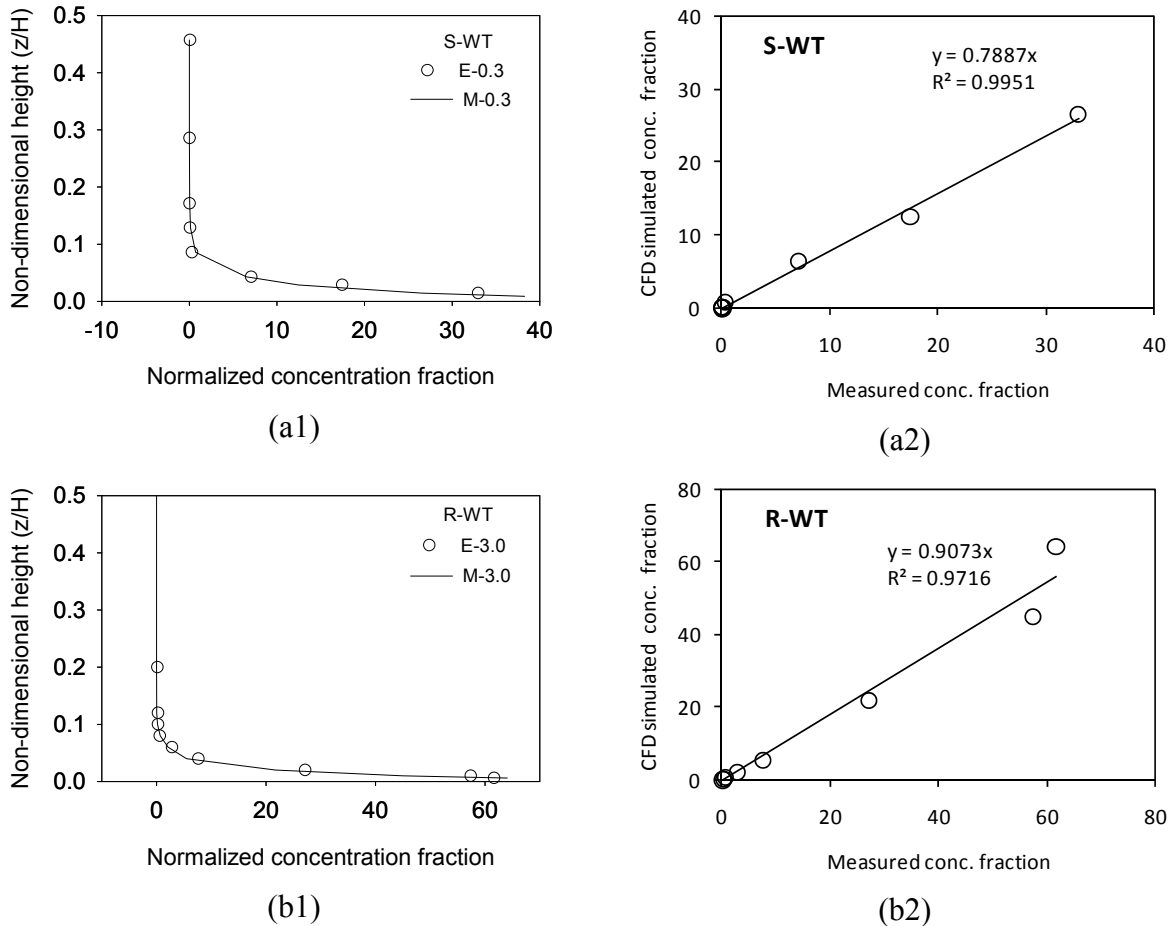
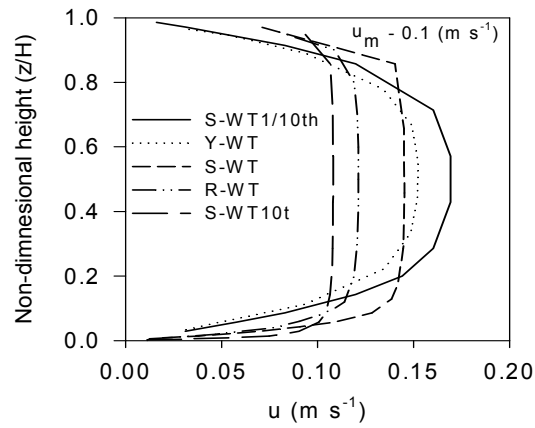


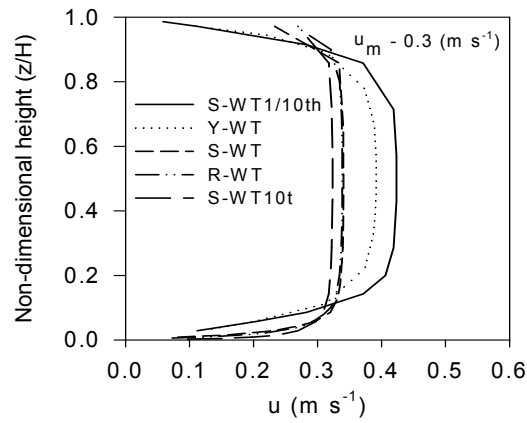
Fig. 3.5 - Comparison of normalized concentration profiles between simulation and measurement results with inlet air velocity of 0.3 m s^{-1} and turbulence intensity of 10% of two wind tunnels (a) S-WT and (b) R-WT. where E represent experiment and M represent model.

On the other hand, air velocity profile was more tapered in the smaller wind tunnels than larger wind tunnels (Fig. 3.6) at the same inlet velocities, where highest velocity was observed in the middle of the smallest wind tunnel than the higher WTs. These tapering rates among the tunnels were big in low inlet velocity (Fig. 3.6a) than in higher velocities (Fig. 3.6b & c). Wind tunnel heights might have played an important role for tapering air velocities. As for example, S-WT10t tunnel height was largest among the WTs, where air velocity tapered less than the other WTs, than might affect on boundary layer thickness. These variations much lower in higher velocities, some

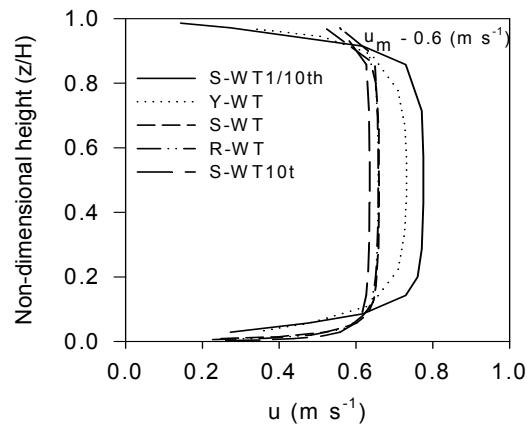
cases diminished if the wind tunnel size difference was not big, such as for wind tunnels S-WT and R-WT (Fig. 3.6c).



(a)



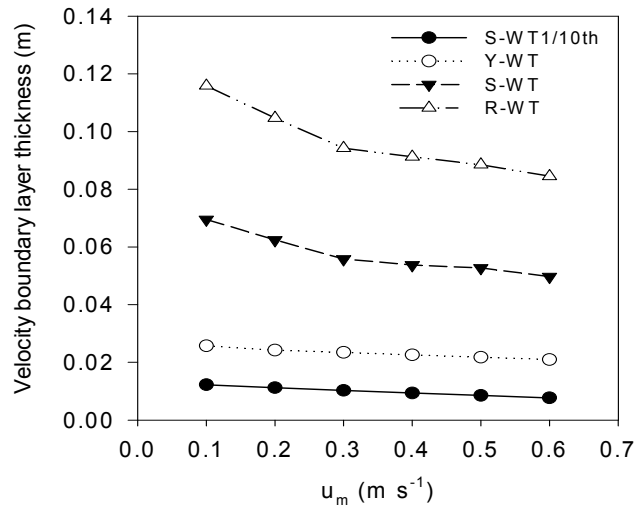
(b)



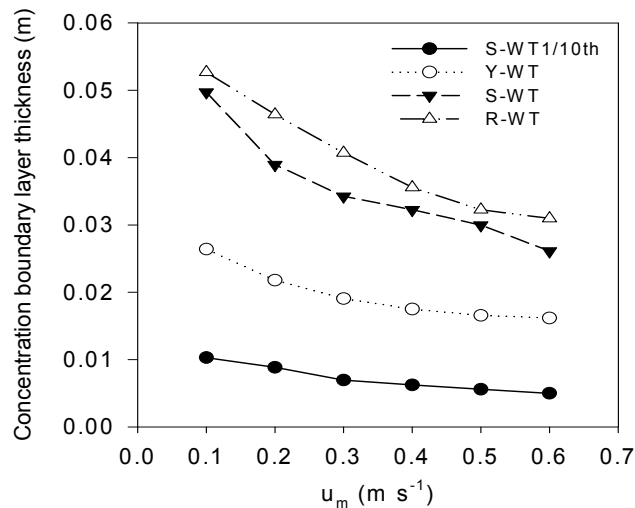
(c)

Fig. 3.6 - Simulated velocity profiles of five different wind tunnels above the emission surface in inlet velocities of (a) 0.1 m s^{-1} , (b) 0.3 m s^{-1} , and (c) 0.6 m s^{-1} respectively.

Effect on average inlet air velocity on velocity and concentration boundary thicknesses are shown in Figs. 3.7a and b, respectively. To maintain resolution of the figure, S-WT10t tunnel thickness data was not presented in these two figures. Air velocity boundary layer thickness (δ_u) decreased with increase of mean inlet air velocity in all wind tunnel sizes (Fig. 3.7a). Increasing air speed inside the tunnel increased wall shear stress and surface friction therefore reduced the boundary layer thickness (Schlichting and Gersten, 2003). The boundary thickness decreased more from 0.1 m s⁻¹ to 0.3 m s⁻¹ and decrease slightly over a velocity ranging from 0.3 m s⁻¹ to 0.6 m s⁻¹



(a)



(b)

Fig. 3.7 - Average inlet velocities and wind tunnel heights affect on (a) velocity boundary layer thickness (δ_u) and (b) concentration boundary layer thickness (δ_c).

for the wind tunnels S-WT and R-WT. But the effect of average inlet velocity on boundary layer thickness was not significant ($P > 0.05$) in that ranges of velocity. The trends are in agreement with study reported by Rong et al (2009). The concentration boundary layer thickness (δ_c) was higher in

low inlet air velocity than higher inlet velocities (Fig. 3.7b), which has same trend as velocity boundary layer thickness. The differences in the thicknesses of the δ_u and δ_c tended to be much smaller in higher velocities, because turbulence induces mixing (Incropera et al., 2007). However, the concentration boundary was thinner than the corresponding velocity boundary layer since mass transfer by molecular diffusion is generally a much slower process than momentum transfer. According to the boundary layer theory, increasing air velocity would result in a thinner concentration boundary layer at the liquid-gaseous interface (Haslam et al., 1924), which will consequently reduce emission resistance.

On the other hand, wind tunnel size had a significant effect on both δ_u and δ_c ($P < 0.001$). In an air velocity range from 0.1 to 0.6 m s⁻¹, smaller size wind tunnel narrowed the air velocity profile than the bigger wind tunnel (Fig. 3.6). At the same inlet air velocity, boundary layer thicknesses were smaller in a small wind tunnel than that in a larger wind tunnel (Figs. 3.7a & b). For example, at the average inlet velocity of 0.3 m s⁻¹, δ_u for S-WT1/10th, Y-WT, S-WT, R-WT, and S-WT10t were 0.01029, 0.02341, 0.05583, 0.09421, and 0.5583 m respectively and δ_c for S-WT1/10th, Y-WT, S-WT, R-WT, and S-WT10t were 0.00695, 0.01904, 0.03425, 0.04069, and 0.2259 m, respectively. The simulation results indicate that although inlet air velocities are maintained the same, the different sizes especially heights of wind tunnels may result in different velocity profiles, therefore different boundary layer thickness. The reduction of tunnel height increases the sweep wind speed (Fig. 3.6) (Frechen et al., 2004), therefore affected on δ_u and δ_c . Smith and Watts (1994) also showed in their analytical simulation that the velocity profiles in the two tunnels are different, with the velocity gradient greatest in the small tunnel. Therefore, mass transfer rate will be increased in smaller wind tunnels.

Using the simulation results, non-linear regressions analysis of air velocity boundary layer thickness (δ_u) with the wind tunnel height (H), and average wind tunnel velocity (u_m) may be established as follows:

$$\delta_u = 0.141 \times H^{0.94} u_m^{-0.18} \quad (R^2=0.97) \quad (3.10)$$

With 95% confidence intervals, the standard errors for the model parameters $a = 0.141$, $b = 0.94$, and $c = -0.18$ are 1.74×10^{-2} , 0.105, and 5.65×10^{-2} , respectively. The standard error of estimate was 5.93×10^{-3} .

Similarly concentration boundary layer thickness (δ_c) may be stated as:

$$\delta_c = 0.039 \times H^{0.51} u_m^{-0.31} \quad (R^2=0.97) \quad (3.11)$$

With 95% confidence intervals, the standard errors for the model parameters $a = 0.039$, $b = 0.51$, and $d = -0.31$ are 4.49×10^{-3} , 6.02×10^{-2} , and 5.89×10^{-2} , respectively. The standard error of estimate was 2.63×10^{-3} .

From Eq. (3.10) and Eq. (3.11), it can be seen that the wind tunnel height (H) has stronger effect on boundary layers development than other parameters. Wind tunnel height has more effect on δ_u than δ_c . The correlations also show that δ_u and δ_c change with average inlet velocity power -0.18 and -0.31 respectively. With the increase of H increased boundary layer thicknesses. On the other hand, boundary layer thickness reduces with the increase of inlet velocity. Both δ_u and δ_c were found sensitive at lower air velocity and smaller wind tunnel heights than higher velocities and heights. Boundary layer thicknesses δ_u and δ_c were more sensitive to wind tunnel height than to average wind tunnel air velocity. As the boundary layer thickness of concentration increase with the wind tunnel size, higher boundary layer thickness will provide bigger resistance to mass transfer processes from the emission surface according to boundary layer theory.

3.4.4. Effect of inlet velocity and wind tunnel sizes on ammonia emission

Simulated emission fluxes of five different wind tunnels at the inlet velocity ranged from 0.1 to 0.6 m s^{-1} is shown in Fig. 3.8. With the increasing inlet air speed, the ammonia emission flux increased. This trend is in line other researcher's studies (Saha et al., 2010; Vlek and Stumpe, 1978; Ye et al., 2008a; Zhang et al., 2008). Increasing inlet air velocity reduced the concentration boundary layer thickness (Fig. 3.7b) and therefore increased mass transfer process and ammonia emission. This result corroborates with Rong et al. (2009).

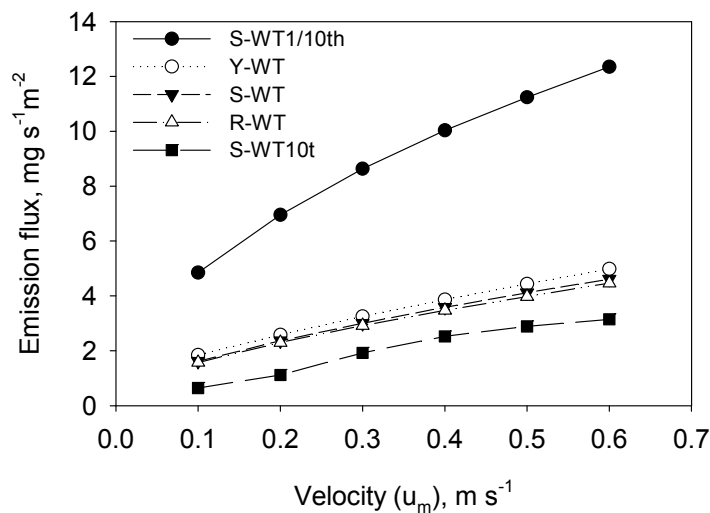


Fig. 3.8 - Simulated emission rates of five different wind tunnels at inlet velocities of 0.1 to 0.6 m s^{-1} .

By examining the simulation results, it was observed that the ammonia emission flux was lower in the higher wind tunnels at the same velocities ($P < 0.001$). Wind tunnels S-WT1/10th, Y-WT, S-WT, and R-WT were 79%, 45%, 40%, and 38% over estimated ammonia emission respectively, compared with the wind tunnel S-WT10t. This is also supported by the results described in the previous sections, i.e., with the increase of height of wind tunnels increased the

velocity and concentration boundary layer thickness, therefore increased resistance, and reduced mass transfer process in the boundary layer. The contour plots of four wind tunnels in Fig. 3.9 showed the ammonia concentration distribution inside tunnels at inlet velocities of 0.3 m s^{-1} . It can be seen that thicker boundary layer was built up in higher wind tunnel height. The relative concentration reference height (defined as the height with concentration of 50 mg m^{-3} compared to wind tunnel height) indicated that majority of air flowed through relatively lower concentration zone in bigger wind tunnels than smaller size of wind tunnels. At the same velocity, more air flushed with low concentration, causing lower concentration at outlet. Therefore emission flux was lower in big wind tunnel than smaller wind tunnels. However, emission flux differences among the different heights of Y-WT, S-WT, and R-WT tunnels were not significant ($P > 0.05$). Comparing with S-WT, Y-WT was given 8.4% over estimation and R-WT was given 3% lower estimation.

According to the simulation results, a statistical correlation of AMTC (k_G) with the wind tunnel height (H), and average wind tunnel velocity (u_m) may be established as follows:

$$k_G = 0.0036 \times H^{-0.48} u_m^{0.54} \quad (R^2=0.84) \quad (3.12)$$

With 95% confidence intervals, the standard errors for the model parameters $a = 0.0036$, $b = -0.48$, and $c = 0.54$ are 1.34×10^{-3} , 0.115, and 0.208, respectively. The standard error of estimate was 1.34×10^{-3} .

Model sensitivity analysis using eq. (3.9) showed that the mass transfer coefficient was more sensitive at lower than at higher wind tunnel heights. The relative sensitivity was -129.48% for height interval between 0.095 and 0.115 m and -26.42% for wind tunnel height interval 0.335 and 0.355 m. A negative value of sensitivity for variation of wind tunnel height means that increasing the wind tunnel height reduced the mass transfer rate. The k_G was also more sensitive at lower than at higher air velocities. The relative sensitivity was 82.53% for velocity interval between 0.05 and 0.1 m s^{-1} and 38.87% for velocity interval 0.35 and 0.4 m s^{-1} . These velocity results were in agreement with the study of Saha et al. (2010). The results also showed that the k_G value was more sensitive to wind tunnel height than to average wind tunnel velocity in lower wind tunnel height and air velocity.

Therefore, much attention should be paid on wind tunnel size, especially on wind tunnel height during wind tunnel design for emission estimation. The effects of wind tunnel height on boundary layer thickness and their effects on mass transfer process highlight the importance of standardization of DFC or wind tunnel for emission measurement from the fields.

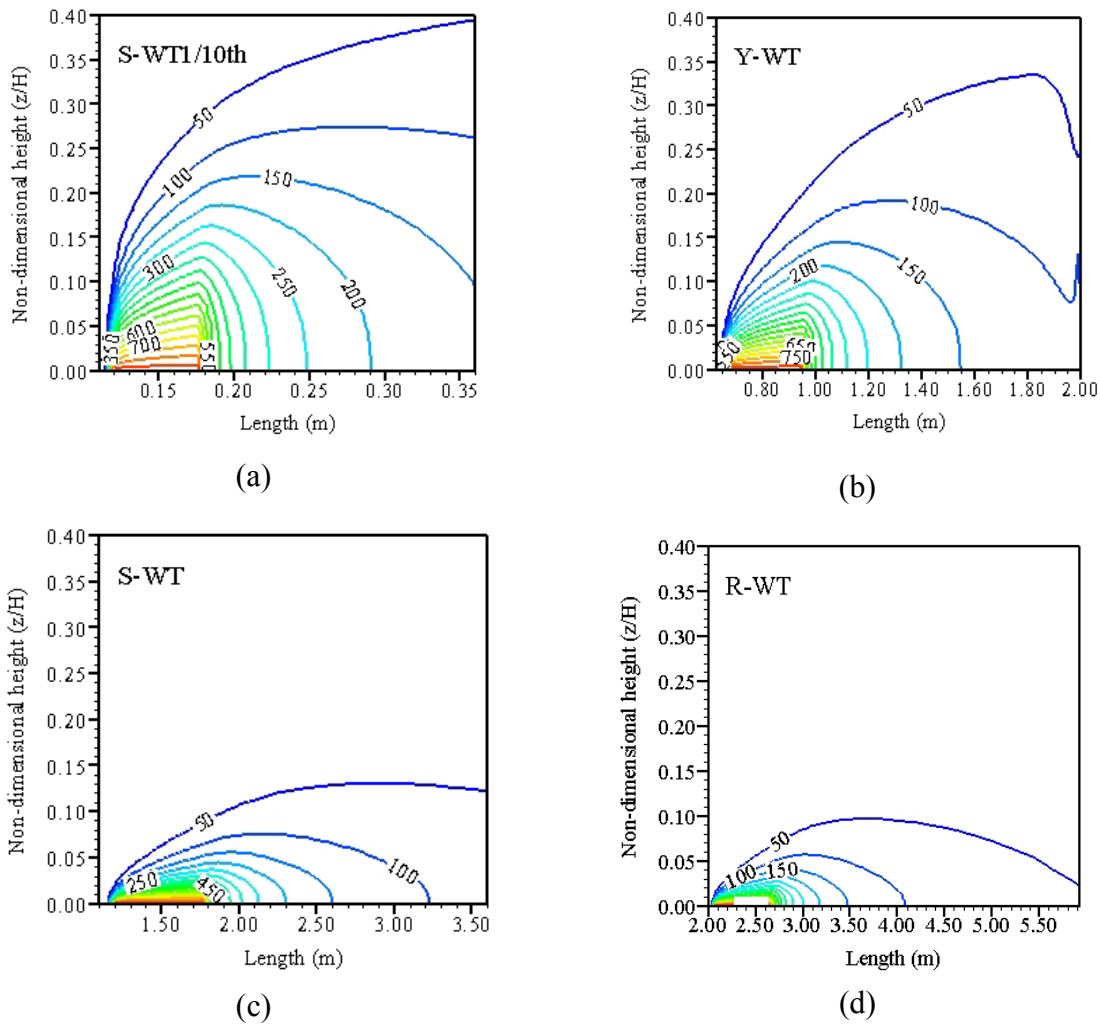


Fig. 3.9 - Contour plot of concentration inside four different wind tunnels at average inlet velocity of 0.3 m s^{-1} . The values in the plots indicate ammonia concentration in mg m^{-3} .

3.5. Conclusions

Computational fluid dynamics (CFD) simulations of velocity and concentration profiles using SST model reasonably agreed with the measurements. The shear stress transport (SST) model was considered to be capable of predicting the transfer process in the boundary layer for further simulation of different scenarios.

Both of experiment and CFD simulation showed that the velocity and concentration boundary layer thickness decreased with the increase of inlet air velocity where the concentration boundary was thinner than the corresponding velocity boundary layer. Wind tunnel size has significant effects on velocity and concentration boundary layer thicknesses ($P < 0.001$). Air velocity boundary layer thickness (δ_u) and concentration boundary layer thicknesses (δ_c) were smaller in small size wind tunnel than the large wind tunnels. Non-linear regression analysis of velocity boundary layer

thickness (δ_u) and concentration boundary layer thicknesses (δ_c) were established with wind tunnel height (H), and average wind tunnel air velocity (u_m) ($R^2=0.97$).

The wind tunnel size especially height has significant effect on ammonia emission and mass transfer process ($P < 0.001$). These differences were not significant among the wind tunnels Y-WT, S-WT, and R-WT ($P > 0.05$). The smaller wind tunnels were over estimated ammonia emission, comparing to the larger wind tunnel or the open field situation. A statistical approach was developed to calculate ammonia mass transfer coefficient (k_G) as a function of wind tunnel height, and average wind tunnel velocity ($R^2 = 0.84$). It was found that k_G was more sensitive to the wind tunnel height than to air velocity.

The work shows that designers and users of wind tunnels for emission estimation have to be aware of wind tunnel height. In addition our results indicated that wind tunnel height needs to be taken into account for generic model development process.

References

- Adre, N., Albright, L. D., 1994. Criterion for Establishing Similar Air-Flow Patterns (Isothermal) in Slotted-Inlet Ventilated Enclosures. *Transactions of the ASAE*, 37 (1), 235-250.
- Baklanov, A., 2000. Application of CFD methods for modelling in air pollution problems: Possibilities and gaps. *Environmental Monitoring and Assessment*, 65(1-2), 181-189.
- Bjerg, B., Morsing, S., Svidt, K., Zhang, G., 1999. Three-dimensional airflow in a livestock test room with two-dimensional boundary conditions. *Journal of Agricultural Engineering Research*, 74 (3), 267-274.
- Bjerg, B., Svidt, K., Zhang, G., Morsing, S., 2000. The effects of pen partitions and thermal pig simulators on airflow in a livestock test room. *Journal of Agricultural Engineering Research*, 77(3), 317-326.
- Bjerg, B., Svidt, K., Zhang, G., Morsing, S., Johnsen, J. O., 2002. Modeling of air inlets in CFD prediction of airflow in ventilated animal houses. *Computers and Electronics in Agriculture*, 34(1-3), 223-235.
- Chen, Q. Y. 2009. Ventilation performance prediction for buildings: A method overview and recent applications. *Building and Environment*, 44 (4), 848-858.
- Frechen, F. B., Frey, M., Wett, M., Loser, C., 2004. Aerodynamic performance of a low-speed wind tunnel. *Water Science and Technology*, 50 (4), 57-64.
- Gao, F., Yates, S. R., 1998. Laboratory study of closed and dynamic flux chambers: Experimental results and implications for field application. *Journal of Geophysical Research-Atmospheres*, 103 (D20), 26115-26125.
- Hansen, M. N., Henriksen, K., Sommer, S. G., 2006. Observations of production and emission of greenhouse gases and ammonia during storage of solids separated from pig slurry: Effects of covering. *Atmospheric Environment*, 40(22), 4172-4181.

- Haslam, R. T., Hershey, R. L., Keen, R. H., 1924. Effect of gas velocity and temperature on rate of absorption. *Industrial and Engineering Chemistry*, 16, 1224-1230.
- Hudson, N., Ayoko, G. A., 2008. Odour sampling. 2. Comparison of physical and aerodynamic characteristics of sampling devices: A review. *Bioresource Technology*, 99 (10), 3993-4007.
- Hudson, N., Ayoko, G. A., 2009. Comparison of emission rate values for odour and odorous chemicals derived from two sampling devices. *Atmospheric Environment*, 43 (20), 3175-3181.
- Hudson, N., Ayoko, G. A., Dunlop, M., Duperouzel, D., Burrell, D., Bell, K., Gallagher, E., Nicholas, P., Heinrich, N., 2009. Comparison of odour emission rates measured from various sources using two sampling devices. *Bioresource Technology*, 100 (1), 118-124.
- Incropera, F. P., DeWitt, D. P., Bergman, T. L., Lavine, A. S., 2007. *Fundamentals of Heat and Mass Transfer*. Sixth Edition, John Wiley & Sons.
- Liang, Z. S., Westerman, P. W., Arogo, J., 2002. Modeling ammonia emission from swine anaerobic lagoons. *Transactions of the ASAE* 45 (3), 787-798.
- Menter, F. R., 1994. 2-Equation Eddy-Viscosity Turbulence Models for Engineering Applications. *AIAA Journal*, 32 (8), 1598-1605.
- Norton, T., Grant, J., Fallon, R., Sun, D. W., 2009. Assessing the ventilation effectiveness of naturally ventilated livestock buildings under wind dominated conditions using computational fluid dynamics. *Biosystems Engineering*, 103 (1), 78-99.
- Norton, T., Grant, J., Fallon, R., Sun, D. W., 2010. Optimising the ventilation configuration of naturally ventilated livestock buildings for improved indoor environmental homogeneity. *Building and Environment* 45 (4), 983-995.
- Norton, T., Sun, D. W., Grant, J., Fallon, R., Dodd, V., 2007. Applications of computational fluid dynamics (CFD) in the modelling and design of ventilation systems in the agricultural industry: A review. *Bioresource Technology*, 98 (12), 2386-2414.
- Peu, P., Beline, F., Martinez, J., 1999. A floating chamber for estimating nitrous oxide emissions from farm scale treatment units for livestock wastes. *Journal of Agricultural Engineering Research*, 73 (1), 101-104.
- Quinn, A. D., Wilson, M., Reynolds, A. M., Couling, S. B., Hoxey, R. P., 2001. Modelling the dispersion of aerial pollutants from agricultural buildings - an evaluation of computational fluid dynamics (CFD). *Computers and Electronics in Agriculture*, 30 (1-3), 219-235.
- Ravikrishna, R., Valsaraj, K. T., Yost, S., Price, C. B., Brannon, J. M., 1998. Air emissions from exposed, contaminated sediment and dredged materials - 2. Diffusion from laboratory-spiked and aged field sediments. *Journal of Hazardous Materials*, 60 (1), 89-104.
- Reichman, R., Rolston, D. E., 2002. Design and performance of a dynamic gas flux chamber. *Journal of Environmental Quality* 31 (6), 1774-1781.

- Rom, H. B., Zhang, G. Q., 2010. Time Delay for Aerial Ammonia Concentration Measurements in Livestock Buildings. *Sensors*, 10 (5), 4634-4642.
- Rong, L., Nielsen, P. V., Zhang, G. Q., 2009. Effects of airflow and liquid temperature on ammonia mass transfer above an emission surface: Experimental study on emission rate. *Bioresource Technology*, 100 (20), 4654-4661.
- Rong, L., Nielsen, P. V., Zhang, G. Q., 2010. Experimental and Numerical Study on Effects of Airflow and Aqueous Ammonium Solution Temperature on Ammonia Mass Transfer Coefficient. *Journal of the Air & Waste Management Association*, 60 (4), 419-428.
- Saha, C. K., Zhang, G., Ni, J. Q., 2010. Airflow and concentration characterisation and ammonia mass transfer modelling in wind tunnel studies. *Biosystems Engineering*, 107 (4), 328-340.
- Schlichting, H., Gersten, K., 2003. *Boundary Layer Theory*. Springer.
- Smith, R. J., Watts, P. J., 1994. Determination of Odor Emission Rates from Cattle Feedlots. 2. Evaluation of 2 Wind Tunnels of Different Size. *Journal of Agricultural Engineering Research*, 58 (4), 231-240.
- Strom, J. S., Zhang, G., Morsing, S., 2002. Predicting near-floor air velocities for a slot-inlet ventilated building by jet velocity decay principles. *Transactions of the ASAE*, 45 (2), 407-413.
- Sun, H., Stowell, R. R., Keener, H. M., Michel, F. C., 2002. Two-dimensional computational fluid dynamics (CFD) modeling of air velocity and ammonia distribution in a High-Rise (TM) hog building. *Transactions of the ASAE*, 45(5), 1559-1568.
- Topp, C., Nielsen, P. V., Heiselberg, P., 2001. Influence of local airflow on the pollutant emission from indoor building surfaces. *Indoor Air-International Journal of Indoor Air Quality and Climate*, 11 (3), 162-170.
- Vallee, C., Hoehne, T., Prasser, H. M., Suehnel, T., 2008. Experimental investigation and CFD simulation of horizontal stratified two-phase flow phenomena. *Nuclear Engineering and Design*, 238 (3), 637-646.
- Versteeg, H. K., Malalasekera, W., 2007. *An Introduction to computational fluid dynamics-the finite volume method*. 2nd edition, Pearson-Prentice Hall, Pearson Education Limited, England.
- Vlek, P. L. G., Stumpe, J. M., 1978. Effects of Solution Chemistry and Environmental-Conditions on Ammonia Volatilization Losses from Aqueous Systems. *Soil Science Society of America Journal*, 42 (3), 416-421.
- Xia, B., Sun, D. W., 2002. Applications of computational fluid dynamics (CFD) in the food industry: a review. *Computers and Electronics in Agriculture*, 34 (1-3), 5-24.
- Ye, Z., Zhang, G., Li, B., Strom, J. S., Dahl, P. J., 2008a. Ammonia Emissions Affected by Airflow in A Model Pig House: Effects of Ventilation Rate, Floor Slat Opening, and Headspace Height in A Manure Storage Pit. *Transactions of the ASABE*, 51 (6), 2113-2122.

- Ye, Z., Zhang, G., Li, B., Strom, J. S., Tong, G., Dahl, P. J., 2008b. Influence of airflow and liquid properties on the mass transfer coefficient of ammonia in aqueous solutions. *Biosystems Engineering*, 100 (3), 422-434.
- Zerihun, D., Feyen, J., Reddy, J. M., 1996. Sensitivity analysis of furrow-irrigation performance parameters. *Journal of Irrigation and Drainage Engineering-ASCE*, 122 (1), 49-57.
- Zhai, Z., Zhang, W., Zhang, Z., Chen, Q. Y., 2007. Evaluation of various turbulence models in predicting airflow and turbulence in enclosed environments by CFD: part 1 - Summary of prevalent turbulence models. *HVAC&R Research*, 13 (6), 853-870.
- Zhang, G., Bjerg, B., Strom, J. S., Morsing, S., Kai, P., Tong, G., Ravn, P., 2008. Emission effects of three different ventilation control strategies - A scale model study. *Biosystems Engineering*, 100 (1), 96-104.
- Zhang, G., Morsing, S., Bjerg, B., Svidt, K., Strom, J. S., 2000. Test room for validation of airflow patterns estimated by computational fluid dynamics. *Journal of Agricultural Engineering Research*, 76 (2), 141-148.
- Zhang, G., Svidt, K., Bjerg, B., Morsing, S., 1999. Buoyant flow generated by thermal convection of a simulated pig. *Transactions of the ASAE*, 42 (4), 1113-1120.

Chapter 4

Ammonia emission process affected by ventilation airflow, pen partition and location of emission surface and ammonia mass transfer modelling in a model pig house

Paper III:

Saha, C. K., Zhang, G., and Kai, P. 2011. Ammonia emission process affected by ventilation airflow, pen partition and location of emission surface and ammonia mass transfer modelling in a model pig house. Submitted to a peer review journal.

Abstract

The influences of airflow characteristics (i.e., floor air velocities and floor air turbulence intensities) on ammonia mass transfer processes were investigated in a model of finishing pig house. The 1:6 scale model was 1.75m×1.00m×0.605m (L×W×H) and had two sidewall inlets and an exhaust in the middle of the ceiling. Different airflow characteristics were generated by using three ventilation control strategies, i.e., constant inlet opening area, constant inlet velocity, and constant inlet momentum. In addition, the effects of pen partition and location of the emission surface on ammonia emission were also examined under different airflow conditions. Non-linear models were developed to relate surface airflow characteristics and ammonia mass transfer coefficient (AMTC) with the inlet opening height, the inlet air velocity and the jet momentum number. The investigations showed that the changes in ventilation control strategies, given the variation of surface air characteristics, changed ammonia emission and AMTC. Ammonia emissions were 8 to 14% less with pen partition than without pen partition. For emission areas located near the side wall, ammonia emissions were about 4 to 22% and 22 to 41% lower compared to those located 0.25m and 0.5m away from the left side wall, respectively. The mean floor air velocities and the root mean square of the floor air velocity fluctuations were correlated to the jet momentum number to the power 0.56 and 0.54 respectively. AMTC increased proportionally to floor air velocity and turbulence intensity at different heights. The AMTC values determined in this experiment were compared to a work using a 1:12.5 model. Correlation of AMTC and jet momentum number for the two models was similar and showed that AMTC was proportional to jet momentum number to the power of 0.23 for fully rotary airflow when the emission source was located in the middle of the pen.

Key words: Ammonia emission, ventilation rate, air velocity, turbulence intensity, jet momentum number, model pig house

Nomenclature

A	ammonia release surface area, m ²	U	average inlet air velocity, m s ⁻¹
a	model constant	u	time average floor air velocity, m s ⁻¹
b	model constant	u'	air velocity fluctuation, m s ⁻¹
C	ammonia concentration, mg m ⁻³	VR	ventilation rate, m ³ s ⁻¹
c	model constant	Δk_G	change in AMTC, m s ⁻¹
E	emission rate, mg s ⁻¹	ΔI	change in input parameter, m s ⁻¹ or %
g	gravitational acceleration rate, m s ⁻²	ΔP	pressure difference, pa
H	room height, m	α_1	model constant
h	height of the inlet opening, m	α_2	model constant
\bar{I}	average value of input parameter, m s ⁻¹ or %	β_1	model constant
J	jet momentum number	β_2	model constant
K_D	dissociation constant	Subscripts	
K_G	ammonia mass transfer coefficient, m s ⁻¹	a	average
K_H	Henry's constant	f	bulk air
L	room length, m	i	inlet
T	temperature, °K	m	mean
TAN	total ammonium nitrogen, mg l ⁻¹	o	outlet/overall
Re	Reynolds number	rms	root mean square
Sr	relative sensitivity, %		

4.1. Introduction

Ammonia emissions to the atmosphere are environmentally important, not only because of its effects on the chemistry of air pollutants in the atmosphere, but also because of undesirable ecological effects of nitrogen compounds when deposited back to land and water bodies (Phillips et al., 2000). Therefore, it is vital that ammonia emissions are regulated to reduce environmental impacts. Approximately 75% of the ammonia emission in Europe originates from livestock production (Webb et al., 2005). Thus, an understanding of the processes leading to ammonia emissions is critical in order to reduce the environmental impact of livestock production.

Approximately 50% of the national ammonia emissions in the Netherlands, Denmark, and France are from pig housing and outside storage of pig slurry (van der Peet-Schwering et al., 1999). The main part of Danish pig farms manage the pig manure as slurry. The floor of the pig pens consists of fully slatted floor or partially slatted floor with a shallow slurry pit underneath. The ammonia is mainly released from the surface of the slurry and the fouled floor surfaces.

Ammonia gas at the liquid-air interface is transported through the laminar boundary layer by molecular diffusion and then in most cases through the turbulent layer to the ventilation air by turbulent diffusion and advection (Ni, 1999; Sommer et al., 2006). The transfer of gas between a slurry surface and the air flow depends mainly on the dynamic structure of the flow in the boundary layer (Bird et al., 2007) and the airflow pattern (Morsing et al., 2008). The airflow patterns are affected by several factors such as ventilation rate (Strom et al., 2002), inlet air-jet momentum (Zhang et al., 2008), floor design (Morsing et al., 2008), height of the pit headspace (Buiter and Hoff, 1998; Ye et al., 2008a), partitions in the room, heat produced by the animals, and animal behaviours (Bjerg et al., 2000; Zhang and Strom, 1999).

The effects of air velocity and air temperature on ammonia emission in a scale model of a dairy cow house were found (Elzing and Monteny, 1997; Wang et al., 2006). Morsing *et al.* (2008) found that the NH_3 emission was significantly affected by the different airflow patterns created by the floor type and the slurry channel layout. Saha et al. (2010a) showed that guiding the airflow using a partial pit ventilation system improved the indoor air quality significantly. The influence of air velocity, turbulence and ventilation rate on NH_3 emission rate was reported by Ye et al. (2008b). The effects of headspace heights on the slurry pit, the slatted floor opening, and the ventilation rate on ammonia emission and airflow characteristics using real slurry were studied (Ye et al., 2008a; Ye et al., 2009b). The scale of a pig building of their study was 1:12.5. Topp et al. (2001) indicated that local airflow affects pollutant emission from the indoor building surface. Zhang et al. (2008) investigated the effects of three different ventilation control strategies on the NH_3 emission and estimated air exchanges between the manure pit headspace and the room space. The scale model that Zhang et al. (2008) and Ye et al. (2008b) used were 1:12.5 pig house models. In these works, the air velocity and the local air flow pattern above the emission surface were not reported. Quantification of airflow characteristics and their effects on the mass transfer process in terms of

inlet air momentum were, however, addressed. To make a step forward to apply the results in full scale, it is very important to assess the correlations of floor air velocities and AMTC from the emission source with room geometry (room height and room length), and with inlet height and mean inlet air velocity. In a full scale pig house, it is difficult to measure floor air velocities in practice, due to animal activity. Based on published literature, it is clear that effects of location, emission areas and physical structures within the livestock house, e.g., pen partitions on ammonia emission remain important topics that need further investigation with focus on the airflow patterns and ventilation.

A scale model may generate airflow conditions more closely related to full-scale room in terms of airflow patterns and the velocity profile (Ye et al. 2008b) as compared to a wind tunnel. Although the flow pattern may be similar in a model with different scales, the differences of model dimensions do affect the emission process. An important characteristic is the turbulence scale. The size of main eddy in a model air space is related to the height of the model and that may affect the mass transfer process. Smith and Watts (1994) found in their field studies that the height of the tunnel could consistently change the estimation of the emission rate. Their study suggested that a smaller tunnel height would enhance the emission rate by increasing the wind speed gradient at the surface for a same bulk wind speed. Bjerg et al. (1999) studied the three dimensional effect on airflow in a full scale test room of a Danish pig rearing unit. They found that the relation between room width and room height had influenced the development of the three-dimensional airflow. Topp et al. (1997) mentioned that using small-scale test chambers, a difference in scale may lead to different emission rates. Chen (2009) mentioned in his recent review that the small-scale experimental models are very effective and economical when studying ventilation performance in buildings. However, in addition to scaling issues associated with thermo-fluid dimensionless parameters, it can be rather challenging to scale down complex flow geometry. The airflow pattern/magnitude of the floor air velocities and emission of scale model should correspond to the full scale situation.

The objective of this study was to contribute to increasing the fundamental knowledge of ammonia mass transfer processes in scale models. The specific objectives were to: 1. characterise the airflow and the aerial boundary layer above an ammonia releasing surface in different ventilation control strategies in a scale model (1:6) ; 2. assess the effect of locations of the emission area and physical structures (pen partition) on ammonia emissions as regulated by different floor airflow characteristics; 3. model ammonia mass transfer as affected by the floor airflow characteristics and by combining inlet opening height and mean inlet air velocities; and 4. compare the results in this study with the work by Ye et al. (2008b) using a 1:12.5 scale model.

4.2. Materials and methods

The experiments were carried out in the Air Physics Lab, Faculty of Agricultural Sciences, Aarhus University, Denmark.

4.2.1. Scale model

The scale model was made of 10 mm thick acrylic glass with an inside dimensions of 1750 mm × 1000 mm × 605 mm (L × W × H) and a corridor with two partition walls of 145 mm height, (Fig. 4.1). Ventilation air was supplied through adjustable flaps at two sides beneath the ceiling spanning the whole width of the model with the maximum opening height of 95 mm. The outlet opening was 78mm under the centre of the ceiling. The exhaust air was extracted through a 70 mm internal diameter pipe by using a variable-speed axial-flow ventilation fan (type K315 L, System air AB, SE-739 30 Skinnskatteberg, Sweden). A Lubcke VARIO[®] variable transformer drive (type RV10806-20, Noratel Lubcke A/S, Brøndby, Denmark) was used to control the fan speed. A pan with surface area of 980 mm × 375 mm and a depth of 70 mm filled with ammonia aqueous solution was used as emission source. The remaining surface areas were covered with a 5 mm thick Polystyrene sheet. The pan with aqueous ammonia may be located in different positions according to the experiment set-up.

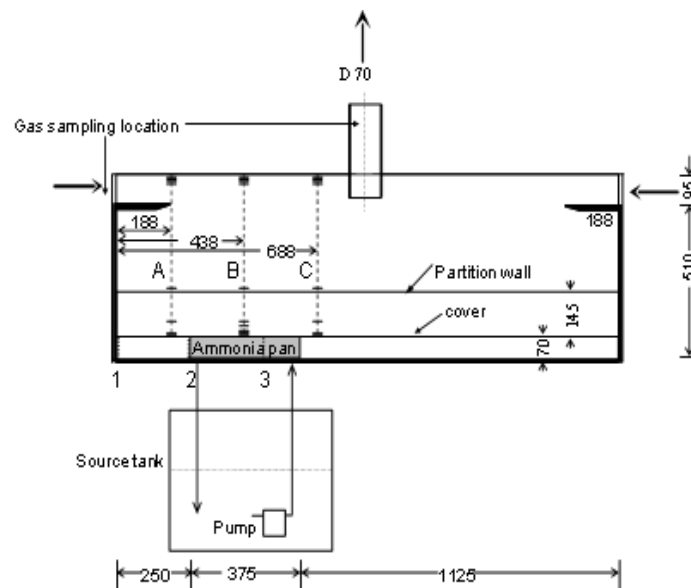


Fig. 4.1- The laboratory study set-up of a 1:6 scale model experiment (all dimensions are in mm). A, B, and C are velocity profile measuring locations and 1, 2, and 3 are slurry pit locations (starting end) from the left side wall.

4.2.2. Ammonia aqueous solution

The ammonia aqueous solution used for the experiment was the combination of a source solution and a buffer solution. An ammonium chloride (NH_4Cl) solution was made as the ammonia source. The buffer solution of sodium carbonate (Na_2CO_3) and sodium hydrogen carbonate (NaHCO_3) was used to maintain the aqueous solution at a constant pH. The ammonia solution had a 23000 mg l^{-1} TAN (total ammoniac nitrogen) concentration and a constant pH value of 8.7. The TAN value was higher than the pig manure to keep a steady state in the solution with respect to available nitrogen and maintain a robust balance between ammonium and ammonia during the experiment. The solution was kept circulating at the flow rate of $0.05 \text{ m}^3\text{hr}^{-1}$ from the ammonia source tank placed under the scale model using a 6-mm diameter hose and a pump (type PA1000, Heissner, Germany). The volume of the total ammonia solution was about 110 L. The stability of the ammonia aqueous solution was tested prior to the experiment to ensure that the ammonia emission rate under specific conditions could allow the experiment to be performed under steady state. The continuous circulation maintained a 70 mm deep reservoir of ammonia solution in the pan and provided a constant free ammonia concentration at the immediate liquid surface (C_s) even during the ammonia release process.

Liquid samples taken from the return flow were used to check the TAN concentrations and pH values before and after each experimental trial. The TAN measurement was made according to ISO 7150/1, while pH was measured with a pH detector (type Sension 1, HACH-LANGE, Bronshoj, Denmark).

4.2.3. Experimental set-ups

To create different airflow conditions above the liquid surface in the scale model studies, the experiments were conducted using four ventilation airflow rates and three control strategies, namely, constant inlet opening area by keeping inlet opening height constant (0.01 m), constant mean inlet velocity (1 m s^{-1}) by changing inlet opening height with the ventilation rates, and constant inlet jet momentum ($0.024 \text{ kg m s}^{-2}$) using combination of inlet opening heights and ventilation rates for emission source location 2, (Fig. 4.1), i.e., 250 mm away from the left side wall (Table 4.1). Inlet jet momentum is defined here as mass flow rate multiplied by average air velocity at the inlet.

To investigate the effects of locations of the ammonia emission surfaces, the distance of the left edge of the emission surface to the left side wall for locations 1, 2, and 3 were 10 mm, 250 mm and 500 mm, respectively (Fig. 4.1). The pen partition wall was removed in one case to investigate its effects on ammonia emission.

Table 4.1- Experiment set up/Control strategies used in the scale model experiment

Control strategies	Emission source distance* (m)	Inlet opening height (m)	Ventilation rate ($\text{m}^3 \text{s}^{-1}$)	Total inlet opening area (m^2)	Inlet velocity (m s^{-1})	Inlet jet momentum, (kg.m s^{-2})	Inlet Re
Constant inlet opening area	0.25	0.010	0.02	0.02	1	0.024	700
	0.25	0.010	0.04	0.02	2	0.096	1400
	0.25	0.010	0.06	0.02	3	0.216	2100
	0.25	0.010	0.08	0.02	4	0.384	2800
Constant inlet velocity	0.25	0.010	0.02	0.02	1	0.024	700
	0.25	0.020	0.04	0.04	1	0.048	1400
	0.25	0.030	0.06	0.06	1	0.072	2100
	0.25	0.040	0.08	0.08	1	0.096	2800
Constant inlet jet momentum	0.25	0.010	0.02	0.02	1	0.024	700
	0.25	0.040	0.04	0.08	0.50	0.024	1400
	0.25	0.092	0.06	0.18	0.33	0.024	2125
Constant inlet opening area	0.01	0.010	0.02	0.02	1	0.024	700
	0.01	0.010	0.04	0.02	2	0.096	1400
	0.01	0.010	0.06	0.02	3	0.216	2100
	0.01	0.010	0.08	0.02	4	0.384	2800
Constant inlet opening area	0.50	0.010	0.02	0.02	1	0.024	700
	0.50	0.010	0.04	0.02	2	0.096	1400
	0.50	0.010	0.06	0.02	3	0.216	2100
	0.50	0.010	0.08	0.02	4	0.384	2800

Note: * Distance of left edge of emission source from the left side wall; Re-Reynolds number

4.2.4. Measurement

4.2.4.1. Ventilation airflow rates and air velocities

A FMU/FMDRU 100-80 flow meter (Lindab A/S, Denmark), which was based on an orifice tapping principle was used to measure the ventilation airflow rates. The error of the flow measuring method was 5-10% depending on the distance to the flow disturbance. By measuring the pressure difference between the measurement nozzles, the ventilation rate in the duct was calculated using Eq (4.1).

$$VR = 0.00732\sqrt{\Delta P} \quad (4.1)$$

where VR is ventilation rate ($\text{m}^3 \text{s}^{-1}$) and ΔP is pressure difference (Pa).

The pressure differences were measured using a differential pressure sensor (Model 694, Huba Control, Würenlos, Switzerland) with a measurement range of 10-300 Pa, an accuracy of \pm

0.7%, and a resolution of 0.1% of full scale. The pressure sampling period was every 10 s and the averaged data were saved every min in a data logger (Model CR215, Campbell Scientific, Logan, Utah, USA). The mean inlet air velocity was calculated using mean ventilation rate divided by inlet cross-sectional area.

A Laser Doppler Anemometer (Type 58N40-FVA enhanced, DANTEC Dynamics, Skovlunde, Denmark) was used to measure the air velocities and velocity fluctuation associated with turbulence or unsteadiness. It measured the velocity using light beams at a point in a flow seeded by small particles which could follow the turbulent motion of the flow. It senses true velocity component and measures that component in a sequence of near instantaneous samples. The velocity of each point was measured for 8 min. Air velocities and turbulence intensities were measured at the three locations A, B, and C of the model (Fig. 4.1). In each location, the air velocity and turbulence intensity profile measurements were taken at 12 different vertical heights (0.005, 0.010, 0.015, 0.020, 0.030, 0.040, 0.150, 0.495, 0.500, 0.505, 515, and 0.525 m above the floor). Air velocity and root mean square (rms) of velocity fluctuation of jet airflow at specific point above the floor surface were defined here as mean floor air velocity (u_m) of time average air speed of 8 min, and root mean square of velocity fluctuation (u_{rms}) of mean floor air velocity (Hoff, 1995). This mean floor air velocity (u_m) and root mean square of velocity fluctuation (u_{rms}) were found directly after each measurement with the Laser Doppler.

Smoke was used in the experiments to indicate the direction of airflow and to provide a quick visualization of the path of the airstreams.

4.2.4.2. Ammonia concentration

Measurements of ammonia concentrations were performed sequentially at the inlet and outlet of the scale model (Fig. 4.1) using a Brüel & Kjær Photoacoustic Multi-gas Monitor (Type 1312, Innova AirTech Instruments, Ballerup, Denmark) and a multiplexer (Type 1309, Innova AirTech Instruments). The minimum detection limit of the Multi-gas Monitor for ammonia measurement was 0.2 ppm depending on the filter setting. The sample integration time configured in the Monitor for the experiment was 20 s. The inlet and outlet measurements provided ammonia concentrations in the incoming and outgoing air. The measurement time at each of the points was 40 min before switching to another point. It was found that at least 10-15 min were required for the ammonia concentration reading to stabilize following measurement of higher ammonia concentration samples (Rom and Zhang, 2010). Therefore, an instrument was vented to ensure correct concentration readings, especially when the concentration of the previous air sample was high. The system was operated for at least 30 min to let the airflow conditions stabilize for each experimental trial.

4.2.4.3. Temperature and relative humidity

The experiments were carried out under isothermal conditions in a laboratory room. To monitor the thermal conditions and variations during the entire experiment period, the air temperature and relative humidity in the scale model exhaust were measured using Vaisala Intercap Humidity and Temperature Probes (Vaisala Humitter 50Y, FI-00421, Helsinki, Finland) that had accuracies of $\pm 0.1^\circ\text{C}$ and $\pm 3\%$ at 20°C , respectively. The data measured were averaged and saved per minute in a data logger (Model CR215, Campbell Scientific, Logan, Utah, USA).

4.2.5. *Estimation of ammonia emission and ammonia mass transfer coefficient*

Surface emission can be described in terms of the convective mass transfer coefficient and the difference between the concentration at the surface and the bulk air concentration. Under steady state conditions and without any sink in the enclosure, ammonia emission equals ammonia release and the core model can be expressed in Eq. (4.2).

$$E = k_G A (C_s - C_f) \quad (4.2)$$

where E is emission rate (mg s^{-1}), k_G is ammonia mass transfer coefficient (AMTC) (m s^{-1}), A is ammonia release surface area (m^2), C_s is gaseous ammonia concentration at immediate liquid surface (mg m^{-3}), and C_f is the ammonia concentration in the bulk air (mg m^{-3}).

Ammonia emission from a scale model can be calculated by:

$$E = VR(C_o - C_i) \quad (4.3)$$

where E is emission rate (mg s^{-1}), VR is the ventilation rate ($\text{m}^3 \text{s}^{-1}$), C_o is the outlet or exhaust ammonia concentration (mg m^{-3}), and C_i is ammonia concentration at the scale model inlet (mg m^{-3}).

Rearranging Eq. (4.2) and Eq. (4.3), Eq. (4.4) is obtained (Ye et al., 2008b).

$$k_G = \frac{VR(C_o - C_i)}{A(C_s - C_f)} \quad (4.4)$$

The measured outlet NH_3 concentrations (C_o) were chosen to represent the values of (C_f) by assuming well mixed concentrations of room air at the outlet (Ye et al., 2008b), C_o and VR can be experimentally determined, and A is a constant, the AMTC (k_G) in scale model can be calculated using Eq. (4.4) if C_s is known. However, although the gaseous ammonia concentration in the bulk air stream can be easily measured, it is still difficult to measure it at the immediate liquid surface (Saha et al., 2010b). Therefore, the C_s was almost always theoretically calculated by using Henry's constant, dissociation constant, association constant, Total ammoniac nitrogen (TAN) concentration, and pH value (Arogo et al., 1999; Bliss et al., 1995; Ni, 1999; Saha et al., 2010b).

The C_s in Eq. (4.4) was calculated using Eq. (4.5)

$$C_s = \frac{[TAN]}{K_H \left(1 + \frac{[H^+]}{K_D} \right)} \quad (4.5)$$

where [TAN] is the concentration of TAN (mg L^{-1}), K_H is the Henry constant, K_D is dissociation constant, and $[H^+]$ is the solution surface proton concentration, can be expressed by pH value in Eq. (4.6).

$$pH = -\log[H^+] \quad (4.6)$$

Eq. (4.7) from Jayweera and Mikkelsen (1990) and Eq. (4.8) from VanderMolen et al. (1990) were used for calculating dissociation constant (K_D) and Henry's constant (K_H).

$$K_D = 10^{-\left(0.0897 + \frac{2729}{T}\right)} \quad (4.7)$$

where K_D is dissociation constant, dimensionless, and T is temperature ($^{\circ}\text{K}$).

$$K_H = 10^{-\left(1.69 + \frac{1477.7}{T}\right)} \quad (4.8)$$

where K_H is Henry's constant, dimensionless, and T is temperature ($^{\circ}\text{K}$).

4.2.6. Modelling and sensitivity analysis

In the data analysis, the values calculated by Eq. (4.4) using the experimental results were used to develop statistical models. Mean floor air velocities and floor air turbulence intensities at specific height above the emission surface were considered for characterizing AMTC (k_{G1}). The non-linear modelling was performed by using the Data Fit program (Version 8.2.79, Oakdale Engineering, Oakdale, PA, USA), in which the k_{G1} was expressed as a function of mean floor air velocity and turbulence intensity:

$$k_{G1} = a u_m^b T_i^c \quad (4.9)$$

where k_{G1} is the ammonia mass transfer coefficient (m s^{-1}), u_m is the mean floor air velocity (m s^{-1}), and T_i is the floor air turbulence intensity (%), a is gain, and b and c are empirical constants.

Floor air turbulence intensity was defined here

$$T_i = \frac{u'_{rms}}{u_m} \times 100 \quad (4.10)$$

where T_i is the turbulence intensity (%), u_m is mean floor air velocity (m s^{-1}), u'_{rms} is root mean square of velocity fluctuations of floor air velocity (m s^{-1}).

For correlation of AMTC with the inlet heights and the mean inlet velocities and room geometry, first the mean floor air velocities and rms of floor air velocities were correlated to the jet momentum number:

$$u_m = \alpha_1 J_i^{\beta_1} \quad (4.11)$$

and

$$u'_{rms} = \alpha_2 J_i^{\beta_2} \quad (4.12)$$

where u_m is the mean floor air velocity ($m s^{-1}$), u'_{rms} is the root mean square of velocity fluctuations of floor airflow ($m s^{-1}$), J_i is the jet momentum number, α_1 , α_2 are gain, and β_1 , β_2 are empirical constants for u_m and u'_{rms} respectively.

The dimensionless jet momentum number would be defined as (Barber et al., 1982)

$$J_i = \frac{VR U_i}{gV} \quad (4.13)$$

where VR is the average ventilation rate ($m^3 s^{-1}$), U_i is mean inlet air velocity ($m s^{-1}$), g is acceleration due to gravity ($m s^{-2}$), V is room volume (m^3).

For an inlet length that is equal to the room width and the inlet openings at both sidewalls, Eq. (4.13) can be written as

$$J_i = \frac{2h_i U_i^2}{gLH} \quad (4.14)$$

where J_i is the dimensionless jet momentum number, U_i is the mean inlet air velocity ($m s^{-1}$), h_i is the inlet opening height (m), g is the gravitational constant, ($m s^{-1}$), L is the length of the scale model (m), and H is the height of the scale model ceiling from the emission surface (m).

By substituting Eq. (4.11) and Eq. (4.12) in Eq. (4.10), Ti relation with jet momentum number was obtained as Eq. (4.15):

$$Ti = \left[\frac{\alpha_2}{\alpha_1} J_i^{(\beta_2 - \beta_1)} \right] \times 100 \quad (4.15)$$

Then relationship of AMTC with J_i was established by putting Eq. (4.11) and Eq. (4.15) in Eq. (4.9), which was found through non-linear regression analysis. Finally the relationship between the inlet opening height (h_i), the mean inlet velocities (U_i), the room length (L), and the room height (H) and the AMTC (k_{G1}) was established using Eq. (4.14) for the particular scale model (1:6).

A sensitivity analysis was performed to determine the relative change rates in the ammonia mass transfer coefficient with changes in the model parameters (air velocity, and turbulence intensity). Relative sensitivity values were calculated for the different input parameter ranges using the method outlined by Zerihun et al. (1996). The relative sensitivity for each input factor was calculated using Eq. (4.16) by varying the factor under analysis in specified ranges while keeping the other factors constants at their mean values (Liang et al., 2002; Ye et al., 2008a).

$$Sr = \frac{\Delta k_{G1} \times \bar{I}}{\Delta I \times \bar{k}_{G1}} \quad (4.16)$$

where Δk_{G1} is the change in mass transfer coefficient (m s^{-1}), $\overline{k_{G1}}$ is the average mass transfer coefficient (m s^{-1}), \bar{I} is the average value of the input parameter, (m s^{-1} or %) ΔI is the change in input parameter over the range being considered (m s^{-1} or %), and Sr is the relative sensitivity (%).

4.2.7. Ammonia emission and ammonia mass transfer coefficient model Comparison

Ammonia emissions and AMTC models based on the results of this study and those of Ye et al. (2008b) were compared. Although the dimensions of the two scale models were different, the methodologies and experimental conditions were comparable. The scale model used by Ye et al. (2008b) was 1:12.5. All the data were obtained under conditions of isothermal and constant liquid surface ammonia concentration in scale model experiments (Table 4.2). The performance of the AMTC (k_{G2}) model by Ye et al. (2008b), where the mean floor air velocity and the mean turbulence intensity at 0.01m and 0.04m above the surface were used and compared to the performance of the AMTC (k_{G1}) defined in this study. The similar procedure was followed to relate k_{G2} with the jet momentum number.

Table 4.2 - Experimental conditions with two scale models (SM) for ammonia mass transfer studies

Parameter	This study	Ye et al., 2008b
SM dimension (L×W×H) (m^3)	1.75×1.0 ×0.605 ^a	0.84×0.50×0.45 ^b
SM maximum inlet height (m)	0.095	0.045
Ammonia release surface area (Ls×W) (m^2)	0.98×0.38	0.5×0.18
Air temperature ($^{\circ}\text{C}$)	22.3±0.4	22±1
Ammonia solution pH	8.7	8.7
TAN concentration (mg l^{-1})	23,000	5,100
Cs (mg m^{-3})	1848	452
Ventilation rate range ($\text{m}^3 \text{s}^{-1}$)	0.02 to 0.08	0.005 to 0.020
Inlet air velocity range (m s^{-1})	1 to 4	1 to 4
Reynolds number (Re)	700-2800	350-1400

Note: Total height of the scale models above the emission surface to ceiling were 0.54 m for this study^a and 0.28 m for Ye et al. 2008b study^b.

4.3. Results and discussion

The room air temperature was maintained at a constant level during the experimental period (Table 4.3). The room air temperature and relative humidity recorded were $22.3 \pm 0.4^{\circ}\text{C}$ and $30.9 \pm 1.5\%$, respectively. The exhaust air temperature and the relative humidity were $21.9 \pm 0.3^{\circ}\text{C}$ and $33.4 \pm 1.4\%$, respectively.

Table 4.3 - Test conditions and relative ammonia concentrations measured at the inlet and outlet of the exhaust air.

Control strategies	Emission source distance* (m)	Ventilation rate ($\text{m}^3 \text{s}^{-1}$)	Inlet air velocity (m s^{-1})	Room air temperature ($^{\circ}\text{C}$)	Exhaust air temperature ($^{\circ}\text{C}$)	Room air RH (%)	Exhaust air RH (%)	Inlet concentration (mg m^{-3}) (SD)	Outlet concentration (mg m^{-3}) (SD)
Constant inlet opening area	0.25	0.02	1	22.41	22.03	29.83	32.75	1.13 (0.08)	46.17 (2.22)
	0.25	0.04	2	22.18	21.85	29.77	32.39	2.58 (0.21)	33.74 (0.94)
	0.25	0.06	3	21.52	21.35	30.07	32.22	1.74 (0.12)	27.71 (0.59)
	0.25	0.08	4	22.49	22.03	33.24	35.59	2.97 (0.05)	23.93 (0.45)
Constant inlet opening area [#]	0.25	0.02	1	21.42	21.22	28.56	31.96	1.85 (0.13)	46.01 (2.22)
	0.25	0.04	2	21.79	21.57	28.56	31.40	1.85 (0.13)	37.59 (1.58)
	0.25	0.06	3	21.85	21.59	28.94	31.40	1.99 (0.13)	28.97 (1.33)
	0.25	0.08	4	22.51	22.09	33.01	35.28	2.12 (0.13)	23.97 (0.61)
Constant inlet velocity	0.25	0.02	1	22.41	22.03	29.83	32.75	2.58 (0.19)	46.17 (2.22)
	0.25	0.04	1	22.73	22.23	29.85	32.39	2.97 (0.05)	26.96 (1.23)
	0.25	0.06	1	22.71	22.41	30.78	32.36	2.15 (0.11)	20.05 (0.85)
	0.25	0.08	1	22.47	22.06	33.29	34.85	2.21 (1.16)	17.93 (0.74)
Constant inlet jet momentum	0.25	0.02	1	22.41	22.03	29.83	32.75	2.58 (0.19)	46.17 (2.22)
	0.25	0.04	0.5	22.51	22.11	32.74	34.51	2.21 (1.16)	24.64 (1.69)
	0.25	0.06	0.33	22.70	22.33	32.26	33.40	1.93 (0.08)	14.85 (1.67)
Constant inlet opening area	0.01	0.02	1	22.26	22.12	29.94	32.63	2.03 (0.11)	35.25 (2.59)
	0.01	0.04	2	22.25	22.07	30.14	32.64	2.21 (0.07)	30.59 (1.41)
	0.01	0.06	3	22.31	22.03	30.18	32.62	2.03 (0.11)	24.62 (0.81)
	0.01	0.08	4	21.87	21.54	31.85	33.80	1.79 (0.08)	21.92 (0.74)
Constant inlet opening area	0.50	0.02	1	22.09	21.77	31.87	35.89	2.31 (0.13)	59.41 (2.72)
	0.50	0.04	2	22.21	21.83	31.97	35.29	2.31 (0.13)	43.03 (1.22)
	0.50	0.06	3	22.24	21.90	32.28	35.07	2.42 (0.14)	33.21 (0.71)
	0.50	0.08	4	22.43	22.00	32.36	34.89	2.54 (0.15)	27.57 (0.72)

[#]without pen partition ; * from left side wall ; SD - Standard deviation

4.3.1. Effect of ventilation control strategies on airflow patterns and airflow characteristics inside the scale model

The airflow pattern in the scale model with two side wall inlets and an exhaust unit at the middle of the ceiling showed that the supply air from two side wall inlets met in the middle of the room and then travelled downwards and mainly entered the headspace near the centre of the room, travelled parallel to the slurry surface and then returned to the room air near the side walls (Fig. 4.2). These symmetric air flow patterns were in line with the results from previous studies (Ye et al., 2009a).

Air velocities were higher close to the ceiling surface and slowed down towards the centre of the model space due to the raised entrainment in flow path by compensating the initial momentum of the air-jet from the inlet. At a constant inlet opening height, the inlet air velocity increased with increasing of ventilation rate, and this resulted in a higher air velocity at the emission surface (Fig. 4.3). The jet air velocity at location B (Fig. 4.1) was higher for an inlet opening height of 0.04m than an opening of 0.01m due to a higher ventilation rate which ultimately resulted in higher floor or return air velocity (Figs 4.3 a and b) where inlet Reynolds numbers (Re) were 700 and 2800

respectively (Table 4.1). On the other hand, turbulence intensity showed opposite characteristics than air velocity (Fig. 4.3c and d). At low air velocity, the turbulence intensity was higher. Turbulence intensity did not show a clear pattern like air velocity except for inlet opening height 0.04m and inlet velocity 0.1 m s⁻¹ in which case strong velocity was observed at location B.

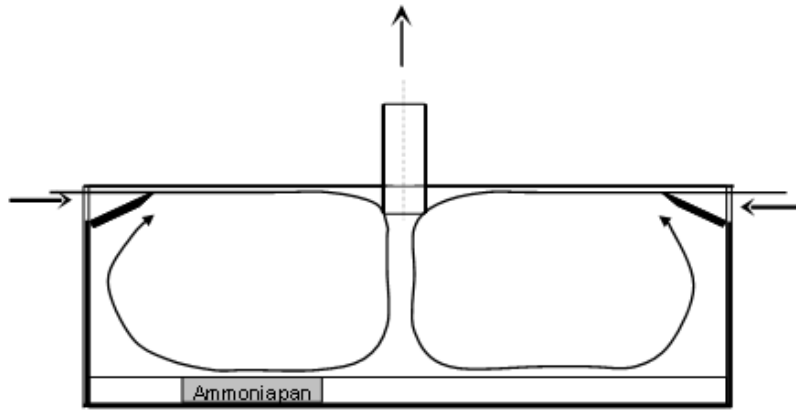


Fig. 4.2 - Air flow pattern in a model pig house from the smoke test.

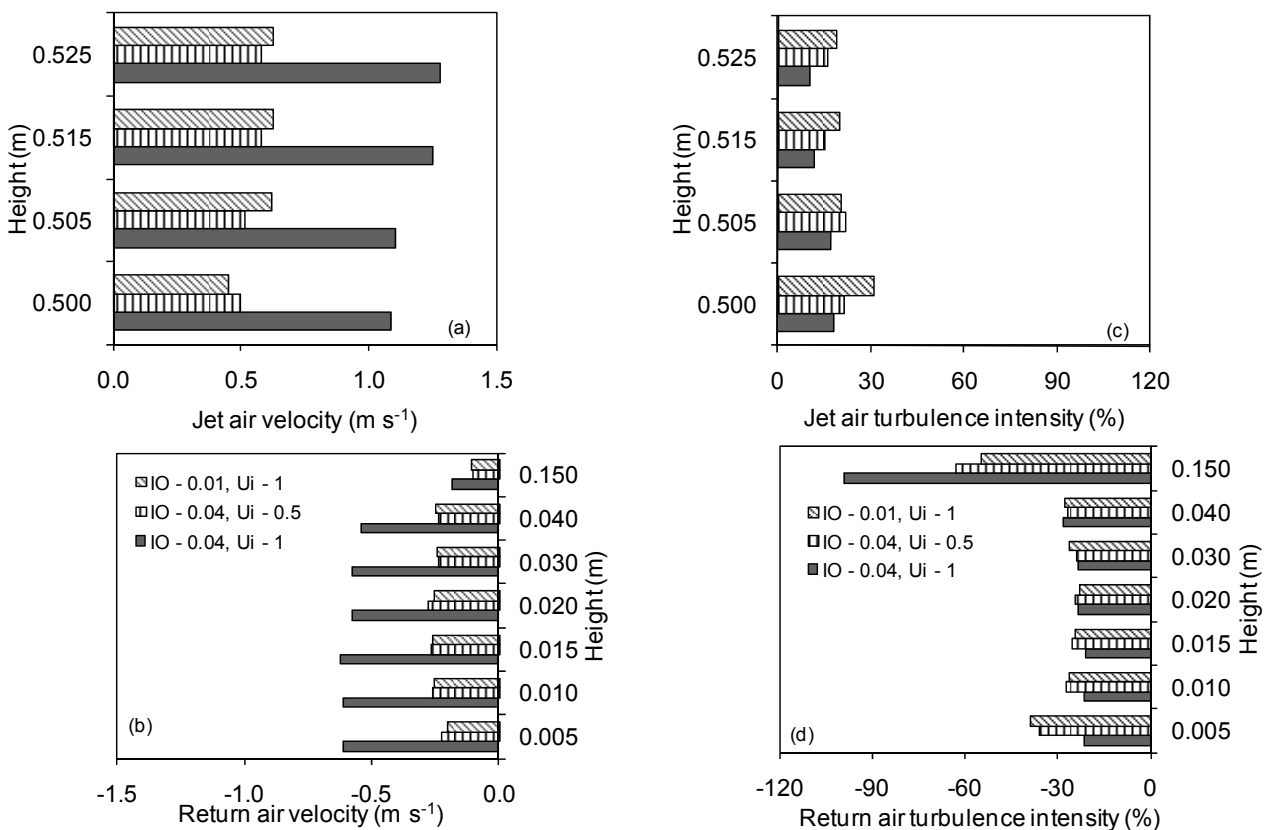


Fig. 4.3 - Air velocity and turbulence measured in the model pig house, (a & b) Velocity at location B, and (c & d) Turbulence intensity at location B. IO – Inlet opening height, m; U_i – Inlet velocity, m s⁻¹. Minus sign in X axis indicates the air velocity and turbulence intensity in opposite direction.

Floor or return air velocities were affected by ventilation rate, inlet air velocity, and inlet opening height. The distribution of measured mean floor air velocities and turbulence intensities at 0.01m above the emission surface (location B) are shown in Fig. 4.4a and Fig. 4.4b. At an average inlet air velocity of 1 m s^{-1} , the floor air velocity was largest at the highest inlet opening height. On the other hand, at the inlet opening height of 0.01m, the floor air velocity was highest at the maximum average inlet velocity of 4 m s^{-1} . For the same Re (e.g., 2100 or 2800 in Table 4.1), the constant inlet opening strategy gave higher floor air velocities than at the constant inlet velocity strategy (Fig. 4.4a). Turbulence intensity did not show clear patterns except in the case with very low inlet air velocity and large inlet opening height (0.092m), which resulted in very high turbulence intensities (Fig. 4.4b).

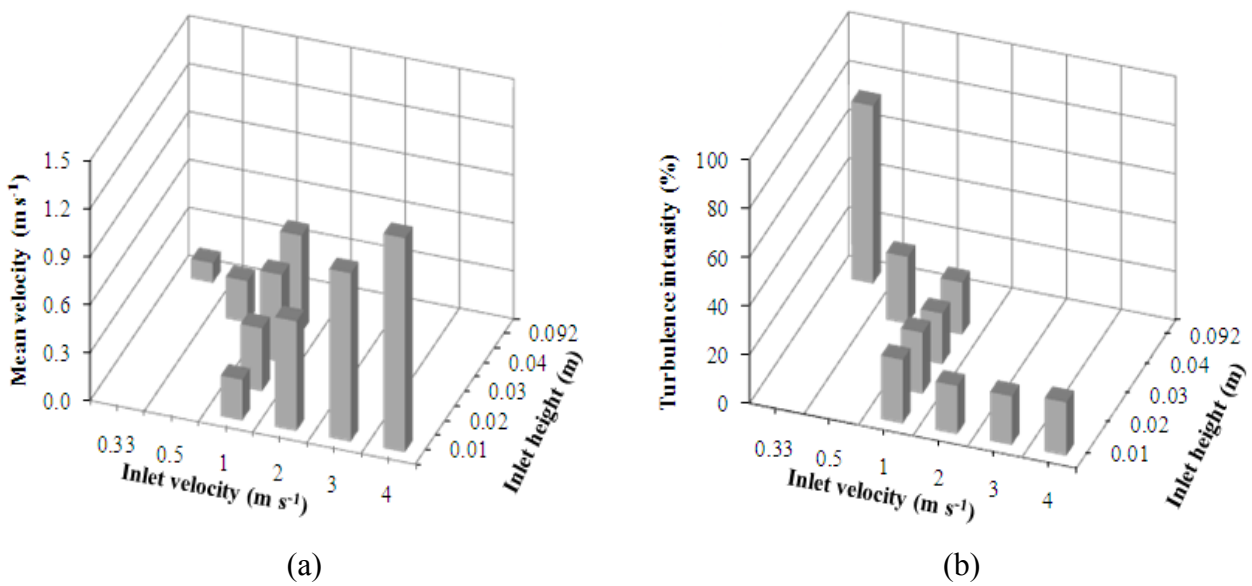


Fig. 4.4 - Measured mean floor air (a) velocities and (b) Turbulence intensities at 0.01m above the emission surface for different combinations of inlet velocity and inlet opening height.

The air velocity and turbulence intensity close to the emission surface affected by different control strategies at location A, B, and C are discussed below.

4.3.1.1. Air velocity profiles above the emission surface

Air velocities recorded at surface level of the scale model are shown in Fig. 4.5i. Floor air velocities were increased with the increased mean inlet air velocities for all three locations A, B, and C at the constant inlet opening of 0.01m (Fig. 4.5ia). The floor air velocity was almost similar, but a little higher at location C than location B in low and high mean inlet air velocity respectively. However, the floor air velocity was much lower at location A than at the locations B, and C. As for example, at the inlet air velocity of 4 m s^{-1} , the air velocities at the height 0.01 m are 0.674, 1.339 and 1.381 m s^{-1} at locations A, B and C respectively.

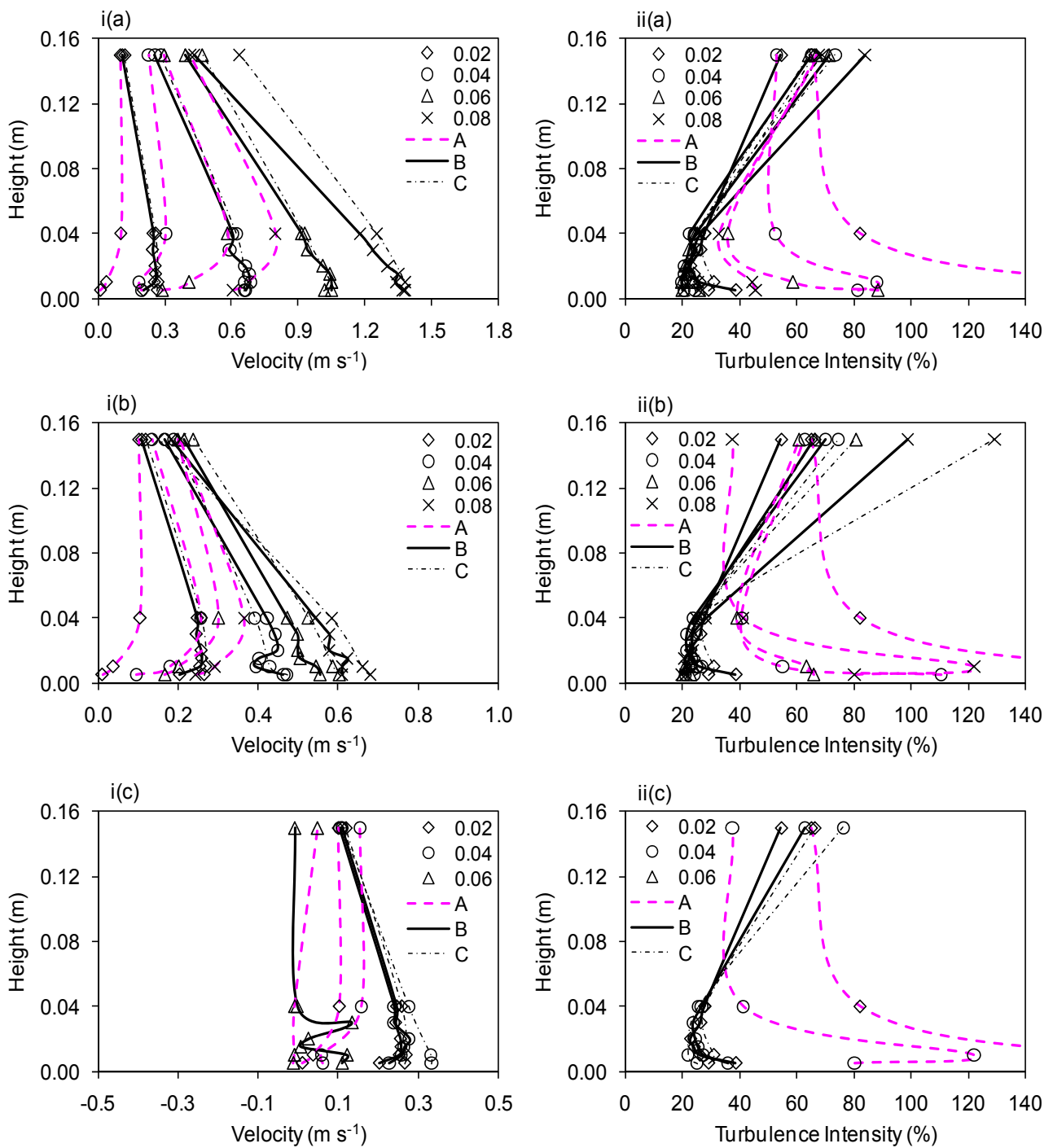


Fig. 4.5 - (i) air velocity profiles and (ii) turbulence intensity profiles at (a) constant inlet opening (0.01 m² each side) , (b) at constant inlet velocity (1 m s⁻¹), and (c) constant inlet jet momentum (0.024 kg.m s⁻²) at different sampling locations A, B, and C respectively. Legends with numbers 0.02, 0.04, 0.06, and 0.08 indicate ventilation rates in m³ s⁻¹.

The highest values occur near where the wall jet reattaches to the surface, and the lowest values occur where the return airflow approaches the inlet wall. As a total room flow eddy, momentum is

added at the inlet and removed by shear at the walls and by mixing with the room air. This phenomenon is consistent with the results from Adre and Albright (1994) and Yu and Hoff (1999). The reduction is not only caused by pressure losses in the corners/airflow changing direction but also by additional momentum losses due to turbulence in the ventilated room space (Strom et al., 2002).

In the cases using the constant inlet air velocity strategy, the return air velocity was increased as the ventilation rates increased (Fig. 4.5ib). At location C, return air velocity was higher than at location A and B which showed a similar pattern as that in the control strategy of the constant inlet opening. The differences in return air velocities between these two strategies were velocity scale though the ventilation rates were the same. The return air velocity was lower in all cases at three locations (A, B and C) in the constant inlet velocity strategy than the constant inlet opening.

At the constant inlet jet momentum, the return air velocities measured are shown in (Fig. 4.5ic). At location B with inlet air velocity 0.33 m s^{-1} with highest inlet opening height of 0.092m, floor air velocity was very low and unstable though the calculated jet momentum was $0.024 \text{ kg.m s}^{-2}$ (Table 4.1). But in reality, we could not even detect a signal at location C.

4.3.1.2. Turbulence intensity profile above the emission surface

The turbulence intensity profiles in the floor level airflow were less distinguishable compared to the air velocity profiles (Fig. 4.5) at the locations B and C than at location A (Fig. 4.1) in all strategies. The general pattern showed a clear inverse relationship between the profiles of the floor air turbulence intensities and the profiles of floor air velocities. The highest turbulence intensities were found where the air velocities were the lowest, i.e., close to floor or the ammonia emitting surface. These characteristics were in good agreement with the results obtained by Sohn et al. (2005). In all experimental setups, turbulence intensity was higher at location A than the locations B and C. At lower inlet air velocities (Fig. 4.5iia) and at lower inlet opening heights (Fig. 4.5iib), turbulence intensities were greater than that at higher inlet air velocities and higher inlet opening heights, respectively. However, using the constant inlet momentum number strategy, the turbulence intensity increased with the increasing inlet air velocity (Fig. 4.5iic). At location C, the local air velocities close to the surface were almost zero and velocity fluctuations were very high. Therefore, very high turbulence intensities were found; in some cases more than 100%. Those were considered as outliers in the data analysis.

4.3.2. *Effect of ventilation control strategies on ammonia concentration and emissions*

The measurement results of the inlet and outlet ammonia concentrations and standard deviations for this scale model study are shown in Table 4.3. The mean values were used to calculate ammonia emission rates and mass transfer coefficients. As the ventilation rate increased, the concentration in

the exhaust air decreased due to dilution and flushing. This reduced concentration might increase the difference in partial pressure between the emission source and indoor air space.

Fig. 4.6a shows the variations in ammonia emission rates as function of the ventilation rate for the different control strategies. Ammonia emission rate increased as the ventilation rate increased for both the constant inlet opening strategy and the constant inlet velocity strategy. The lower ammonia emission rates were found at higher ventilation rates in the constant inlet velocity strategy than in the constant inlet opening strategy. However, using the constant inlet jet momentum strategy the emission rates maintained the same level or with a little decreasing pattern when ventilation rates increased.

The airflow dynamics in the boundary layer of emission surface showed that with the constant inlet opening strategy the inlet air velocity increases as ventilation rate increases (Fig. 4.5ia). This resulted in higher velocities at the emission surface leading to reduce the velocity boundary layer thickness (Incropera et al., 2007) at the emission surface, hence reducing the resistance and increasing the emission. The higher the air velocity is at the emission surface, the higher the emission rate will be (Arogo et al., 1999; Saha et al., 2010b; Zhang et al., 2008). Since partial pressure difference is the driving force for ammonia release from the source surface, the emission rates increased.

The inlet air momentum was lower in connection with the constant inlet velocity strategy than in connection with the constant inlet opening strategy (Table 4.1) even though ventilation rates were increased with the same interval, which resulted in lower velocities at the emission surface (Fig. 4.5ib), a decreased ammonia concentration at the exhaust air (Table 4.3) and reduced emission (Fig. 4.6a).

With the constant inlet air momentum strategy, the higher ventilation rate resulted in a lower inlet air velocity and, consequently, a lower air velocity at the emission surface (Fig. 4.5ic). The size of the inlet opening rapidly became a limiting factor when compensating for a higher ventilation rate. The emission rate was maintained at almost a constant level and decreased slightly with the increasing ventilation rate. This result can be explained by very low and unstable air velocity at the emission surface. For example, at the inlet opening height 0.092m and inlet air velocity 0.33 m s^{-1} , local air velocities were 0.11 to -0.002 m s^{-1} (minus sign indicates opposite air flow direction) from height 0.005m to 0.15m, respectively.

4.3.3. Effect of emission source locations and pen partition on ammonia emissions

Locations of the emission surface showed significant effect on ammonia emission. The emission surface located closest to the side wall (location1) resulted in an ammonia emission of 4 to 22% and 22 to 41% lower than that at the locations of 0.25m and 0.5m away from the left side wall (locations 2 and 3) respectively (Fig. 4.6c). Following the travelling distance of the airflow from the inlet, the

floor air velocity was lower at the location close to the side wall (location A) than at locations B and C (Fig. 4.5i). Floor air velocities were lower at location A, B than at location C, which were above the middle of the emission source locations of 1, 2, and 3 respectively. Therefore, the ammonia emission was lower when the emission surface was located at location 1 than at the locations 2 and 3.

Ammonia emission in the scale model with pen partition was 8 to 14% lower than without pen partition (Fig. 4.6d). Bjerg et al. (2000) showed that introducing a pen partition reduced the air velocity in the occupied zone which might be the cause for reduction of ammonia emission.

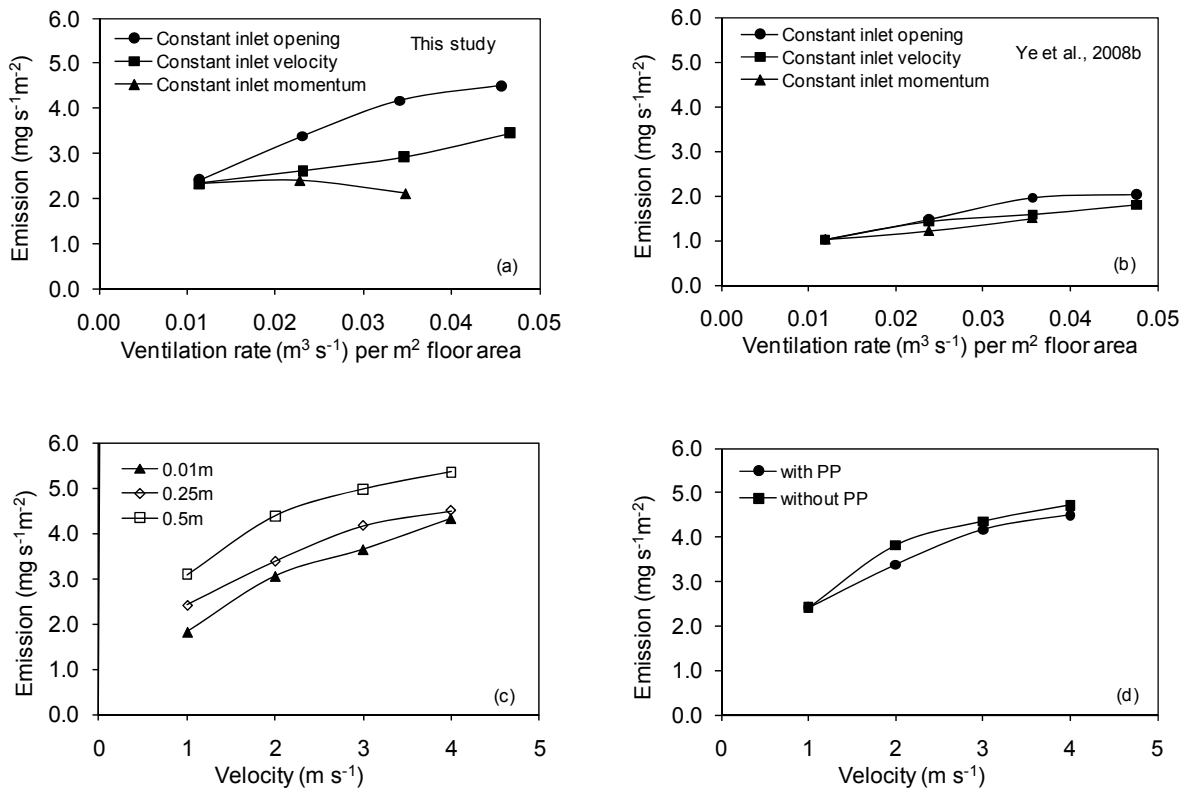


Fig. 4.6 - Comparison of ammonia emission fluxes of the scale model studies for (a) This work & (b) work by Ye et al., 2008b using three ventilation control strategies, (c) emission surface locations from left side wall and (d) with and without pen partition.

4.3.4. Modelling of ammonia mass transfer coefficient

Using a nonlinear model fitting, AMTC models ($R^2 \geq 0.95$) were obtained for this study (Table 4.4).

The model was described with Eq. (4.9) as a function of mean floor air velocity, and turbulence intensity at different heights and at different measurement locations (A, B, and C) above the middle of the ammonia emitting surface. At locations A, B and C, the exponent b of floor air velocity

model of Eq. (4.9) did not show a large difference between the heights, but the turbulence intensity influenced the exponent c between the heights and between the locations.

Table 4.4 - Model values and mass transfer coefficient in relation to u_m and Ti at 95% confidence interval in different heights above the emission surface

Study	Location	Height (m)	S.E.E.	R^2	Gain	Exponent	Exponent	n DoF
					$a \pm SE$	$b \pm SE$	$c \pm SE$	
This	A	0.01	5.17×10^{-5}	0.985	$4.05 \times 10^{-4} \pm 2.17 \times 10^{-4}$	0.48 ± 0.08	0.52 ± 0.45	9
		0.04	7.65×10^{-5}	0.968	$7.75 \times 10^{-5} \pm 5.92 \times 10^{-4}$	0.48 ± 0.104	0.37 ± 0.18	9
	B*	0.01	8.44×10^{-5}	0.961	$1.56 \times 10^{-3} \pm 2.13 \times 10^{-3}$	0.41 ± 0.07	0.11 ± 0.45	9
		0.02	8.42×10^{-5}	0.961	$9.07 \times 10^{-4} \pm 2.66 \times 10^{-3}$	0.42 ± 0.07	0.29 ± 0.95	9
	C	0.01	8.19×10^{-5}	0.964	$1.39 \times 10^{-3} \pm 1.74 \times 10^{-3}$	0.43 ± 0.07	0.14 ± 0.39	9
		0.04	9.17×10^{-5}	0.954	$2.81 \times 10^{-4} \pm 5.62 \times 10^{-4}$	0.45 ± 0.09	0.64 ± 0.62	9
Ye et al., 2008b	B*	0.01	2.29×10^{-4}	0.923	$7.38 \times 10^{-4} \pm 4.21 \times 10^{-4}$	0.56 ± 0.12	0.64 ± 0.21	10
		0.04	2.63×10^{-4}	0.897	$8.19 \times 10^{-4} \pm 4.54 \times 10^{-4}$	0.47 ± 0.17	0.55 ± 0.26	10

* 1/4 of the total length from the left side wall for both scale models

At locations B and C, the turbulence intensity's exponents were lower at the height 0.01m than at the height 0.04m. At location A, exponent c was higher at the height 0.01m than the height of 0.04 m. The airflow pattern and magnitude of floor velocity might be the cause of those differences. Three different equations of k_{G1} value were found at three different heights of location B.

at 0.01 m height
$$k_{G1} = 0.00156 \times u_m^{0.41} Ti^{0.11} \quad (4.17)$$

at 0.02 m height
$$k_{G1} = 0.00091 \times u_m^{0.42} Ti^{0.29} \quad (4.18)$$

and at 0.04 m height
$$k_{G1} = 0.00074 \times u_m^{0.43} Ti^{0.35} \quad (4.19)$$

From Eqs (4.17), (4.18), and (4.19), it can be seen that Ti played a leading role on the AMTC value as the height increased. AMTC was much more sensitive to the variations of air velocity or turbulence intensity at lower than at higher velocity ranges.

The return air velocities were also correlated to the jet momentum number (J_i) as shown in Table 4.5. The u_m and u_{rms} were proportional to J_i power 0.53 to 0.56 for both cases at locations B and C. The result is consistent with the result of Jin and Ogilvie (1992). But differences were observed in location A. Average of the model parameters of different heights of location B (Table 4.5) were used for prediction of overall $u_{m,o}$ and $u_{rms,o}$ at location B, which are follows:

$$u_{m,o} = 8.6 \times J_i^{0.56} \quad (4.20)$$

and

$$u'_{rms,o} = 1.8 \times J_i^{0.54} \quad (4.21)$$

Table 4.5 - Statistics and empirical constants for u_m and u_{rms} related to J_i at 95% confidence interval at different heights above the emission surface

Study	Location	Height (m)	Dependent variable	Equation number	S.E.E.	R ²	Gain	Exponent	n
							a ± SE	b ± SE	
This	A	0.01	u_m	11	0.0414	0.958	9.80 ± 5.83	0.79 ± 0.15	9
		0.04	u_m	11	0.0033	0.979	6.92 ± 2.23	0.64 ± 0.08	9
		0.01	u_{rms}	12	0.0075	0.991	1.75 ± 0.29	0.52 ± 0.04	9
		0.04	u_{rms}	12	0.0097	0.976	1.13 ± 0.26	0.43 ± 0.06	9
	B*	0.01	u_m	11	0.0405	0.988	9.62 ± 3.04	0.57 ± 0.08	9
		0.02	u_m	11	0.0355	0.990	8.85 ± 1.72	0.56 ± 0.05	9
		0.04	u_m	11	0.0300	0.991	7.55 ± 1.09	0.55 ± 0.03	9
		0.01	u_{rms}	12	0.0042	0.996	1.77 ± 0.18	0.54 ± 0.02	9
	C	0.01	u_{rms}	12	0.0038	0.997	1.86 ± 0.17	0.55 ± 0.02	9
		0.02	u_{rms}	12	0.0045	0.996	1.77 ± 1.64	0.53 ± 0.22	9
		0.04	u_m	11	0.0293	0.993	9.10 ± 1.38	0.56 ± 0.04	9
		0.04	u_m	11	0.0186	0.996	8.06 ± 0.86	0.55 ± 0.03	9
Ye et al., 2008b	B*	0.01	u_{rms}	12	0.0070	0.993	2.11 ± 0.31	0.54 ± 0.03	9
		0.04	u_{rms}	12	0.0031	0.998	1.97 ± 0.14	0.54 ± 0.02	9
		0.01	u_m	11	0.0251	0.993	4.73 ± 0.64	0.53 ± 0.04	9
		0.04	u_m	11	0.0312	0.981	3.98 ± 0.88	0.56 ± 6.12	9
		0.01	u_{rms}	12	0.0105	0.946	0.58 ± 0.17	0.41 ± 0.11	9
		0.04	u_{rms}	12	0.0708	0.988	0.98 ± 0.16	0.51 ± 0.04	9

* 1/4 of the total length from the left side wall for both scale models

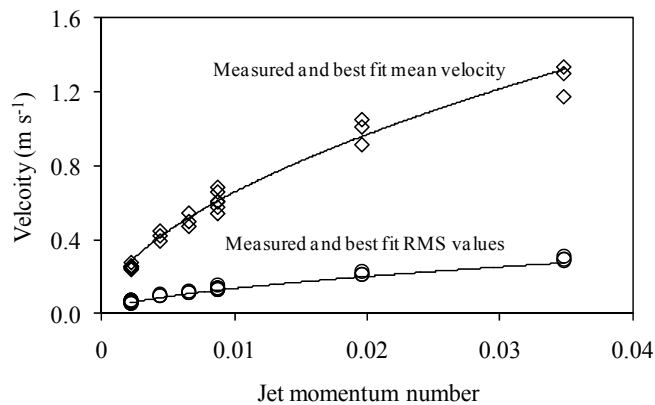


Fig. 4.7 - Measured and fitted mean air velocity and RMS value at the floor correlated with inlet jet momentum number

Fig. 4.7 shows best fit predictions using model Eq. (4.20) and Eq. (4.21) and measured values of u_m and u_{rms} at location B for the jet momentum number of three control strategies. The average values of the model parameters in Eqs. (4.20) and (4.21) were given representative prediction of $u_{m,o}$ and $u'_{rms,o}$ regardless of measuring heights when the jet momentum was used. Therefore, when we substituted Eq (4.20) and Eq. (4.21) in Eqs (4.17), (4.18), and (4.19), interesting results were found for AMTC values in relation to the jet momentum number (J_i).

at 0.01m height

$$k_{G1} = 0.00528 \times J_i^{0.227} \quad (4.22)$$

at 0.02m height

$$k_{G1} = 0.00541 \times J_i^{0.229} \quad (4.23)$$

and at 0.04m height

$$k_{G1} = 0.00544 \times J_i^{0.234} \quad (4.24)$$

Eqs. (4.22), (4.23), and (4.24) may be stated as single equation Eq. (4.25), which is average of gain and exponent.

$$k_{G1} = 0.00538 \times J_i^{0.23} \quad (4.25)$$

The model Eq. (4.25) gave good prediction of AMTC in relation to J_i when compared to the measured values (Fig. 4.8) i.e., AMTC was proportional to the $J_i^{0.23}$. Again, the gain value in Eq. (4.25) should contain the appropriate unit. By putting Eq. (4.14) in Eq. (4.25) following relation can be obtained

$$k_{G1} = 0.00373 \times h_i^{0.23} U_i^{0.46} L^{-0.23} H^{-0.23} \quad (4.26)$$

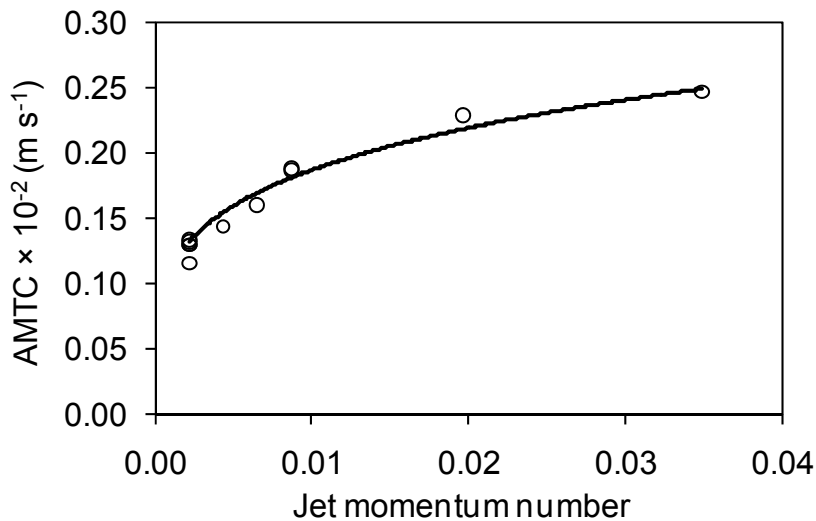


Fig.4.8 - Measured and fitted mean AMTC (k_{G1}) value at the floor correlated with jet momentum number. o and —, represent the measured and modelled values respectively.

However, the AMTC was modelled in this study to describe the relationship between the airflow characteristics and inlet opening height, inlet velocity, length and height of the scale model. The ammonia emissions were only obtained in laboratory experiments using a particular scale model (1:6). The quantitative correlation could be different from other model scales, real slurry, or in full scale production buildings with pigs, due to scale effect and other factors.

4.3.5. Comparison of different scale model studies

4.3.5.1. Ammonia emission

Ammonia emissions rates measured in the current study and that by Ye et al. (2008b) are shown in (Fig. 4.6a, and Fig. 4.6b). The summarized experimental conditions of the two studies are listed in Table 4.2. The ammonia emission rates from this study were generally higher than those obtained by Ye et al. (2008b). The two experiments conducted using the similar methodology and lab experimental setups but different model scales and the TAN concentration in ammonia solution (Table 4.2). Due to the difference in TAN, it is difficult to make direct comparison for the two sets of data. The scale model in the current study had a larger inlet cross section area than in the scale model used by Ye et al. (2008b). Therefore, in this study, ventilation rates were adjusted accordingly to maintain the same inlet air velocities and the same ventilation rate per unit floor area.

As shown in Table 4.2, the TAN concentration used in this study was about four times what was reported by Ye et al. (2008b), but the pH values were similar. The calculated C_s was 1848 and 452 mg m⁻³ in this study and in Ye et al. (2008b), respectively. However, the measured ammonia emission rates in this work were about double of those reported by Ye et al. (2008b). These results indicated that the mass transfer coefficients were different in the two studies. It also suggested that the model dimensions played an important role in emissions and agreed with the work of other researchers such as, Hudson and Ayoko (2008) who pointed out that different devices cannot be expected to provide equivalent emission rate estimates. However, limited information is available to quantify the effect due to dimension differences.

4.3.5.2. Mass transfer coefficients

Statistically modelled AMTCs, as a function of the mean floor air velocity, and turbulence intensity above the emission surfaces for the two scale model studies showed differences among the two studies as observed for ammonia emissions (Fig. 4.6), although all the AMTC values ranged from 1.3×10^{-3} to 3.38×10^{-3} m s⁻¹ and were within the range of 1.17×10^{-2} to 1.3×10^{-6} m s⁻¹ reviewed by Ni (1999). The k_{G1} and k_{G2} were positively correlated to mean floor air velocity, and turbulence intensity at location B (Table 4.4).

at 0.01m height

$$k_{G2} = 0.000738 \times u_m^{0.56} Ti^{0.64} \quad (4.27)$$

and at 0.04m height

$$k_{G2} = 0.000819 \times u_m^{0.47} Ti^{0.55} \quad (4.28)$$

In the results of this work, AMTC (k_{G1}) value was function of floor air velocity power of 0.41-0.43, and of floor air turbulence intensity power of 0.11-0.35, where air velocity was the more dominating factor than turbulence intensity. Comparatively, in the work by Ye et al. (2008b), AMTC (k_{G2}) was influenced by air velocity and turbulence intensity with the power of 0.47-0.56 and 0.55-0.64 respectively where turbulence intensity worked as the dominating factor. This disagreement among the two studies was expected in that the airflow characteristics were quite different in this study than the study of Ye et al. (2008b) (Table 4.5). The AMTCs were obtained based on the known ammonia emission rates as shown in Fig. 4.6. Therefore, the discrepancy could also be contributed to the differences in scale model sizes.

The work by Smith and Watts (1994) and Hudson and Ayoko (2008) showed that the relationship between the AMTC and the airflow characteristics was highly device-dependent. A non-linear relationship existed between ammonia mass transfer and the sizes of scale models and inlet opening area cross sections. Therefore, while the factors such as airflow characteristics, air and liquid temperature, pH and TAN of the emission source, etc. are indispensable in AMTC (Ye et al., 2008b) on boundary layers and ammonia emissions.

Considering a similar approach as described in section 4.3.4, by putting average model parameters values of $u_{m,o}$ and $u'_{rms,o}$ study which were related to J_i from Table 4.5 of Ye et al. (2008b), the following relationships were found as Eq. (4.29) and Eq. (4.30):

at 0.01m height

$$k_{G2} = 0.0107 \times J_i^{0.25} \quad (4.29)$$

at 0.04m height

$$k_{G2} = 0.0079 \times J_i^{0.21} \quad (4.30)$$

The power of J_i were also little different from this study. But the average value of J_i power was 0.23 for both studies. Also there were differences in gain values between the two studies. Gain values at different heights were not changed significantly in this study. In the work by Ye et al. (2008b), however, the gain value was lower at 0.04m height than 0.01m height. The measurement point of 0.04m height in Ye et al. (2008b) could be beyond the boundary layer zone of floor air flow which might make differences. From the comparison of the two scale models, the jet momentum number relation with AMTC (i.e., $k_G \propto J_i^{0.23}$) might give a reasonable prediction of the mass transfer process and ammonia release from the emission surface in scale model studies regardless of geometric dimensions if the other parameters are known. The relationship of the mass transfer coefficient with the jet momentum number was based on two scale model studies of different geometric sizes, but this relationship need to be validated in full scale. However, more

investigations are needed to find out suitable criteria for comparing different scale model studies with full scale studies.

4.4. Conclusion

A symmetric airflow pattern was observed in the scale model study. Return air velocities above the floor were different. The mean floor velocity decreased as the main airflow travelling distance from the inlet opening increased, as showed in sequences of locations C-B-A in all experimental setups. However, turbulence intensity was increased following the decay of the air velocity.

Ventilation control strategies significantly affected the floor level airflow characteristics and therefore the ammonia emission and mass transfer coefficient in the pig model house. The ammonia emission reduced when pen partition was present in the room compared to without pen partition. Emission surface located close to the side wall (location 1) resulted in ammonia emission of about 4 to 22% and 22 to 41% lower than the surface located at location 2 and close to the location 3 respectively.

Statistical models of AMTC were developed based on the air velocity, and turbulence intensity of different heights above the emission surface. The measurement position heights were important for the representative air velocity and turbulence measurements for modelling purpose. AMTC was much more sensitive to the variations of air velocity at lower than at higher velocity ranges. Similar response was obtained for turbulence intensity.

Mean floor air velocity ($u_{m,a}$) and rms of floor velocity fluctuation ($u'_{rms,a}$) were correlated with the jet momentum number successfully ($R^2 = 1$) and were proportional to $J_i^{0.56}$ and $J_i^{0.54}$ respectively as the room airflow patterns stayed in the fully rotary flow zone. AMTC was also correlated with the jet momentum number for fully rotary airflow and was proportional to $J_i^{0.23}$. Finally, AMTC relation with the inlet opening height, the inlet air velocity, the length and the height of the scale model was established.

Comparison of two different sizes of scale models showed that airflow characteristics and AMTC was very much device-dependent. But using jet momentum number might resolve of estimating of AMTC from scale model study where J_i power for both models was 0.23. These studies were limited by the data based on only two model dimensions. Further systematic studies on the effects of model dimensions on determination of ammonia mass transfer and emission modelling are needed in the future.

Acknowledgements

This research was performed as part of ROSES project “Reduction of Odour Source in and Emission from Swine Buildings” under the program “Animal Husbandry, the Neighbours and the Environment” funded by the Danish Ministry of Food, Agriculture and Fisheries (Grant

Number:3304-VMP-05-032-01). The authors also appreciate the technical support of Preben Jensen Dahl at Air Physics Lab, University of Aarhus, Denmark.

References

- Adre, N., and L. D. Albright. 1994. Criterion for Establishing Similar Air-Flow Patterns (Isothermal) in Slotted-Inlet Ventilated Enclosures. *Trans. ASAE* 37(1): 235-250.
- Arogo, J., Zhang, R. H., Riskowski, G. L., Christianson, L. L., and D.L. Day. 1999. Mass transfer coefficient of ammonia in liquid swine manure and aqueous solutions. *J. Agric. Eng. Res.* 73(1): 77-86.
- Barber, E. M., Sokhansanj, S., Lampman, W. P., and J. R. Ogilvie. 1982. Stability of airflow patterns in ventilated airspaces. *Paper presented in winter meeting of American Society of Agricultural Engineers*, Palmer House, Chicago, Illinois, December 14-17, 1982.
- Bird, B. R., Stewart, W. E., and E. E. Lightfoot. 2007. *Transport Phenomena* (revised second edition). New York, N. Y. :John Wiley and Sons.
- Bjerg, B., Morsing, S., Svidt, K., and G. Zhang. 1999. Three-dimensional airflow in a livestock test room with two-dimensional boundary conditions. *J. Agric. Eng. Res.* 74(3): 267-274.
- Bjerg, B., Svidt, K., Zhang, G., and S. Morsing. 2000. The effects of pen partitions and thermal pig simulators on airflow in a livestock test room. *J. Agric. Eng. Res.* 77(3): 317-326.
- Bliss, P. J., Jiang, K. Y., and T. J. Schulz. 1995. The Development of A Sampling System for the Determination of Odor Emission Rates from Areal Surfaces .2. Mathematical-Model. *J. Air Waste Mgmt Assoc.* 45(12): 989-994.
- Buiter, J. J., and S. J. Hoff. 1998. Ammonia distribution in a pit-ventilated confinement building: One-half scale model study. *Trans. ASAE* 41(6): 1817-1827.
- Chen, Q. Y. 2009. Ventilation performance prediction for buildings: A method overview and recent applications. *Build. Environ.* 44(4): 848-858.
- Elzing, A., and G. J. Monteny. 1997. Ammonia emission in a scale model of a dairy-cow house. *Trans. ASAE* 40(3): 713-720.
- Hoff, S. J. 1995. Isothermal airflow characteristics in the animal-occupied zone of a slot-ventilated swine facility. *Trans. ASAE* 38(6): 1843-1852.
- Hudson, N., and G. A. Ayoko. 2008. Odour sampling. 2. Comparison of physical and aerodynamic characteristics of sampling devices: A review. *Bioresource Tech.* 99(10): 3993-4007.
- Incropera, F. P., DeWitt, D. P., Bergman, T. L., and A. S. Lavine. 2007. *Fundamentals of Heat and Mass Transfer. Sixth Edition, John Wiley & Sons.*
- Jayaweera, G. R., and D. S. Mikkelsen. 1990. Ammonia Volatilization from Flooded Soil Systems - A Computer-Model .1. Theoretical Aspects. *Soil Sci. Soc. America J.* 54(5): 1447-1455.

- Jin, Y., and J. R. Ogilvie. 1992. Air-Flow Characteristics in the Floor Region of A Slot Ventilated Room (Isothermal). *Trans. ASAE* 35(2): 695-702.
- Liang, Z. S., Westerman, P. W., and J. Arogo. 2002. Modeling ammonia emission from swine anaerobic lagoons. *Trans. ASAE* 45(3): 787-798.
- Morsing, S., Strom, J. S., Zhang, G., and P. Kai. 2008. Scale model experiments to determine the effects of internal airflow and floor design on gaseous emissions from animal houses. *Biosystems Eng.* 99(1): 99-104.
- Ni, J. Q. 1999. Mechanistic models of ammonia release from liquid manure: a review. *J. Agric. Eng. Res.* 72(1): 1-17.
- Phillips, V. R., Scholtens, R., Lee, D. S., Garland, J. A., and R. W. Sneath. 2000. A review of methods for measuring emission rates of ammonia from livestock buildings and slurry or manure stores, part 1: Assessment of basic approaches. *J. Agric. Eng. Res.* 77(4): 355-364.
- Rom, H. B., and G. Zhang. 2010. Time delay for aerial ammonia concentration measurements in livestock buildings. *Sensors* 10(5): 4634-4642.
- Saha, C. K., Zhang, G. Q., Kai, P., and B. Bjerg. 2010a. Effects of a partial pit ventilation system on indoor air quality and ammonia emission from a fattening pig room. *Biosystems Eng.* 105(3): 279-287.
- Saha, C. K., Zhang, G., and J. Q. Ni. 2010b. Airflow and concentration characterisation and ammonia mass transfer modelling in wind tunnel studies. *Biosystems Eng.* 107(4): 328-340.
- Smith, R. J., and P. J. Watts. 1994. Determination of Odor Emission Rates from Cattle Feedlots .2. Evaluation of 2 Wind Tunnels of Different Size. *J. Agric. Eng. Res.* 58(4): 231-240.
- Sohn, J. H., Smith, R. J., Hudson, N. A., and H. L. Choi. 2005. Gas sampling efficiencies and aerodynamic characteristics of a laboratory wind tunnel for odour measurement. *Biosystems Eng.* 92(1): 37-46.
- Sommer, S. G., Zhang, G. Q., Bannink, A., Chadwick, D., Misselbrook, T., Harrison, R., Hutchings, N. J., Menzi, H., Monteny, G. J., Ni, J. Q., Oenema, O., and J. Webb. 2006. Algorithms determining ammonia emission from buildings housing cattle and pigs and from manure stores. *Advan. in Agro.* 89: 261-335.
- Strom, J. S., Zhang, G., and S. Morsing 2002. Predicting near-floor air velocities for a slot-inlet ventilated building by jet velocity decay principles. *Trans. ASAE* 45(2): 407-413.
- Topp, C., Nielsen, P. V., and P. Heiselberg. 1997. Evaporation controlled emission in weighted rooms. *Proceedings of Healthy Building/IAQ' 97, Washington D C, USA*3: 557-562.
- Topp, C., Nielsen, P. V., and P. Heiselberg. 2001. Influence of local airflow on the pollutant emission from indoor building surfaces. *Indoor Air-Int. J. Indoor Air Quality and Climate* 11(3): 162-170.

- van der Peet-Schwering, C., Aarnink, A. J. A., Rom, H. B., and J. Y. Dourmad. 1999. Ammonia emissions from pig houses in The Netherlands, Denmark and France. *Livestock Prod. Sci.* 58(3): 265-269.
- Vandermolen, J., Beljaars, A. C. M., Chardon, W. J., Jury, W. A., and H. G. Vanfaassen. 1990. Ammonia Volatilization from Arable Land After Application of Cattle Slurry .2. Derivation of A Transfer Model. *Netherlands J. Agric. Sci.* 38(3): 239-254.
- Wang, C. Y., Li, B. M., Zhang, G. Q., Rom, H. B., and J. S. Strom. 2006. Model estimation and measurement of ammonia emission from naturally ventilated dairy cattle buildings with slatted floor designs. *J. Air Waste Mgmt Assoc.* 56(9): 1252-1259.
- Webb, J., Menzi, H., Pain, B. F., Misselbrook, T. H., Dammgen, U., Hendriks, H., and H. Dohler. 2005. Managing ammonia emissions from livestock production in Europe. *Environ. Pollution* 135(3): 399-406.
- Ye, Z., Saha, C. K., Li, B., Tong, G., Wang, C., Zhu, S., and G. Zhang. 2009a. Effect of environmental deflector and curtain on air exchange rate in slurry pit in a model pig house. *Biosystems Eng.* 104(4): 522-533.
- Ye, Z., Zhang, G., Li, B., Strom, J. S., and P. J. Dahl. 2008a. Ammonia Emissions Affected by Airflow in A Model Pig House: Effects of Ventilation Rate, Floor Slat Opening, and Headspace Height in A Manure Storage Pit. *Trans. ASABE* 51(6): 2113-2122.
- Ye, Z., Zhang, G., Li, B., Strom, J. S., Tong, G., and P. J. Dahl. 2008b. Influence of airflow and liquid properties on the mass transfer coefficient of ammonia in aqueous solutions. *Biosystems Eng.* 100(3): 422-434.
- Ye, Z., Zhang, G., Seo, I. H., Kai, P., Saha, C. K., Wang, C., and B. Li. 2009b. Airflow characteristics at the surface of manure in a storage pit affected by ventilation rate, floor slat opening, and headspace height. *Biosystems Eng.* 104(1): 97-105.
- Yu, H., and S. J. Hoff. 1999. Airflow pattern similarity criteria for ceiling slot-ventilated agricultural enclosures under isothermal conditions. *Trans. ASAE* 42(2): 459-469.
- Zerihun, D., Feyen, J., and J. M. Reddy. 1996. Sensitivity analysis of furrow-irrigation performance parameters. *J Irrig. Drainage Eng.* 122(1): 49-57.
- Zhang, G., Bjerg, B., Strom, J. S., Morsing, S., Kai, P., Tong, G., and P. Ravn. 2008. Emission effects of three different ventilation control strategies - A scale model study. *Biosystems Eng.* 100(1): 96-104.
- Zhang, G., and J. S. Strom. 1999. Jet drop models for control of non-isothermal free jets in a side-wall multi-inlet ventilation system. *Trans. ASAE* 42(4): 1121-1126.

Chapter 5

Similarity criteria for estimating gas emission from scale models

Paper IV:

Saha, C.K., Zhang, G, Ni, J.-Q. and Ye, Z. 2011. **Similarity criteria for estimating gas emission from scale models**. Biosystems Engineering, Vol 108 (3), P 227-236.

Abstract

Similarity, or the relationship between a model and a prototype, is an important issue when using physical modelling techniques. The objective was to investigate similarity criteria using Reynolds number (Re) and jet momentum ratio (Rm) in two scale models (SM-1 of 1:6 and SM-2 of 1:12.5) of a pig house under isothermal conditions for predicting airflow and ammonia emission. Experiments were conducted using two ventilation control strategies (constant inlet opening and constant inlet velocity) in SM-1 and SM-2 by (1) keeping the same inlet Re with constant inlet opening, and (2) keeping the same Rm with constant inlet opening and constant inlet velocity. Aqueous ammonia solutions with four different total ammoniacal nitrogen (TAN) concentrations and two different pH levels were used as emission sources inside the scale models. Non-dimensional normalised emission rate, defined as the ratio of the measured emission rate and the reference emission rate at inlet air velocity of 1 m s^{-1} of the scale models, was proposed for when using Re and Rm as similarity. Rm was found to be a better scaling parameter than Re for predicting the influence of airflow on ammonia emission rate when using the non-dimensional normalised emission rate in scale models with both ventilation control strategies and ammonia solutions of different TAN and pH.

Key words: Ammonia emission; non-dimensional emission rate; similarity; ventilation

Nomenclature		<i>SM</i>	scale model
<i>A</i>	area, m^2	<i>W</i>	model width, m
<i>C</i>	ammonia concentration, mg m^{-3}	<i>U</i>	mean air velocity, m s^{-1}
<i>D</i>	diameter of exhaust pipe, m	μ	dynamic viscosity, N s m^{-2}
<i>ds</i>	depth of ammonia pan, m	ρ	density of air, kg m^{-3}
<i>E</i>	emission rate, $\text{mg s}^{-1} \text{m}^{-2}$	ΔP	pressure difference, N m^{-2}
<i>Eu</i>	Euler number	<i>Subscripts</i>	
<i>Fr</i>	Froude number	<i>i</i>	inlet
<i>g</i>	gravitational acceleration rate, m s^{-2}	<i>m</i>	model
<i>H</i>	model or prototype height, m	<i>max</i>	maximum
<i>h</i>	air inlet opening height, m	<i>o</i>	outlet
<i>L</i>	model or prototype length, m	<i>p</i>	prototype
<i>Lf</i>	flap length, m	<i>r</i>	return air
<i>n</i>	geometry scale ratio of prototype to model	<i>s</i>	ammonia release surface
<i>Re</i>	Reynolds number	<i>t</i>	sum of inlet cross-sections of two side walls
<i>Rm</i>	jet momentum ratio, $\text{m}^2 \text{s}^{-2}$	<i>1</i>	test condition at inlet velocity of 1 m s^{-1}
<i>Sw</i>	width of ammonia pan emission surface, m		

5.1. Introduction

Gas and odour emissions from livestock production buildings are major air pollutant to the environment. These pollutants are mostly transported by air motion from slurry surface to the room space and eventually to the outside environment. Ventilation is important to regulate indoor environment and keep an appropriate microclimate for the thermal comfort and air quality of the occupants and farm workers. Ventilated airflow inside an enclosure influences the air distribution, thermal environment, and contaminant concentration (Aarnink and Wagemans, 1997; Saha et al., 2010; Topp et al., 2001; Zhang et al., 2005; Zhang et al., 2008). Jet air supplies are used in most mechanically ventilated rooms. The performance of air-jets determines the distribution of thermal energy, moisture, and fresh air inside the rooms (Awabi, 1991) as well as gas and odour emissions from the rooms (Morsing et al., 2008).

The characteristics of enclosed air-jet and their effect on gas emissions have been studied by using prototype buildings, scale-models, and numerical simulation (Buller and Hellickson, 1978; Morsing et al., 2008; Strom et al., 2002; Zhang et al., 2008). However, precise mathematical models are not feasible for the extremely complex micro-structures occurring in room airflows (Yu et al., 2006).

Experiments with full scale buildings are expensive and it is often difficult to observe the specific behaviour of airflow and emission by controlling parameters such as wind velocity, humidity, air temperature etc. Therefore, scale model tests are necessary if dimensional uncertainty is not known and a precise mathematical-physical prediction model is not established. Scale model studies are practical for simulating the air motion of a prototype and can be used to validate numerical simulations. Similarity, or the relationship between a model and a prototype, is an important issue for experiments with scale models. Similitude engineering can be a useful technique for predicting the performance of a prototype animal housing system from scaled models (Adre and Albright, 1994). Nevertheless, only partial similarity between the model and the prototype is satisfied for most of the dimensionless parameters because usually there is conflict between the similarity requirements.

Reynolds number (Re) has been widely used as the similarity parameter for an isothermal airflows in scale models (Jin and Ogilvie, 1992; Pattie and Milne, 1966; Timmons and Baughman, 1981). However, differences in inlet air velocity profiles between the model and the prototype can result in greater dimensionless inlet jet momentum for the scale model even though the inlet Re remains the same, especially when the room airflow is not fully turbulent (Adre and Albright, 1994; Yu et al., 2006; Yu and Hoff, 1999; Zhang et al., 1991). The jet momentum ratio (Rm), or the ratio of the inlet jet momentum and the momentum loss due to shear along the enclosure walls, has been validated as an appropriate scaling parameter for airflow pattern similarity under isothermal

conditions. However, direct comparison studies of the effect of Re and Rm on gas emission, have not been found in the literature.

When comparing the similarity between gas emission rates from two models, there can be differences in prevailing conditions, i.e., the temperature, moisture content, concentration of aqueous solution/source, pH value, and emission surface area etc. To reduce these effects, Smith and Watts (1994) used a non-dimensional emission rate (E_l) for comparing two wind tunnel results, where E_l was the emission rate at a velocity of 1 m s^{-1} . This was viewed as a base emission rate for the prevailing conditions. However, limited knowledge is available on the similarity of gas emission estimates using scale model experiment data.

Laboratory experiments were recently conducted on ammonia emissions from two 1:6 and 1:12.5 scale models of a pig barn operating under isothermal conditions. The objectives of this work were to 1) investigate Re and Rm as similarity parameters for estimating airflow and gas emissions from scale models, and 2) assess two-dimensional wall jet air flow patterns in confined spaces and their effect on gas emissions using scale models.

5.2. Theory

Complete similarity of turbulent plane-wall air-jets diffused into a slot-ventilated enclosure under isothermal conditions requires geometric, kinematic, and dynamic similarity, and similar boundary conditions (Awabi, 1991; Baturin, 1972; Szucs, 1980; Yu and Hoff, 1999). Similarity of boundary conditions must occur to reach complete similarity between geometric, kinematic and dynamic conditions at all solid boundaries of the model and prototype. Geometric similarity requires the model to be the same shape as the prototype, usually scaled. In kinematic similarity, fluid flow of both the model and prototype must undergo motion changes with similar time scales, i.e., accurate scaling flow boundaries including air supply opening, exhaust outlet, and roughness of all surfaces. Dynamic similarity requires keeping constant ratios of all forces acting on corresponding fluid particles and boundary surfaces, including inertial, viscous, pressure, and buoyant forces.

Similarity analysis indicates that similarity parameters for isothermal airflow are geometry, Froude number (Fr), Reynolds number (Re), and Euler number (Eu) between the model and the prototype. The Fr represents the ratio of inertial to gravitational forces:

$$Fr = \frac{U_i}{\sqrt{gL}} \quad (5.1)$$

where Fr is Froude number; U_i is mean inlet air velocity at air inlet, m s^{-1} ; g is gravitational acceleration rate, m s^{-2} ; L is model or prototype length, m .

For isothermal airflow in a slot-ventilated enclosure, Fr does not need to be considered, because it is only important for compressible flows and for motions with free liquid-vapour surfaces (Schlichting, 1979). The Reynolds number Re has traditionally been used as the scaling factor; but an anomaly in the use of Re as the kinematic similarity parameter for the scale modelling of slot-

ventilated enclosures has occurred (Rousseau and Albright, 1996). This dimensionless similarity parameter (Re) for isothermal conditions represents the ratio of inertial to viscous forces:

$$Re = \frac{\rho U_i h_i}{\mu} \quad (5.2)$$

where Re is Reynolds number; ρ is density of air, kg m^{-3} ; h_i is inlet opening height, m; μ is dynamic viscosity, N s m^{-2} .

Similarity between the model and the prototype requires:

$$\left(\frac{\rho U_i h_i}{\mu} \right)_m = \left(\frac{\rho U_i h_i}{\mu} \right)_p \quad (5.3)$$

where subscripts m and p represent scale model and prototype, respectively.

If the same working fluid is used in the model and the prototype, then $\rho_m = \rho_p$ and $\mu_m = \mu_p$, resulting in the following requirement between diffuser airspeeds:

$$\frac{U_{i,m}}{U_{i,p}} = \frac{h_{i,p}}{h_{i,m}} = n \quad (5.4)$$

where $U_{i,m}$ is mean inlet velocity of the model, m s^{-1} ; $U_{i,p}$ is mean inlet velocity of the prototype; $h_{i,p}$ is inlet opening height of the prototype, m; $h_{i,m}$ is inlet opening height of the model; n is the geometric scale between the model and the prototype.

For slot-ventilated enclosures, Re has a negligible effect on the governing equations of fluid dynamics compared with that of the Euler number (Eu), which becomes an alternative kinematic similarity parameter instead of Re (Rousseau and Albright, 1996). The Eu represents the ratio of pressure to momentum forces:

$$Eu = \frac{2\Delta P}{\rho U_i^2} \quad (5.5)$$

where Eu is Euler number; ΔP is total pressure difference between inlet and outlet, N m^{-2} .

For a two-dimensional wall jet in mechanically ventilated spaces under isothermal condition, Eu may not be the appropriate similarity parameter (Yu et al., 2006). In scale model studies with confined wall jets where airflow pattern and air-jet penetration distance similarity were measured, the jet momentum ratio (Rm) was proposed (Adre and Albright, 1994) and verified (Adre and Albright, 1994; Yu et al., 2006; Yu and Hoff, 1999) as a more appropriate scaling criterion. The Rm is functionally equivalent to the Eu number for similarity in diffuser airspeeds between a scale model and a prototype. The Rm was defined by Adre and Albright (1994) as:

$$Rm = \frac{U_i^2 h_i}{L + H} \quad (5.6)$$

where Rm is jet momentum ration, $\text{m}^2 \text{s}^{-2}$; H is model or prototype height, m.

The Rm implies that, to acquire similar wall jet flows in slotted inlet ventilated enclosures of different sizes, the jet momentum at the inlet (source) must vary proportionally to the cross-sectional perimeter of the enclosure.

Using Rm as the similarity criterion, the design condition between the model and the prototype is

$$\left(\frac{U_i^2 h_i}{L + H} \right)_m = \left(\frac{U_i^2 h_i}{L + H} \right)_p \quad (5.7)$$

as

$$\left(\frac{h_i}{L + H} \right)_m = \left(\frac{h_i}{L + H} \right)_p \quad (5.8)$$

the relationship further simplifies to:

$$U_{i,m} = U_{i,p} \quad (5.9)$$

In this study, two similarity parameters Re and Rm are compared for estimating floor level airflows and gas emissions using two scale models.

5.3. Materials and Methods

5.3.1. Experimental facilities

The experiments were carried out in Air Physics Lab, Faculty of Agricultural Sciences, Aarhus University, Denmark. Two geometrically similar scale models representing a pig grower barn were used to study airflow parameters and ammonia emissions. The 1:6 and the 1:12.5 scale models were denoted as SM-1 and SM-2, respectively, and are illustrated in Fig. 5.1. The dimensions of SM-1 and SM-2 are given in Table 5.1. The scale models were made

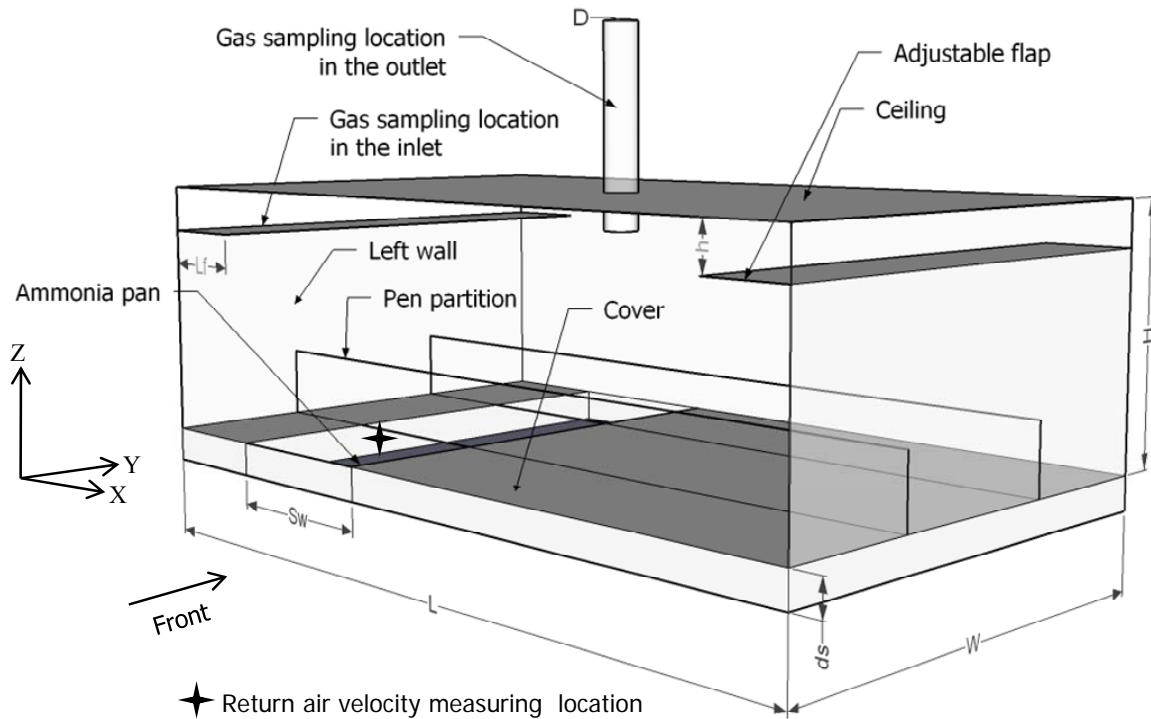


Fig. 5.1 - Schematic diagram of the scale models used in the study.

of thick transparent acrylic plastic. Ventilation air was supplied through adjustable flaps at two sides beneath the ceiling. The flaps spanned the whole width of the model with maximum opening heights of 0.095 m and 0.045 m for SM-1 and SM-2, respectively. Exhaust air was extracted using variable-speed axial-flow ventilation fans type K315 L (System air AB, SE-739 30 Skinnskatteberg, Sweden) and type QBU100D (Lindab, Denmark) through 0.070 and 0.035-m internal diameter pipes for SM-1 and SM-2, respectively. A Lubcke VARIO[®] variable transformer drive (type RV10806-20, Noratel Lubcke A/S, Brøndby, Denmark) and a Danfoss VLT[®] variable-speed drive (type 3508, Danfoss A/S, Nordborg, Denmark) were used to control fan speeds for SM-1 and SM-2 respectively.

Table 5.1 - Dimensions of the two scale models SM-1 (1:6) and SM-2 (1:12.5).

Parameters	SM-1, m	SM-2, m
Model length, L	1.750	0.840
Model width, W	1.000	0.500
Model height from the emission surface, H	0.535	0.290
Maximum inlet opening height, h_{max}	0.095	0.045
Diameter of exhaust pipe, D	0.070	0.035
Flap length, L_f	0.188	0.090
Width of ammonia pan emission surface, S_w	0.375	0.180
Depth of ammonia pan, d_s	0.070	0.130

A duct was fitted between the circular exhaust port and the exhaust fans. A calibrated FMU/FMDRU 100-80 flow meter (Lindab A/S, Haderslev, Denmark) and an orifice plate were used to select desired airflow rates through SM-1 and SM-2, respectively. In SM-1, the pressure difference between the upstream and the downstream side of the flow meter, was measured using a differential pressure sensor (Model 694, Huba Control, Würenlos, Switzerland), which had a measurement range of 10-300 Pa, an accuracy of $\pm 0.7\%$, and a resolution of 0.1% of full scale. In SM-2, pressures across the orifice plates were measured by a Micro-manometer (type FC0510, Furness control Ltd., East Sussex, England), which had a measurement range of 0–2000 Pa, an accuracy of 0.3% and a resolution of 0.01 Pa. The averaged data of a sampling period of 1s were saved every min in a data logger (Model CR215, Campbell Scientific, Logan, Utah, USA).

At a distance of 1/4 the length from the left sidewalls, $0.980 \text{ m} \times 0.375 \text{ m}$ and $0.500 \text{ m} \times 0.180 \text{ m}$ surface areas of the uncovered ammonia pans were used in SM-1 and SM-2, respectively (Fig. 5.1). The remaining bottom surface areas were covered with 0.005m thick polystyrene sheet in SM-1 and 0.001m thick neoprene in SM-2.

5.3.2. Ammonia aqueous solution

The aqueous solutions of ammonia used for the experiment were combinations of a source solution and a buffer solution. An ammonium chloride (NH_4Cl) solution was made as the ammonia source.

The buffer solution of sodium carbonate (Na_2CO_3) and sodium hydrogen carbonate (NaHCO_3) was used to keep the constant pH of the aqueous solution. The solution was kept circulating during the measurement at the flow rate of $0.05 \text{ m}^3 \text{ hr}^{-1}$ using a 6-mm diameter hose and a pump (type PA1000, Heissner GmbH, Lauterbach, Germany) from the ammonia source tank. This kept a 0.25 m deep ammonia solution underneath the scale model and fed the ammonia pan inside the model. The stability of the ammonia aqueous solution was tested prior to the experiment to ensure that the ammonia emission rate under specific conditions could allow the experiment to be performed under steady state conditions. The continuous circulation of solution in the ammonia pan provided a stable free ammonia concentration at the immediate liquid surface even during the ammonia release process.

Liquid samples were taken from the return flow of the ammonia solution before and after each experiment to measure the total ammoniacal nitrogen (TAN) concentration according to ISO 7150/1 and the pH value using a pH detector (type Sension 1, HACH-LANGE, Bronshoj, Denmark).

5.3.3. Experimental design

To create different airflow conditions above the liquid surface, the experiments were carried out using four airflow rates and two ventilation control strategies (constant inlet opening and constant inlet velocity). Three set-ups were used during the four experiments. Set-up 1 and set-up 2 were conducted with constant inlet opening and constant inlet velocity, respectively. The same Rm was kept between the two models at corresponding ventilation rates in both set-ups (Table 5.2). In set-up 3, a constant inlet opening was used and Re was kept the same

Table 5.2 - Experimental set-ups 1 and 2 with two ventilation control strategies to keep similar Rm in two scale models.

Set-up	Control strategy	Rm , $\text{m}^2 \text{ s}^{-2}$	Inlet velocity, m s^{-1}	SM-1			SM-2		
				Inlet opening, m	Ventilation, $\text{m}^3 \text{ s}^{-1}$	Re	Inlet opening, m	Ventilation, $\text{m}^3 \text{ s}^{-1}$	Re
1	Constant inlet opening	0.0044	1	0.01	0.02	700	0.005	0.005	350
		0.0177	2	0.01	0.04	1400	0.005	0.010	700
		0.0398	3	0.01	0.06	2100	0.005	0.015	1050
		0.0708	4	0.01	0.08	2800	0.005	0.020	1400
2	Constant inlet velocity	0.0044	1	0.01	0.02	700	0.005	0.005	350
		0.0088	1	0.02	0.04	1400	0.010	0.010	700
		0.0133	1	0.03	0.06	2100	0.015	0.015	1050
		0.0177	1	0.04	0.08	2800	0.020	0.020	1400

between the two models at the controlling ventilation rates (Table 5.3). Three different TAN concentrations were used in SM-1 to study the effect of TAN on total ammonia emission rate. Ammonia solutions with TAN 8400 mg l^{-1} (pH 9.0) and 23000 mg l^{-1} (pH 8.7) were used for set-ups

1 and 2. Ammonia solution with TAN of 6700 mg l⁻¹ (pH 9.0) was used in set-ups 1 and 3. These selected TAN concentrations were higher than found in the pig manure to facilitate the study and maintain a robust balance between ammonium and ammonia during the experiment. Ammonia aqueous solution with TAN concentration of 5100 mg l⁻¹ and pH of 8.7 was used in SM-2 in all three set-ups.

Table 5.3 - Experimental set-up 3 with one ventilation control strategy to keep similar *Re* in two scale models.

Set-up	Control strategy	<i>Re</i>	SM-1				SM-2			
			Inlet opening, m	Inlet velocity, m s ⁻¹	Ventilation, m ³ s ⁻¹	<i>Rm</i> , m ² s ⁻²	Inlet opening, m	Inlet velocity, m s ⁻¹	Ventilation, m ³ s ⁻¹	<i>Rm</i> , m ² s ⁻²
3	Constant inlet	350	0.01	0.5	0.01	0.0012	0.005	1.0	0.005	0.0044
		700	0.01	1.0	0.02	0.0044	0.005	2.0	0.010	0.0177
	opening	1050	0.01	1.5	0.03	0.0098	0.005	3.0	0.015	0.0398
		1400	0.01	2.0	0.04	0.0175	0.005	4.0	0.020	0.0708

5.3.4. Measurement

Temperature and the relative humidity (RH) of the air in the experimental room and the SM-1 exhaust air were measured using two Vaisala Intercap humidity and temperature probes (Humitter 50Y, Vaisala, Helsinki, Finland) that had accuracies of $\pm 0.1^\circ\text{C}$ for temperature and $\pm 3\%$ at 20°C for RH. The air temperature and RH data were averaged and saved every minute in a data logger (Model CR215, Campbell Scientific, Logan, Utah, USA). During the SM-2 study, the room air temperature and RH were monitored with a Testo 174 mini temperature/humidity data logger (Testo Inc., Sparta, New Jersey, USA).

Smoke was used in the experiments to visualise the direction of the local air stream flow paths and the pressure differentials. Measurements of return air velocity and turbulent intensity were taken at non-dimensional measurement height (measurement point height/total height (*H*)) = 0.035 above the ammonia emission surface in both scale models at corresponding ventilation rates and inlet air velocities (Fig. 5.1). The return air velocity is the velocity of the floor air at above mentioned height of rotary air jet. A laser Doppler anemometer (Type 58N40-FVA enhanced, DANTEC Dynamics, Skovlunde, Denmark) was used to measure the air velocity and velocity fluctuations associated with turbulence or unsteadiness. The integration time for velocity measurement at each measurement point was 8 min. The inlet air velocity was calculated using the mean ventilation rate divided by the model inlet cross-sectional area.

Ammonia concentration in the incoming and outgoing air was measured sequentially at the scale model inlet and outlet, respectively, using a Brüel & Kjær Photoacoustic Multi-gas Monitor (Type 1312, Innova AirTech Instruments, Ballerup, Denmark) and a multiplexer (Type 1309, Innova AirTech Instruments, Ballerup, Denmark). The accuracy of the Multi-gas monitor for ammonia measurement was ± 0.1 ppm depending on the filter setting. The sample integration time configured in the monitor for the experiment was 20 s. The measurement time at each point was 40

min before switching to another point. It was found that at least 10-15 min were required for the ammonia concentration reading to stabilise following a measurement of air with higher ammonia concentration. Therefore, the 'old' air in the instruments was flushed to ensure the replacement of new air, especially when ammonia concentration of 'old' air was very high (Rom and Zhang, 2010). The system operated for at least 30 min to let the airflow conditions to stabilise in each experiment before ammonia concentrations were measured.

5.3.5. Estimation of ammonia emission rate and calculation of non-dimensional parameters

Ammonia emission from the scale models were calculated as:

$$E = U_i \frac{A_t}{A_s} (C_o - C_i) \quad (5.10)$$

where E is emission rate, $\text{mg s}^{-1}\text{m}^{-2}$; A_t is total inlet opening area, m^2 ; A_s is ammonia release surface area, m^2 ; C_o is outlet ammonia concentration, mg m^{-3} ; C_i is inlet ammonia concentration, mg m^{-3} .

The average inlet velocities ranged from 1.0 to 4.0 m s^{-1} for most of the tests. Therefore, emission rate at the inlet velocity of 1 m s^{-1} was used as a base emission rate, a method successfully used by Smith and Watts (1994), to calculate the non-dimensional normalised emission rate (Eq. 5.11) for model comparisons.

$$\text{Normalised emission rate} = \frac{E}{E_1} \quad (5.11)$$

where E_1 is reference emission rate at inlet air velocity of 1 m s^{-1} for the corresponding experiment set-up, $\text{mg s}^{-1}\text{m}^{-2}$.

The non-dimensional normalized return air velocity was calculated as

$$\text{Normalised return air velocity} = \frac{U_r}{U_i} \quad (5.12)$$

where U_r is the return air velocity, m s^{-1} .

5.4. Results and discussion

5.4.1. Air flow pattern

The smoke test of airflow patterns in the scale models showed that the supply air entering from the two side-wall inlets travelled horizontally until they met in the middle of the model before turning downwards and forming two cycles of opposite directions (Fig. 5.2a). The two contra-rotating flows were symmetric about the vertical centre line across the widths of the model. These ventilation air streams were in direct contact with the floor in the model (Fig. 5.1), which because the model did not have slatted floors was equivalent to pit manure level in pig houses. This symmetrical air flow pattern was similar to that achieved by Ye et al. (2009) and Zhang et al. (2008). Details of the air flow patterns depend on ventilation rate, inlet air velocity, and inlet opening height (Saha and

Zhang, 2010). A linear correlation ($R^2=0.89$) between the inlet air velocity and the return air velocity was demonstrated in this study (Fig. 5.2b). A similar relationship was also found by Strøm *et al.* (2002) in a full-scale room study. At constant inlet air velocity of 1 m s^{-1} but with different inlet opening height and ventilation rates, the return air velocities were different. Because the airflow patterns at the two sides of the ventilated enclosure were symmetric, only the left side of the model was considered for the study of surface air velocity, ammonia emission, and similarity criteria.

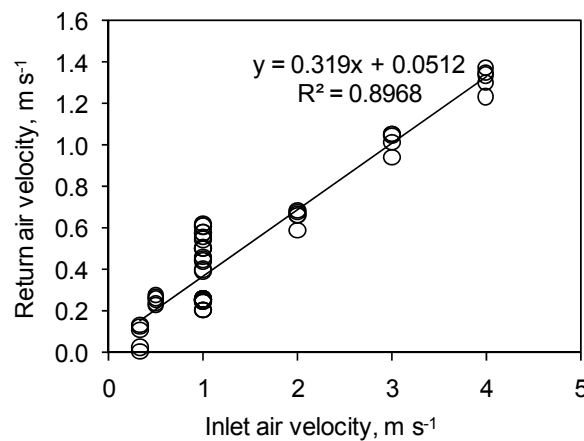
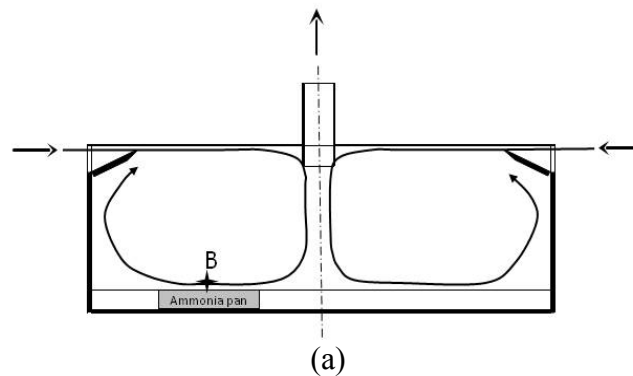


Fig. 5.2 - (a) Air flow pattern in a model pig house from smoke test and (b) relationship between inlet air velocity and return air velocity measured at location B.

5.4.2. Ammonia concentration

At the exhaust air temperature of $21.9 \pm 0.25^\circ\text{C}$ was measured when the laboratory room air temperature was kept at $22.3 \pm 0.28^\circ\text{C}$; ammonia concentrations at the outlets varied and were correlated to the different TAN concentrations and pH values in the ammonia aqueous solutions among different trials and in SM-1 (Table 5.4) and SM-2 (Table 5.5). Higher TAN in the solutions resulted in higher outlet ammonia concentrations (Table 5.4).

Table 5.4 - Experimental conditions and study results in SM-1

Trial	Set-up	Ventilation, Inlet velocity,		Re	Rm , $m^2 s^{-2}$	TAN, $mg l^{-1}$	pH	Ammonia, $mg m^{-3}$	
		$m^3 s^{-1}$	$m s^{-1}$					Inlet*	Outlet*
1	1	0.02	1	700	0.0044	23000	8.7	1.13±0.08	46.17±2.22
		0.04	2	1400	0.0175	23000	8.7	2.58±0.20	33.74±0.94
		0.06	3	2100	0.0394	23000	8.7	1.74±0.12	27.71±0.59
		0.08	4	2800	0.0700	23000	8.7	2.97±0.05	23.93±0.45
	2	0.02	1	700	0.0044	23000	8.7	2.58±0.19	46.17±2.22
		0.04	1	1400	0.0088	23000	8.7	2.97±0.05	26.96±1.23
		0.06	1	2100	0.0131	23000	8.7	2.15±0.11	20.05±0.85
		0.08	1	2800	0.0175	23000	8.7	2.20±1.16	17.93±0.74
2	1	0.02	1	700	0.0044	8400	9.0	0.94±0.06	20.67±0.98
		0.04	2	1400	0.0175	8400	9.0	1.08±0.07	15.23±0.65
		0.06	3	2100	0.0394	8400	9.0	1.02±0.09	12.02±0.35
		0.08	4	2800	0.0700	8400	9.0	1.16±0.09	10.26±0.30
	2	0.02	1	700	0.0044	8400	9.0	0.94±0.06	20.67±0.98
		0.04	1	1400	0.0088	8400	9.0	0.89±0.13	13.03±0.86
		0.06	1	2100	0.0131	8400	9.0	0.82±0.08	9.76±0.61
		0.08	1	2800	0.0175	8400	9.0	0.75±0.07	8.57±0.82
3	1	0.02	1	700	0.0044	6700	9.0	0.83±0.07	17.25±0.96
		0.04	2	1400	0.0175	6700	9.0	1.07±0.12	12.67±0.53
		0.06	3	2100	0.0394	6700	9.0	1.00±0.08	9.83±0.28
		0.08	4	2800	0.0700	6700	9.0	0.91±0.10	8.02±0.22
4	3	0.01	0.5	350	0.0012	6700	9.0	0.67±0.07	22.47±3.48
		0.02	1.0	700	0.0044	6700	9.0	0.83±0.07	17.25±0.96
		0.03	1.5	1050	0.0098	6700	9.0	0.95±0.08	14.25±0.73
		0.04	2.0	1400	0.0175	6700	9.0	1.07±0.12	12.67±0.53

* mean±standard deviation.

Ammonia concentrations at the outlets of scale models decreased as the ventilation rate increased due to the effect of dilution and flushing. This reduced concentration could increase the difference in partial pressures between the emission source and the ventilated air space. Partial pressure difference is the driving force for ammonia release from liquid solutions.

5.4.3. Ammonia emission rate

Ammonia emission rates increased as the inlet air velocities increased with all three different ammonia concentrations in aqueous solutions (Fig. 5.3a). Moreover, at the same inlet air velocities, ammonia emission rates were higher when the TAN concentrations were higher in the aqueous solutions. At the same pH in the aqueous solutions, a 25% higher TAN resulted in almost 25% higher emission rates (Fig. 5.3a). On the other hand, an aqueous ammonia solution with 23000 $mg l^{-1}$ TAN and pH of 8.7 resulted in 2.8 times higher ammonia emission rate than the solution with

6700 mg l⁻¹ TAN and pH of 9.0, though there was a 3.4-time difference between the two TAN concentrations. This result indicated that pH value also affected ammonia emission rates. The higher the pH value, the more dissolved ammonia was in the solution and thus the higher concentration of gaseous ammonia was available at the solution surface. Ye *et al.* (2008) also confirmed that increased pH value of ammonia solution enhanced ammonia mass transfer rate.

Table 5.5 - Experimental conditions and test results in SM-2.

Trial	Set-up	Ventilation, m ³ s ⁻¹	Inlet velocity, m s ⁻¹	<i>Re</i>	<i>Rm</i> , m ² s ⁻²	Ammonia, mg m ⁻³	
						Inlet*	Outlet*
1	1	0.005	1	350	0.0044	8.9±0.2	27.2±1
		0.010	2	700	0.0177	8.3±0.1	21.5±0.6
		0.015	3	1050	0.0399	8.5±0.3	20.2±1.1
		0.020	4	1400	0.0709	7.8±0.1	16.9±0.5
	2	0.005	1	350	0.0044	8.9±0.2	27.2±1
		0.010	1	700	0.0089	8.3±0.1	21.1±1
		0.015	1	1050	0.0133	8.5±0.1	18±0.5
		0.020	1	1400	0.0177	7.8±0.2	15.9±0.4

TAN = 5100 mg l⁻¹, and pH = 8.7. * mean±standard deviation.

The relationship between the emission-related variables was masked by large differences in the magnitude of emissions among the different trials. This problem was solved by using a non-dimensional emission rate as used by Smith and Watts (1994) who compared experimental results between two wind tunnels of different sizes. By considering ammonia emission rate at 1 m s⁻¹ air velocity (E_1) as the base emission rate for prevailing conditions with the TAN and pH in aqueous solution, temperature, moisture content, and solution age, etc., the non-dimensional normalised emission rates were almost the same at different air velocities, although the aqueous solution properties were quite different among the three experiments (Fig. 5.3b). If the relationship between the normalised emission rate and the air velocity shown in Fig. 5.3b assumed to be a power curve, then Eq. 5.11 can be written as:

$$\frac{E}{E_1} = 1.018 \times U_i^{0.43} \quad (R^2 = 0.98) \quad (5.13)$$

where R^2 is the co-efficient of determination.

Compared with the work of Smith and Watts (1994), the ammonia emission rates in this study had two more dependent variables, the TAN and the pH in aqueous solution between the scale models. However, the experimental results shown in Fig. 5.3b demonstrated that the non-dimensional normalised emission rate could be a good tool to compare the similarity parameters Re and Rm .

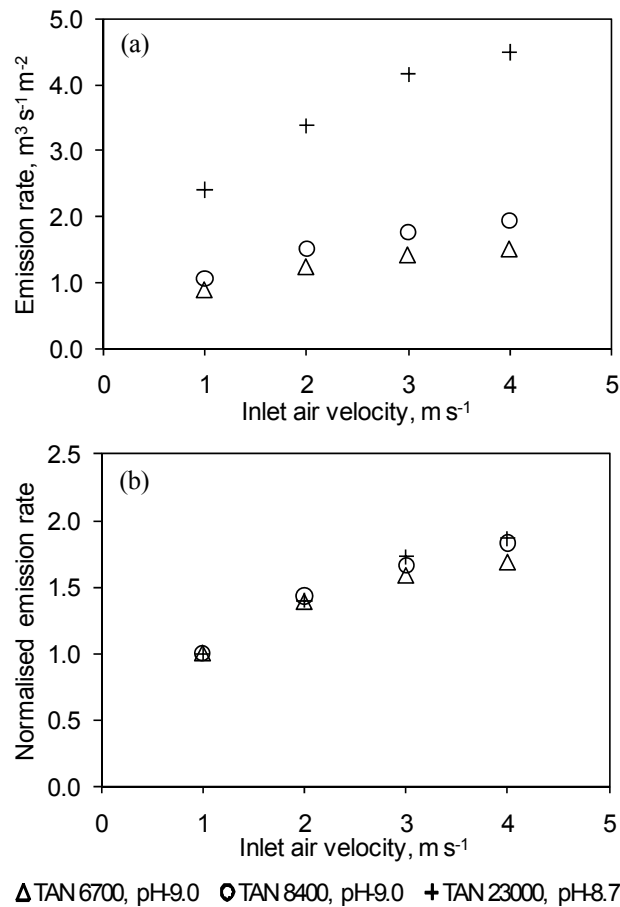


Fig. 5.3 - (a) Ammonia emission rate and (b) normalised ammonia emission rate at different inlet air velocities.

5.4.4. Comparison of similarity parameters Re and Rm

5.4.4.1. Return air velocity

The normalised return air velocities calculated using Eq. 5.12 at constant inlet openings and constant inlet air velocities were compared with the Re and Rm and presented in Fig. 5.4. By keeping similar Rm in the two models in set-ups 1 and 2, the calculated Re values were from 700 to 2800 and from 350 to 1400 in SM-1 and SM-2, respectively (Table 5.2). In set-up 3, the Re range was 350 to 1400 for both models (Table 5.3). These results made it difficult to directly compare the normalised return air velocities for $Re > 1400$ (Figs. 5.4a and 5.4b). At the same inlet Re , the inlet air velocity was always lower in the SM-1 than in the SM-2. The return air velocities above the emission surface could be expected to be lower in SM-1 than SM-2 as the return air velocity was linearly correlated to the inlet air velocity. But at constant inlet opening, the normalised return air velocity above the emission surface was similar in the two models when using Re as a similarity parameter (Fig. 5.4a). This result was in line with the study of Yu and Hoff (1999). Additionally, Yu and Hoff (1999) found that air velocity profile along the ceiling for a model and a prototype were not consistently based on Re although the dimensionless peak air velocities between the model

and the prototype were similar in the floor region. Using the constant inlet air velocity strategy, the normalised return air velocities were always higher in SM-2 than SM-1 at the same Re (Fig. 5.4b). At constant inlet air velocity but with different air inlet heights and ventilation rates in the scale models, the return air velocities above the emission surfaces were different.

When using Rm as the similarity parameter, the normalised return air velocities for SM-1 and SM-2 were similar for both ventilation control strategies, although some non-significant differences were observed at higher Rm , i.e., at higher inlet air velocities and larger inlet opening (Figs. 5.4c and 5.4d). These differences might be related with the higher h/H ratio in SM-1 than in SM-2.

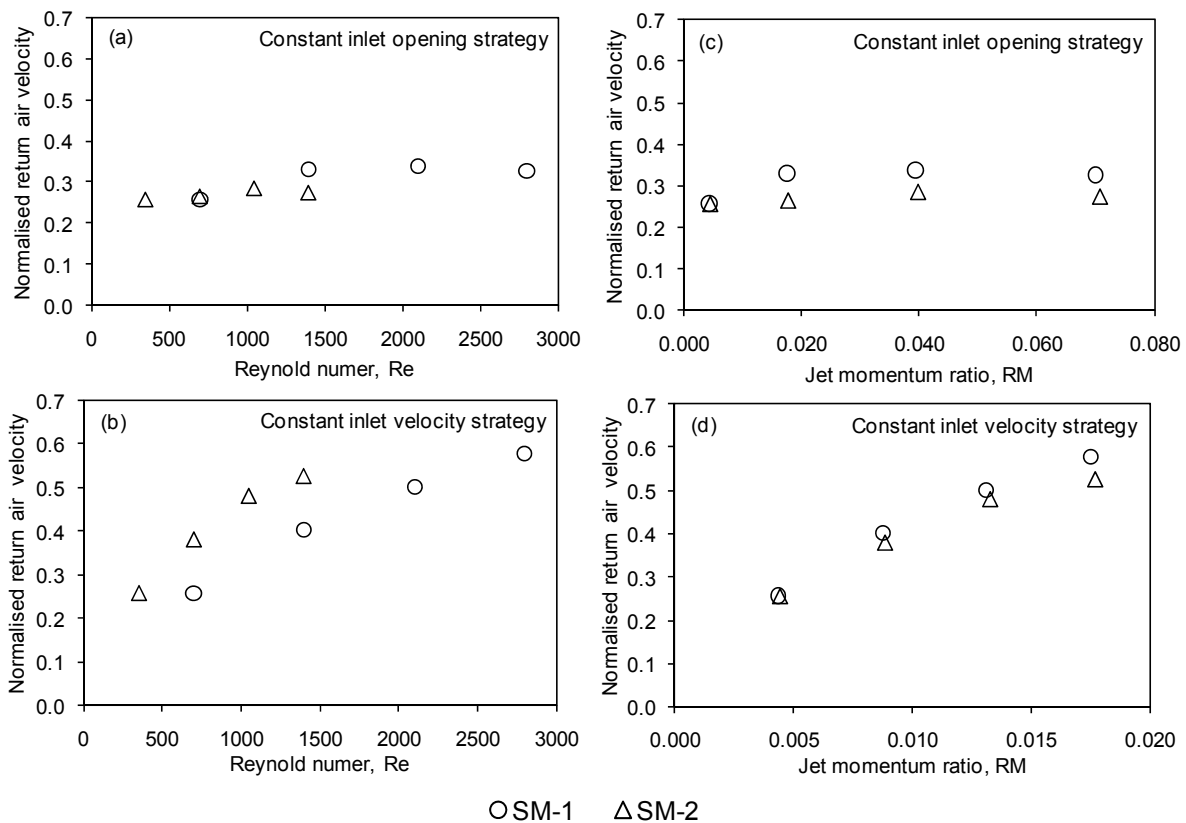


Fig. 5.4 - Comparison of normalised return air velocity based on Re and Rm at two ventilation control strategies.

5.4.4.2. Ammonia emission rate

The non-dimensional normalised ammonia emission rates increased as Re or Rm increased with both control strategies (Figs. 5.5 and 5.6). This was expected because gas emission rates are directly proportional to the surface air velocity in scale models studies (Saha et al., 2010, Ye et al., 2008). The normalised emission rates were higher in SM-2 than in SM-1 at the same Re values for both control strategies and at different TAN concentrations (Figs. 5.5a, 5.5b, and 5.5c). Air velocities in the air-jets were lower in SM-1 than SM-2 at the same Re , therefore reducing jet momentum, mass transfer, and normalised emission rate with SM-1 (Fig. 5.5c).

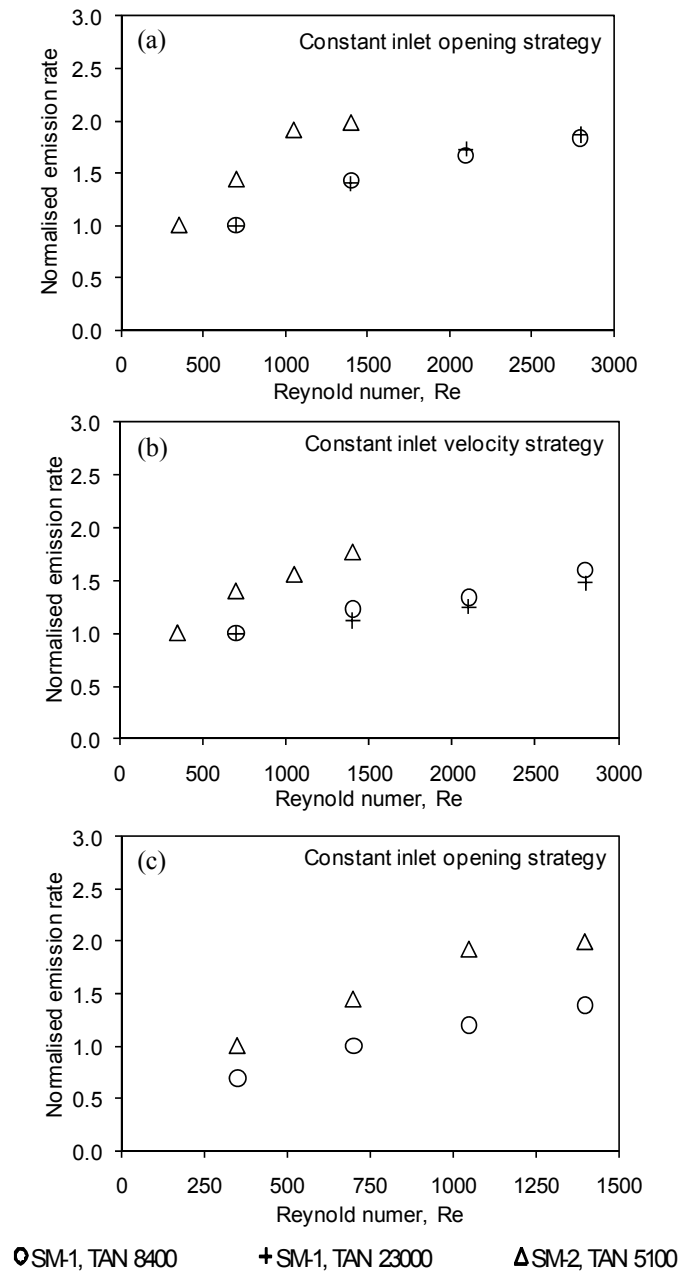


Fig. 5.5- Comparison of normalised ammonia emission rate based on Re at three set-ups with two ventilation control strategies.

However, the plot of normalised emission rate against Rm (Figs. 5.6a and 5.6b) shows that the non-dimensional normalised emission rate was similar irrespective of the ventilation control strategies adopted with the models. This indicated that Rm was the preferable similarity parameter rather than Re in scale model studies for prototype emission rate estimation. The small differences found between the normalised emission rates with SM-1 and SM-2 were expected because of the small differences in h/H ratio that resulted the differences in velocity distributions and turbulence scales in boundary layers.

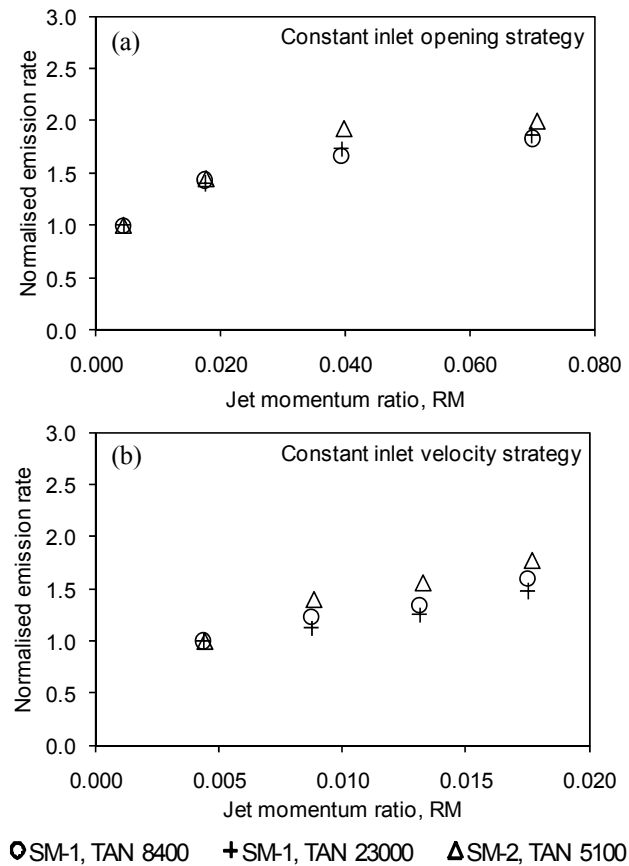


Fig. 5.6- Comparison of normalised ammonia emission rate based on R_m at two ventilation control strategies.

The regression equations of normalised emission rates as functions of Re and R_m in Table 5.6 indicate that, when using Re as the similarity criterion, the differences between the two scale models within the same control strategy were significant. However, because the coefficient of determination (R^2) for each of the six single-model equations in Table 5.6 were high, the equations for a single scale model using Re can be applied to estimate the emission rate for individual models. The normalised emission rate did not correlate well between the two models in all strategies when Re was used as the similarity parameter. When R_m was used as the similarity parameter, the normalised emission rates between the two models were very close, demonstrating good correlations between the two scale models. Using constant inlet opening and constant inlet velocity control strategies, R^2 were 0.97 and 0.83, respectively. Therefore, R_m can be used as similarity parameter for comparing two model results or comparing model results with the prototype.

Table 5.6 - Regression equations of normalised emission rates (E/E_1) in the two scale models.

Parameter	Strategy	Model	E/E_1	R^2
Re	Constant inlet opening	SM-1	$0.0528R_e^{0.4513}$	0.9903
		SM-2	$0.0470R_e^{0.5238}$	0.9776
		SM-1 & SM-2	$0.1523R_e^{0.3194}$	0.6104
Re	Constant inlet velocity	SM-1	$0.1451R_e^{0.2917}$	0.9056
		SM-2	$0.0949R_e^{0.4047}$	0.9881
		SM-1 & SM-2	$0.3451R_e^{0.1853}$	0.3661
Re^*	Constant inlet opening	SM-1	$0.0371R_e^{0.5008}$	0.9999
		SM-2	$0.0470R_e^{0.5238}$	0.9776
		SM-1 & SM-2	$0.0421R_e^{0.5123}$	0.6279
Rm	Constant inlet opening	SM-1 & SM-2	$3.6837R_m^{0.2379}$	0.9713
	Constant inlet velocity	SM-1 & SM-2	$5.9370R_m^{0.3293}$	0.8299

*Used the same Re in the two scale models.

5.5. Conclusions

Comparison of airflow and ammonia release in the two scale models revealed several characteristics in the model studies. Air streams were symmetric about the vertical centre line inside the models. A linear correlation ($R^2=0.89$) was established between the inlet air velocity and the return air velocity. Higher concentration and pH of the aqueous ammonia solution resulted in higher gaseous ammonia concentrations in the model outlets and ammonia emissions from the models. The non-dimensional normalised emission rate was proved to be a good tool to compare the similarity parameters Re and Rm .

Our study confirmed that Rm was the preferred similarity parameter rather than Re for modelling the airflow and non-dimensional ammonia emission rates at different experimental conditions, including two ventilation control strategies and different TAN and pH in ammonia solutions. This was demonstrated because when using Rm as the similarity parameter, the normalised emission rates between the two scale models had R^2 of 0.97 and 0.83 for constant inlet opening and constant inlet velocity control strategies, respectively.

Acknowledgements

This research was conducted as part of ROSES project “Reduction of Odour Source in and Emission from Swine Buildings” under the program “Animal Husbandry, the Neighbours and the Environment” funded by the Danish Ministry of Food, Agriculture and Fisheries (Grant Number 3304-VMP-05-032-01). The authors also appreciate the technical support of Preben Jensen Dahl,

Academic employee, and Shen Xiong, PhD student, Department of Biosystems Engineering, Aarhus University, Denmark.

References

- Aarnink A J A; Wagemans M J M (1997). Ammonia volatilization and dust concentration as affected by ventilation systems in houses for fattening pigs. *Transactions of the ASAE*, 40(4), 1161-1170.
- Adre N; Albright L D (1994). Criterion for establishing similar air-flow patterns (Isothermal) in slotted-inlet ventilated enclosures. *Transactions of the ASAE*, 37(1), 235-250.
- Awabi H B (1991). *Ventilations of Buildings*. Chapman & Hall, London, UK.
- Baturin V V (1972). *Fundamental of Industrial Ventilation*. Pergamon Press, Oxford, UK.
- Buller G W; Hellickson M A (1978). Model study of swine manure pit ventilation systems. St. Joseph, Mich.: ASAE.
- Jin Y; Ogilvie J R (1992). Air-flow characteristics in the floor region of a slot ventilated room (Isothermal). *Transactions of the ASAE*, 35(2), 695-702.
- Morsing S; Strom J S; Zhang G; Kai P (2008). Scale model experiments to determine the effects of internal airflow and floor design on gaseous emissions from animal houses. *Biosystems Engineering*, 99(1), 99-104.
- Pattie D R; Milne W R (1966). Ventilation airflow patterns by use of models. *Transactions of the ASAE*, 9 (5), 646-649.
- Rom H B; Zhang G (2010). Time delay for aerial ammonia concentration measurements in livestock buildings. *Sensors*, 10(5), 4634-4642.
- Rousseau A N; Albright, L D (1996). An alternative kinematic similarity criterion for slot-ventilated enclosures . *Transactions of the ASAE*, 38(6), 1887-1889.
- Saha C K; Zhang G Q; Kai P; Bjerg B (2010). Effects of a partial pit ventilation system on indoor air quality and ammonia emission from a fattening pig room. *Biosystems Engineering*, 105(3), 279-287.
- Saha C K; Zhang G Q (2010). Effect of ventilation control strategies, pen partition, and slurry pit location on ammonia emission in a model pig house. In: *Towards Environmental Technologies – Proceedings of AgEngg2010 International Conference on Agricultural Engineering*, 6-8 September 2010, Clermont-Ferrand, France. Paper no. REF485 in Proceedings CD.
- Schlichting H (1979). *Boundary-layer Theory*. MacGraw-Hill Inc., NewYork, USA.

- Smith R J; Watts P J (1994). Determination of odor emission rates from cattle feedlots. 2. Evaluation of two wind tunnels of different size. *Journal of Agricultural Engineering Research*, 58(4), 231-240.
- Strom J S; Zhang G; Morsing S (2002). Predicting near-floor air velocities for a slot-inlet ventilated building by jet velocity decay principles. *Transactions of the ASAE*, 45(2), 407-413.
- Szucs E (1980). *Similitude and Modeling*. Elsevier Scientific Publishing Co., Amsterdam, The Netherlands.
- Timmons M B; Baughman G (1981). Similitude analysis of ventilation by stack effect from an open ridge livestock structure. *Transactions of the ASAE*, 14(4), 1030-1034.
- Topp C; Nielsen P V; Heiselberg P (2001). Influence of local airflow on the pollutant emission from indoor building surfaces. *Indoor Air-International Journal of Indoor Air Quality and Climate*, 11(3), 162-170.
- Ye Z; Saha C K; Li B; Tong G; Wang C; Zhu S; Zhang G (2009). Effect of environmental deflector and curtain on air exchange rate in slurry pit in a model pig house. *Biosystems Engineering*, 104(4), 522-533.
- Ye Z; Zhang G; Li B M; Strom J S; Tong G H; Dahl P J (2008). Influence of airflow and liquid properties on the mass transfer coefficient of ammonia in aqueous solutions. *Biosystems Engineering*, 100(3), 422-434.
- Yu H; Hoff S J (1999). Airflow pattern similarity criteria for ceiling slot-ventilated agricultural enclosures under isothermal conditions. *Transactions of the ASAE*, 42(2), 459-469.
- Yu H; Jou L J; Ouyang H T; Liang H M; Liao C M (2006). Similitude criteria for a two-dimensional wall jet in an isothermal mechanically ventilated enclosure. *Biosystems Engineering*, 93(4), 415-425.
- Zhang G; Bjerg B; Strom J S; Morsing S; Kai P; Tong G; Ravn P (2008). Emission effects of three different ventilation control strategies - A scale model study. *Biosystems Engineering*, 100(1), 96-104.
- Zhang G; Strom J S; Li B; Rom H B; Morsing S; Dahl P; Wang C (2005). Emission of ammonia and other contaminant gases from naturally ventilated dairy cattle buildings. *Biosystems Engineering*, 92(3), 355-364.
- Zhang J S; Christianson L L; Riskowski G L (1991). Effect of diffuser air velocity profiles on scaling methods for predicting room air motion. ASAE Paper No.91-4558, St Joseph, MI.

Chapter 6

Effect of airflow on odorants emissions in a model pig house- A laboratory study using proton-transfer-reaction mass spectrometry (PTR-MS)

Paper V:

Saha, C.K., Feilberg, A., Zhang, G., and Adamsen, A. P. (2011). **Effect of airflow on odorants emissions in a model pig house- A laboratory study using Proton-Transfer-Reaction Mass Spectrometry (PTR-MS).** Submitted to a peer review journal.

Abstract

Identification of different factors that affect emissions of gases, including volatile organic compounds (VOCs) are necessary to develop emission abatement technology. The objectives of this research were to quantify and study temporal variation of gas emissions from a model pig house under varying ventilation rates. The model was 0.84 m×0.5 m×0.32 m (L×W×H), had two sidewall inlets and an exhaust in the middle of the ceiling, and is a scale of 1:12.5 of a section of a commercial finishing pig house. The experiments were conducted under controlled isothermal laboratory condition using four ventilation rates. The concentrations at inlet, outlet, and slurry pit of the model space were measured using Proton-Transfer-Reaction Mass Spectrometry (PTR-MS). PTR-MS can measure the temporal variations of odour compounds emission from the slurry pit in real time. The emissions of H₂S and 14 VOCs were lower than at real pig buildings except for ammonia, which indicated possible other sources of those compounds than the slurry in the slurry pit. One or more of the four factors, such as (1) pH increase at the surface, (2) dry matter enrichment at the surface layer, (3) surface concentration reduction due to evaporation combined with reduced diffusivity in the enriched surface, and (4) oxidation of the oxic surface layer might be the main reasons for the temporal variations of NH₃, H₂S, and 14 VOCs. The ventilation rate affected significantly on ammonia and trimethylamine emission ($p < 0.05$). The hydrogen sulphide (H₂S) emission was independent of ventilation rate. VFAs emission dependency on ventilation rate increased with the increase of carbon chain. Phenols, indoles, and ketones showed the positive correlation with ventilation rate to some extent. Generally, compounds with high solubility (low Henry's constant) showed stronger correlation with ventilation rates than the compounds with high Henry's constant.

Key words: ammonia; hydrogen sulphide; volatile organic compounds; temporal variation; emission; ventilation rate

6.1. Introduction

Emission of volatile organic compounds (VOCs) and volatile inorganic compounds (VICs) from intensive livestock production facilities is a source of offensive odour in indoor and outdoor air (Aneja et al., 2009). The odorous VOCs includes volatile reduced sulphur compounds, phenols, indoles, aldehydes, ketones, amines, and volatiles fatty acids (VFAs) (Feilberg et al., 2010b). Two of the primary VICs emitted from pig production are ammonia (NH_3) and hydrogen sulphide (H_2S) (Blunden and Aneja, 2008; Ni et al., 2000a). In atmospheric chemistry, VOCs play central roles through their reactions with the hydroxyl radical (OH), by indirect production of ozone and organic aerosol following their photochemical oxidation (Andreae and Crutzen, 1997). Both ozone and organic aerosol have direct health effects for humans as they are harmful to our respiratory system. Moreover, ammonia and hydrogen sulphide have negative effects on human and animal health as well as the surrounding ecosystems and cause malodorous emission (Bull and Sutton, 1998; Campagna et al., 2004; Cupr et al., 2005; Portejoie et al., 2002). Hydrogen sulphide is considered the most dangerous gas in animal buildings and manure storage facilities, and has been reported responsible for animal as well as human death in animal facilities (Oesterhelweg and Puschel, 2008). The quantification and transport behaviour of VOCs and VICs emissions from pig production facilities are important not only for estimation of emission factors from a regulatory standpoint, but also important for developing efficient emission abatement technologies and airflow control strategies for reducing emission and odours.

Odorous compounds in livestock facilities have several sources, such as the animals themselves, their excretions, the animal feed, and dust particles in animal building could serve as both VOC sources and sinks (Alanis et al., 2010; Ngwabie et al., 2008). Measurements of VOCs and H_2S in full-scale buildings have been conducted recently (Feilberg et al., 2010b), with results indicating that emissions from both slurry and floor surfaces were important. Influences of air exchange rate, temperature, and animal activity were observed, but the relative importance of these factors could not be completely elucidated due to covariance between the variables. Gaseous emissions from specific sources (e.g., pig slurry) that may contribute significantly to the total emission from pig buildings, need to be identified and quantified. In addition, the effects of single factors need to be investigated under controlled conditions.

Most research on emission from pig facilities has been focused on ammonia (Arogo et al., 1999a; Chaoui et al., 2009; Cortus et al., 2008; Elzing and Monteny, 1997; Griffing et al., 2007; Misselbrook et al., 2000; Ni, 1999; Rong et al., 2009; Saha et al., 2010a; Sommer and Sherlock, 1996; Ye et al., 2008b; Zhang et al., 2008) and in few a cases on hydrogen sulphide (Arogo et al., 1999b; Blunden et al., 2008; Griffing et al., 2007; Ni et al., 2000a; Ni et al., 2009) because of unavailability of reliable measurement methods for studying emission dynamics under variable

conditions (airflow, temperature, pH etc.). Furthermore, research on VOC emissions from slurry based on a limited number of discrete samples has been published (Blanes-Vidal et al., 2009b; Chen et al., 2009) giving, however, little insight of the emission dynamic process.

Analysis of air samples in gas bags by olfactometry has been used to assess the odour impact on people of single compounds or complex mixture. This measurement method is time-consuming and associated with significant systematic and random errors (Bliss et al., 1996; Clanton et al., 1999; Hansen et al., 2011; Schulz and vanHarreveld, 1996) and cannot be used for continuous measurements. Measurements of VOCs in agricultural emissions have largely been done using gas chromatography coupled with mass spectrometry (GC/MS) for analysis of air samples that were either collected in canisters, on adsorbents or in cryostats (Blanes-Vidal et al., 2009a; Chen et al., 2009; Trabue et al., 2006; Trabue et al., 2008; Wright et al., 2005). GC/MS measurements provide detailed information of gaseous VOC composition, but are not suitable for following rapid changes in concentrations. Feilberg et al. (2010a) presented continuous Membrane Inlet Mass Spectrometry (MIMS) data on odorant reduction in biological air filters treating air from pig slurry. However, lack of adequate field calibration, reduced selectivity and sensitivity were identified as major shortcomings of the method with respect to quantification and specific odorant emission estimates.

Proton-Transfer-Reaction Mass Spectrometry (PTR-MS) has been demonstrated to be a promising tool for time-resolved measurement of emissions of selected VOCs from dairy farms (Ngwabie et al., 2008; Shaw et al., 2007) and pig farms (Feilberg et al., 2010b). The method is based on chemical ionization by protonated water and is characterized by sufficient selectivity and high sensitivity together with short response times (de Gouw and Warneke, 2007; Hewitt et al., 2003). Since PTR-MS is a direct method without request for sample collection, it holds a potential for overcoming sampling issues observed in previous methods for measuring odorants (Feilberg et al., 2010a). Therefore, PTR-MS can be used to study VOC release behaviour by direct continuous measurement.

Experiments in full scale buildings are very expensive and often it is difficult to observe the specific influence of airflow on emissions. Therefore, model studies under controlled laboratory conditions are practical for simulating the air motion of a prototype and can be used to study VOCs and VICs release behaviour from specific emission sources (e.g., from slurry surface). Several studies have been done in model buildings (Elzing and Monteny, 1997; Morsing et al., 2008; Zhang et al., 2008) and in wind tunnels (Saha et al., 2010b; Ye et al., 2008b) to investigate correlations of ammonia emissions and airflow, pH, and temperature. The influence of air velocity, turbulence and ventilation rate on NH₃ emission rate was reported by Ye et al. (2008b), Rong et al. (2009) and Saha et al. (2010b). Recently, Ni et al. (2009) studied emissions from pig wastes in two different ventilation rates in cylindrical chambers and found that different release mechanisms are correlated to gas solubility. The degree of involvement of convective mass transfer and bubble-release was

different for NH₃, H₂S, CO₂, and SO₂, which have different solubilities. VOCs were not included in their study.

Therefore, investigation of emissions of odorous VOCs from pig slurry at different ventilation rates is needed. The main objective of this research is to provide fundamental knowledge on odorant emissions from pig slurry under different conditions. This can be achieved by using PTR-MS. The specific objectives were (i) to quantify emissions of NH₃, H₂S, and VOCs only from pig slurry, (ii) to study temporal variation of emissions with constant ventilation rate, and (iii) to study the effect of ventilation rates on emissions from pig slurry under isothermal conditions in a model pig house.

6.2. Materials and Methods

6.2.1. Experimental room and model pig house

The model pig house used was a 1:12.5 scale model of a section of a commercial finishing pig house and placed in a laboratory room at Research Centre Foulum, Aarhus University. A detail of the scaling of a full scale pig building is described in Zhang et al. (2008). The experimental model pig house is made of a 5 mm clear acrylic sheet and consists of two parts: the top part is the pig house, and the bottom part a slurry pit (Fig. 6.1). The dimension of the top part was 840 × 500 mm (L × W), and the total height was 320 mm (Fig. 6.1). The slatted floor is 10 mm thick and was placed on two partitions with a height of 100 mm, leaving 210 mm height from the floor to the ceiling surface. The slurry pit was 850 mm long, 510 mm wide and 245 mm high. The headspace height is the distance between the underside of the slatted floor and the slurry surface, which was kept at 82 mm in all experimental set-ups. Ventilation air was supplied through adjustable slits spanning the whole width of the model in the two end-walls beneath the ceiling. The maximum opening height of each inlet is 45 mm. Air was drawn into the model by a SCL lateral channel blowers-exhausters (type SCL V4, FPZ Effepizeta s. r. l., Milano, Italy), connected to a central ceiling outlet made of clear acrylic pipe with 35 mm in diameter (Fig. 6.1). A Mitsubishi variable-speed drive inverter (type FR-S500, Mitsubishi Electric Corporation, Japan) was used as the fan speed controller.

Experiments were conducted with a slatted floor opening ratio of 33% and with four ventilation rates under isothermal conditions (Table 6.1). The resulting inlet air velocities were between 1 and 4 m s⁻¹, which were at the same level as inlet air velocities found under practical conditions. These velocities were calculated using average ventilation rates by total inlet opening area.

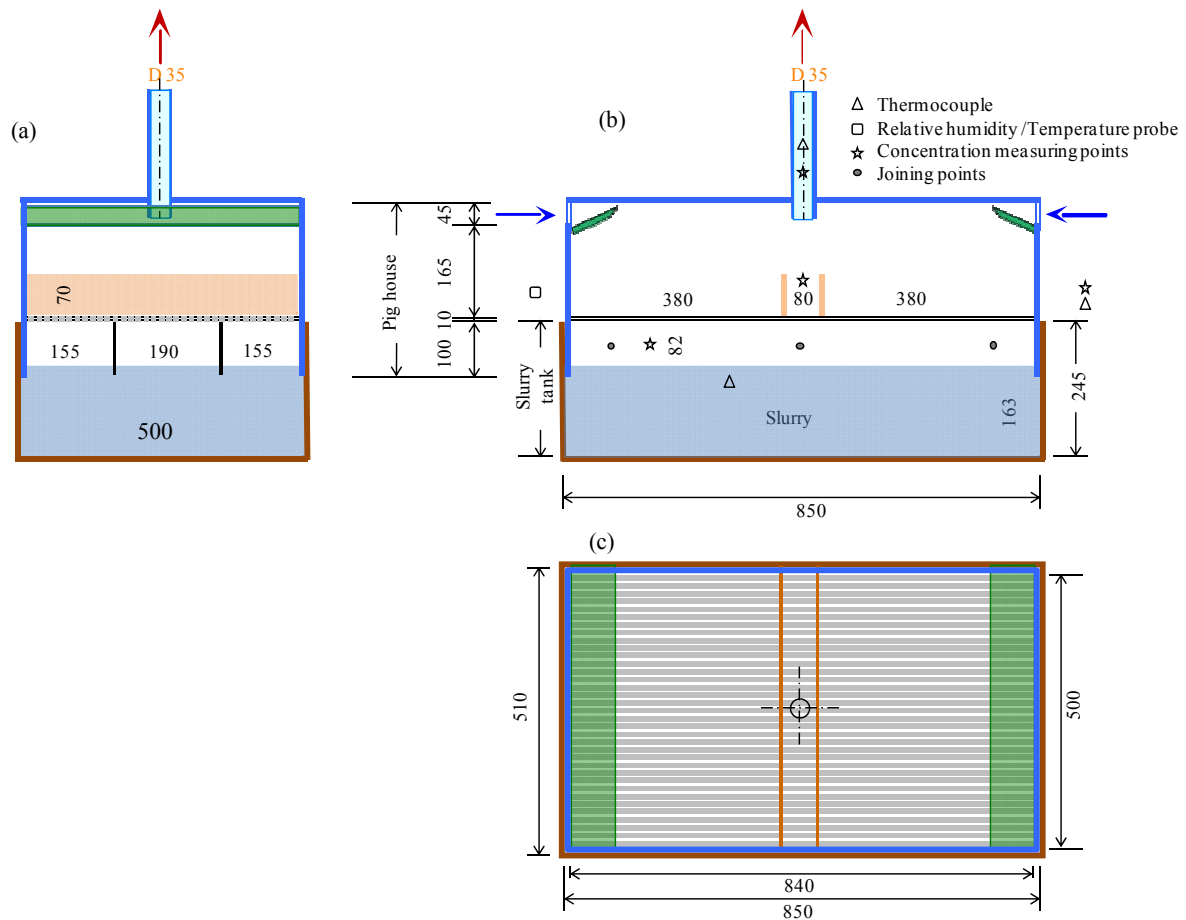


Fig. 6.1 - Different views of the 1:12.5 scale pig house section's experimental set-up with double rows of pens (a) front views, (b) side view with measuring locations and (c) plan view (all dimensions are in mm).

Table 6.1 - Control strategies were used in the scale model experiment at the headspace height of 82mm, the floor opening ratio of 33%, and the inlet opening height of 5 mm.

Velocity, ms^{-1}	Ventilation rate, m^3s^{-1}	Reynolds number, Re	Jet momentum number, J
1.00	0.005	350	5.8×10^{-3}
2.00	0.010	700	2.3×10^{-2}
3.00	0.015	1050	5.2×10^{-2}
4.00	0.020	1400	9.3×10^{-2}

6.2.2. Pig slurry

The pig slurry was collected directly from the slurry pit of an experimental pig production facility and stored using an intermediate bulk container. It was kept outside the laboratory building during the experimental period (September, 2010). The slurry was stirred and moved into a small tank, and

kept one day at constant room temperature ($20 \pm 0.5^\circ\text{C}$) for allowing slurry temperature to come into equilibrium. This was done repeatedly for each experimental run. Ye et al. (2008a) found that one day is enough to achieve temperature equilibrium because of the small amount of new slurry that was exchanged. The slurry pit of the scale model was always filled with the slurry from the small tank to a level of 160 mm above the bottom and stored overnight before starting experiments. After each experimental trial, 1/3 of the slurry in the manure container was replaced with new slurry to be ready for the experiment in the next day.

6.2.3. Measurements and instruments.

6.2.3.1. Temperature and relative humidity

The experimental room temperature and relative humidity was measured with Vaisala Intercap Humidity and Temperature Probe (Vaisala Humitter 50Y, FI-00421, Helsinki, Finland) that has accuracies of $\pm 0.1^\circ\text{C}$ and $\pm 3\%$ of the relative humidity at 20°C . The averaged of every minute room air temperature and relative humidity data was saved in a data logger (Model CR215, Campbell Scientific, Logan, Utah, USA).

The room air, exhaust air, and slurry temperatures were also measured continuously with three T-type thermocouples. The averaged of every minute temperature data were saved in ELTEK 1000 series squirrel data logger (type 1033-130K, Eltek Ltd. Haslingfield Cambridge CB3 7LL, England).

6.2.3.2. Ventilation airflow

The ventilation airflow rate was measured using an orifice plate designed according to ISO 5167-1. The pressures was measured with a differential pressure transmitter (type 694, Huba Control, Würenlos, Switzerland) with a measurement range of 0-300 Pa, an accuracy of $\pm 0.7\%$, and a resolution of 0.1% of full scale. The data was collected through Campbell Scientific CR1000 data logger (Campbell Scientific, Logan, Utah, USA). The sampling period was 10 s and averages were saved each 1 min. Ventilation airflow rate is related to the measured differential pressure and was determined by:

$$VR = \frac{C_d}{\sqrt{1-\beta^4}} \times \frac{\pi}{4} d^2 \times \sqrt{\frac{2\Delta P}{\rho}} \quad (6.1)$$

where VR is ventilation rate, $\text{m}^3 \text{s}^{-1}$; C_d is the coefficient of discharge; d is the diameter of the orifice, m; β is diameter ratio (diameter of the orifice/diameter of the vent pipe); ΔP is pressure difference between upstream and downstream side of the orifice, Pa.

The new ventilation rate was started each morning about 18 hours after replacing slurry in the slurry pit. The ventilation system was operated for at least 30 min to let the airflow conditions stabilize for each experimental trial before concentration measurement.

6.2.3.3. Manure analysis

Three slurry samples from the slurry surface in the manure container were taken before and after each experimental run for checking variations of manure characteristics such as pH value, dry matter (DM), total Kjeldahl nitrogen (TKN), total ammoniacal nitrogen (TAN), and volatile fatty acids (VFAs). DM, total nitrogen TKN and ammonium nitrogen $\text{NH}_4\text{-N}$ (Kjeldahl-N method) were measured according to the standard methods (APHA, 1998). The concentration of VFAs was measured as described by Kaparaju et al. (2009). The pH was measured in slurry samples and also 10 mm below the slurry surface using a pH electrode (type Sension 1, Hach-Lange GmbH, Germany) before and after each experimental run.

6.2.3.4. PTR-MS calibration and concentration measurement

The continuous measurement of VOCs and gaseous NH_3 and H_2S measurement were conducted by a High-Sensitivity PTR-MS (Ionicon Analytik, Innsbruck, Austria). The principle of PTR-MS has been described in detail in review papers (de Gouw and Warneke, 2007). In short, the sample molecules are ionized by a proton transfer from protonated water, H_3O^+ , in the drift tube. If the protonated sample molecules do not part into smaller fragments, the resulting protonated ion will have the molecular mass plus one from the proton. The ions are separated in a quadrupole mass filter according to the mass-to-charge ratio (m/z) and detected by an electron multiplier. The PTR-MS was operated under standard ion drift tube conditions applying a total voltage of 600 V and maintaining the pressure in the range of 2.1-2.2 mbar (210-220 pa). The temperature of the drift tube was controlled at 60 °C. The inlet flow during measurements as well as calibrations was $\sim 100 \text{ mL min}^{-1}$.

The humidity dependency of the sensitivity of the PTR-MS towards H_2S was investigated by diluting the output from the permeation oven with zero-air bubbled through a water trap via a frit diffuser. Calibrations were performed in the laboratory before the experiments. Mass dependent transmission factors were adjusted based on a standard mixture (Restek, P/N 34423-PI, Bellefonte, PA, USA) of aromatic compounds with known concentrations (in the range of 100 – 120 ppbv; $\pm 10\%$) and known proton transfer rate constants.

For compounds of which calibration standards were not available, the sensitivity was calculated based on the proton transfer rate constant and the estimated drift tube residence time as described in the literature (de Gouw and Warneke, 2007). Proton transfer rate constants were estimated if necessary as described by Feilberg et al. (2010b).

The uncertainties in concentration measurements were estimated by error propagation to be in the range of 10-26% depending on the calibration method (details given in Feilberg et al. (2010b)).

Detection limits were determined based on blank measurements of zero air. Dry zero-air for the laboratory tests and calibrations were produced from pressurized air by using a cold trap (obtained dewpoint: ~ -30 °C) and a charcoal filter. Further hydrocarbon removal was ensured by purification via a Supelpure HC filter (Supelco, USA). Zero air controlled by a mass flow controller (Sierra Instruments, USA) was passed through the permeation oven. The output was further diluted by using a mass flow controller. Values in the range of 0.2 to 2 $\mu\text{g m}^{-3}$ were generally observed using a mass dwell time of 2 s. The samples were collected and measured continuously in five locations for five minutes at each sampling point: at the ceiling exhaust unit, above and below the slatted floor, at the inlet, and blank. Thus, a complete measurement cycle was 25 min. All five sampling lines of 3 m Teflon (FEP) (3.18 mm OD, 1.59 mm ID) were used to draw air to the PTR-MS. These were connected to the instrument inlet system and drift tube via a 1 m PEEK sampling line (ID: 1 mm). The main sampling lines were insulated and temperature controlled at 40 °C by heater strips, whereas the PEEK tube was controlled at 60 °C. Measurements were carried out continuously by means of selected ion monitoring (SIM) mode with dwell times of 2 s. Masses for SIM mode were selected based on chemical compositions reported for similar systems, known PTR-MS fragmentation patterns, and ion abundance in full scan mode as reported by Feilberg et al. (2010b). The ions monitored together with compound assignments are presented in Table 6.2.

The concentration was measured at least five hours for each ventilation run to get sufficient data for comparison. One case was run at lowest ventilation rate (i.e., 0.005 $\text{m}^3 \text{s}^{-1}$) for 18 hours, just after filling the slurry in the tank to check the temporal variation VOCs and VICs.

6.2.4. Concentration and emission flux calculations

The first cycle (i.e., 25 min) of VOCs and gas concentration measurement were not considered in calculation of average concentration calculation because to be sure of stabilization of ventilation air. The first 1 min of the 5 min of VOCs and gas concentration data for each sampling site was not included in data processing allowing sufficient system equilibrium time. The averages of outlet concentration and inlet concentrations during measurement of each ventilation rate were used for emission flux calculation.

The rate of gas emission flux from the model pig house was calculated with Eq. (6.2).

$$E = \frac{VR}{A_s} (C_o - C_i) \quad (6.2)$$

where, E is gas emission flux, $\mu\text{g s}^{-1} \text{m}^{-2}$; VR is the ventilation rate, $\text{m}^3 \text{s}^{-1}$; C_o is the outlet air concentration, $\mu\text{g m}^{-3}$; C_i is inlet air concentration, $\mu\text{g m}^{-3}$; and A_s is emission surface area, m^2 .

The surface pH is expected to be higher than the pH in the bulk slurry due to higher evaporation rate of CO₂ than NH₃ (Ni et al., 2009). To estimate how much surface pH increased in the liquid phase boundary layer, and to get the approximate equilibrium gas phase surface concentration of ammonia and VFAs, equilibrium gas phase surface concentration was calculated from the liquid phase surface concentration using dimensionless Henry's constant (K_H^{cc}) as in Eq. (6.3) (Sawyer and McCarty, 1998).

$$K_H^{cc} = \frac{C_s}{C_l} \quad (6.3)$$

where C_s is the equilibrium concentration in gas phase boundary layer, $\mu\text{g m}^{-3}$; and C_l is the equilibrium concentration in liquid phase boundary layer, $\mu\text{g m}^{-3}$.

The concentrations in liquid slurry (C_l) for an organic acid and for a base were calculated by Eq. (6.4) and Eq. (6.5) respectively (Schwarzenbach et al., 2003).

For an organic acid

$$C_l = \frac{C_{l,tot}}{1 + 10^{(pH - pK_a)}} \quad (6.4)$$

For an organic base

$$C_l = \frac{C_{l,tot}}{1 + 10^{(pK_a - pH)}} \quad (6.5)$$

where $C_{l,tot}$ is the total concentration of the acid or base (nondissociated and dissociated) at saturation ; pK_a is a measure of the strength of an organic acid relative to the acid-base pair $\text{H}_3\text{O}^+/\text{H}_2\text{O}$.

The dimensionless Henry's constant (i.e., Eq (6.3)) is then calculated from k_H using Eq. (6.6) (Sander, 1999).

$$K_H^{cc} = \frac{12.2}{k_H T} \quad (6.6)$$

where k_H is Henry's law constant, M atm^{-1} at temperature T , K. Henry's law constants vary with temperature, therefore k_H is corrected using the following equation (Sander, 1999):

$$k_H = k_H^\ominus \exp\left(\frac{-\Delta_{soln}H}{R} \left(\frac{1}{T} - \frac{1}{T^\ominus}\right)\right) \quad (6.7)$$

where k_H^\ominus is Henry's law constant, M atm^{-1} at standard of $T^\ominus = 298.15\text{K}$, and $\frac{\Delta_{soln}H}{R}$ is the temperature dependent factor, K which is also defined as $\frac{-d \ln k_H}{d(1/T)}$. $\Delta_{soln}H$ is changes in enthalpy of solution, J M^{-1} ; R is the gas constant, $\text{J M}^{-1}\text{K}^{-1}$.

Statistical linear regression model was fit to find slopes or trends of VOCs and gas emission flux with the ventilation rates. Single factor analysis of variance (ANOVA) was used for tests of significance when comparing mean values.

6.3. Results and Discussion

The recorded room air temperature and relative humidity during the experiment were about $20\text{ }^{\circ}\text{C} \pm 0.5\text{ }^{\circ}\text{C}$ and $35\% \pm 3\%$, respectively. The slurry temperature and exhaust air temperature were $19.3\text{ }^{\circ}\text{C} \pm 0.4\text{ }^{\circ}\text{C}$ and $20\text{ }^{\circ}\text{C} \pm 0.6\text{ }^{\circ}\text{C}$ respectively.

6.3.1. Manure composition

Manure characteristics during the experiments were presented in Table 6.2. The mean dry matter content of manure samples was 6.0% (Table 6.2). There were no significant differences ($P > 0.05$) of dry matter content among the samples under different experimental setups as well as before and after each run.

Table 6.2 - Analysis results of the pig slurry used in the experiment (mean \pm standard deviation)

Ventilation rate, $\text{m}^3\text{ s}^{-1}$	Sampling time	Dry matter, %	Total nitrogen, g l^{-1}	Ammonium nitrogen, g l^{-1}	Acetic acid, g l^{-1}	Propionic acid, g l^{-1}	Butanoic acid, g l^{-1}	C5-carboxylic acid, g l^{-1}	pH (in bulk slurry)
0.005	Before	8.3 ± 0.59	5.3 ± 0.16	2.9 ± 0.19	8.3 ± 0.33	2.8 ± 0.11	2.2 ± 0.08	0.7 ± 0.02	6.6 ± 0.04
	after	6.3 ± 0.46	5.2 ± 0.15	2.9 ± 0.08	8.4 ± 0.46	2.9 ± 0.29	2.3 ± 0.15	0.7 ± 0.06	6.7 ± 0.02
0.010	Before	6 ± 0.21	5.3 ± 0.11	2.9 ± 0.04	8.7 ± 0.54	3.1 ± 0.32	2.4 ± 0.17	0.7 ± 0.07	6.9 ± 0.01
	after	5.5 ± 1.25	5.2 ± 0.13	2.9 ± 0.02	9 ± 0.09	3.3 ± 0.04	2.5 ± 0.03	0.8 ± 0.01	6.8 ± 0.05
0.015	Before	6.2 ± 0.31	5.2 ± 0.14	3 ± 0.16	9.2 ± 0.16	3.3 ± 0.06	2.5 ± 0.04	0.8 ± 0.01	6.6 ± 0.04
	after	4.5 ± 0.26	5.1 ± 0.03	3.1 ± 0.14	9.3 ± 0.17	3.4 ± 0.06	2.5 ± 0.04	0.8 ± 0.01	6.8 ± 0.04
0.020	Before	5.9 ± 0.46	5 ± 0.17	3.1 ± 0.12	9.2 ± 0.26	3.3 ± 0.09	2.5 ± 0.07	0.8 ± 0.02	6.7 ± 0.02
	after	5.6 ± 0.44	4.9 ± 0.24	2.9 ± 0.33	8.5 ± 1.21	3 ± 0.47	2.4 ± 0.17	0.8 ± 0.03	6.7 ± 0.07
Mean \pm SD		6 ± 1.01	5.2 ± 0.14	2.8 ± 0.12	8.8 ± 0.37	3.1 ± 0.21	2.4 ± 0.11	0.8 ± 0.05	6.7 ± 0.09
P-value ^a		0.35	0.04	0.99	0.86	0.93	0.64	0.58	0.32
P-value ^b		0.14	0.78	0.04	0.30	0.49	0.75	0.28	0.63

^aP-value at 95% confidence interval (i.e. $\alpha = 0.05$), compared among the ventilation rates, ^bP-value at 95% confidence interval, compared between sampling time before and after experiment run.

The mean total nitrogen and ammonium nitrogen were 5.2 g l^{-1} and 2.8 g l^{-1} , respectively. The differences in total nitrogen and ammonium nitrogen among the ventilation rates were not significant ($P > 0.05$). The mean concentration of total VFAs in slurry samples was 16 g l^{-1} , in which acetic acid, propanoic acid, butanoic acid, and pentanoic acid were 8.2 , 3.1 , 2.4 , and 0.8 g l^{-1} respectively. No significant differences were found in VFAs of slurry used in the experiment for the different ventilation rates and between the sampling times ($P > 0.05$). The pH measured in the

slurry was quite stable during the experimental run ($P > 0.05$). The average pH measured at 10 mm below the slurry surface was 6.7, which was closed to other researchers' measurement (Ni et al., 2009). The above results indicated that the slurry used for the experiment was sufficiently stable for studying ventilation effects on VICs and VOCs emission fluxes over several days.

Calculated gas phase surface concentrations at immediate liquid surface considering bulk pH (6.7) and adjusted pH (7.4), and measured slurry pit concentration of ammonia and VFAs for the ventilation rate of $0.005 \text{ m}^3 \text{ s}^{-1}$ were presented in Table 6.3. The calculated equilibrium gaseous concentration immediately above the liquid slurry surface using Henry's law constant, pH, and reaction rate constant indicated that the concentrations of NH_3 and VFAs in the air boundary layer were relatively higher than the concentrations at the slurry pit. Saha et al. (2010b) also found the large ammonia concentration gradients within the 0.1 m thick boundary in their study and reported difficulty to experimentally determine the surface concentration, because a small change in height above the slurry surface give a significant difference in ammonia concentrations in gas phase. The calculated surface concentration of NH_3 using bulk pH (6.7) was relatively lower than the NH_3 concentration measured at the slurry pit at the fixed ventilation rate (i.e., $0.005 \text{ m}^3 \text{ s}^{-1}$). Therefore, higher pH value might be expected at the slurry surface. Adjusted pH (7.42) given a higher equilibrium gas phase NH_3 concentration than the measured slurry pit concentration. The ratio of slurry pit concentration with equilibrium gas phase surface concentration of NH_3 (base) and acetic acid were 0.58 and 0.57 respectively, for balanced conditions. In this case, the pH was increased 0.7 units in the slurry surface. The data presented in the Table 6.3 clearly indicate that there was a pH gradient, which might be affected by the ventilation rate, and higher CO_2 release. The

Table 6.3 - Calculated gas phase surface concentrations at immediate liquid surface considering bulk pH (6.7) and adjusted pH (7.4), and measured slurry pit concentration of ammonia and VFAs for the ventilation rate of $0.005 \text{ m}^3 \text{ s}^{-1}$.

Compounds	Gas phase surface concentration (Cs)		Slurry pit concentration at $0.005 \text{ m}^3 \text{ s}^{-1}$, $\mu\text{g m}^{-3}$
	at bulk pH	at adjusted pH	
	$\mu\text{g m}^{-3}$	$\mu\text{g m}^{-3}$	$\mu\text{g m}^{-3}$
Ammonia	4660	24200	14000
Acetic acid	482	92.7	53.1
Propanoic acid	187	36.0	2.6
Butanoic acid	179	34.5	0.4
C5-carboxylic acid	112	21.6	1.8

existence of the pH gradient was in good agreement with the study of Zhang and Day (1996), who reported that the pH in the top layers of settled manure was 0.5 and 0.9 higher than the pH of bottom layers of manure.

6.3.2. Concentration and temporal variations

Concentrations of 14 detectable VOCs and 2 VICs (NH₃ and H₂S) from the pig slurry were measured in the slurry pit and at the outlet are presented in Table 6.4. For all compounds, higher concentrations in the outlet and slurry pit air were observed in lower ventilation rate than in higher ventilation rate. The concentrations were much higher in slurry pit air than in the outlet air. As for example, at the ventilation rate of 0.010 m³ s⁻¹, slurry pit concentrations of NH₃, H₂S, acetic acid, & 4MP were 65%, 52%, 46%, and 54 % higher, respectively, than the concentrations at the outlet. The lower concentrations at outlet than in the slurry pit can be explained by dilution due to higher air exchange rate above the slatted floor.

Table 6.4 - Compound assignment together with ions monitored by PTR-MS, Mean concentration ± standard deviation for selected compounds at outlet and in slurry pit of pig scale model house for four ventilation rates. (The concentrations were corrected for background contributions).

Compounds	ion(s) (m/z)	Concentration (µg m ⁻³)							
		at VR 0.005 m ³ s ⁻¹		VR 0.01 m ³ s ⁻¹		at VR 0.015 m ³ s ⁻¹		at VR 0.02 m ³ s ⁻¹	
		Outlet	Slurry-pit	Outlet	Slurry-pit	Outlet	Slurry-pit	Outlet	Slurry-pit
ammonia	18	4600 ± 200	14000 ± 200	3500 ± 200	9900 ± 400	3200 ± 300	9000 ± 1000	2500 ± 300	5900 ± 800
hydrogen sulphide	35	54 ± 12.64	152 ± 158.66	13.7 ± 1.57	28.7 ± 6.79	6.4 ± 1.51	14.9 ± 2.85	7.2 ± 1.49	16.1 ± 4.5
methanethiol	49	0.1 ± 0.03	0.34 ± 0.06	0.1 ± 0.02	0.2 ± 0.05	0.1 ± 0.03	0.2 ± 0.07	0.1 ± 0.04	0.3 ± 0.08
acetone	59	7.4 ± 2.08	19.7 ± 2.61	6.1 ± 0.54	18 ± 1.53	9 ± 0.64	23.7 ± 1.46	5.5 ± 0.73	14.5 ± 1.8
trimethylamine	60	3.4 ± 1.06	5.7 ± 1.25	1.8 ± 0.47	3.9 ± 0.63	1.9 ± 0.17	4.7 ± 0.95	1.6 ± 0.31	2.7 ± 0.35
acetic acid	61	47 ± 11.64	53.1 ± 14.73	11.2 ± 2.18	20.9 ± 2.88	4.2 ± 1.36	19 ± 4.26		
dimethyl sulphide	63	0.7 ± 0.43	1.6 ± 0.46	0.1 ± 0.08	0.3 ± 0.08	0.1 ± 0.06	0.3 ± 0.12	0.1 ± 0.11	0.1 ± 0.11
C4-carbonyls (e.g., 2-butanone)	73	0.8 ± 0.28	2.5 ± 0.38	4 ± 0.32	11 ± 0.76	3.2 ± 0.38	8.2 ± 1.2	2.1 ± 0.23	4.9 ± 0.52
propanoic acid	75	1.9 ± 0.66	2.6 ± 0.34	1.3 ± 0.51	2 ± 0.65	0.9 ± 0.43	2.7 ± 0.73	0.6 ± 0.48	1 ± 0.39
2,3-butanedione	87	1.1 ± 0.7	1.6 ± 0.81	1.7 ± 0.74	1.8 ± 0.65	0.7 ± 0.18	3 ± 0.73	0.6 ± 0.26	2.5 ± 0.39
butanoic acid	89		0.4 ± 0.81	1.5 ± 0.54	3.8 ± 0.56	1.5 ± 0.29	4.6 ± 0.62	1.4 ± 0.56	4.9 ± 1.41
phenol(+dimethyl disulphide)	95	9.4 ± 1.61	32.6 ± 2.54	4.9 ± 0.59	13.8 ± 1.04	2.8 ± 0.34	6.6 ± 0.69	3.9 ± 0.17	7.5 ± 0.62
C5 carboxylic acids	103	3.5 ± 0.99	5.4 ± 0.13	1.7 ± 0.28	3.9 ± 0.79	1.6 ± 0.28	4.9 ± 0.72	1.5 ± 0.52	5.4 ± 0.98
4-methylphenol	109	7 ± 1.28	16.1 ± 2.23	3.5 ± 0.46	7.5 ± 0.86	2.7 ± 0.38	5.7 ± 0.8	2.9 ± 0.42	5.7 ± 0.39
indole	118	0.1 ± 0.05	0.2 ± 0.07	0.2 ± 0.12	0.3 ± 0.14	0.1 ± 0.1	0.2 ± 0.13	0.1 ± 0.06	0.2 ± 0.1
4-ethylphenol	123	4.7 ± 2.58	5 ± 2.9	2.5 ± 0.43	4.9 ± 1.05	1.3 ± 0.23	3.9 ± 0.81	1.6 ± 0.46	2.6 ± 0.37
dimethyl trisulphide	127	0.1 ± 0.33	0.5 ± 0.35	0.1 ± 0.08	0.4 ± 0.15	0.1 ± 0.03	0.1 ± 0.13	0.2 ± 0.06	0.2 ± 0.08
3-methyl-1H-indole	132	0.1 ± 0.06	0.4 ± 0.17	1.5 ± 0.58	9.2 ± 1.69	1.7 ± 1.31	6.2 ± 2.05	1.9 ± 1.06	5.7 ± 2.78

The outlet NH₃ concentration was very high compared to other compounds measured in the slurry pit (Table 6.4), and was close to the full scale measurements (Saha et al., 2010a). The significant amount of H₂S, acetic acid was emitted from the slurry. Considerable amounts of acetic acid, propanoic acid, butanoic acid, C5-carboxylic acid, phenol and 4-methylphenol (4-MP) were observed from the slurry at first 6 to 8 h of the measurement period (Fig. 6.2). The outlet concentrations of methanethiol, dimethyl sulphide, and dimethyl trisulphide were very low (< 1 µg m⁻³), and did not change with the ventilation rates (Table 6.4), and also in some cases were lower than the detection limit in this study. Therefore, these three compounds have not been considered in the correlation analysis of emission and ventilation rates.

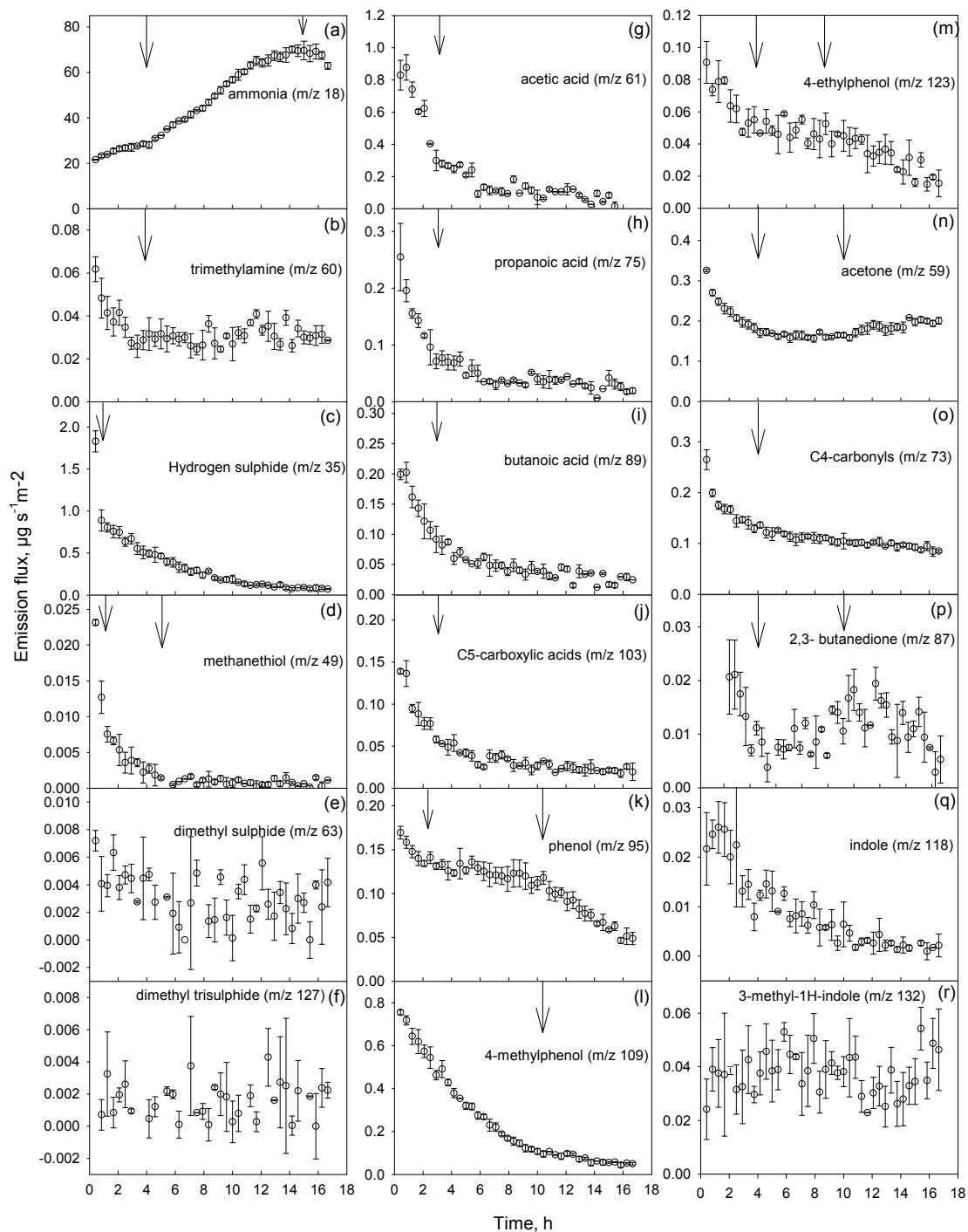


Fig. 6.2 - Temporal variation of different gases and VOCs emission at the ventilation rate of $0.005 \text{ m}^3 \text{ s}^{-1}$, just after filling slurry in the tank. Down arrows indicate emission trend changing time.

The measured 14 VOCs and H_2S emission (Fig. 6.2) were much lower than what were measured by Feilberg et al. (2010b) in a full scale pig house. In this case, the ventilation rate per square meter emission surface area corresponded to full scale study. In a full scale pig house, there might be other sources of VOCs and H_2S such as slats, soiled surface, and feed etc. However, animal and

workers activities or movements, and agitation of slurry surfaces by urination and defecation in real pig houses might also contribute to VOCs and H₂S emission (Patni and Clarke, 1990). Aarnink et al. (1996) found that the pigs urinate and defecate 7.1 and 6.1 times a day, respectively. Therefore continuous renewal of slurry and soiled surfaces in certain interval might contribute to higher emission of full scale pig buildings.

Temporal variations of NH₃, H₂S and 14 VOCs emissions at the ventilation rate of 0.005 m³ s⁻¹ from the scale model of a pig house shows that the ammonia emission pattern over time was different, compared to H₂S and VOCs (Fig. 6.2). In general, four factors are likely to influence the change in emissions over time: (1) pH increase due to a faster surface evaporation of CO₂ (acidic) compared to NH₃ (basic) (Ni et al., 2000b; Sommer and Sherlock, 1996), (2) build-up of a dry matter-enriched surface layer due to buoyancy of large particles (Fig. 6.3), (3) slurry surface concentration reduction due to evaporation combined with reduced diffusivity in the enriched surface layer, and (4) oxidation of the compounds by O₂ in the oxic surface layer (Nielsen et al., 2010a) or in the sub-oxic zone by e.g., NO₃⁻ (Nielsen et al., 2010b).



(a)



(b)

Fig. 6.3 - Formation surface layers with dry matter, (a) after renewal with new slurry before experiment run, and (b) after the experiment run.

In the following the emission patterns for different compound groups are discussed in terms of these four factors:

6.3.2.1. Nitrogen compounds

The ammonia (m/z 18) emission increased linearly in the first 4 hrs, and then the rate increased, and continued until 15 hrs (Fig. 6.2a). This can be explained by a steady increase of pH in the slurry surface in the beginning due to release of CO₂ (Sommer and Sherlock, 1996). The higher the pH value in the surface, the higher the NH₃ release (Ni et al., 2009; Ye et al., 2008b). There is no increasing trend of NH₃ emission after 15 h, which might be because of pH did not change and/or surface TAN decreased. On the other hand, the emission of trimethylamine (m/z 60, pKa = 9.8) decreased faster until 3.5 h, and after that trimethylamine release remain approximately at the same level (Fig. 6.2b). But we expected same trend as NH₃, which was not the case. The difference might be because of faster diffusion rate of NH₃ (i.e., almost twice as rule of thumb) in the bulk slurry than trimethylamine.

6.3.2.2. Sulphur compounds

Hydrogen sulphide (m/z 35) emission had its maximum value ($\sim 1.8 \mu\text{g s}^{-1} \text{m}^{-2}$) at the starting point, and dropped significantly to $\sim 0.89 \mu\text{g s}^{-1} \text{m}^{-2}$ after $\sim 1/2$ h, and subsequently decreased gradually with time (Fig. 6.2c). The similar behaviour was observed by Ni et al. (2010) in their multi reactors experimental study with the pig slurry. This can partly be explained by increasing pH at surface level with time which will increase the dissociation of H₂S to HS⁻. This could also be due to oxidation of H₂S in the aerobic surface layer or in the suboxic zone by NO₃⁻, ferric iron, or indirectly by O₂ through a network of natural electrical conductors reaching to the oxic surface layer (Nielsen et al., 2010b). Similar behaviour was observed for methanethiol (m/z 49) until 5 h from the start of ventilation, afterwards no changes in emission level was observed (Fig. 6.2d), because the concentration measured at this stages were below or very close to the detection limit ($0.2 \mu\text{g m}^{-3}$). The emissions of dimethyl sulphide (DMS) (m/z 63) and dimethyl trisulphide (DMTS) (m/z 127) were also very low during the measurement period (Fig. 6.2e and f) because the concentrations were close to the detection limit.

6.3.2.3. Volatile fatty acids

The volatile fatty acids (VFA) all have a similar pattern, i.e., an exponentially decreasing trend as showed in Fig. 6.2g-j. VFAs decreased steeply at first 3 h, probably because of sharp increase of pH at the slurry surface. The emissions drop of acetic acid, propanoic acid, butanoic acid, C5-carboxylic acid within the above mentioned hours were from 0.83, 0.23, 0.19, and $0.14 \mu\text{g m}^{-3}$ to 1.8, 0.08, 0.08, and $0.05 \mu\text{g s}^{-1} \text{m}^{-2}$ respectively. The higher concentration of acetic acid in the slurry

compared with the other VFAs (Table 6.2), gave a corresponding higher concentration at the outlet. After 3 h VFAs emissions did not change much possibly due to formation of a thick surface layer (Fig. 6.3) and possibly oxidation at the top, and surface depletion.

6.3.2.4. Phenols and indoles

Emissions of phenolic compounds such as phenol, 4-MP (p-cresol), and 4-EP also exhibited decreasing trends as shown in Fig. 6.2k, Fig. 6.2l, and Fig. 6.2m, respectively. Phenol (m/z 95) and 4EP (m/z 123) emissions were $0.17 \mu\text{g s}^{-1} \text{m}^{-2}$, and $0.09 \mu\text{g s}^{-1} \text{m}^{-2}$, respectively, at the beginning, and were $0.05 \mu\text{g s}^{-1} \text{m}^{-2}$, and $0.015 \mu\text{g s}^{-1} \text{m}^{-2}$ at the end of the measurement period. On the other hand, 4-MP emission was found $0.76 \mu\text{g s}^{-1} \text{m}^{-2}$ at the first hour, which was approximately 4.5 and 8 times higher than phenol and 4-EP respectively. At the end of the measurement hours, the 4-MP emission was $0.05 \mu\text{g s}^{-1} \text{m}^{-2}$. The 4-MP losing rate was higher than the phenol and 4-EP. Hobbs et al. (1999) also found the highest 4-MP emission of the phenols present. The decreasing trend of phenols could also be explained by dry matter enrichment at surface layer (Fig. 6.3) due to its increasing buoyancy, and the thickness of surface layers therefore typically reflects the duration over which material has been allowed to build up (age) (Smith et al., 2007).

Indole (m/z 118) and 3-methyl-1H-indole (m/z 132) has decreasing and fluctuation trends respectively over time (Fig. 6.2q-r). The concentration levels of these compounds were very low; therefore, those phenomena were hard to explain, and need further study.

6.3.2.5. Ketones

Ketones (acetone (m/z 59), c4-carbonyls (m/z 73), and 2, 3-butanedione (m/z 87)) behaved differently over the time (Fig. 6.2n-p). Acetone dropped quickly in first 4 h due to oxidation, and remained steady until approximately ~10 h. After that time, acetone emission started to increase slowly (Fig. 6.2n), which might be because of increased microbial production. C4-carbonyls also had quick drop at the beginning and decreased steeply until 4 h, and later continued to decrease slowly. 2, 3-Butanedione showed a trend similar to acetone and C4-carbonyls in the first 4 h after which the emission increased until 10 h, and decreased again. The 2, 3-butanedione concentration was low (0.3 to $1.7 \mu\text{g m}^{-3}$) compared to acetone and c4-carbonyls.

6.3.3. *Effect of ventilation rate on VICs and VOCs emissions*

Effect of ventilation rates on VICs (NH_3 , and H_2S) and VOCs released from slurry are shown in Fig. 6.4. The graphs are presented with 95% confidence band. The linear regression data of gases and VOCs with ventilation are presented in Table 6.5. Large slopes are indicative of higher source concentrations.

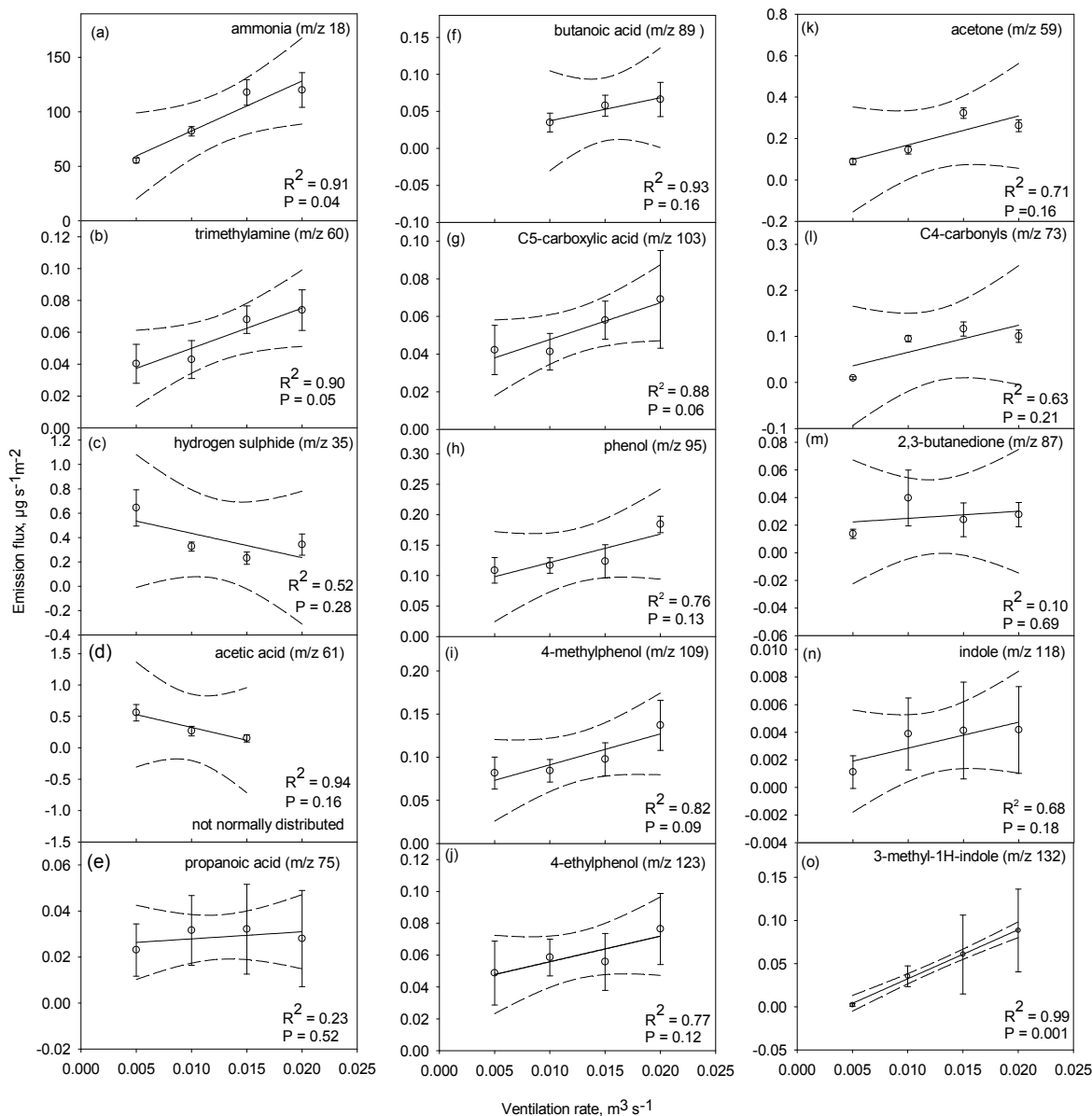


Fig. 6.4 - Emission of different gases and VOCs in different ventilation rates. Full lines represent linear regressions of the data. ----- indicate 95% confidence range, which refers to the region of uncertainties in the predicted values over a range of values for the independent variable. P value less than 0.05 indicates highly significant. All data of each compound passed normality test, except acetic acid.

Ammonia and trimethylamine emission rates are strongly correlated with ventilation rate (Fig. 6.4a-b) ($P < 0.05$). The emission rates increased with the increase of ventilation rate. Higher ventilation rates increase the air velocity near the manure surface (Ye et al., 2009), which lead to increase ammonia emissions (Ye et al., 2008a). Both concentration and air velocity changes affected the concentration gradient above the emission surface, and therefore increased convective mass transfer process for NH_3 . This explained the increase in NH_3 release at higher airflow rates, and confirmed that convective mass transfer governed the NH_3 release process. In contrast,

hydrogen sulphide (H₂S) was decreased with the increase of ventilation rate ($R^2 = 0.52$) (Fig. 6.4c). Arogo et al. (1999b) found the slight decrease of the H₂S mass transfer coefficient in both aqueous solution and liquid manure as the air velocity increased over the surface. However, mass transfer process of H₂S is mainly limited by liquid film control (Hudson and Ayoko, 2008; Parker et al., 2010), therefore less effect/no effect of ventilation rate on H₂S emission process was observed (Feilberg et al., 2010b; Ni et al., 2009).

Table 6.5 - Linear orthogonal regression data for correlation between selected compounds' emissions ($\mu\text{g m}^{-2} \text{s}^{-1}$) (dependent variable) and ventilation rates ($\text{m}^3 \text{s}^{-1}$) (independent variable). $E = a \times \text{VR} + b$.

Compound	ion(s) (m/z)	Model parameter		R^2
		Slope	Intercept	
ammonia	18	4600	36.50	0.91
hydrogen sulphide	35	-20.0	0.64	0.52
acetone	59	14.0	0.03	0.71
trimethylamine	60	2.5	0.00	0.90
acetic acid	61	-40.9	0.74	0.94
C ₄ -carbonyls (e.g., 2-butanone)	73	5.9	0.01	0.63
propanoic acid	75	0.3	0.02	0.23
2,3-butanedione	87	0.5	0.02	0.10
butanoic acid	89	3.1	0.01	0.93
phenol(+dimethyl disulfide)	95	4.7	0.07	0.77
C ₅ carboxylic acids	103	2.0	0.03	0.88
4-methylphenol	109	3.6	0.06	0.82
indole	118	0.2	0.00	0.68
4-ethylphenol	123	1.6	0.04	0.77
3-methyl-1H-indole	132	5.7	-0.03	0.99

Among the volatile fatty acids (VFAs), acetic acid (m/z 61) and propanoic acid (m/z 75) emission rates showed decreasing trend and slightly increasing trend, respectively, with the increase of ventilation rate (Fig. 6.4d-e). On the other hand, butanoic acid (m/z 89) and C₅-carboxylic acid (m/z 103) emission rates increased with the increase of ventilation rate (Fig. 6.4f and g). The oxidation rate at the slurry surface might be higher for acetic acid because of the short carbon chain (C₂), and then followed by propanoic acid (C₃), butanoic acid (C₄), C₅- carboxylic acid in the higher ventilation rates. Therefore the concentration of these acids at outlet air reduced significantly with higher ventilation rates, resulting lower emission. However, generation of acetic acid and diffusivity in slurry may not be faster than the gas phase mass transfer process in higher ventilation rate. Feilberg et al. (2010b) found positive correlation with ventilation rate in real pig barn,

indicating possible other sources of these compounds. Alanis et al. (2008) found that VFA emissions per unit area are much higher from animal feed than from animal waste.

Phenolic compounds (Phenol, 4-MP, and 4-EP) were positively correlated with the ventilation rate (Fig. 6.4h-j). 4-MP was significantly correlated with ventilation rate ($R^2 = 0.91$ and $P < 0.05$). Acetone (m/z 59) and C4-carbonyls (m/z 73) emission rate increased with the increase of ventilation rate where both air side and liquid side resistances might be affected on emission process (Fig. 6.4k and l). In contrast, 2, 3-butanedione (m/z 87) was not very dependent of ventilation rate (Fig. 6.4m). Indole compounds were also positively correlated to the ventilation rates (Fig. 6.4n and o).

Broadly, the differences for these emission fluxes correlated with ventilation rates could be related to the Henry's constant of the compounds. For compounds with higher Henry's constant K_H (sulphur compounds), the liquid side mass transfer resistance is expected to dominate, and the influence of air velocity therefore less significant. On the other hand, for compounds with low K_H (e.g., ammonia, VFAs, Phenols, indoles), the emission rate is increased with the higher ventilation rate which reduces air side mass transfer resistance dominating over liquid side resistance for these relatively soluble compounds (Hudson and Ayoko, 2008; Parker et al., 2010). The results of emission rate related to ventilation rate for most of the compounds are in line with the study by Feilberg et al (2010b). However, for acetic acid the trend was different. H_2S and VOCs emissions in Feilberg et al. (2010b) were also higher than in this study, despite ammonia emissions were comparable. There may be other sources (e.g., slats, soiled surfaces, straw, feed, and silage) than the slurry, which contributed to the total VOCs emissions from real pig production facilities in Feilberg et al. (2010b) study.

In addition, it can be seen that sampling time is very important for some of the compounds for comparing emission with the ventilation rates. For a longer duration of waiting time in scale model, some compounds may quickly disappear (e.g., methanethiol, DMS, and DMTS) and might be given lower concentration values than expected (Fig. 6.2), sometimes below detection limit. This could make it difficult to find correlations of emission with the ventilation rates for some of the compounds, which need to be taken care of. Further studies are needed to clarify some of the anomalies and to study VOCs emission behaviour under non-isothermal condition.

6.4. Conclusion

Using PTR-MS gave a unique opportunity to study temporal variation of different gases and VOCs concentration and emission correlation with ventilation rates. The ammonia concentration measured in this study was close to the full scale. H_2S , acetic acid, 4-MP, and acetone were also other major compounds after ammonia, which emitted from the pig slurry. H_2S and 14 VOCs emitted from the slurry were lower than the concentration measured at real pig building, which indicates that there

might be other sources of these compounds. Temporal variations of these odorous compounds at a constant ventilation rate and isothermal condition were varied differently, depending on the solubility of these compounds, and one or more of the mentioned factors. The pH increase and dry matter enrichment at the surface layer, surface depletion due to evaporation combined with reduced diffusivity in the enriched surface, oxidation either in the oxic surface layer or in the sub-oxic zone might be the main reasons for the temporal variations of NH₃, H₂S, and 14 VOCs.

Ventilation rate increased the ammonia and trimethylamine emissions significantly ($p < 0.05$). The hydrogen sulphide (H₂S) was independent of ventilation rate. The complex relationships of VFAs with ventilation rate were observed. VFAs emission dependency on ventilation rate increased with the increase of carbon chain. Phenols, indoles, and ketones showed the positive correlation with ventilation rate to some extent. In general, compounds with high solubility (low Henry's constant) showed stronger correlation with ventilation rates than the compounds with high Henry's constant.

Acknowledgements

This research was performed as part of ROSES project "Reduction of Odour Source in and Emission from Swine Buildings" under the program "Animal Husbandry, the Neighbours and the Environment" funded by the Danish Ministry of Food, Agriculture and Fisheries (Grant Number: 3304-VMP-05-032-01). The authors gratefully acknowledged financial support by the Department of Biosystems Engineering, Aarhus University, Denmark. The authors also appreciate the technical support of Claudia Nagy, lab technician, Department of Biosystems Engineering, Aarhus University, Denmark.

References

- Aarnink AJA, vandenBerg AJ, Keen A, Hoeksma P, Verstegen MWA. Effect of slatted floor area on ammonia emission and on the excretory and lying behaviour of growing pigs. *Journal of Agricultural Engineering Research* 1996; 64: 299-310.
- Alanis P, Sorenson M, Beene M, Krauter C, Shamp B, Hasson AS. Measurement of non-enteric emission fluxes of volatile fatty acids from a California dairy by solid phase micro-extraction with gas chromatography/mass spectrometry. *Atmospheric Environment* 2008; 42: 6417-6424.
- Alanis P, Ashkan S, Krauter C, Campbell S, Hasson AS. Emissions of volatile fatty acids from feed at dairy facilities. *Atmospheric Environment* 2010; 44: 5084-5092.
- Andreae MO, Crutzen PJ. Atmospheric aerosols: Biogeochemical sources and role in atmospheric chemistry. *Science* 1997; 276: 1052-1058.
- Aneja VP, Schlesinger WH, Erisman JW. Effects of Agriculture upon the Air Quality and Climate: Research, Policy, and Regulations. *Environmental Science & Technology* 2009; 43: 4234-4240.

APHA. Standard Methods for the Examination of Water and Wastewater. American Public Health Association, Washington, DC 1998

Arogo J, Zhang RH, Riskowski GL, Christianson LL, Day DL. Mass transfer coefficient of ammonia in liquid swine manure and aqueous solutions. *Journal of Agricultural Engineering Research* 1999a; 73: 77-86.

Arogo J, Zhang RH, Riskowski GL, Day DL. Mass transfer coefficient for hydrogen sulfide emission from aqueous solutions and liquid swine manure. *Transactions of the ASAE* 1999b; 42: 1455-1462.

Blanes-Vidal V, Hansen MN, Adamsen APS, Feilberg A, Petersen SO, Jensen BB. Characterization of odor released during handling of swine slurry: Part I. Relationship between odorants and perceived odor concentrations. *Atmospheric Environment* 2009a; 43: 2997-3005.

Blanes-Vidal V, Hansen MN, Sousa P. Reduction of Odor and Odorant Emissions from Slurry Stores by Means of Straw Covers. *Journal of Environmental Quality* 2009b; 38: 1518-1527.

Bliss PJ, Schulz TJ, Senger T, Kaye RB. Odour measurement - Factors affecting olfactometry panel performance. *Water Science and Technology* 1996; 34: 549-556.

Blunden J, Aneja VP. Characterizing ammonia and hydrogen sulfide emissions from a swine waste treatment lagoon in North Carolina. *Atmospheric Environment* 2008; 42: 3277-3290.

Blunden J, Aneja VP, Overton JH. Modeling hydrogen sulfide emissions across the gas-liquid interface of an anaerobic swine waste treatment storage system. *Atmospheric Environment* 2008; 42: 5602-5611.

Bull KR, Sutton MA. Critical loads and the relevance of ammonia to an effects-based nitrogen Protocol. *Atmospheric Environment* 1998; 32: 565-572.

Campagna D, Kathman SJ, Pierson R, Inserra SG, Phifer BL, Middleton DC, Zarus GM, White MC. Ambient hydrogen sulfide, total reduced sulfur, and hospital visits for respiratory diseases in northeast Nebraska, 1998-2000. *Journal of Exposure Analysis and Environmental Epidemiology* 2004; 14: 180-187.

Chaoui H, Montes F, Rotz CA, Richard TL. Volatile Ammonia Fraction and Flux from Thin Layers of Buffered Ammonium Solution and Dairy Cattle Manure. *Transactions of the ASABE* 2009; 52: 1695-1706.

Chen LD, Hoff S, Cai LS, Koziel J, Zelle B. Evaluation of Wood Chip-Based Biofilters to Reduce Odor, Hydrogen Sulfide, and Ammonia from Swine Barn Ventilation Air. *Journal of the Air & Waste Management Association* 2009; 59: 520-530.

Clanton CJ, Schmidt DR, Nicolai RE, Goodrich PR, Jacobson LD, Janni KA, Weisberg S, Buckel JA. Dynamic olfactometry variability in determining odor dilutions-to-threshold. *Transactions of the ASAE* 1999; 42: 1103-1112.

- Cortus EL, Lemay SP, Barber EM, Hill GA, Godbout S. A dynamic model of ammonia emission from urine puddles. *Biosystems Engineering* 2008; 99: 390-402.
- Cupr P, Skarek M, Bartos T, Ciganek M, Holoubek I. Assessment of human health risk due to inhalation exposure in cattle and pig farms in south Moravia. *Acta Veterinaria Brno* 2005; 74: 305-312.
- de Gouw J, Warneke C. Measurements of volatile organic compounds in the earth's atmosphere using proton-transfer-reaction mass spectrometry. *Mass Spectrometry Reviews* 2007; 26: 223-257.
- Elzing A, Monteny GJ. Ammonia emission in a scale model of a dairy-cow house. *Transactions of the ASAE* 1997; 40: 713-720.
- Feilberg A, Adamsen APS, Lindholm S, Lyngbye M, Schafer A. Evaluation of Biological Air Filters for Livestock Ventilation Air by Membrane Inlet Mass Spectrometry. *Journal of Environmental Quality* 2010a; 39: 1085-1096.
- Feilberg A, Lu DZ, Adamsen APS, Hansen MJ, Jonassen KEN. Odorant Emissions from Intensive Pig Production Measured by Online Proton-Transfer-Reaction Mass Spectrometry. *Environmental Science & Technology* 2010b; 44: 5894-5900.
- Griffing EM, Overcash M, Westerman P. A review of gaseous ammonia emissions from slurry pits in pig production systems. *Biosystems Engineering* 2007; 97: 295-312.
- Hansen MJ, Adamsen APS, Feilberg A, Jonassen KE. Storage stability of odorants from pig production in sampling bags for olfactometry. *Journal of Environmental Quality* (accepted) 2011.
- Hewitt CN, Hayward S, Tani A. The application of proton transfer reaction-mass spectrometry (PTR-MS) to the monitoring and analysis of volatile organic compounds in the atmosphere. *Journal of Environmental Monitoring* 2003; 5: 1-7.
- Hobbs PJ, Misselbrook TH, Cumby TR. Production and emission of odours and gases from ageing pig waste. *Journal of Agricultural Engineering Research* 1999; 72: 291-298.
- Hudson N, Ayoko GA. Odour sampling 1: Physical chemistry considerations. *Bioresource Technology* 2008; 99: 3982-3992.
- Kaparaju P, Serrano M, Thomsen AB, Kongjan P, Angelidaki I. Bioethanol, biohydrogen and biogas production from wheat straw in a biorefinery concept. *Bioresource Technology* 2009; 100: 2562-2568.
- McGill AEJ, Jackson N. Changes in Short-Chain Carboxylic-Acid Content and Chemical Oxygen-Demand of Stored Pig Slurry. *Journal of the Science of Food and Agriculture* 1977; 28: 424-430.
- Misselbrook TH, Van der Weerden TJ, Pain BF, Jarvis SC, Chambers BJ, Smith KA, Phillips VR, Demmers TGM. Ammonia emission factors for UK agriculture. *Atmospheric Environment* 2000; 34: 871-880.

Morsing S, Strom JS, Zhang G, Kai P. Scale model experiments to determine the effects of internal airflow and floor design on gaseous emissions from animal houses. *Biosystems Engineering* 2008; 99: 99-104.

Ngwabie NM, Schade GW, Custer TG, Linke S, Hinz T. Abundances and flux estimates of volatile organic compounds from a dairy cowshed in Germany. *Journal of Environmental Quality* 2008; 37: 565-573.

Ni JQ. Mechanistic models of ammonia release from liquid manure: a review. *Journal of Agricultural Engineering Research* 1999; 72: 1-17.

Ni JQ, Heber AJ, Diehl CA, Lim TT. Ammonia, hydrogen sulphide and carbon dioxide release from pig manure in under-floor deep pits. *Journal of Agricultural Engineering Research* 2000a; 77: 53-66.

Ni JQ, Heber AJ, Sutton AL, Kelly DT. Mechanisms of gas releases from swine wastes. *Transactions of the ASABE* 2009; 52: 2013-2025.

Ni JQ, Heber AJ, Sutton AL, Kelly DT, Patterson JA, Kim ST. Effect of swine manure dilution on ammonia, hydrogen sulfide, carbon dioxide, and sulfur dioxide releases. *Science of the Total Environment* 2010; 408: 5917-5923.

Ni JQ, Hendriks J, Vinckier C, Coenegrachts J. A new concept of carbon dioxide accelerated ammonia release from liquid manure in pig house. *Environment International* 2000b; 26: 97-104.

Nielsen DA, Nielsen LP, Schramm A, Revsbech NP. Oxygen Distribution and Potential Ammonia Oxidation in Floating, Liquid Manure Crusts. *Journal of Environmental Quality* 2010a; 39: 1813-1820.

Nielsen LP, Risgaard-Petersen N, Fossing H, Christensen PB, Sayama M. Electric currents couple spatially separated biogeochemical processes in marine sediment. *Nature* 2010b; 463: 1071-1074.

Oesterhelweg L, Puschel K. "Death may come on like a stroke of lightning ..." - Phenomenological and morphological aspects of fatalities caused by manure gas. *International Journal of Legal Medicine* 2008; 122: 101-107.

Parker DB, Caraway EA, Rhoades MB, Cole NA, Todd RW, Casey KD. Effect of Wind Tunnel Air Velocity on Voc Flux from Standard Solutions and Cafo Manure/Wastewater. *Transactions of the ASABE* 2010; 53: 831-845.

Patni NK, Clarke SP. Transient Hazardous Conditions in Animal Buildings Due to Manure Gas Released During Slurry Mixing. 1990, 449-459 pp.

Portejoie S, Martinez J, Landmann G. Ammonia of farm origin: impact on human and animal health and on the natural habitat. *Productions Animales* 2002; 15: 151-160.

Rong L, Nielsen PV, Zhang GQ. Effects of airflow and liquid temperature on ammonia mass transfer above an emission surface: Experimental study on emission rate. *Bioresource Technology* 2009; 100: 4654-4661.

Saha CK, Zhang GQ, Kai P, Bjerg B. Effects of a partial pit ventilation system on indoor air quality and ammonia emission from a fattening pig room. *Biosystems Engineering* 2010a; 105: 279-287.

Saha CK, Zhang G, Ni JQ. Airflow and concentration characterisation and ammonia mass transfer modelling in wind tunnel studies. *Biosystems Engineering* 2010b; 107: 328-340.

Sander R. Compilation of Henry's law constants for inorganic and organic species of potential importance in environmental chemistry. Version 3 Mainz, Germany: Max-Planck Institute for Chemistry Available at: www.mpch-mainz-mpg.de/~sender/res/henry.html 1999.

Sawyer CN, McCarty PL. *Chemistry of Environmental Engineering*. 3rd ed New York, N Y : McGraw-Hill 1998.

Schulz TJ, vanHarreveld AP. International moves towards standardisation of odour measurement using olfactometry. *Water Science and Technology* 1996; 34: 541-547.

Schwarzenbach R, Gschwend P, Imboden D. *Environmental Organic Chemistry*. 2nd Edition, John Wiley & Sons, New York 2003.

Shaw SL, Mitloehner FM, Jackson W, Depeters EJ, Fadel JG, Robinson PH, Holzinger R, Goldstein AH. Volatile organic compound emissions from dairy cows and their waste as measured by proton-transfer-reaction mass spectrometry. *Environmental Science & Technology* 2007; 41: 1310-1316.

Smith K, Cumby T, Lapworth J, Misselbrook T, Williams A. Natural crusting of slurry storage as an abatement measure for ammonia emissions on dairy farms. *Biosystems Engineering* 2007; 97: 464-471.

Sommer SG, Sherlock RR. pH and buffer component dynamics in the surface layers of animal slurries. *Journal of Agricultural Science* 1996; 127: 109-116.

Trabue SL, Anhalt JC, Zahn JA. Bias of Tedlar bags in the measurement of agricultural odorants. *Journal of Environmental Quality* 2006; 35: 1668-1677.

Trabue SL, Scoggin KD, Li H, Burns R, Xin HW. Field sampling method for quantifying odorants in humid environments. *Environmental Science & Technology* 2008; 42: 3745-3750.

Wright DW, Eaton DK, Nielsen LT, Kuhrt FW, Koziel JA, Spinhirne JP, Parker DB. Multidimensional gas chromatography-olfactometry for the identification and prioritization of malodors from confined animal feeding operations. *Journal of Agricultural and Food Chemistry* 2005; 53: 8663-8672.

Ye Z, Zhang G, Li B, Strom JS, Dahl PJ. Ammonia Emissions Affected by Airflow in A Model Pig House: Effects of Ventilation Rate, Floor Slit Opening, and Headspace Height in A Manure Storage Pit. *Transactions of the ASABE* 2008a; 51: 2113-2122.

Ye Z, Zhang G, Li B, Strom JS, Tong G, Dahl PJ. Influence of airflow and liquid properties on the mass transfer coefficient of ammonia in aqueous solutions. *Biosystems Engineering* 2008b; 100: 422-434.

Ye Z, Zhang G, Seo IH, Kai P, Saha CK, Wang C, Li B. Airflow characteristics at the surface of manure in a storage pit affected by ventilation rate, floor slat opening, and headspace height. *Biosystems Engineering* 2009; 104: 97-105.

Zhang G, Bjerg B, Strom JS, Morsing S, Kai P, Tong G, Ravn P. Emission effects of three different ventilation control strategies - A scale model study. *Biosystems Engineering* 2008; 100: 96-104.

Zhang RH, Day DL. Anaerobic decomposition of swine manure and ammonia generation in a deep pit. *Transactions of the ASAE* 1996; 39: 1811-1815.

Chapter 7

Effect of environmental deflector and curtain on air exchange rate in slurry pit in a scaled livestock building

Paper VI:

Ye, Z., **Saha, C.K.**, Li, B., Tong, G., Wang, C., Zhu, S., and Zhang, G. 2009. **Effect of environmental deflector and curtain on air exchange rate in slurry pit in a scaled livestock building**. Biosystems Engineering, Vol. 104 (4), P 522-533.

Abstract

The main source of ammonia and odour from most livestock buildings is the slurry pit. The ammonia emission rate is affected by the air exchange rate in the slurry pit. Reduction of air exchange between slurry pit and room air may reduce the emissions. The hypothesis that using an environmental deflector in the room and curtains in the slurry pit may affect air exchange rate between the slurry pit and the room air was validated. In the experiment, three position angles for the deflector and three arrangements of curtains were investigated in a two-dimensional ventilation chamber under isothermal conditions at two ventilation airflow rates. The airflow pattern, air velocity and turbulence intensity inside the chamber were also recorded. The results showed that the airflow patterns, air velocities and turbulence intensities in the room space near the slatted floor and in the headspace of the pit were influenced by changing deflector angles and curtain numbers. It was found that the lowest pit ventilation and the highest concentration in the headspace of the pit could be achieved by using a deflector's position angle of 45° at both of two airflow rates. On the other hand, it was also found that more curtain numbers under the slatted floor and lower room ventilation rate caused lowest pit air exchange rate and the highest concentration in the headspace of pit.

7.1. Introduction

Odour and ammonia (NH_3) release from livestock buildings is a major concern of public and government due to the issue of negative environmental impacts on water and air quality. NH_3 in and from animal houses is one of the most important agricultural air pollutants related to human and animal health and ecological damage (Webb *et al.*, 2005). Approximately 50% of the NH_3 emissions in The Netherlands, Denmark and France originated from pig housing and slurry storage of pig production (Van der Peet-Schwering *et al.*, 1999). Airflow in the room and slurry channel mainly affects odour and NH_3 transport in and total emission from ventilated livestock production buildings. Consequently, effective and practical methods to guide the airflow for reduction of the odour and NH_3 emissions from livestock buildings are highly desired. Furthermore, local air velocities and turbulence levels play important roles in contaminant emissions. Zhang *et al.* (1994) indicated that increasing the air velocities over the manure surface result in increased NH_3 releasing from manure pits with a given ammonia concentration at the manure surface. (Ye *et al.*, 2008a) and (Ye *et al.*, 2008b) and Ye *et al.* (2009) found that turbulence intensity had a significant effect on NH_3 emission at low velocities. Therefore, reducing the air ventilation from the slurry pit has become important to reduce emissions from the slurry surface and improve air quality inside and outside livestock buildings.

Air motion inside livestock buildings is mainly controlled by ventilation, and its pattern is related to the distribution of contaminants inside the building (Arogo *et al.*, 1997; Zhang and Strøm, 1999; Demmers *et al.*, 2000; Morsing *et al.*, 2008). The ventilation effectiveness will affect local air mixing and consequently emission from the ventilated room space. Many attempts have been made to improve the ventilation effectiveness and guide the airflow pattern, such as by changing inlet and outlet locations (Buiter and Hoff, 1998; Chung and Hsu, 2001; Zhang *et al.*, 2001), location of the pollutant source (Demmers *et al.*, 2000), ventilation rates (Buiter and Hoff, 1998; Demmers *et al.*, 2000; Zhang *et al.*, 2008; Ye *et al.*, 2008a; Ye *et al.*, 2008b), floor type and slurry channel layout (Aarnink *et al.*, 1997; Morsing *et al.*, 2008), by using pen partitions (Bjerg *et al.*, 2000) and manipulating slat orientations and manure depths (Buiter and Hoff, 1998; Ye *et al.*, 2008b; Ye *et al.*, 2009).

Placing an environmental deflector inside the room and curtains inside the slurry pit may change the airflow pattern and reduce airflow between the slurry pit and the room. Tong *et al.* (2008) investigated influence of four deflector angles on air exchange rate using a two-dimensional (2D) chamber. However, the important parameters like air velocity and turbulence intensity were not measured. Morsing *et al.* (2008) found 23% reduction of NH_3 concentration by using slurry channels perpendicular to the supply air jet compared to using parallel channels below the fully slatted floor. However, the air exchange rate between the slurry pit and the room air was not recorded. Therefore, the key objective of this study was to investigate the effects of environmental

deflector and slurry pit curtain on air exchange rates between the slurry pit and the room air, and to record general airflow patterns, air velocities and turbulence intensities.

7.2. Materials and methods

7.2.1. Experimental facility

7.2.1.1. Two-dimensional chamber

A 2D ventilation chamber with inside dimensions $2.18 \text{ m} \times 0.62 \text{ m} \times 2.41 \text{ m}$ ($L \times W \times H$) was made as a sub-section of a pig house which corresponds to $4.36 \text{ m} \times 4.96 \text{ m} \times 2.41 \text{ m}$ ($L \times W \times H$) full scale room, Fig. 7.1. The chamber was the same as used in the investigation by Tong et al. (2008). The front face was made of 2 panes of laminated glass 220 cm long and 240 cm high and 0.6 cm thick, and the back and side plywood surfaces were painted in dark colours in order to facilitate visualization of airflow patterns with illuminated smoke (Fig. 7.2). Ventilation air was supplied

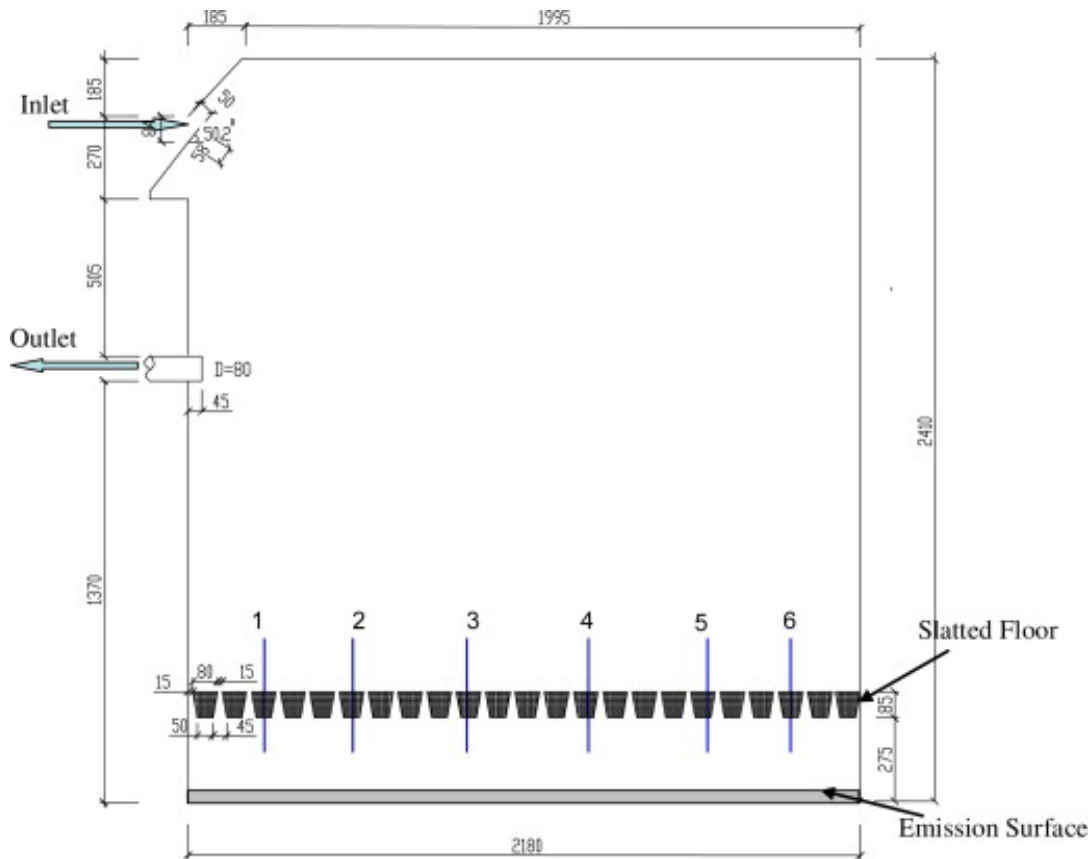


Fig. 7.1 - 2D ventilation chamber and six concentration sampling positions, mm.

through adjustable slats with dimensions $540 \text{ mm} \times 50 \text{ mm}$ ($L \times W$) in one side beneath the ceiling. The opening height of the inlet was kept at 45 mm . Room air was exhausted through a clear acrylic pipe outlet, 80 mm in diameter from the middle of the side wall. The pipe was connected *via* a

flexible duct to a channel fan with ventilation rate range of 0–300 m³ h⁻¹ (Lindab-type CBU200B, Denmark) discharging the air to the outside. The fully slatted floor used for this study was made with polystyrene sheet with 15.6% opening ratio and placed 0.275 m above the chamber bottom, leaving 2.05 m height from the floor to the ceiling surface.

7.2.1.2. Environmental deflector

The environmental deflector made of Polyvinyl chloride board with dimensions 620 mm × 200 mm × 5 mm ($L \times W \times H$) was installed at the side wall of the chamber opposite the inlet wall and placed 590 mm above the slatted floor (Fig. 7.2). Different positions of deflector could be achieved by adjusting the height of one side of the deflector using string. Three angles of the deflector, namely 0° (parallel to the side wall), 45° and 90°, were used in the investigations.

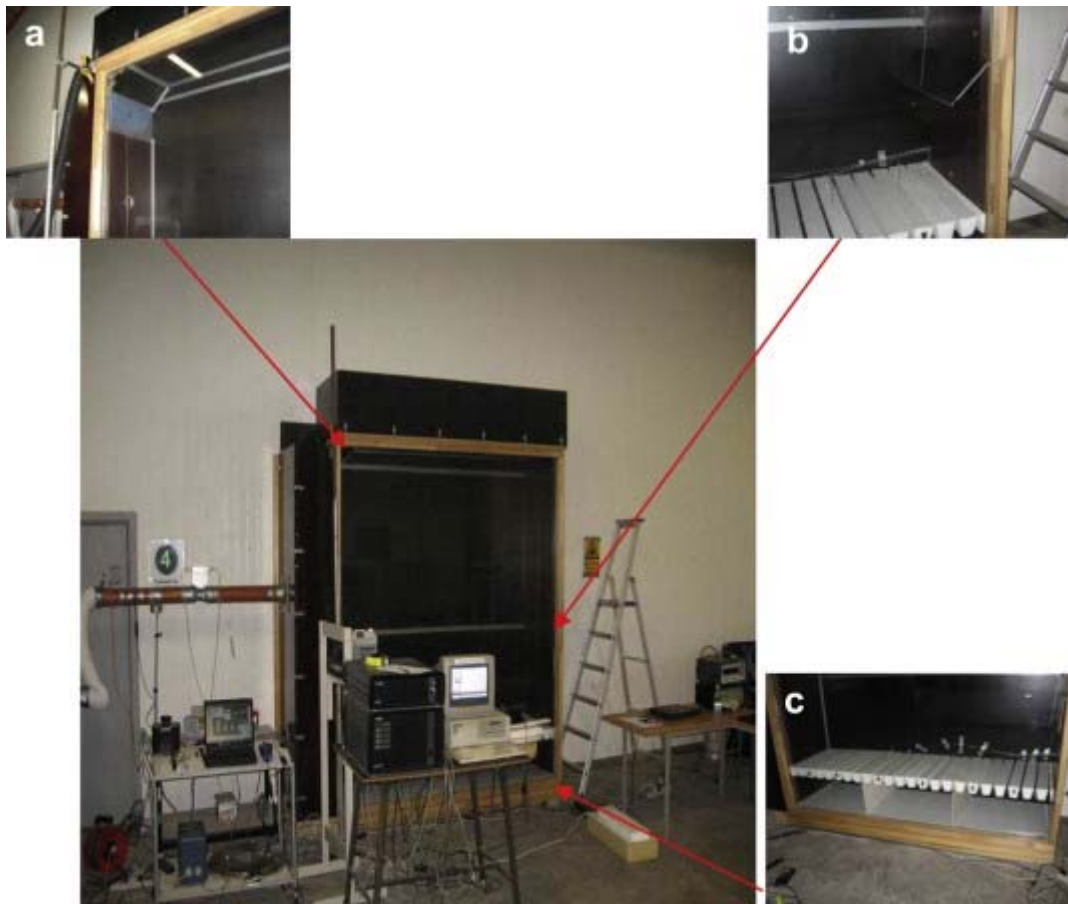


Fig. 7.2 – Experimental 2D ventilation chamber: a – air inlet and outlet; b – deflector; c – slurry pit curtain.

7.2.1.1. Slurry pit curtain

The curtains were placed under the slatted floor to evaluate the effects on air exchange rate between the slurry pit and room air. The curtain was made of polystyrene sheet with dimensions 620 mm × 360 mm ($L \times W$) and thickness of 5 mm. Three treatments, namely without curtain, one curtain and two curtains were investigated in this study. The slurry pit can be divided into two or three parts by using one or two curtains, respectively (Fig. 7.2). One curtain was placed under the slatted floor at a distance of 1125 mm from the inlet wall and two curtains were placed at distances of 745 mm and 1425 mm, respectively.

7.2.2. *Measurements*

Experiments were carried out under isothermal conditions in the Air Physics Lab, Research Centre Bygholm, Faculty of Agricultural Sciences, Aarhus University, Denmark. The measurements were conducted at two ventilation airflow rates with fixed inlet opening height. The airflow characteristics in the 2D chamber are shown in Table 7.1. In addition, the experimental treatments are shown in Table 7.2 and Table 7.3.

Table 7.1 – Airflow characteristics in the 2D chamber

Ventilation rate ($\text{m}^3 \text{h}^{-1}$)	Inlet height (mm)	Inlet velocity (m s^{-1})	Inlet Re	Inlet Rm ($\text{m}^2 \text{s}^{-2}$)	J^a	ACH ^b
100	45	1	3154	0.015	8.9×10^{-4}	37
180	45	1.8	5679	0.048	28.5×10^{-4}	65

^a Jet momentum number as proposed by Barber et al. (1982)

^b Air change per hour

Table 7.2 – Experimental treatment for environmental deflector

Numbers of curtain	Angles of deflector ($^\circ$)	Ventilation rate ($\text{m}^3 \text{h}^{-1}$)
0	0	100
		180
	45	100
		180
	90	100
		180

Table 7.3 – Experimental treatment for slurry pit curtain

Angles of deflector (°)	Numbers of curtain	Ventilation rate (m ³ h ⁻¹)
0	0	100
		180
	1	100
		180
	2	100
		180

7.2.2.1. Ventilation airflow rate

The Lindab FMU/FMDRU 100-80 flow meter (Denmark) was used to measure the ventilation airflow rates. The accuracy of the flow measuring method is 5–10% depending on the distance to the flow disturbance. The ventilation flow in the duct was determined using the equation

$$VR = 26.32\sqrt{\Delta P} \quad (7.1)$$

where VR is ventilation rate, m³ h⁻¹; ΔP is pressure difference between upstream and downstream side of the orifice, Pa. The pressure differences were measured using a differential pressure transmitter (Model 694, Huba control, Switzerland) with a measurement range of 0–300 Pa and an accuracy of $\pm 0.7\%$ and a resolution of 0.1% of full scale. The data were recorded and collected through a Campbell Scientific CR215 data logger. The sampling period was 10 s and averages saved each 1 min.

7.2.2.2. CO₂ concentration

CO₂ was used as a tracer gas in this study. A constant CO₂ flux of 50 ml min⁻¹ was supplied uniformly into a conditioning space with a mixing fan and emitted through 30 holes each 5 mm in diameter, located on the emission surface (Fig. 7.1). A reference point in the conditioning space, 20 mm beneath the emission surface, was used to monitor the CO₂ concentration in the air before it defused *via* the emission surface into the slurry channel. Prior to each measurement of CO₂ concentrations at the six sampling points 150 mm above and below the slatted floor, there was an initialization period to allow the reference CO₂ concentration to achieve a steady-state condition. During the initialization period, the inlet and outlet CO₂ concentrations were also recorded.

The CO₂ concentration at the reference point was monitored by Testo 400 (Testo GmbH & Co., Germany). The outlet CO₂ concentration was measured by Vaisala GM343 carbon dioxide

probe which has accuracy of ± 3 ppm, while CO₂ concentrations at inlet and six points above and below the slatted floor were measured by a Brüel & Kjær Photoacoustic Multi-gas Monitor (type 1312, Denmark) and a multiplexer (type 1309, Denmark). The sampling period for each CO₂ measurement was 20 s, followed by 20 s cleaning time to replace the air in the measuring chamber of the Monitor before a new measurement was started. The total sampling time was 2 h for each treatment. It should be mentioned that the CO₂ is assumed to come only from the compressed tank and there were no other CO₂ emission sources inside the chamber.

7.2.2.3. Air velocity and turbulence intensity

After finishing CO₂ concentration measurements at six points above and below the slatted floor, airflow patterns were observed using smoke from a Dräger Air Flow Tester (Dräger Sicherheitstechnik GmbH, Germany) that was back illuminated using a fluorescent tube. A single-dimensional Laser Doppler Anemometer (type 58N40, DANTEC FVA enhanced, Skovlunde, Sweden) was used to measure air velocity and turbulence intensity at the same six points. Each point was measured for 8 min.

7.2.2.4. Air temperature and relative humidity

The air temperature and relative humidity inside the testing room were recorded by Vaisala 50Y temperature and humidity probe. The data were recorded every minute in CR215 data logger (Campbell Scientific, Inc). During the experiments, the air temperature and relative humidity were kept around 24.0 ± 1.0 °C and 30–40%, respectively.

7.2.3. *Statistical and estimation methods*

Analysis of variance (ANOVA) utilizing SPSS statistical analysis package (SPSS 16.0, SPSS Inc., Chicago, IL, USA) was executed to compare and validate the experimental values.

7.2.3.1. Environmental deflector

In order to describe the air exchange rates in the slurry channel under different experimental conditions, the ratio between air exchange rate in the pit and room ventilation rate was applied to evaluate the effects of the deflector (Tong et al., 2008). The smaller the value of the air exchange ratio, the more effective the position of deflector is for contaminant control. This air exchange ratio is expressed by Eq. (7.2)

$$R_p = \frac{Q_{pit}}{Q_{out}} = \frac{C_{outlet} - C_{inlet}}{C_{pit} - C} \times 100 \quad (7.2)$$

where R_p is the pit air exchange ratio, %, Q_{pit} is the pit ventilation airflow rate, $m^3 h^{-1}$, Q_{out} is the experimental airflow rate, $100 m^3 h^{-1}$ and $180 m^3 h^{-1}$, and C_{outlet} , C_{inlet} , C_{pit} and C_{room} are average CO_2 concentrations at outlet, inlet, under the slatted floor and above the slatted floor, $mg m^{-3}$, respectively.

Zonal ventilation is the ventilation of only a portion of the airspace where thermal comfort or air quality is the primary concern. To evaluate such zonal ventilation effectiveness affected by the deflector, the ventilation effectiveness factor (VEF) for a zone of concern, or i th location, defined by Zhang et al. (2001) was used.

$$VEF_i = \frac{C_{outlet} - C_{inlet}}{C_i - C_{inlet}} \quad (7.3)$$

where VEF_i is the ventilation effectiveness factor at i th location; C_i is the average CO_2 concentration, $mg m^{-3}$, at the i th sampling position above or below the slatted floor (the zone of concern), and C_{outlet} and C_{inlet} are CO_2 concentrations of room exhaust air and inlet air, $mg m^{-3}$, respectively.

The dimensionless VEF is used in this study to compare the local concentration distribution above or below slatted floor compared with that at outlet for different deflector positions. The smaller the value of the VEF below the slatted floor near the outlet side, the more effective the deflector position is.

7.2.3.2. Slurry pit curtain

The following formula was used to evaluate the effects of the curtains on air exchange rates between the slurry channel and room air under different experimental conditions. The air exchange rate ratio is expressed as

$$R = \frac{C_{room}}{C_{pit}} \quad (7.4)$$

where R is the air exchange ratio, %, and C_{room} and C_{pit} are the average CO_2 concentrations in the exhaust air and pit air, $mg m^{-3}$, respectively.

7.3. Results and discussion

The reference CO_2 concentrations used for environmental deflector and slurry pit curtain experiments with different ventilation rates are shown in Table 7.4.

Table 7.4 – Reference CO₂ concentrations used in the study

Terms	VR(m ³ h ⁻¹)	Reference CO ₂ concentration (mg m ⁻³)	Standard deviation (SD) (mg m ⁻³)
Environmental deflector	100	5347.0	43.4
	180	3137.5	34.6
Slurypit curtain	100	8923.9	96.6
	180	5127.8	46.3

7.3.1. Effect of environmental deflector

7.3.1.1. CO₂ concentration

With a ventilation rate of 100 m³ h⁻¹, the mean concentrations of CO₂ for six sampling points above the floor were 872.0 (±32.3), 877.4 (±27.0) and 967.1 (±30.0) mg m⁻³ for a deflector angle of 0°, 45° and 90°, respectively (Fig. 8.3a). As shown in Fig. 7.3b, the mean CO₂ concentrations at six sampling points above the floor for a deflector's position angle of 0°, 45° and 90° were 835.8 (±14.4), 856.9 (±14.8) and 857.8 (±11.2) mg m⁻³ by the levels of 180 m³ h⁻¹. There were no significant differences in CO₂ concentrations above the floor among the levels of ventilation rate and three positions of deflector ($p > 0.05$). However, the CO₂ concentration at point 6 was influenced by the positions of deflector especially at the lower ventilation rate. For example, the CO₂ concentration at point 6 with a deflector angle of 90° was 37% higher than for 0°.

In Fig. 7.3c, the mean concentrations of CO₂ for six sampling points below the floor were 1262.3 (±120.8), 1798.1 (±152.1) and 1430.7 (±130.8) mg m⁻³ for a deflector angle of 0°, 45° and 90° for the ventilation rate of 100 m³ h⁻¹, respectively. The mean CO₂ concentrations at six sampling points below the floor for a deflector angle of 0°, 45° and 90° were 963.1 (±56.9), 1162.6 (±78.3) and 959.8 (±50.0) mg m⁻³ for ventilation rate of 180 m³ h⁻¹ (Fig. 7.3d). There were significant differences in pit CO₂ concentrations among the levels of ventilation rate and three positions of deflector ($p < 0.05$). Moreover, the multiple comparisons showed that there were significant differences in pit CO₂ concentrations with a deflector angle of 45° compare to 0° and 90° ($p < 0.05$). However, no significant difference in pit CO₂ concentrations was found between 0° and 90° ($p > 0.05$).

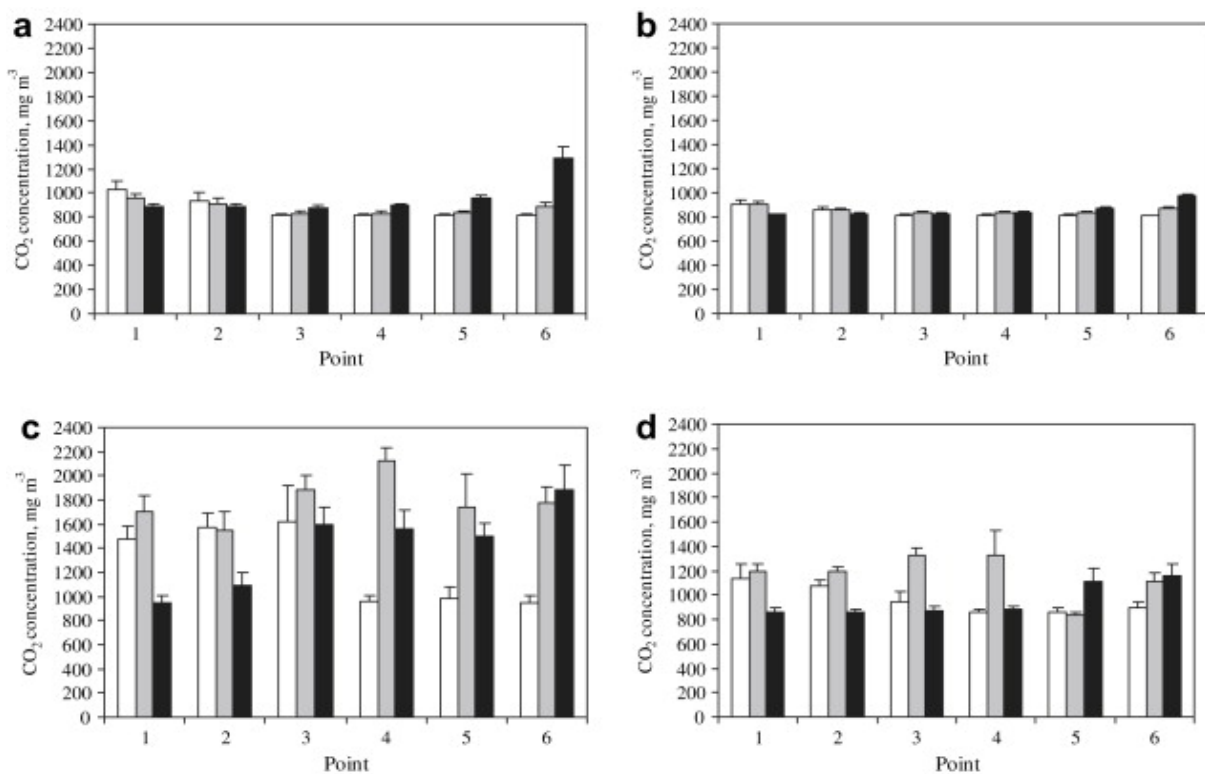


Fig. 7.3 - Relation between deflector position and CO₂ concentration at six sampling points, where, □, ■ and ■ represent 0°, 45° and 90°: (a) and (c) represent above and below the floor with 100 m³ h⁻¹ ventilation rate; (b) and (d) represent above and below the floor with 180 m³ h⁻¹ ventilation rate, respectively.

The results in Fig. 7.3 show that the highest CO₂ concentration in the slurry pit and lower CO₂ concentration in the room air could be achieved by using lower ventilation rate and 45° deflector angle. The contaminants like NH₃ and odour emissions from the animal house may be reduced if more contaminants can be kept inside the pit. In addition, lower CO₂ concentration in the room air result in better air quality inside livestock buildings.

7.3.1.2. Air exchange ratio in the slurry pit

The pit air exchange ratios for different deflector angles and ventilation rates are estimated as shown in Fig. 7.4. In a ventilated pig building with slatted floor without pit ventilation, the air exchange rate in the slurry pit is influenced by changing positions of deflector in the room. In a ventilated room space, the floor slots function as both air inlets and outlets for the headspace of the slurry pit.

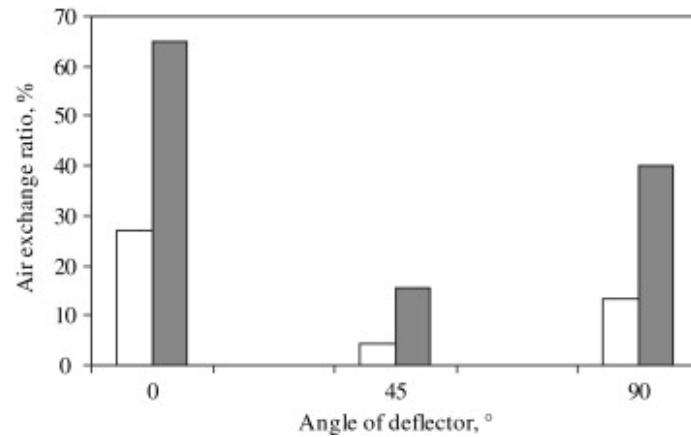


Fig. 7.4 - Pit air exchange ratios for different deflector angles, where, □ and ■ represent ventilation rate of 100 m³ h⁻¹ and 180 m³ h⁻¹, respectively.

It can be clearly seen that lower ventilation rate and 45° of deflector's position angle resulted in lowest air exchange ratio. A deflector angle of 45° reduced air exchange rate by 83.6% and 76.2% at the ventilation rates of 100 m³ h⁻¹ and 180 m³ h⁻¹ respectively, compare to 0°. The lower pit air exchange rate means less contaminant emission from the slurry pit.

7.3.1.3. Local ventilation effectiveness factor

The VEFs for the two ventilation rates were substantially different with the values lower for 100 m³ h⁻¹ and higher for 180 m³ h⁻¹ ($p < 0.05$), Fig. 7.5. However, Zhang et al. (2001) found ventilation effectiveness was primarily affected by the ventilation system and much less affected by ventilation rate. The contrary conclusions may be caused by different ventilation rate ranges and model scales. The ventilation rates used were much higher than this study. Hence, more investigations are needed to draw a definite conclusion.

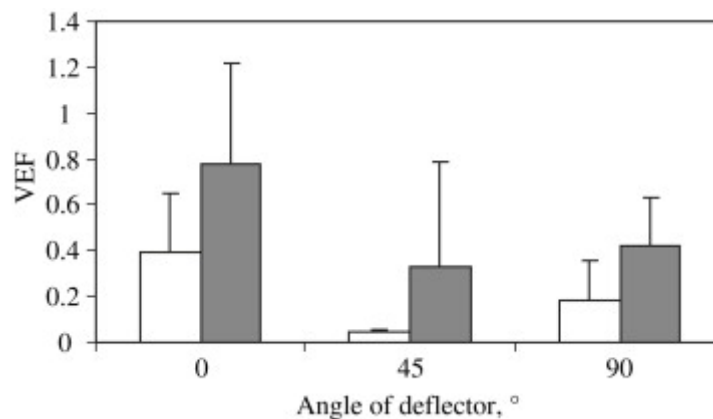


Fig. 7.5 - Local mean VEFs below the slatted floor for different deflector angles, where, □ and ■ represent ventilation rate of 100 m³ h⁻¹ and 180 m³ h⁻¹, respectively.

The results also showed that, using the deflector angles of 45° and 90°, the VEFs obviously varied in the headspace of the pit compared with 0° ($p < 0.05$). The mean effectiveness factor below the floor for a deflector angle of 45° was smaller than that for 0° and 90°. Therefore, it could be concluded that a deflector's position angle of 45° is much more effective for reducing air exchange rate between slurry pit and room air. This conclusion is shown to agree well with results in Fig. 7.4.

7.3.1.4. Airflow pattern

As shown in Fig. 7.6, the inlet airflow observed using the smoke system attached to the ceiling and continued down the far end wall. On reaching the floor it generally split into two: a primary airflow returning above the floor and another penetrating into the slurry pit below the slatted portion of the floor. The deflector's position affected normal airflow behaviour both in the room and the slurry pit. With a deflector angle of 0°, the primary airflow at floor level was from points 2 to 6. However, by adjusting deflector angle to 45° or 90°, the primary airflow was moved forward to points 1–5. Furthermore, the contact area and inlet as well as outlet of secondary airflow in the pit were also influenced by the deflector angle.

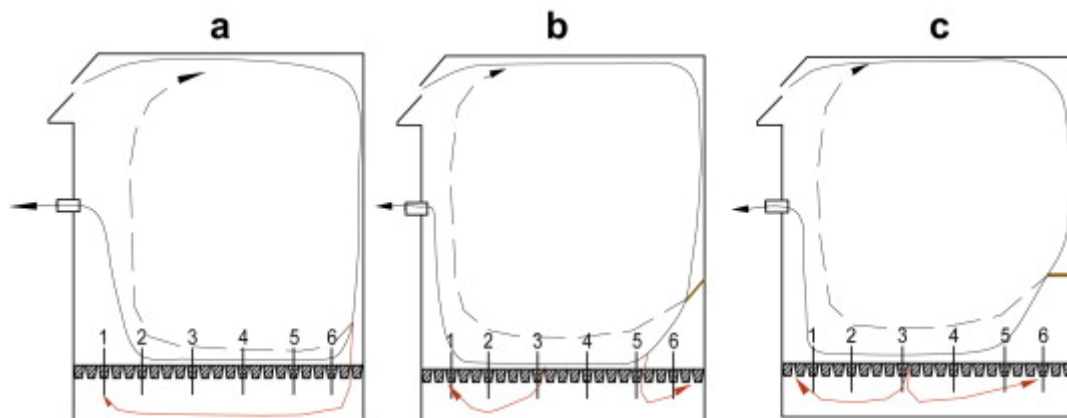


Fig. 7.6 - General airflow patterns in the 2D chamber with different deflector angles: (—) and (---) primary airflow; (—) secondary airflow; (a) 0°, (b) 45° and (c) 90°.

The primary and secondary airflows also influence the flow type and air velocity as well as CO₂ concentration above and below the floor. In this study, the main concern is the effect of deflector angle on airflow variation in local areas, such as point 6. The highest CO₂ concentration at point 6 above the floor for a deflector angle of 90° may result from the lowest airflow. For a deflector angle of 0°, the secondary airflow was able to penetrate into the slurry pit with unrestricted access to the total emission surface area, Fig. 7.6a. When changing the deflector angle (Fig. 7.6b, c), however, the secondary airflow was broken into smaller volumes, restricting the

secondary airflow contact between air and emission surface. The least airflow penetrated into the slurry pit was found at a deflector angle of 45° and resulted in highest average CO₂ concentration.

7.3.1.5. Air velocity

The similar tendency for air velocity changes above and below the floor with two ventilation rates is shown in Fig. 7.7. Increasing ventilation rate increased air velocities above and below the floor. The mean air velocity above the floor with ventilation rate of 180 m³ h⁻¹ was around 1.7 times than that with 100 m³ h⁻¹ ($p < 0.05$). However, no significant difference of air velocity above the floor was observed for the three deflector angles ($p > 0.05$). There was significant difference in air velocity below the floor among the levels of ventilation rate and deflector angle ($p < 0.05$). Moreover, the multiple comparisons showed that there were significant differences in air velocity with a deflector angle of 45° compare to 0° and 90° ($p < 0.05$). However, no significant difference in air velocity was found between deflector's position angles of 0° and 90° ($p > 0.05$).

The air velocity at each sampling point is highly related to airflow pattern in the room and slurry pit. As shown in Fig. 7.6, in case of air velocity above the floor, the primary airflow mainly passed points 3 and 4, resulting in higher air velocities at these points. By contrast, the air velocities at points 1 and 6 were low because very little air passed. In the case of air velocity below the floor, the airflow pattern in the slurry pit was affected by which floor slot functioned as air inlet or outlet for the headspace of the slurry pit. Therefore, the air velocities at sampling points below the floor were more complex.

The air velocities at sampling points also affect the CO₂ concentrations and the air exchange rate between room air and slurry pit. Higher air velocity at sampling point causes lower CO₂ concentration because of air dilution. For example, the air velocity at point 6 above the floor with a deflector's position angle of 90° was 7 times less than at 0° which could explain why it had highest CO₂ concentration. A linear correlation between inlet air velocity and floor air velocity in a full scale room has been confirmed by Strøm et al. (2002). The inlet air velocity increased with increasing ventilation rate due to the constant inlet opening in this study and resulted in a higher air velocity close to the floor. This increased the air exchange rate in the pit room and the air velocity above the emission surface (Tong et al., 2008 and Ye et al., 2009). Consequently, the reduction of pit air exchange ratio by reducing ventilation rate as depicted in Fig. 7.4 can be explained by reducing air velocity at the emission surface.

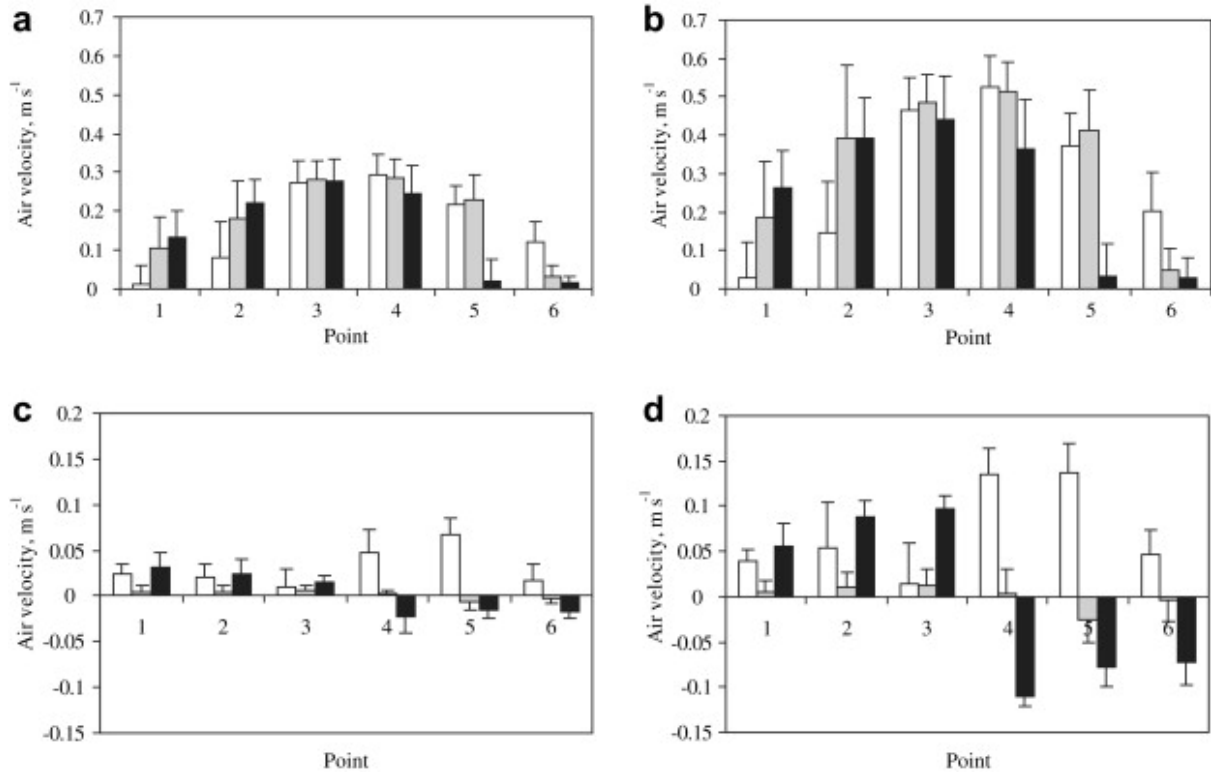


Fig. 7.7- Relation between deflector angle and air velocity at six sampling points, where, □, ■ and ■ represent 0°, 45° and 90°: (a) and (c) represent above and below the floor with 100 m³ h⁻¹ ventilation rate; (b) and (d) represent above and below the floor with 180 m³ h⁻¹ ventilation rate, respectively.

7.3.1.6. Turbulence intensity

The similar tendency for Ti changes above the floor for two ventilation rates is shown in Fig. 7.8. There was no significant difference in Ti above the floor among the levels of ventilation rate and three deflector angles ($p > 0.05$). This may be caused by similar primary airflow above the floor and also indicated that the CO₂ concentrations at sampling points above the floor are mainly influenced by air velocities. However, there was no significant difference in Ti below the floor among the levels of ventilation rate ($p > 0.05$) but there were significant difference among three deflector angles ($p < 0.05$). Moreover, the multiple comparisons showed that there were significant differences in Ti with a deflector angle of 45° compare to 0° and 90° ($p < 0.05$). However, no significant difference in Ti was found between a deflector's position angle of 0° and 90° ($p > 0.05$).

Ti is defined as the ratio of the root mean square (RMS) value of the velocity fluctuations to the mean velocity. It should be mentioned that vertical velocity fluctuations may still exist and affect the concentrations at sampling points. However, the Laser Doppler Anemometer used in this study was only one-dimensional and Ti in the vertical plane was not recorded.

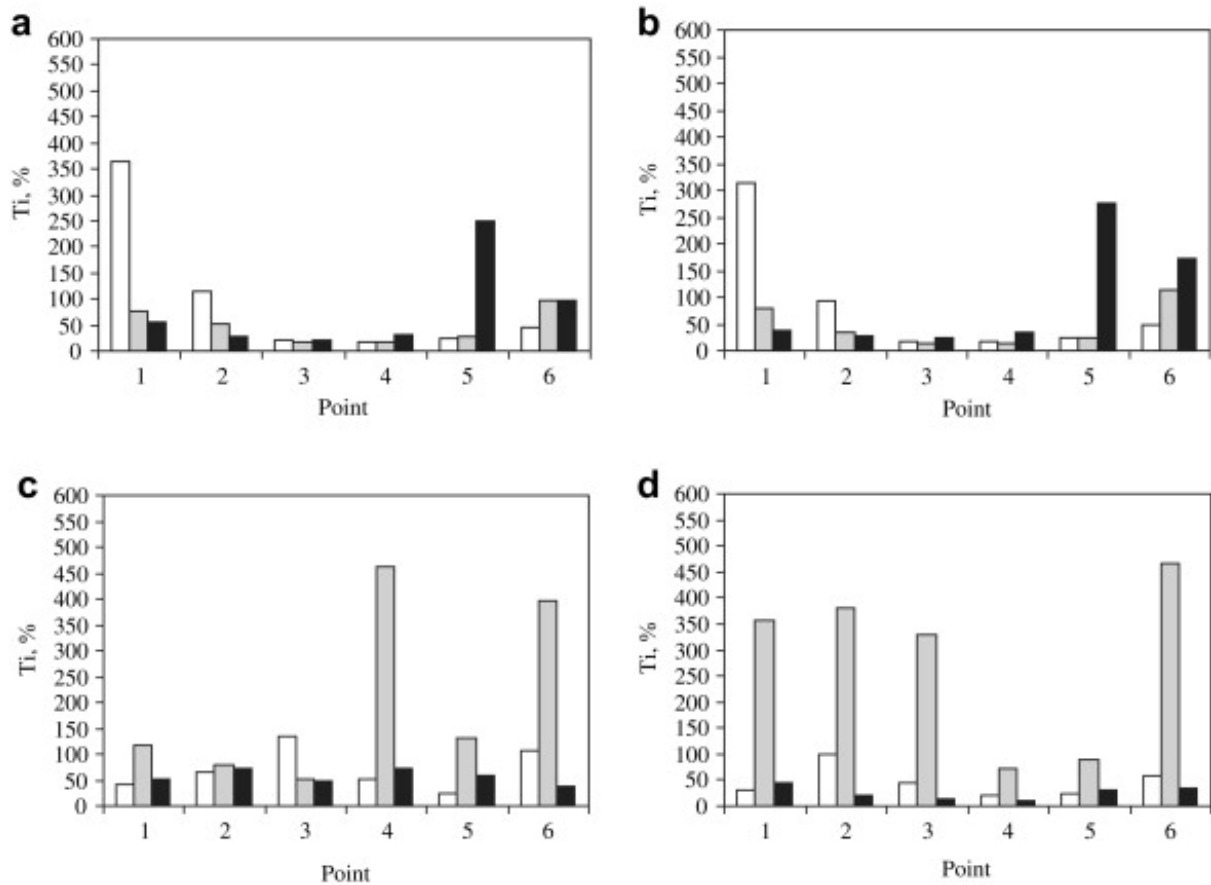


Fig. 7.8 - Relation between deflector angle and turbulence intensity at six sampling points, where, □, ■ and ■ represent 0°, 45° and 90°: (a) and (c) represent above and below the floor with 100 m³ h⁻¹ ventilation rate; (b) and (d) represent above and below the floor with 180 m³ h⁻¹ ventilation rate, respectively.

7.3.2. Effect of slurry pit curtain

7.3.2.1. CO₂ concentration

At the ventilation rate of 100 m³ h⁻¹, the mean concentrations of CO₂ for six sampling points above the floor were 934.0 (±40.8), 873.3 (±55.8) and 838.0 (±21.6) mg m⁻³ with no curtain, one curtain and two curtains, respectively (Fig. 7.9a). As shown in Fig. 7.9b, the mean CO₂ concentrations at six sampling points above the floor with no curtain, one curtain or two curtains were 923.9 (±18.6), 832.7 (±14.7) and 852.1 (±13.8) mg m⁻³ at the levels of 180 m³ h⁻¹. There was no significant difference in room CO₂ concentrations among the levels of ventilation rate ($p > 0.05$) but was significant difference among three numbers of curtains ($p < 0.05$). Moreover, the multiple comparisons showed that there were significant differences in room CO₂ concentrations without curtain compare to with one curtain and two curtains ($p < 0.05$). However, no significant difference in room CO₂ concentrations was found between one curtain and two curtains ($p > 0.05$).

In Fig. 7.9c, the mean concentrations of CO₂ for six sampling points below the floor were 1738.5 (\pm 132.5), 2449.0 (\pm 245.3) and 3031.5 (\pm 178.9) mg m⁻³ with no curtain, one curtain and two curtains for the ventilation rate of 100 m³ h⁻¹, respectively. The mean CO₂ concentrations at six sampling points below the floor were 1108.2 (\pm 68.9), 1146.9 (\pm 74.1) and 1466.9 (\pm 137.8) mg m⁻³ at 180 m³ h⁻¹ ventilation rate with no curtain, one curtain and two curtains, respectively (Fig. 7.9d).

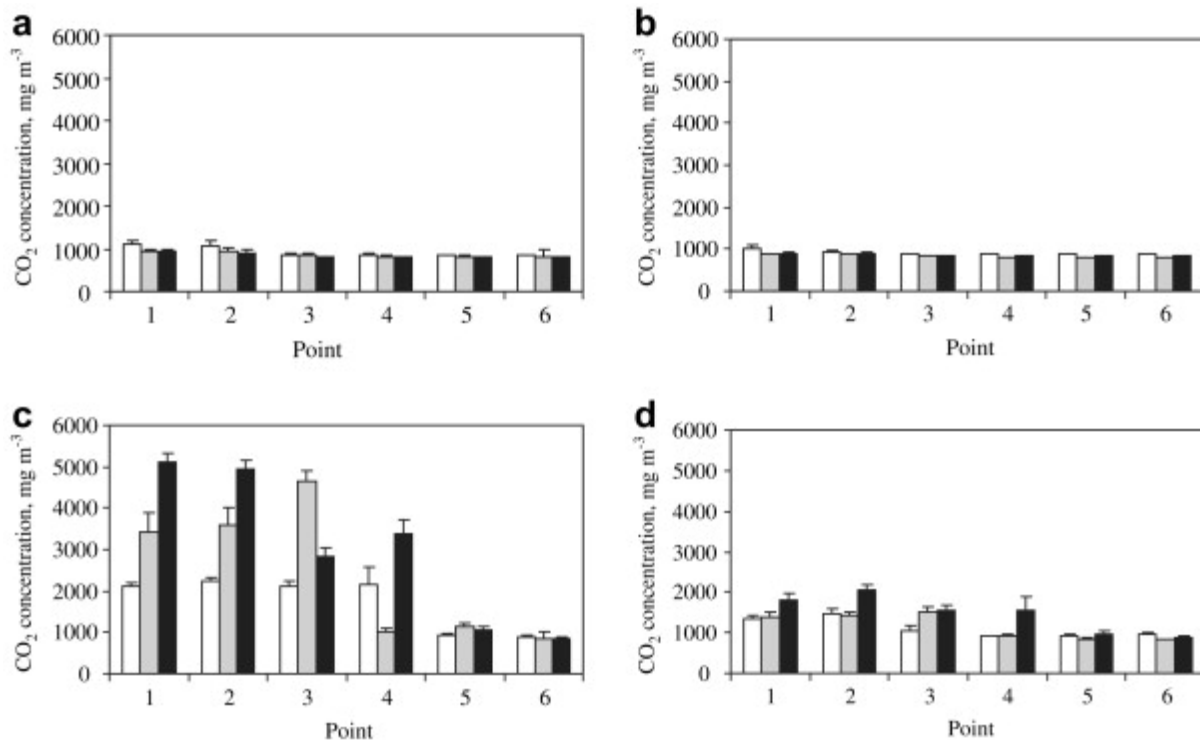


Fig. 7.9 - Relation between curtain number and CO₂ concentration at six sampling points, where, □, ▒ and ■ represent with no curtain, one curtain and two curtains: (a) and (c) represent above and below the floor with 100 m³ h⁻¹ ventilation rate; (b) and (d) represent above and below the floor with 180 m³ h⁻¹ ventilation rate, respectively.

There were significant differences in pit CO₂ concentrations between the levels of ventilation rate ($p < 0.05$), however, no significant difference in pit CO₂ concentrations was observed among different curtain numbers ($p > 0.05$).

The results in Fig. 7.9 showed that the highest CO₂ concentration in the slurry pit and lower CO₂ concentration in the room air could be achieved by using lower room ventilation rate and more slurry pit curtains. The contaminants like NH₃ and odour emissions may be reduced from animal house if more contaminants can be kept inside the pit. In addition, lower CO₂ concentration in the room air results in better air quality inside livestock buildings.

7.3.2.2. Air exchange ratio in the slurry pit

The estimated pit air exchange ratios are shown in Fig. 7.10. In a ventilated pig building with slatted floor without pit ventilation, the air exchange rate in the slurry pit is influenced by room ventilation rate and curtain under the slatted floor. It can be clearly seen that lower ventilation rate and more curtains under the slatted floor resulted in lower air exchange ratios in the slurry pit. One curtain under the slatted floor reduced pit air exchange rate by 31.1% and 9.8% ($p < 0.05$) at the room ventilation rates of $100 \text{ m}^3 \text{ h}^{-1}$ and $180 \text{ m}^3 \text{ h}^{-1}$ respectively compare to without curtain. On the other hand, reductions of pit air exchange rate were 45.6% and 27.4% ($p < 0.05$) at the room ventilation rates of $100 \text{ m}^3 \text{ h}^{-1}$ and $180 \text{ m}^3 \text{ h}^{-1}$ respectively with two curtains in comparison to no curtain.

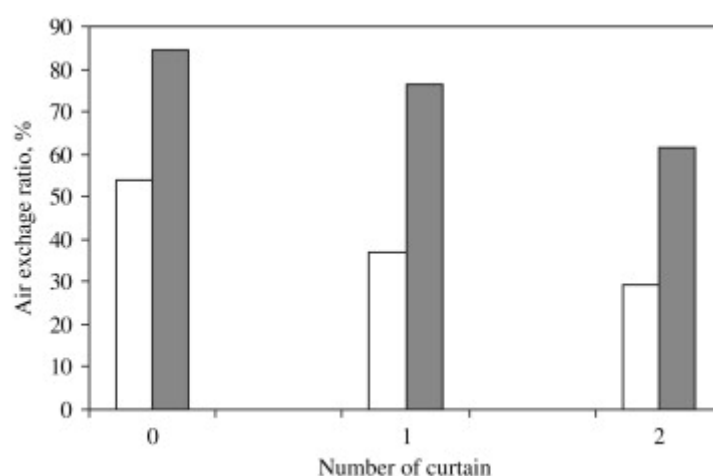


Fig. 7.10 - Pit air exchange ratio for different curtain numbers, where □ and ■ represent ventilation rates of $100 \text{ m}^3 \text{ h}^{-1}$ and $180 \text{ m}^3 \text{ h}^{-1}$, respectively.

From the results, it is clear that curtains reduce the air exchange rate between the slurry pit and room air, which ultimately reduces emissions. But use of curtains under slatted floors in practical situations could be difficult. It may affect manure removal and handling procedures. Therefore, further tests would be needed in full scale pig buildings with suitable curtain designs.

7.3.2.3. Airflow pattern

Slurry pit curtain affects airflow behaviour in the slurry channel. With no slurry pit curtain (Fig. 7.11a), the secondary airflow was able to penetrate into the slurry pit with unrestricted access to the total emission surface area. When the slurry pit was divided by using the curtains (Fig. 7.11b, c), however, the secondary airflow was broken into several smaller volumes in each space, restricting the secondary airflow contact between air and emission surface, and thus reducing the pit air exchange rate and CO_2 concentration in the room air.

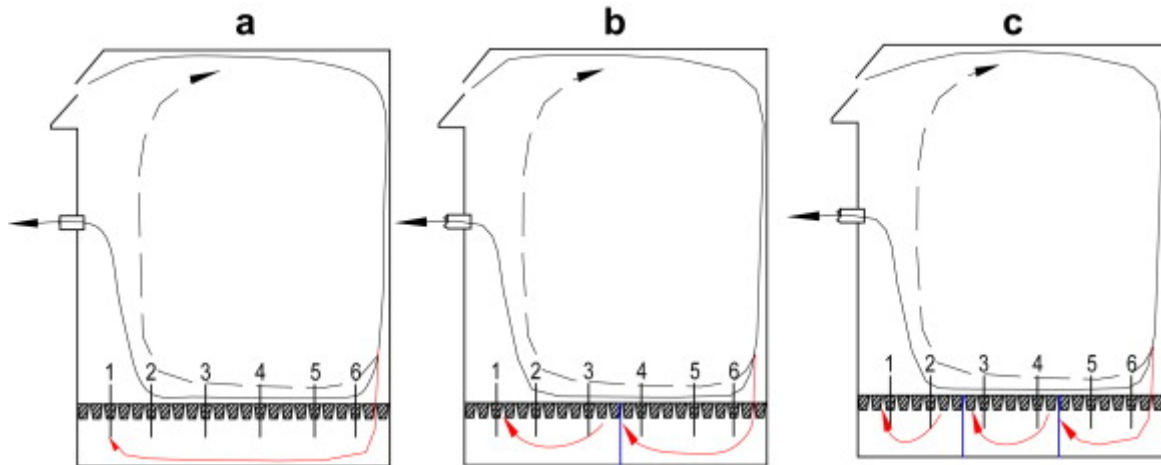


Fig. 7.11 - Airflow patterns in the 2D chamber with different curtain numbers: (—) and (---) primary airflow; (—) secondary airflow; (a) without curtain, (b) one curtain and (c) two curtains.

7.3.2.4. Air velocity

Increasing ventilation rate increased air velocities above and below the floor. The mean air velocity above the floor with ventilation rate of $180 \text{ m}^3 \text{ h}^{-1}$ was around twice than that at $100 \text{ m}^3 \text{ h}^{-1}$ ($p < 0.05$). No significant difference in air velocity above the floor was observed among numbers of curtains ($p > 0.05$) due to the lack of effect on primary airflow. There was a significant difference in air velocity below the floor among the levels of ventilation rate and three numbers of curtains ($p < 0.05$). Moreover, the multiple comparisons showed that there were significant differences in air velocity below the floor with no curtain compared to one curtain or two curtains ($p < 0.05$). However, no significant difference in air velocity below the floor was found between one curtain and two curtains ($p > 0.05$).

The airflow pattern in the slurry pit was affected by the positions and numbers of curtains. Comparing to without curtain, there were higher air velocities at points 4, 5 and 6.

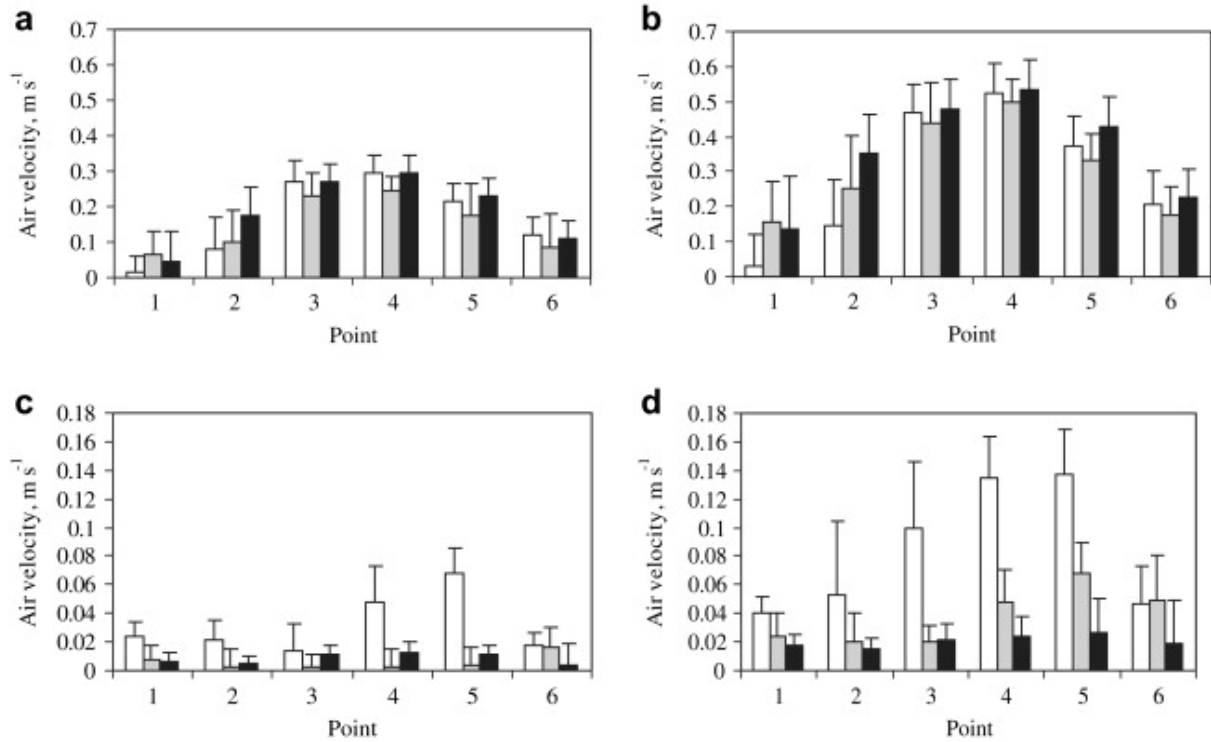


Fig. 7.12 - Relation between curtain number and air velocity at six sampling points, where, □, ■ and ■ represent with no curtain, one curtain and two curtains: (a) and (c) represent above and below the floor with 100 m³ h⁻¹ ventilation rate; (b) and (d) represent above and below the floor with 180 m³ h⁻¹ ventilation rate, respectively.

The inlet air velocity increased with increasing ventilation rate due to the constant inlet opening in this study and resulted in a higher air velocity at the emitting surface. Consequently, the reduction of pit air exchange ratio with reduced ventilation rate in Fig. 7.10 can be explained by reducing air velocity at the emission surface.

7.3.2.1. Turbulence intensity

Increasing ventilation rate reduced Ti both above and below the floor. There was no significant difference in Ti above the floor among the levels of ventilation rate and three numbers of curtains ($p > 0.05$). However, significant differences in Ti below the floor among the levels of ventilation rates and numbers of curtains can be observed ($p < 0.05$). The big values of Ti in Fig. 7.13c may be caused by the very small mean velocities as shown in Fig. 7.12c. Furthermore, vertical velocity fluctuations still may exist and affect the concentrations and emissions.

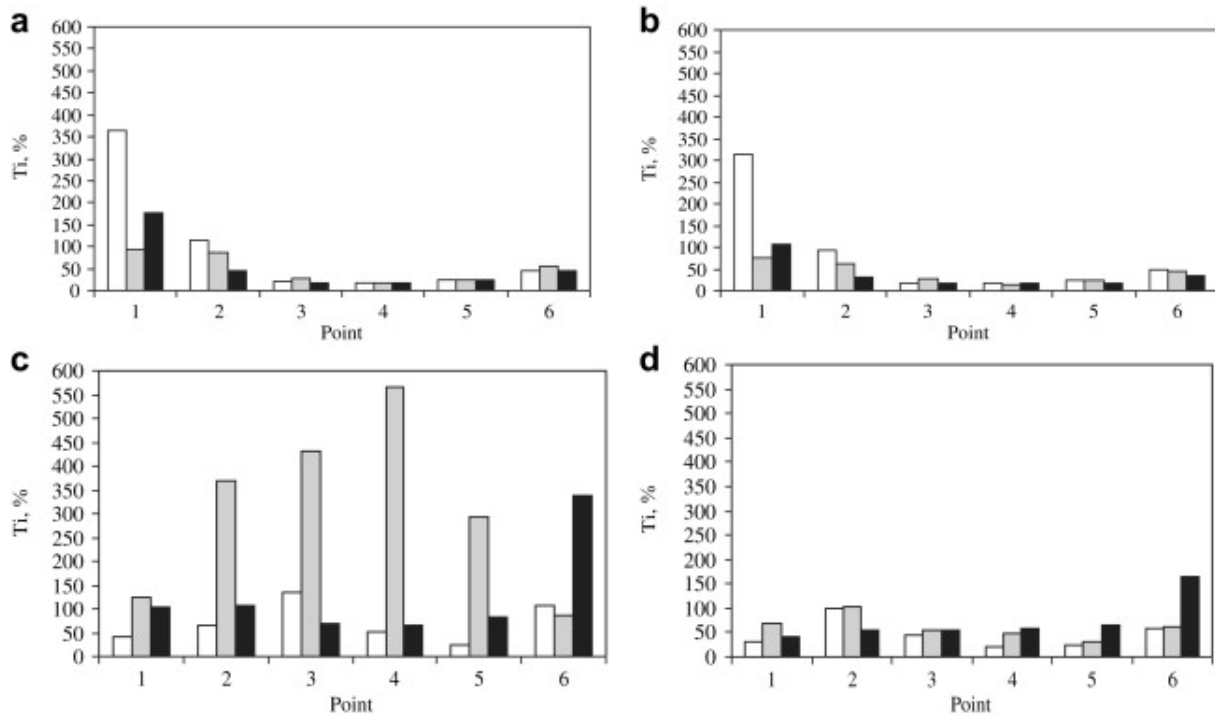


Fig. 7.13 - Relation between curtain number and turbulence intensity at six sampling points, where □, ■ and ■ represent with no curtain, one curtain and two curtains: (a) and (c) represent above and below the floor with 100 m³ h⁻¹ ventilation rate; (b) and (d) represent above and below the floor with 180 m³ h⁻¹ ventilation rate, respectively.

7.4. Conclusions

The airflow patterns, air velocities and turbulence intensities in the room space near the slatted floor and in the headspace of the pit were affected by changing the angle of a deflector and by the presence of pit curtains numbers. It was found that the lowest pit ventilation and the highest concentration in the headspace of the pit could be achieved by using a deflector angle of 45° for both of two ventilation rates. Moreover, the lowest pit air exchange rate and the highest concentration in the headspace of the pit were found in higher curtain numbers and lower ventilation rate. However, to define an optimal deflector angle and number of pit curtains will require further studies. Furthermore, the results from the model chamber experiments should be validated in future investigations with full scale buildings.

Acknowledgements

The research was performed as part of ROSES project “Reduction of Odour Source in and Emission from Swine Buildings” under the Program “Animal Husbandry, the Neighbours and the Environment” funded by the Danish Ministry of Food, Agriculture and Fisheries (Grant No. 3304-

VMP-05-032-01). The authors appreciate the supports by the National Science and Technology Support Project of China (Grant No. 2006BAD14B01) and NSFC (Grant No. 30901046). The authors also thank to the technical supports of Peter Ravn and Jan Ove Johnsen at Air Physics Lab, Research Centre Bygholm, University of Aarhus, Denmark.

References

- Aarnink A J A; Swierstra D; van den Berg A J; Speelman L (1997). Effect of type of slatted floor and degree of fouling of solid floor on ammonia emission rates from fattening piggeries. *Journal of Agricultural Engineering Research*, 66 (2), 93–102.
- Arogo J; Zhang R; Riskowski G L; Christianson L L; Day D L (1997). Mass transfer coefficient of ammonia in liquid swine manure and aqueous solutions. *Journal of Agricultural Engineering Research*, 73, 77–86.
- Barber E M; Sokhansanj S; Lampman W P (1982). Stability of airflow patterns in ventilated airspaces. ASAE Paper No. 82-4551, St Joseph, MI.
- Bjerg B; Svidt K; Zhang G; Morsing S (2000). The effects of pen partitions and thermal pig simulators on airflow in a livestock test room. *Journal of Agricultural Engineering Research*, 77 (3), 317–326
- Buiter J J; Hoff S J (1998). Ammonia distribution in a pit-ventilated confinement building: one-half scale model study. *Transactions of the ASAE*, 41 (6), 1817–1827.
- Chung K; Hsu S (2001). Effect of ventilation pattern on room air and contaminant distribution. *Building and Environment*, 36, 989–998.
- Demmers T G M; Burgess L R; Phillips V R; Clark J A; Wathes C M (2000). Assessment of techniques for measuring the ventilation rate, using an experimental building section. *Journal of Agricultural Engineering Research*, 76, 71–81.
- Morsing S; Strøm J S; Zhang G; Kai P (2008). Scale model experiments to determine the effects of internal air-flow and floor design on gaseous emissions from animal houses. *Biosystems Engineering*, 99 (1), 99–104.
- Strøm J S; Zhang G.; Morsing S. (2002). Predicting near-floor air velocities for a slot-inlet ventilation building by jet velocity decay principles, *Transactions of the ASAE*, 45 (2), 407–413.
- Tong G; Zhang G; Ravn P; Rong L; Nielsen P V (2008). Effect of environmental deflector on air exchange in slurry pit and concentration distribution in a two-dimensional ventilation chamber. In: *Agricultural & Biosystems Engineering for a Sustainable World – Proceedings of AgEng2008 International Conference on Agricultural Engineering*, 23–25 June 2008, Crete, Greece. Paper No. OP-550 on Proceeding CD.

- Van der Peet-Schwering C M C; Aarnink A J A; Rom H B; Dourmad J Y (1999). Ammonia emissions from pig houses in the Netherlands, Denmark and France. *Livestock Production Science*, 58, 265–269.
- Webb J; Menzi H; Pain B F; Misselbrook T H; Dämmgen U; Hendriks H; Döhler H (2005). Managing ammonia emissions from livestock production in Europe. *Environmental Pollution*, 135, 399–406.
- Ye Z; Zhang G; Li, B; Strøm J S; Tong G; Dahl P J (2008). Influence of airflow and liquid properties on the mass transfer coefficient of ammonia in aqueous solutions. *Biosystems Engineering*, 100 (3), 422–434.
- Ye Z; Zhang G; Li, B; Strøm J S; Dahl P J (2008). Ammonia emissions affected by airflow in a model pig house: effects of ventilation rate, floor slat opening, and headspace height in a manure storage pit. *Transactions of the ASABE*, 51 (6), 2113–2122.
- Ye Z; Zhang G; Seo I-H; Kai P; Saha C K; Wang C; Li B (2009). Airflow characteristics at the surface of manure in a storage pit affected by ventilation rate, floor slat opening, and headspace height. *Biosystems Engineering*, 104 (1), 97–105.
- Zhang G; Strøm J S (1999). Jet drop models for control of non-isothermal free jets in a side-wall multi-lint ventilation system, *Transactions of the ASAE*, 42 (4), 1121–1126.
- Zhang G; Bjerg B; Strøm J S; Morsing S; Kai P; Tong G; Ravn P(2008). Emission effects of three different ventilation control strategies—a scale model study. *Biosystems Engineering*, 100 (1), 96–104.
- Zhang R; Day D L; Christianson L L; Jepson W P (1994). A computer model for predicting ammonia release rates from swine manure pits. *Journal of Agricultural Engineering Research*, 58 (4), 223–229.
- Zhang Y; Wang X; Riskowski G L; Christianson L L (2001). Quantifying ventilation effectiveness for air quality control. *Transactions of the ASAE*, 44 (2), 385–390.

Chapter 8

Effects of a partial pit ventilation system on indoor air quality and ammonia emission from a fattening pig room

Paper VII:

Saha, C.K., Zhang, G, Kai, P. and Bjerg, B. 2010. **Effects of a partial pit ventilation system on indoor air quality and ammonia emission from a fattening pig room.** Biosystems Engineering, Vol. 105 (3), P 279-287.

Abstract

The investigation was based on a hypothesis that applying an extra pit ventilation system may remove the highly concentrated gases and odours from the headspace above the liquid manure surface. This would improve air quality in the animal occupation zone, and utilising an air purification system to clean the pit-exhaust air may result in a reduction of the total emission from livestock buildings. In the investigations, an experimental fattening room with two pens and 30 pigs was used. The room was equipped with an automatically controlled negative pressure ventilation system with ceiling diffusion air inlet and a ceiling–roof top ventilator as a major exhaust unit. Additionally, an extra pit-exhaust unit was also installed. During the experiments, the major exhaust unit was automatically controlled by the climate computer according to indoor thermal conditions. About 10% of the maximum ventilation capacity was dedicated to the pit ventilation in each of two two-week periods. Ammonia concentrations, in air inlet and outlet, in the headspace above the slurry pit and in the slurry-pit exhaust were measured continuously. We found that the combination of ceiling and pit ventilation resulted in significantly lower ammonia concentrations in the room air (42.6%, $p < 0.001$) and in the slurry-pit headspace (22.3%, $p < 0.001$) compared with only ceiling ventilation. Total ammonia emissions increased slightly due to this new combination of ventilation systems. However, using an air cleaning system such as bioscrubber for pit exhaust, reductions in the ammonia emission of 37–53% from pig building might be achieved. The capacity required for the air cleaning needs only be 10% of the system capacity for cleaning all exhaust air. We conclude that indoor air quality can be significantly improved, and emission from the buildings significantly reduced, by utilising partial pit ventilation together with an exhaust air cleaning in pig buildings with ceiling ventilation system, without affecting pigs' behaviour.

Key words: Ammonia, Air quality, Emission, Pit ventilation, Pig room

8.1. Introduction

Indoor air quality and gas as well as odour emission from pig buildings are major concerns for ventilation engineers due to the negative effects on the well-being of animals, workers in the buildings and neighbours. Ammonia is considered a main variable for determining air quality and a significant contributor to health and equipment deterioration (Bull and Sutton, 1998; Cupr *et al.*, 2005; Webb *et al.*, 2005). Most European countries have emphasised the importance of ammonia and odour reduction to reduce the negative impact on the environment and local society. In Denmark, producers with livestock farms producing more than 7500 kg nitrogen in the manure prior to application must obtain environmental authorisation and the ammonia emission must be reduced by 25% in 2009 and onwards compared with a reference pig facility (partially slatted floor). In practice this corresponds to a reduction of approximately 40% if the farmer wishes to build a pig house with fully slatted floor (Anonymous, 2007). To achieve the goals for reducing the emission from livestock production, different technologies are under development. Air purification systems, including wet-scrubber, bioscrubber, biofilter and chemical-filter for application to exhaust ventilation can be found in the market. However, to clean the total exhaust air from a ventilation system requires considerable energy and cleaning capacity. Therefore, more consideration is needed to find an optimal technical solution.

Ammonia emissions from liquid manure inside pig houses are related to the ammonia concentration difference between the manure and the air above the manure, manure pH, manure temperature and air temperature and air velocity over the manure surface (Arogo *et al.*, 1999; Ni, 1999; Ye *et al.*, 2008b; Zhang *et al.*, 2008). The ammonia concentration difference is the driving force of mass transfer of ammonia release. The pH and temperature affect the free ammonia concentration in liquid manure. The temperature and air velocity govern the convective mass transfer process. The air velocity over the manure surface in a pig house is directly related to the ventilation of the house (Ni, 1999).

The purpose of the ventilation system is to maintain a desired indoor thermal condition while controlling levels of humidity and removing gaseous contaminants introduced by the animal and their waste. Efficient removal of gases depends on proper ventilation system designs. Ventilation design characteristics that may affect ammonia levels in a building include: the location of air inlets and outlets, the total ventilation rate, obstructions to airflow, and temperature profiles within the space (Buiter and Hoff, 1998). An environment with a high concentration of gases and odours in room air cannot be controlled effectively by a conventional roof or ceiling ventilation system, especially when minimum ventilation rates are employed during winter, and during manure agitations prior to pumping of the manure pit (Pohl and Hellickson, 1978). During winter an ammonia level of 5–50 ppm has been found in fully slatted floor buildings with under-floor manure

storage, and ammonia exceeding a threshold value may affect adversely the health of stockmen and animals (Koerkamp et al., 1998). Therefore, employing a partial pit ventilation system might remove the gases and odours from the space above the liquid manure surface before natural convection currents or mechanically induced air movement above the slatted floor transfer the gases to the livestock environment. However, it would be easier to improve air quality inside room and clean concentrated exhaust air in one place using an air cleaner or ammonia scrubber. The capacity required for air cleaning will also be lower than for cleaning of total exhaust air.

The influence of pit ventilation on airflow pattern in animal buildings has been reported by some researchers (Keller and Day, 1975; Ross et al., 1975). Ross et al. (1975) found that tapered exhaust ducts equipped with variable speed fans resulted in acceptable air distribution and temperature control, but unsatisfactory odour control in a pig structure. Pohl and Hellickson (1978) compared five types of pit ventilation systems in a 1/12 scale model and concluded that the centred duct system produced the best ventilation characteristics. Buiter and Hoff (1998) studied the effects of building design and management factors on the distribution of ammonia in the airspace with pit ventilation in a 1:2 scale model. Gas used in these studies may not be representative of actual gas concentrations of ammonia and the authors recommended a full scale study. Gustafsson (1987) compared buildings with above-floor exhaust with buildings with only pit exhaust; pit ventilation reduced ammonia levels by 25–30% in the occupied zones. The effect of partial pit ventilation with major ceiling ventilation unit on indoor air quality and ammonia emission from fattening pig rooms has not been investigated in previous studies. Study on the behavioural pattern of the pigs using different ventilation systems may also give an indication of the feasibility of partial pit ventilation.

The objective of this study was to investigate the effect of a partial pit ventilation system on indoor air quality and ammonia emission from a fattening pig room, and to estimate the potential for applying an air purification system to the pit-exhaust unit only. Additionally, the effect of the ventilation system on animal behaviour was also analysed.

8.2. Material and methods

8.2.1. Experimental pig house

The investigation was carried out in one of the four rooms of an experimental building for fattening pigs (Fig. 8.1) at Research Centre Bygholm (University of Aarhus, Denmark). The room had two pens and each pen had two thirds fully slatted and one third drained floor. The room dimension, pen layout and the numbers of pigs in pens were similar to a commercial production unit. The opening area of the slatted floor was 16.5% and for the drained floor 8.5%. Each of the two pens had its own slurry pit of 0.9 m depth, with draining pipes of 0.25 m diameter and a central valve per room for the removal of slurry. The pen partition wall was 1.2 m high. The inspection alley was 1.2 m wide.

The building was equipped with an inlet duct of 0.8 m, located in the roof above the diffuse ceiling of room, to connect the attic and outside air.

8.2.2. Ventilation systems

A negative pressure ventilation system with ceiling diffuse inlet was installed in the room, since it is commonly used in Denmark. The system had two parallel exhaust units, one was placed in the ceiling (major exhaust unit, Fig. 8.1a) and another was under the slatted floor in the pit (partial pit exhaust). In the ventilation process, fresh air came into the attic through the roof duct and into the room through diffuse ceiling due to negative pressure. The ceiling exhaust unit was in continuous operation from 24th September 2008 until the whole experiment was terminated. The pit-exhaust unit was in operation for two weeks in conjunction with the ceiling ventilation from 10th October to 24th October 2008 and from 7th November to 18th November 2008.

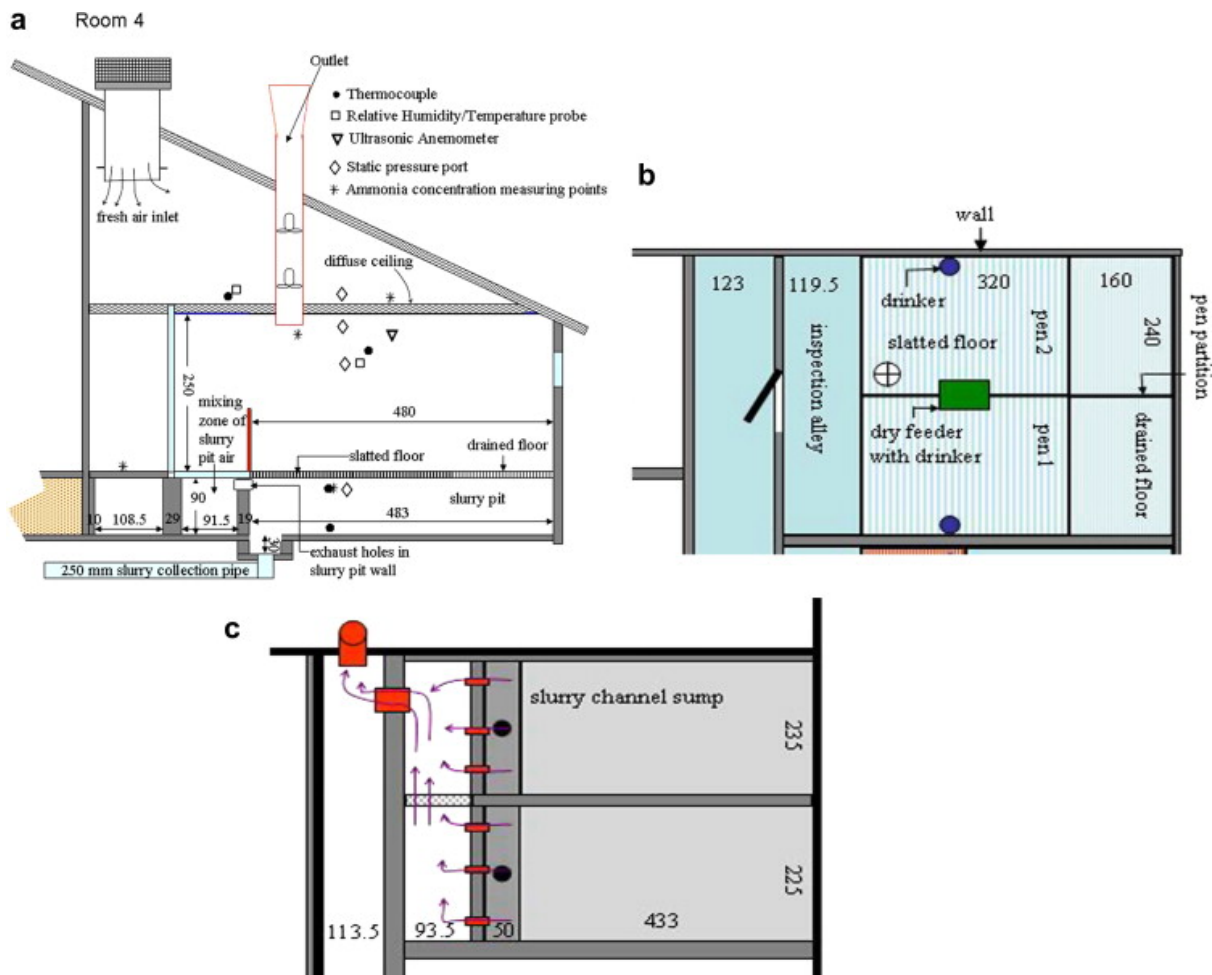


Fig. 8.1 - Cross-section of the experimental room with (a) measurement and sampling locations, (b) layout of a pen and (c) pit ventilation arrangement under the slatted floor. All dimensions are in cm.

8.2.2.1. Ceiling exhaust unit

An exhaust fan was installed in a ceiling chimney of 0.4 m diameter (Fancom BV). Under the fan, a free propeller (model AT40, Fancom BV) was installed to measure the airflow rate. The outlet opening was about 0.4 m beneath the ceiling in the middle of the room. The capacity of the ceiling exhaust was 3400 m³ h⁻¹ at 40 Pa static pressure. The ventilation rate was controlled automatically by a climate controller (FC14-T6, Fancom BV) with a reference temperature sensor located at 1.2 m above the pig lying area.

8.2.2.2. Pit-exhaust unit

Three exhaust openings of 0.16 m in diameter and made of PVC (Polyvinyl chloride) tubes were installed in the slurry-pit wall between an air exhaust channel and the slurry pit for each pen (Fig. 8.1c). The air exhaust channel was located under the inspection alley. The exhaust air from the manure pit was extracted through the six pit openings to the exhaust channel and further through a 0.2 m diameter pipe by means of an exhaust ventilator located outside the room when pit ventilation was in operation. A pit ventilation rate of 10% of maximum system ventilation rate was pre-set for the experiments with the pit ventilation. The pit ventilation rate was pre-adjusted manually by means of a fan motor voltage regulator.

8.2.3. *Animals and feeding*

The experiment was carried out over 56 days, from 24th September to 18th November 2008. 30 pigs, randomly picked from a group of 120 pigs, were divided equally and put into the two pens in the room. Mean initial weight of the pigs was 35.8 kg and mean final weight was 76.1 kg. Feed and drinking water were available all the time. The type of feed for the pigs was “DLG Finale Plus U Fuldfoder til slagtesvin” (eng. DLG Finale Plus U Complete Feed) (DLG a.m.b.a., Copenhagen, Denmark) containing 40% wheat, 30% barley, 12% rapeseed, 7.45% wheat bran, 4.85% soya bean, 2.40% beet molasses, plus vitamins and minerals. The diet contained 15.5% raw protein. Feed was delivered to the two pens *via* a feed hopper positioned between the pens (Fig. 8.1b) with a water nipple placed inside the feed hopper. Straw was supplied as a rooting material according to Danish regulations.

8.2.4. *Measurements*

8.2.4.1. Ventilation airflow rates and air velocity inside the room

Ventilation rates through the ceiling exhaust were measured by a Fancom free running impeller in the exhaust chimney. The sensor was calibrated before the experiment. A FMU/FMDRU 200-160 flow meter (Lindab A/S, Denmark) based on an orifice taping principle, was used to measure the

ventilation airflow rates in pit exhaust. The accuracy of the flow measuring method is 5–10% depending on the distance to the flow disturbance. By measuring the pressure difference, ΔP , between the measurement nozzles, the ventilation flow in the duct was estimated by

$$VR = 29.4\sqrt{\Delta P} \quad (8.1)$$

where VR is ventilation rate, $\text{m}^3 \text{h}^{-1}$; ΔP is pressure difference between upstream and downstream side of the orifice, Pa. The pressure differences were measured using a differential pressure transmitter (Model 694, Huba control, Switzerland) with a measurement range of 10–300 Pa and an accuracy of $\pm 0.7\%$ and a resolution of 0.1% of full scale. The data was sampled every 10 s and recorded as 1 min averages using a Campbell Scientific CR1000 data logger.

8.2.4.2. Ammonia measurements

To estimate the ammonia emission from the room and to quantify the emission rate from the two exhaust units, ammonia concentrations in sample air collected (i) in the attic just above the ceiling (background), (ii) in the ceiling exhaust unit, (iii) in the slurry pit: 0.10 m beneath the slats in the middle of the pit, and (iv) in the pit-exhaust pipe (Fig. 8.1a), were measured using an infrared 1312 photoacoustic multi-gas analyser and a multiplexer 1303 (Innova Air Tech Instruments A/S, Denmark). According to the specifications of the instrument, the detection limit of ammonia measurement instrument was 0.2 ppm (1 atm.; 20 °C). Suction pumps (Model Eg 7130-4AY-RLT, 19W, GEFEG Motoren) were used to collect air samples from these locations and deliver the sample air to the multiplexer and the multi-gas analyser *via* FEP (Fluorinated ethylene propylene or Teflon-FEP) tubes of 6 mm inside diameter and 1 mm of tube thickness. The tubes were insulated and heated using heating wire in order to avoid condensation.

8.2.4.3. Air temperature and relative humidity

The air temperature was measured using type T thermocouples in attic (air inlet), inside the room, and 0.10 m beneath the slats in the middle of the slurry pit (Fig. 8.1a). A Vaisala 50Y temperature and relative humidity probe was also used for measuring temperature and relative humidity in the attic. Outside temperature data for Bygholm, Horsens, Denmark was collected from the local weather station, which is available in the climate database of Department of Agro-ecology and Environment, Aarhus University, Denmark.

8.2.5. *Observations*

The lying locations of the pigs were monitored by video camera during the experimental period. Snapshots at 1 h intervals were collected automatically. These snapshots were used to determine the

lying locations of pigs. The following locations were distinguished in the pen: wall side slatted floor; pen partition side of the slatted floor; wall side of the drained floor and pen partition side of the drained floor (Fig. 8.1b).

8.2.6. Computation of ammonia emission rate and data analysis

The ammonia emission for ceiling ventilation and pit ventilation was calculated by the following eqs. (8.2) and (8.3).

Ammonia emission for ceiling ventilation

$$E_{NH_3,ceil} = V_{ceil} (C_{out} - C_{in}) \quad (8.2)$$

where $E_{NH_3,ceil}$ is the ammonia emission for ceiling ventilation, $mg\ h^{-1}\ pig^{-1}$ or $mg\ d^{-1}\ pig^{-1}$; V_{ceil} is the ceiling ventilation rate, $m^3\ h^{-1}\ pig^{-1}$ or $m^3\ d^{-1}\ pig^{-1}$; C_{out} is the outlet ammonia concentration of room air, $mg\ m^{-3}$; C_{in} is the inlet/attic air ammonia concentration, $mg\ m^{-3}$.

Ammonia emission for pit ventilation

$$E_{NH_3,pit} = V_{pit} (C_{pit-exhaust} - C_{in}) \quad (8.3)$$

where $E_{NH_3,pit}$ is the ammonia emission from pit ventilation, $mg\ h^{-1}\ pig^{-1}$ or $mg\ d^{-1}\ pig^{-1}$; V_{pit} is the pit ventilation rate, $m^3\ h^{-1}\ pig^{-1}$ or $m^3\ d^{-1}\ pig^{-1}$; $C_{pit-exhaust}$ is the ammonia concentration of pit-exhaust air, $mg\ m^{-3}$; C_{in} is the inlet/attic air ammonia concentration, $mg\ m^{-3}$.

The single factor ANOVA (analysis of variance) analysis was used to determine the effect of ceiling and pit ventilation on ammonia emissions and concentrations. The dependent variables considered for each analysis were the daily mean ammonia emission ($g\ d^{-1}\ pig^{-1}$), ammonia concentrations ($mg\ m^{-3}$) and pig activity. The independent variable considered for these analyses was the ventilation system.

8.3. Results and discussion

The mean values of climate during the measurement periods of 15 days for each stage are shown in Table 8.1. The temperature in the measuring locations is shown in Fig. 8.1a. Room temperature was maintained at the set points regulated by the ventilation control system: from $19.9 (\pm 0.6)^\circ C$ at the beginning, gradually reduced to $15.9 (\pm 0.8)^\circ C$ at the end of the experiments (Fig. 8.2). The average slurry-pit air temperature was $16.7 (\pm 0.6)^\circ C$ during the first stage and this temperature was $0.8^\circ C$ lower during stage four. There was no significant difference in the slurry-pit temperature when ceiling ventilation was in single operation compared with ceiling plus pit ventilation. During the experimental run, outside and attic temperature were $8-10^\circ C$ lower than the inside room temperature.

Table 8.1- Means and standard deviation (between brackets) of temperatures at the different locations and the ventilation rates through the ceiling and pit

Systems run/measurement		Stages (Test period in 2008)			
		1st (24 Sept. to 9 Oct)	2nd (10 to 24 Oct)	3rd (25 Oct. to 6 Nov.)	4th (7 to 18 Nov.)
Ventilation system		System C ^a	System C + P ^b	System C ^a	System C + P ^b
Temperature (°C)	Slurry-pit	16.7 (0.6)	16.6 (0.6)	15.8 (0.6)	15.9 (0.5)
	Room	19.9 (0.6)	18.5 (0.9)	16.8 (0.8)	15.9 (0.8)
	Attic	11.9 (2.5)	11.4 (2.3)	7.5 (2.7)	8.3 (2.0)
	Outside	10 (3.3)	10.5 (2.7)	6.3 (3.4)	7.5 (2.4)
Ceiling ventilation rate m ³ h ⁻¹ pig ⁻¹		39.1 (12.5)	53.3 (14.7)	58.3 (15.7)	69.5 (18.5)
Pit ventilation rate m ³ h ⁻¹ pig ⁻¹		–	11.4 (0.7)	–	11.8 (1.0)

a System C – ceiling exhaust unit.
b System C + P – ceiling plus pit-exhaust unit.

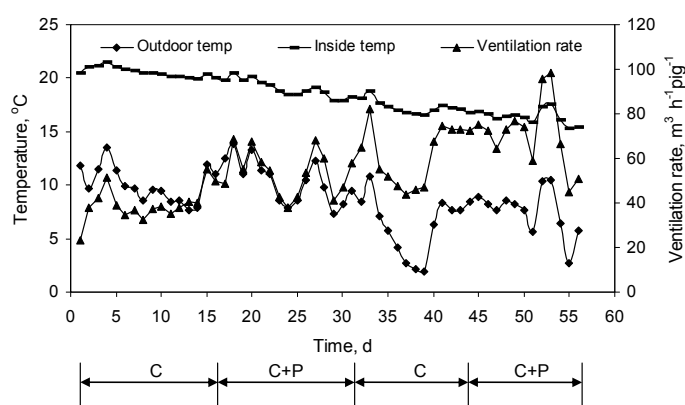


Fig. 8.2 –Daily mean inside and outside temperatures and ceiling ventilation rate during the growing period. C, only ceiling exhaust in operation; C+P, both ceiling and pit exhaust in operation.

The pit ventilation was run during the 2nd and 4th stages together with ceiling ventilation system. The average fixed pit ventilation rates were 11.4 (± 0.7) and 11.8 (± 1) m³ h⁻¹ pig⁻¹ during the 2nd and 4th stage respectively. Since the pit ventilation rate was not automatically controlled, the actual pit ventilation rate fluctuated to some extent due to variations in the system ventilation rate. A little variation was observed in pit ventilation rate over 24 h, but was generally maintained at 11.1–11.8 m³ h⁻¹ pig⁻¹.

The ceiling ventilation rate per pig was increased as the pigs grew, since the heat production of pigs increases with body weight increase (Fig. 8.2). However, ventilation requirement also depends on outdoor temperature, indoor air temperature set point, pig activity etc. (Jeppsson, 2002). Fig. 8.2 shows that ventilation rate followed a similar pattern to the outdoor air temperature. At lower temperatures, the ventilation requirement was lower. In the experiment period, the lowest outdoor temperature period was from days 33 to 39 where the ventilation rate was also lower in 3rd stage (system C). The highest ventilation rate (98.3 m³ h⁻¹ pig⁻¹) was on day 53 during the 4th stage (system C + P) when the pigs were much bigger and the outdoor temperature was relatively high.

8.3.1. Ammonia concentration

The mean and standard deviation (in brackets) of the daily values of ammonia concentrations at different locations and ammonia emission in different ventilation systems for each set-up are given in Table 8.2. The system C + P had a significant effect on lowering ammonia concentration in the slurry pit as well as in the room air ($p < 0.001$). On the other hand, in the slurry-pit exhaust, the ammonia concentration was much higher in system C + P than system C. We did not expect higher concentration differences in slurry-pit exhaust between the two ventilation systems. The reasons could be that the pit-exhaust duct was not closed tightly enough while pit ventilation was off. Therefore, a little outdoor fresh air might have leaked into the pit exhaust due to the negative pressure of the system and resulted in the lower concentration in the measurement locations. The ammonia concentration of attic air was at a constant level of 0.8–1.0 mg m⁻³.

Table 8.2 – Mean and standard deviation (between brackets) of the daily values of ammonia concentrations at different locations and ammonia emission in different ventilation systems

Systems run/measurement		Stages				Effect of ventilation systems ^b
		1st (24 Sept. to 9 Oct)	2nd (10 to 24 Oct)	3rd (25 Oct. to 6 Nov.)	4th (7 to 18 Nov.)	
Ventilation systems		System C	System C + P	System C	System C + P	
Ammonia concentration ^a , mgm ⁻³	Slurry-pit	7.6 (1.7)	5.8 (1.1)	8.7 (1.7)	6.8 (1.7)	$P < 0.001$
	Slurry-pit exhaust	0.7 (0.1)	8.3 (1.0)	0.9 (0.3)	7.0 (0.8)	$P < 0.001$
	Ceiling exhaust (room)	4.9 (1.4)	3.1 (0.4)	4.3 (0.6)	2.3 (1.9)	$P < 0.001$
	Attic	1.0 (0.1)	1.0 (0.2)	0.9 (0.1)	0.8 (0.1)	$P > 0.05$
Ammonia emission, mg h ⁻¹ pig ⁻¹	Through ceiling	150.9 (15.1)	111.5 (11.2)	197.2 (8.9)	98.8 (9.0)	$P < 0.001$
	Through pit	–	82.9 (4.0)	–	73.5 (3.3)	–
	Total	150.9	194.4	197.2	172.3	–

^a See Fig. 8.1 for different locations

^b main effects calculated with the statistical model.

The ammonia concentration in room air using ventilation system C + P showed significant reduction by about 42.6% compared to system C (Fig. 8.3a). Ammonia concentration just under slatted floor was also reduced in system C + P. The average reduction of the concentration in the pit was 22.3% (Fig. 8.3a). These reductions of ammonia concentration in ceiling exhaust air and in the slurry pit indicate the improvement in air quality within the room (Fig. 8.3a).

The mean diel (24 h) pattern shows less variation in ammonia concentration in different locations (Fig. 8.3b) for the two ventilation systems. Ammonia concentrations at ceiling outlet were higher until 0800 h for both, and then started to drop when the ventilation rate increased (Fig. 8.3b). When ceiling ventilation was reduced, ammonia concentration at outlet was increased. Ammonia concentration in ceiling exhaust air for system C was higher than system C + P between 0000 and 0800 h, but concentration for system C was lower at higher ventilation rates than system C + P from

1200 to 2000 h. On the other hand, there was less variation of ammonia concentration in slurry-pit air in system C than system C + P. Ammonia concentration in slurry-pit air was lower from 0400 to 1400 h in system C + P than system C.

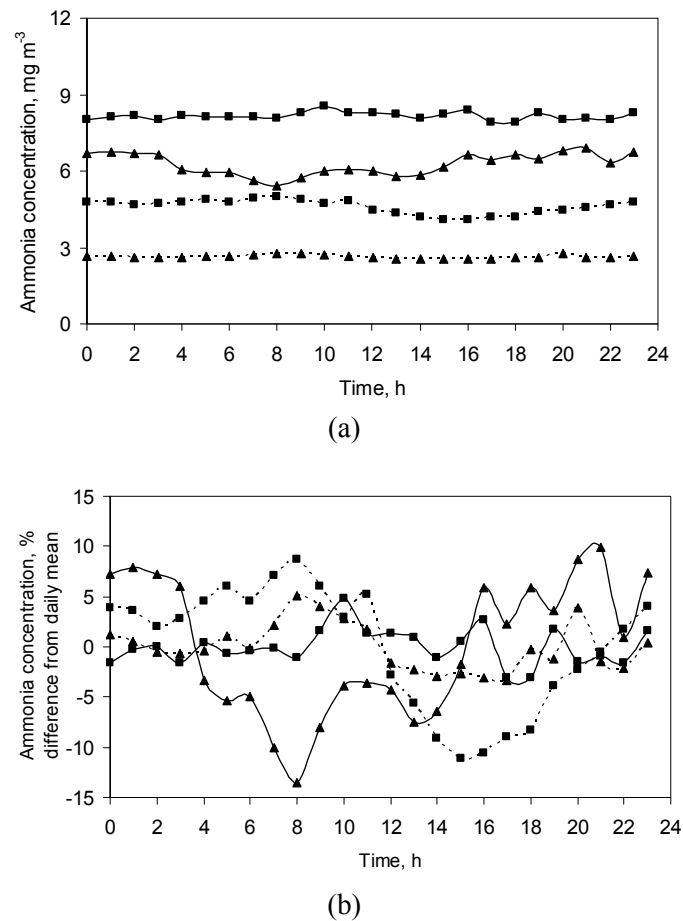


Fig. 8.3 –(a) Mean ammonia concentrations at the same hours of the experiment days and (b) mean diel pattern of ammonia concentrations in room (dotted line) and in the slurry pit (solid line) in two different ventilation systems. ■, system C; ▲, system C + P.

Fig. 8.4 shows the daily variation of ammonia concentration in different locations in the experimental room. The concentration data were not available from days 25 to 27 because of a technical problem with data acquisition. The experiment was started when pigs were 10 weeks old. The ammonia concentration in the room and slurry pit at the beginning was low, because of the small amount of slurry in the slurry pit. The concentration in the room and slurry pit then increased until day 10 (Fig. 8.4). After that, there were small fluctuations in ammonia concentrations in both room and pit but the concentrations did not increase. After week two and week six, when the pit ventilation was started, the ammonia concentration in room air and in slurry-pit dropped; on average it was 1.9 mg m^{-3} in both locations and in both cases. On the other hand, the average ammonia concentration in slurry-pit exhaust was increased to 7.7 mg m^{-3} . The ammonia

concentration in attic air remained almost constant during the entire experimental period. These differences in ammonia concentrations were mainly caused by differences in airflow patterns and air exchange rate. In system C + P, pit air was extracted from the slurry pit, and therefore the ammonia concentration above and beneath the slatted floor were lower than in system C. Minimum flow rate with a negative pressure in the headspace of the pit with partial pit ventilation may prevent upward motion of air from the pit and thus decreased ammonia concentration in the pig room (Gustafsson, 1987; Aarnink and Wagemans, 1997). Another reason for the lower concentration inside the room could be the lower slurry temperature in system C + P because of enhancement of airflow above the slurry surface.

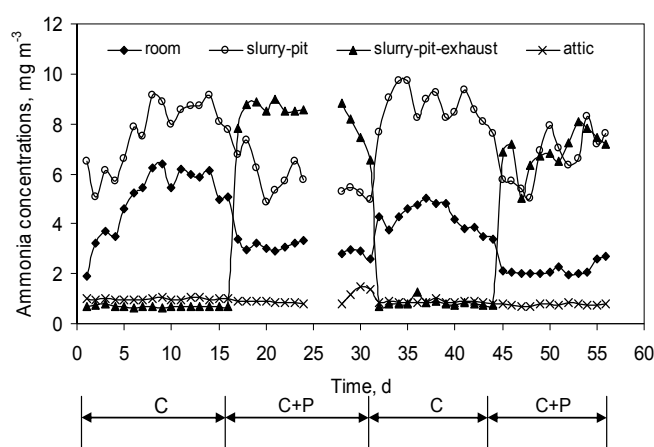


Fig. 8.4 – Daily mean ammonia concentration in different locations of room during the growing period of fattening pigs.

8.3.2. Ammonia emission

The pattern of ammonia emission was similar for both ventilation systems (system C and system C + P) and followed that of the ventilation rate (Fig. 8.5). There was a low emission in the morning and a broader peak in the afternoon. With increasing ventilation rate, ammonia emission was increased. This is consistent with other studies in different systems and approaches (Depraetere and Vanderbiest, 1990; Aarnink et al., 1995; Aarnink and Wagemans, 1997; Arogo et al., 1999; Ye et al., 2008a; Zhang et al., 2008). Increased ventilation to maintain the desired indoor thermal condition resulted in higher emissions.

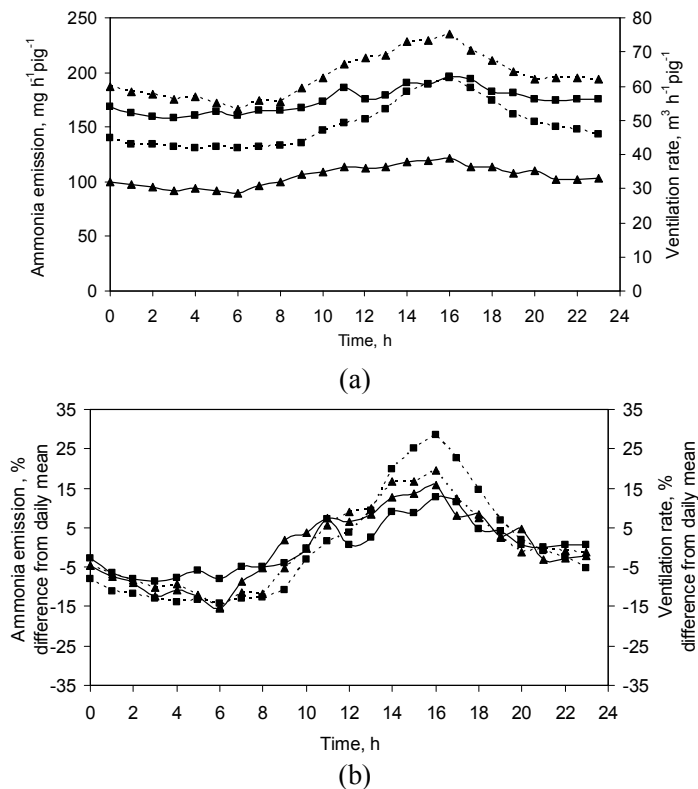


Fig. - 8.5 (a) Mean at the same hours of the experiment days and (b) Mean diel pattern (% difference from daily mean) of ammonia emission (solid line) and ventilation rate (dotted line) respectively through ceiling exhaust in two different ventilation systems. ■ system C; ▲ system C + P.

Ammonia emission through ceiling vent was significantly higher in the system C than system C + P (Fig. 8.5a) although the ceiling ventilation rate was higher in system C + P. The higher ammonia emission in system C could be because of the higher concentration difference between room and pit air. With system C + P, the polluted air in the pit did not move up *via* floor openings to mix with room air, but was taken away by the pit exhaust. In addition, some polluted air above the slatted floor surface was also moving down into pit headspace and leaving *via* the pit-exhaust channel. Average ammonia emission through ceiling vent for system C was 174.0 mg h⁻¹ pig⁻¹ and for system C + P was 105.1 mg h⁻¹ pig⁻¹.

On the other hand, there was less variation in ammonia emission from the pit during the hours when pit ventilation was running (Table 8.2). The average ammonia emission through the pit was 78.2 mg h⁻¹ pig⁻¹. In the system C + P, total emission through the ceiling and pit was 183.4 mg h⁻¹ pig⁻¹ (i.e., 5% higher in system C + P than system C). However, the amount of air passing through the pit could be cleaned effectively by using an air cleaning devices. Phillips *et al.* (1999) found that bioscrubber could abate 97.6% of ammonia from the exhaust air.

Applying such a bioscrubber to treat the pit-exhaust air has the potential to make a significant reduction of total ammonia emission. Fig. 8.6 shows the measured daily mean ammonia emission from the pig room and also simulates what might be expected with bioscrubber at pit exhaust. Emission increases with time at the beginning following a similar pattern of ventilation rate (Fig. 8.6), although climate factors such as indoor and outdoor temperature were changing during the growing period (Fig. 8.2). Without application of any air cleaning, the minimum ammonia emission was $0.5 \text{ g d}^{-1} \text{ pig}^{-1}$ at day one and maximum ammonia emission was $5.6 \text{ g d}^{-1} \text{ pig}^{-1}$ at day 33 of the fattening period. The average ammonia emission through the partial pit exhaust was $1.9 \text{ g d}^{-1} \text{ pig}^{-1}$. Ammonia emission reduction of 37–53% was estimated for using bioscrubber at the pit exhaust (Fig. 8.6). This would be a significant reduction for a pig production room.

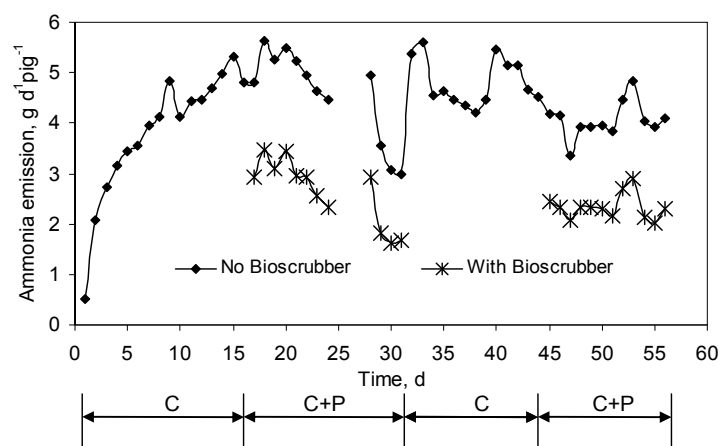


Fig. 8.6 - Daily mean ammonia emissions from pig room during the growing period with (simulated) and without bio-scrubbers at pit exhaust.

8.3.3. Lying locations

On average the pigs lay for 79% of their time during the observation days and on average 37.6% of lying pigs lay on the wall side of the drained floor, 27.1% on the pen partition side of the drained floor, 25.7% on the wall side of the slatted floor and only 9.6% on the pen partition side of the slatted floor (for location see Fig. 8.1b). In system C, on average 39.4% of the lying pigs laid on the wall side of the drained floor where in system C + P about 35.9%. On the other hand, in system C, on average 22.5% of the lying pigs laid on the wall side of the slatted floor where 28.9% in system C + P. At temperatures within the comfort zone, pigs prefer lying on a solid insulated floor to slatted floor (Fraser, 1985). However, at high temperatures they will prefer the slatted floor (Aarnink et al., 1996). In this experiment, most pigs preferred to lie on the drained floor (8.5% opening area) rather than the slatted floor (16.5% opening area). The air exchange between pit and room air was lower in this area (Ye et al., 2008a), which probably provided better comfort climate

to pigs. Very little difference was found in lying behaviour of pigs between the two ventilation systems.

No significant difference in the degree of activity of the pigs was found between two ventilation systems ($p > 0.05$). Using the definition of Aarnink and Wagemans (1997), the pig activity was described as numbers of pigs that were not lying. Mean activity of 20.8% in system C and 21.0% in system C + P were found.

The diel activity pattern was very similar for both ventilation systems (Fig. 8.7). There was a small peak in the morning and a broad peak in the afternoon. Fig. 8.7 shows that pigs were more active between 1000 and 1800 h in both cases.

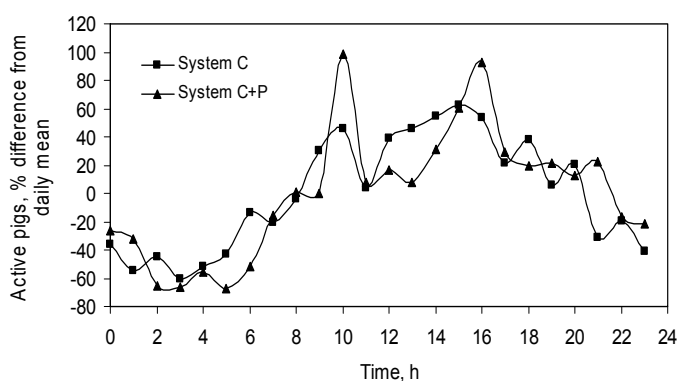


Fig. 8.7 - Mean diel pattern of pig activity (calculated as the percent difference from the daily mean number of pigs not lying) for the ventilation systems C and C + P.

8.4. Conclusion

Applying a partial pit ventilation system may remove the highly concentrated gases and odours from the headspace above the liquid manure surface. A partial pit exhaust of 10% of maximum ventilation capacity in a system with diffusion ceiling inlet and a ceiling exhaust significantly reduced indoor ammonia concentration by 42.6%. The total ammonia emission was 5% higher in ceiling plus pit exhaust than only using ceiling exhaust. If an air purification system were used to clean the pit-exhaust air, the total ammonia emission could be reduced significantly. The differences in the pigs' lying behaviour and activity were not significant between ventilation systems.

Acknowledgements

The research was performed as part of ROSES project “Reduction of Odour Source in and Emission from Swine Buildings” under the Program “Animal Husbandry, the Neighbours and the Environment” funded by the Danish Ministry of Food, Agriculture and Fisheries (Grant Number:

3304-VMP-05-032-01). The authors also thank to the technical support of Jan Ove Johnsen at Air Physics Lab, Research Centre Bygholm, University of Aarhus, Denmark. We would also like to thank the anonymous reviewers for their careful review of the manuscript and their helpful comments.

References

- Aarnink A J A; Keen A; Metz J H M; Speelman L; Verstegen M W A (1995). Ammonia emission patterns during the growing periods of pigs housed on partially slatted floors. *Journal of Agricultural Engineering Research*, 62(2), 105-116
- Aarnink A J A; VandenBerg A J; Keen A; Hoeksma P; Verstegen M W A (1996). Effect of slatted floor area on ammonia emission and on the excretory and lying behaviour of growing pigs. *Journal of Agricultural Engineering Research*, 64(4), 299-310
- Aarnink A J A; Wagemans M J M (1997). Ammonia volatilization and dust concentration as affected by ventilation systems in houses for fattening pigs. *Transactions of the ASAE*, 40(4), 1161-1170
- Anonymous (2007). Annual report on Danish Pig production-Research and Development. Danish Pig Production, 1st edition, October 2007, Published by Tafdrup@co, Denmark
- Arogo J; Zhang R H; Riskowski G. L; Christianson L L; Day D L (1999). Mass transfer coefficient of ammonia in liquid swine manure and aqueous solutions. *Journal of Agricultural Engineering Research*, 73(1), 77-86
- Buiter J J; Hoff S J (1998). Ammonia distribution in a pit-ventilated confinement building: One-half scale model study. *Transactions of the ASAE*, 41(6), 1817-1827
- Bull K R; Sutton M A (1998). Critical loads and the relevance of ammonia to an effects-based nitrogen Protocol. *Atmospheric Environment*, 32(3), 565-572
- Cupr P; Skarek M; Bartos T; Ciganek M; Holoubek I (2005). Assessment of human health risk due to inhalation exposure in cattle and pig farms in south Moravia. *Acta Veterinaria Brno*, 74(2), 305-312
- Depraetere K; Vanderbiest W (1990). Air-flow patterns in piggeries with fully slatted floors and their effect on ammonia distribution. *Journal of Agricultural Engineering Research*, 46(1), 31-44
- Fraser D (1985). Selection of bedded and unbedded areas by pigs in relation to environmental-temperature and behavior. *Applied Animal Behaviour Science*, 14(2), 117-126
- Gustafsson G. (1987). Reduction of ammonia in swine houses. Latest Developments in Livestock Housing. Seminar, Second Technical Section, C.I.G.R. Urbana-Champaign. St. Joseph: ASABE, 9-22

- Jeppsson K H (2002). Diurnal variation in ammonia, carbon dioxide and water vapour emission from an uninsulated, deep litter building for growing/finishing pigs. *Biosystems Engineering*, 81(2), 213-223
- Keller R A; Day D L (1975). Pit ventilation system for swine buildings. ASAE Paper No. 75-4048. ASAE, St. Joseph, Mich..
- Koerkamp P W G; Metz J H M; Uenk G H; Phillips V R; Holden M R; Sneath R W; Short J L; White R P; Hartung J; Seedorf J; Schroder M; Linkert K H; Pedersen S; Takai H; Johnsen J O ; Wathes C M (1998). Concentration and emission of ammonia in livestock buildings in Northern Europe. *Journal of Agricultural Engineering Research*, 70(1), 79-95
- Ni J Q (1999). Mechanistic models of ammonia release from liquid manure: a review. *Journal of Agricultural Engineering Research*, 72(1), 1-17.
- Phillips V R; Cowell D A; Sneath R W; Cumby T R; Williams A G.; Demmers T G M; Sandars D L (1999). An assessment of ways to abate ammonia emissions from UK livestock buildings and waste stores. Part 1: ranking exercise. *Bioresource Technology*, 70(2), 143-155.
- Pohl S H; Hellickson M A (1978). Model study of 5 types of manure pit ventilation systems. *Transactions of the ASAE*, 21(3), 542-549.
- Ross D S; Aldrich R A; Younkin D E; Sherritt G W; McCurdy J A (1975). Exhaust systems for under-floor manure pits. In *Managing Livestock Wastes: Proceeding of 3rd International Symposium on Livestock Wastes*, 366-368. ASAE, St. Joseph, Mich..
- Webb J; Menzi H; Pain B F; Misselbrook T H; Dammgen U; Hendriks H; Dohler H (2005). Managing ammonia emissions from livestock production in Europe. *Environmental Pollution*, 135(3), 399-406.
- Ye Z; Zhang G; Li B; Strom J S; Dahl P J (2008a). Ammonia emissions affected by airflow in a model pig house: effects of ventilation rate, floor slat opening, and headspace height in a manure storage pit. *Transactions of the ASABE*, 51(6), 2113-2122.
- Ye Z; Zhang G.; Li B; Strom J S; Tong G H; Dahl P J (2008b). Influence of airflow and liquid properties on the mass transfer coefficient of ammonia in aqueous solutions. *Biosystems Engineering*, 100(3), 422-434.
- Zhang G.; Bjerg B; Strom J S; Morsing S; Kai P; Tong G.; Ravn P (2008). Emission effects of three different ventilation control strategies - A scale model study. *Biosystems Engineering*, 100(1), 96-104.

Chapter 9

General discussion and conclusions

In this chapter, the main findings from each study described in this thesis are summarised and discussed in a boarder context and their implication for future research on fundamental study in laboratory scale and how to control odorants in and from livestock houses are given.

9.1. Effect of air velocity & turbulence intensity on boundary layer and ammonia emission from aqueous ammonia solution

Airflow is considered a main medium in livestock buildings of conveying pollutants from the slurry and the soiled surfaces to the room air and to the atmosphere. Therefore, the characteristics of air velocity and turbulence intensity above the emission surface are essential to study ammonia release behaviour. The results of this study confirmed that increasing wind velocity had evident effect on increasing ammonia emissions at all three RTIs. Increasing RTI also caused a general trend of increase in ammonia emission fluxes. Comparison of ammonia mass transfer co-efficient (AMTC) models as a function of only air velocity and as a function of both air velocity and RTIs showed that the effects of turbulence intensity on the mass transfer modeling cannot be ignored. Characteristics of ammonia emissions obtained in this study (Chapter 2) were similar to those by Rong et al. (2009) and other studies (Arogo et al. 1999; Mackay and Yeun 1983; Rong et al. 2009; Vlek and Stumpe 1978). The AMTC models developed in this study and those of Rong et al. (2009) were positively correlated to wind velocity and turbulence intensity; but the AMTC model presented by Ye et al. (2008a) was inversely correlated to wind velocity although positively correlated to turbulence intensity, indicating a higher uncertainty when using wind velocity and turbulence intensity to model ammonia emissions with different sizes of wind tunnels.

Airflow characteristics above emission surface showed inverse relationship between air velocities and turbulence intensity. The velocity and concentration boundary layer thickness could not be distinguished at different average inlet velocities in the wind tunnel experiments (Chapter 2). The ammonia concentration gradients within a 0.1m-thick quasi-constant boundary layer demonstrated technical difficulty to experimentally determine the ammonia concentration at the immediate liquid surface, because a small variation in height meant significant difference in ammonia concentrations. The available instruments for concentration measurement at boundary layer interfered with inlet air, and also measuring more points were needed to get the exact thickness of the concentration boundary layer. However, there is a risk of damaging the expensive instruments (e.g. Innova Photoacoustic multi-gas monitor), if we take measurement very close to the aqueous emission surface, because liquid may be sucked through the sampling tube into the instrument. Therefore, it is important to find alternative methods or approaches to measure concentration at boundary layer. To solve the problem, an advanced numerical approach, the computational fluid dynamics (CFD), was applied to investigate the details of the velocity and concentration boundary layer above the emission surface. The CFD simulation study (Chapter 3)

showed that the velocity and concentration boundary layer thicknesses decreased with the increase of inlet velocities, causing increased mass transfer rate, and therefore increased ammonia emission.

Comparing with wind tunnel, airflow pattern in a model pig house was different. The airflow direction over the floor (Chapter 4) and the slurry pit (Ye et al., 2009) were not always parallel to the emission surface as in the wind tunnel. In the ventilation room space, airflow characteristics and magnitudes in different locations above floor surface and slurry pit will not be the same at same ventilation condition. In the scale model study (Chapter 4), air velocity was the highest where jet reaches to the surface, and the lowest where the return air approaches the inlet wall. As a total room flow eddy, momentum was added at the inlet and gradually decayed by shear at the walls and by mixing with the room air (Adre and Albright 1994; Yu and Hoff 1999). The reduction in air velocity was not only caused by pressure losses in the corners/airflow changing direction but also by additional momentum losses due to turbulence in the ventilated space (Strom et al. 2002). In addition, combinations of inlet opening height and inlet air velocity induced different air velocities and turbulence intensities at floor level, which altered ammonia emission. The turbulence intensity profiles at the floor level were less distinguishable, compared with the air velocity profiles. Because of the fully rotary flow in the scale model, the airflow characteristics were different at different measurement heights. But, the representative measurement height was important for AMTC modelling in the scale model. Jet momentum number was found a good dimensionless number for avoiding this anomaly, investigating general airflow characteristics over the emission surface, and for modelling AMTC. The relationship of the AMTC with the inlet opening height, inlet air velocity, and length (i.e., total width of a pig house model cross-section) and height of the scale model was established.

9.2. Effect of chamber or wind tunnel dimensions on airflow characteristics and mass transfer process

Due to the covariance between the variables (turbulence level, aqueous concentration, and pH), the wind tunnels' size effect could not be completely elucidated through experiment (Chapter 2). However, the quantification and estimation of the effects of geometry, especially height of the tunnels, on airflow characteristics in boundary layer and odorant emission processes were important to utilise the research results using different chamber or tunnel dimensions for building efficient models and to design a new experimental facility.

The CFD simulation study (Chapter 3), showed that air velocity and ammonia concentration boundary layer thickness were lower in smaller wind tunnels than larger wind tunnels. The results of non-linear regression analysis of velocity boundary layer thickness and concentration boundary layer thickness provided significant evidence of the wind tunnel size effect on boundary thicknesses ($P < 0.001$). These results also helped to explain why the wind tunnel height had significant effect

on ammonia mass transfer process and ammonia emission ($P < 0.001$). Ammonia emission was higher in smaller wind tunnels than in larger wind tunnels because of thinner boundary layer thickness. This PhD work demonstrated that the emission measured using devices of different geometric sizes may not directly comparable. Therefore, standardisation of wind tunnel or dynamic flux chamber is necessary to measure gas and odour emissions from area sources. Direct application of the laboratory study results in field conditions can cause over estimation of emissions and is not recommended. The laboratory results should be at least adjusted to corresponding field conditions using correction factors. Moreover, in field conditions, different heights of slurry pit head space characteristics of odorant emissions. Higher emissions are expected in slurry pit with smaller head space height than that with larger head space height (Ye et al., 2008b). Therefore, odorant emissions may vary dynamically from slurry pits in real pig buildings. This needs to be taken into account in generic emission model development process.

It is always difficult to comprehend the knowledge obtained from a scale model in comparison with that obtained from models of different sizes or from full size buildings due to different experimental conditions and scale effects on airflow and emission process (Chapter 4). The size of eddies in scale model cannot be the same in full size building. Using similitude approach combined with non-dimensional normalised emission rate in this thesis (Chapter 5), the jet momentum ratio (R_m) was found the preferable criterion over Reynolds number (Re) in ammonia emission rate studies in scale models. This conclusion was obtained in isothermal without pigs inside the confined space. Scale model comparison with the real pig production building will be much more complex. Therefore, further researches are needed.

9.3. Mass transport behaviour of different gases and odours

Mass transfer processes of odorants from slurry under different ventilation rates are very important in air pollution research. In most of the scientific studies, ammonia was selected as a representative odorant, because it is a major gas, emitted from livestock buildings and is relatively easy to measure. However, if the measurement is limited to ammonia while our interest is in a wide range of odorants, it is essential to know which odorants from slurry follow the same emission behaviour as ammonia, so that similar techniques may be applied to reduce the emission of all these odorants.

Before introduction of Proton-Transfer-Reaction Mass Spectrometry (PTR-MS), we could measure only ammonia, carbon dioxide, hydrogen sulphide, nitrous oxide, and methane in real time (Blanes-Vidal et al. 2008; Ni et al. 2010), and other VOCs from slurry by collecting discrete samples (Blanes-Vidal et al. 2009; Chen et al. 2009). Our study (Chapter 6) and the study by Feilberg et al. (2010) showed that the PTR-MS could measure odorants precisely in real time.

Temporal variation of odorants at constant ventilation rate immediately after filling the slurry into the slurry tank showed that the head space ammonia concentration increased with time. On the

other hand, concentrations of H₂S, VFAs, and phenol compounds were decreased with time. The temporal variation of DMS, DMTS, 2,3 butanedione, and indoles could not be explained either due to their concentrations being too low to be detected or some other reasons. We have explained that the differences and increasing or decreasing trend might be because of one or more of these four factors : (1) pH increase at the slurry surface over time (Ni et al. 2009), (2) build-up of a dry matter-enriched surface layer due to buoyancy of large particles, (3) slurry surface concentration reduction due to evaporation combine with reduced diffusivity in the enriched surface layer, and (4) oxidation of the compounds by O₂ in the oxic surface layer or in the sub-oxic zone (Nielsen et al. 2010). These explanations were based on theory, our observation, and other researchers' studies. These are the topics which need detail investigations to understand the complex release behaviour of compounds from slurry. An integrated research (i.e., measuring all those factors at the same time) with suitable instruments is needed to understand these phenomena.

The differences of emission fluxes of VICs and VOCs were correlated to the ventilation rate. For compounds with higher Henry constant (sulphur compounds) (Hudson and Ayoko 2008), the liquid mass transfer resistance was expected to dominate, and therefore, these compounds were independent of ventilation rate. On the other hand, for compounds with low Henry constant (e.g., ammonia, VFAs, phenols, and indoles), the emission rates showed positive correlation with the ventilation rates significantly or to some extents (Chapter 6). Parker et al. (2010) showed significant positive correlation of phenol and acetic acid fluxes with air velocity. But this was not the case in our study and neither in the study by Feilberg et al. (2010). The regeneration rate of these compounds, pH development process in the surface, and the reaction rate of these compounds (acid and base) in slurry might be different for different compounds than a single compound in aqueous solution. Emissions of most of these compounds are positively correlated with the ammonia in different ventilation rates (Table 9.1). There might be also other sources of VOCs such as feed, straw bedding etc (Alanis et al. 2010; Blanes-Vidal et al. 2008). In our experiment, there were some technical challenges in using real slurry in laboratory experiment, because slurry surface characteristics changed with time. The experiments required several hours of preparation and also to bring slurry in stable form before conducting measurement. By the time the measurement started, some of the compounds (e.g. acetic acid, phenols, DMS, etc) might disappear from the open surface in a tank, or dropped to concentrations below the instrument detection limit. These are the challenges, which should be taken care of in future laboratory studies.

Table 9.1 – Correlation of ammonia emission with emissions of other odour compounds in laboratory scale study (chapter 6) under different ventilation rates.

<i>Compounds</i>	<i>correlation with ammonia</i>
Trimethylamine	0.95
Hydrogen sulfide	-0.85
Acetic acid	-0.84
Propanoic acid	0.64
Butanoic acid	0.97
C ₅ carboxylic acid	0.88
Phenol	0.43
4-methylphenol	0.75
4-ethylphenol	0.25
Acetone	0.96
C4-carbonyls	0.88
2,3-butanedione	0.30
Indole	0.87
3-methyl-1H-indole	0.96

Though there were some challenges to find the correlation of odorants with the ventilation rates in laboratory scale test device due to their complex behaviour in slurry. The emission of the compounds that were positively correlated with ammonia might also be reduced by controlling ventilation rate or guiding airflow using the same techniques for ammonia emission reduction.

9.4. Technologies for improving indoor air quality, and reducing odorants emissions

As discussed above, there are many VIC (e.g., NH₃) and VOC (e.g., VFAs, phenols, ketones, and indoles) which are affected by ventilation airflow or air phase boundary conditions. Therefore, by controlling ventilation rate or guiding airflow above the emission surface (i.e., either slurry surface or floor surface), the indoor air quality for animals and workers might be improved and the emission of above mentioned odorants could be reduced. A few case studies of improving indoor air and emission reduction strategies from our investigations are discussed below:

9.4.1. Ventilation strategy

In constant inlet momentum strategy, the ammonia emission was nearly independent of ventilation rate. Further investigation (Chapter 4) showed that by changing ventilation strategy, the local/floor air velocity close to the emission surface was changed under the same ventilation rate. In general, when there was low air velocity or less contact with the emission surface, we got less emission from the scale models.

9.4.2. Location of emission surface

One of our studies (Chapter 4) demonstrated that, the emission source located closer to the side wall (or back of the pen) could result in an ammonia emission of 4 to 22% and 22 to 41% lower than the emission source located at the middle and front of the pen, respectively. It was found that floor air velocities were lower at the back of the pen than at the middle and front of the pen. The results indicated that the local flow including the velocity and turbulence intensity has significant effect on ammonia emission.

9.4.3. Deflector and curtain

Placing an environmental deflector inside the room and curtains inside the slurry pit could change the air exchange ratio between the slurry pit and the room, and reduce emission (Chapter 7). The results from the 2D chamber experiment with environmental deflector inside the room showed that the highest carbon dioxide concentration in the slurry pit and lower carbon dioxide concentration in the room could be achieved by using lower ventilation rate and a 45° deflector angle, compared with the deflector angles of 0° and 90°. In a ventilated pig building with slatted floor without pit ventilation, the air exchange rate in the slurry pit was influenced by the angle of the deflector in the room. The 45° deflector angle resulted in the lowest air exchange ratio, and therefore, less contaminant emission from the slurry pit. On the other hand, higher carbon dioxide concentration in the slurry pit and lower carbon dioxide concentration in the room air could be achieved by using lower room ventilation rate and more slurry pit curtains, because lower ventilation rate and more curtain under slatted floor resulted in lower air exchange in the slurry pit.

Therefore, emissions of contaminants like ammonia and odours can be reduced from animal house if more contaminants are kept inside the pit. In addition, lower odour concentration in the room air results in better air quality inside livestock buildings. However, to define an optimal deflector angle and number of pit curtains will require further studies in field conditions.

9.4.4. Partial pit ventilation

According to Aarnink et al. (1996), 60% of emission from a pig production building comes from slurry pit; therefore, removing the contaminated air directly from the slurry pit may improve indoor air quality. A partial pit ventilation that apply a small portion of the total required ventilation capacity to remove the polluted air with relatively high concentration from the slurry pit, can provide better indoor air quality and make the exhaust air cleaning more efficient by treating only the pit exhaust air.

Our investigations in a negative pressure ventilation system with diffusion ceiling inlet and ceiling exhaust showed a partial pit exhaust of 10% of maximum ventilation capacity can reduce

indoor ammonia concentration by 42.6% (Chapter 8). Without an air cleaning connects to pit exhaust, the total ammonia emission was 5% higher in ceiling plus pit exhaust than only using ceiling exhaust. The 37 to 53% or even more of ammonia emission reduction is possible if high efficient (97.6%) air purification is used at the pit exhaust. This study also showed that partial pit ventilation did not affect pig behaviour significantly. Airflow characteristics in slurry pit were difficult to measure in this real pig production facility.

Overall, this thesis has contributed to the new knowledge related to some technologies for odour emission reduction. However, on-farm evaluation of these technologies is a critical step before they can be applied in commercial farms. Although in theory some of the emission reduction technologies can have high application potentials, they should always be tested, evaluated, and validated using the integrated approach in practical conditions, preferably in commercial houses.

9.5. Future perspectives

Odorant emissions from intensive livestock productions are a growing concern for environmental scientists, livestock farmers, rural residents, politicians, and welfare organizations, because of their negative effects on human and animal health, and atmosphere. More stringent environmental regulations on animal productions can be expected in the near future. Public interest and investment in controlling odorant emissions will be continued. In this thesis, the initial objectives were fulfilled with certain limitations, which discussed below. The discussion can serve for improving future studies on source apportionment of odorants from livestock houses and odour reduction. Several areas need further investigation:

- Factors, which were studied in this thesis (i.e., air velocity, turbulence intensity, geometric scale) and found to have influence on emission processes, need to be verified, and tested in real livestock production facilities for feasible model development.
- Odour release behaviours were studied only in steady state and isothermal conditions. Odour release behaviour in non-isothermal case should be studied and should also include manure from different animal species (e.g., pig, dairy, poultry etc.) because different manure may release different quantities of gases and VOCs. Chemical compounds found in one type of slurry may not be present in others.
- A knowledge gap has been identified in the liquid side diffusion rates and reaction rates of different compounds in slurry, and the pH development process in slurry surface. These are the topics that deserved thorough study using advanced instruments.
- Some of the odour reduction and indoor air quality improvement techniques presented in this thesis should be tested in real production facilities. Improvement and optimisation are

needed for the partial pit ventilation system with the air purification system at building ventilation exhaust.

9.6. General conclusions

The following general conclusions were drawn from this thesis:

- Airflow inside the pig buildings played a dominant role for transporting major odorants from slurry pit to room air and to outdoor air.
- Both air velocity and turbulence intensity affected ammonia emission process. Turbulence intensity, together with the air velocity, was confirmed to be an important parameter for increasing accuracy of emission models.
- Wind tunnel height significantly affected air velocity and concentration boundary layer and therefore ammonia emission estimation. This factor should be considered when interpreting result from laboratory scale to full scale. Also it should be taken into account for developing any model through wind tunnel study.
- Advanced numerical approach CFD is a good tool for studying details of different factors affecting on boundary layers or studying distribution of air velocity and concentration in space, which are expensive and difficult to achieve through experiment.
- Correlation of jet momentum number and the AMTC was established for the model pig houses. Using this correlation, the measurements of air velocity and turbulence above the emission surface can be avoided.
- Non-dimensional normalized emission rate and jet momentum ratio could be a good option for comparing emission measurements in the scale model with full scale or with another scale of slot ventilated pig house in isothermal case.
- Proton-Transfer-Reaction Mass Spectrometry (PTR-MS) was found very effective instruments for measuring odour compounds precisely in real time.
- Ammonia and trimethylamine emissions were significantly correlated with ventilation rate. Volatile fatty acids emission dependency on ventilation rate increased with the increase of carbon chain and source. Phenols, indoles, and ketones showed positive correlation with ventilation rate to some extent. The reduction of emission of most of the compounds is possible through controlling ventilation.
- Guiding airflow using deflector, curtain, and partial pit ventilation, the indoor air quality could be improved significantly, and the emission could be reduced substantially by using air purification system at the end of partial pit vent.

References

- Aarnink, A. J. A., vandenBerg, A. J., Keen, A., Hoeksma, P., and Verstegen, M. W. A. (1996). Effect of slatted floor area on ammonia emission and on the excretory and lying behaviour of growing pigs. *Journal of Agricultural Engineering Research*, 64(4), 299-310.
- Adre, N., and Albright, L. D. (1994). Criterion for Establishing Similar Air-Flow Patterns (Isothermal) in Slotted-Inlet Ventilated Enclosures. *Transactions of the ASAE*, 37(1), 235-250.
- Alanis, P., Ashkan, S., Krauter, C., Campbell, S., and Hasson, A. S. (2010). Emissions of volatile fatty acids from feed at dairy facilities. *Atmospheric Environment*, 44(39), 5084-5092.
- Arogo, J., Zhang, R. H., Riskowski, G. L., Christianson, L. L., and Day, D. L. (1999). Mass transfer coefficient of ammonia in liquid swine manure and aqueous solutions. *Journal of Agricultural Engineering Research*, 73(1), 77-86.
- Blanes-Vidal, V., Hansen, M. N., Pedersen, S., and Rom, H. B. (2008). Emissions of ammonia, methane and nitrous oxide from pig houses and slurry: Effects of rooting material, animal activity and ventilation flow. *Agriculture Ecosystems & Environment*, 124(3-4), 237-244.
- Blanes-Vidal, V., Hansen, M. N., and Sousa, P. (2009). Reduction of Odor and Odorant Emissions from Slurry Stores by Means of Straw Covers. *Journal of Environmental Quality*, 38(4), 1518-1527.
- Chen, L. D., Hoff, S., Cai, L. S., Koziel, J., and Zelle, B. (2009). Evaluation of Wood Chip-Based Biofilters to Reduce Odor, Hydrogen Sulfide, and Ammonia from Swine Barn Ventilation Air. *Journal of the Air & Waste Management Association*, 59(5), 520-530.
- Feilberg, A., Lu, D. Z., Adamsen, A. P. S., Hansen, M. J., and Jonassen, K. E. N. (2010). Odorant Emissions from Intensive Pig Production Measured by Online Proton-Transfer-Reaction Mass Spectrometry. *Environmental Science & Technology*, 44(15), 5894-5900.
- Hudson, N., and Ayoko, G. A. (2008). Odour sampling 1: Physical chemistry considerations. *Bioresource Technology*, 99(10), 3982-3992.
- Mackay, D., and Yeun, A. T. K. (1983). Mass-Transfer Coefficient Correlations for Volatilization of Organic Solutes from Water. *Environmental Science & Technology*, 17(4), 211-217.
- Ni, J. Q., Heber, A. J., Sutton, A. L., and Kelly, D. T. (2009). Mechanisms of Gas Releases from Swine Wastes. *Transactions of the ASABE*, 52(6), 2013-2025.

- Ni, J. Q., Heber, A. J., Sutton, A. L., Kelly, D. T., Patterson, J. A., and Kim, S. T. (2010). Effect of swine manure dilution on ammonia, hydrogen sulfide, carbon dioxide, and sulfur dioxide releases. *Science of the Total Environment*, 408(23), 5917-5923.
- Nielsen, L. P., Risgaard-Petersen, N., Fossing, H., Christensen, P. B., and Sayama, M. (2010). Electric currents couple spatially separated biogeochemical processes in marine sediment. *Nature*, 463(7284), 1071-1074.
- Parker, D. B., Caraway, E. A., Rhoades, M. B., Cole, N. A., Todd, R. W., Casey, K. D. (2010). Effect of wind tunnel air velocity on voc flux from standard solutions and cafo manure/wastewater. *Transactions of the ASABE*, 53 (3), 831-845.
- Rong, L., Nielsen, P. V., and Zhang, G. Q. (2009). Effects of airflow and liquid temperature on ammonia mass transfer above an emission surface: Experimental study on emission rate. *Bioresource Technology*, 100(20), 4654-4661.
- Strom, J. S., Zhang, G., and Morsing, S. (2002). Predicting near-floor air velocities for a slot-inlet ventilated building by jet velocity decay principles. *Transactions of the ASAE*, 45(2), 407-413.
- Vlek, P. L. G., and Stumpe, J. M. (1978). Effects of Solution Chemistry and Environmental-Conditions on Ammonia Volatilization Losses from Aqueous Systems. *Soil Science Society of America Journal*, 42(3), 416-421.
- Ye, Z., Zhang, G., Li, B., Strom, J. S., Tong, G., and Dahl, P. J. (2008a). Influence of airflow and liquid properties on the mass transfer coefficient of ammonia in aqueous solutions. *Biosystems Engineering*, 100(3), 422-434.
- Ye, Z., Zhang, G., Li, B., Strom, J. S., and Dahl, P. J. (2008b). Ammonia Emissions Affected by Airflow in A Model Pig House: Effects of Ventilation Rate, Floor Slat Opening, and Headspace Height in A Manure Storage Pit. *Transactions of the ASABE*, 51(6), 2113-2122.
- Ye, Z., Saha, C. K., Li, B., Tong, G., Wang, C., Zhu, S., and Zhang, G. (2009). Effect of environmental deflector and curtain on air exchange rate in slurry pit in a model pig house. *Biosystems Engineering*, 104(4), 522-533.
- Yu, H., and Hoff, S. J. (1999). Airflow pattern similarity criteria for ceiling slot-ventilated agricultural enclosures under isothermal conditions. *Transactions of the ASAE*, 42(2), 459-469.

Appendix – A

Pictorial views of different experimental set-ups

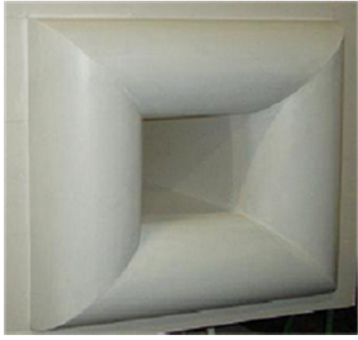


(a)

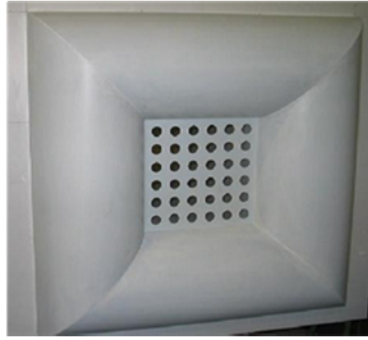


(b)

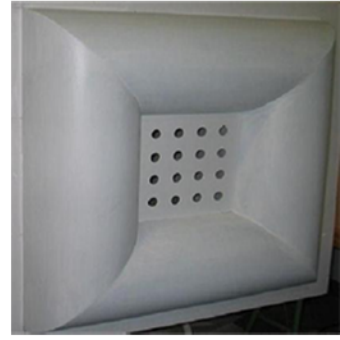
Fig. A1 - Experimental set-up of wind tunnel experiment, (a) Wind tunnel (cross-section (W×H) - 0.35×0.35), and (b) velocity and concentration profile measuring section.



S-0



S-1



S-2

Fig. A2 - Inlet conditions of wind tunnel for generating different average turbulence intensities above the middle of the emission surface (S-0) Ti - 11%, (S-1) Ti -20%, and (S-2) Ti -30%.



(a)



(b)

Fig. A3 - Pictorial views of experimental set-ups with two scale models of different sizes of a pig house; (a) 1:6 scale model and (b) 1:12.5 scale model.

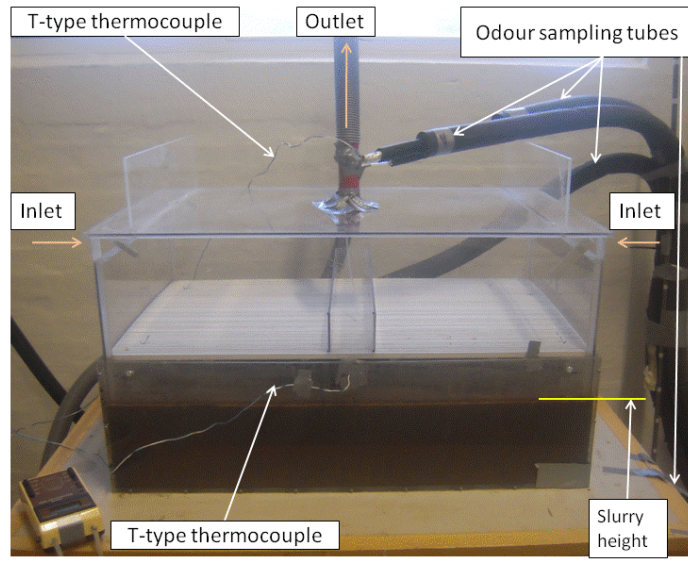


Fig. A4 - Experimental set-up using real slurry in a model pig house (1:12.5)



Airflow inside livestock building is considered a main transport medium of odorants, which have negative impacts on environment pollution, animals' wellbeing, and workers' health. Identification of different factors that influence release behaviours of odorants is essential to understand the mechanisms of air pollution related to livestock buildings and to develop emission abatement technologies. The main objective of the PhD thesis was to generate fundamental knowledge about mass transfer processes of odorants from slurry surface boundary layer to room air space. Emphases were given on the effects of air velocity, turbulence intensity, ventilation rate, and geometric size on mass transfer processes. Turbulence intensity was found an important parameter, together with air velocity, to affect mass transfer processes of odorants. Laboratory-scale studies using wind tunnel and scale model demonstrated that their scale/geometric dimension also had significant effects on mass transfer process and emission estimation. Computational Fluid Dynamics approach was found to be a good tool for studying mass transfer process in boundary layer. New methods investigated in this thesis showed that indoor air quality could be improved and odorant emission could be reduced by controlling air motion above the emission surface.

